TECHNISCHE UNIVERSITÄT MÜNCHEN

Lehrstuhl für Technische Chemie II

Selective Cleavage of C-O Bonds and Hydrodeoxygenation of Lignin Fragment Molecules

Jiayue He

Vollständiger Abdruck der von der Fakultät für Chemie der Technischen Universität München zur Erlangung des akademischen Grades eines

Doktors der Naturwissenschaften (Dr. rer. nat.)

genehmigten Dissertation.

Vorsitzender: Univ.-Prof. Dr.-Ing. Kai-Olaf Hinrichsen

Prüfer der Dissertation:

1. Univ.-Prof. Dr. Johannes A. Lercher

2. Univ.-Prof. Dr. Dr. h.c. Bernhard Rieger

3. Prof. Dr. Gary L. Haller (nur schriftliche Beurteilung),

   Yale University, New Haven / USA

   Univ.-Prof. Dr. Thomas Brück (nur mündliche Prüfung)

Die Dissertation wurde am 15.05.2014 bei der Technischen Universität München eingereicht und durch die Fakultät für Chemie am 18.06.2014 angenommen.

"No power, a little knowledge, a little wisdom, as much flavor as possible."

Roland Barthes (1915 – 1980)

Acknowledgements

My sincere thanks go to my revered teacher Professor Dr. Johannes A. Lercher for this interesting topic, for the unlimited trust, for the research freedom, for the invaluable scientific discussion and for all the support which were crucial for the success of this thesis.

My heartfelt thanks go out to:

Prof. Dr. Chen Zhao, for the supervision of my work progress, for the excellent discussion we shared throughout these years, for the uncountable assistance in the laboratory and for the kind encouragements during my graduate career.

Dr. Eszter Baráth, for being my mentor in the last few months of my PhD study. I am grateful for the encouragement, patience, support I have received from her.

Prof. Dr. Xuebing Li, for being my supervisor in the beginning of PhD study and for the interesting discussion, tips and help.

Prof. Dr. Andreas Jentys, for his assistance in the laboratory and joyful discussion.

YiChao Chu, Fan Chen, Albert Albert, Yu Lou, Xueyin Cui, Lu Lu, Harry Renges, Céline Nathalie Schweitzer, Miriam Pfab, Ang Li, for making their internship, bachelor or master thesis under my supervision, for the precious help and fruitful collaboration with all of you.

Dr. Donghai Mei, for the DFT calculations and the kind encouragement.

Xaver Hecht, for the help to solve all the technical problems, and for BET and hydrogen chemisorption measurements.

Martin Neukamm, for AAS and SEM measurement and the order of chemicals and labware.

Jiayue

Mar. 2014

Abstract

The mechanisms for catalytic cleavage of C-O bonds and hydrodeoxygenation of the lignin fragment molecules over metals (Ni, Pd) and acid catalysts (HZSM-5) have been systematically investigated. With Ni/SiO_2 the C-O bonds of α-O-4 (benzyl phenyl ether) and β-O-4 (2-phenylethyl phenyl ether) ether bonds could be selectively cleaved by hydrogenolysis at 373 K in the presence of 0.6 MPa H_2 in the aqueous phase, while the C-O bond of 4-O-5 (diphenyl ether) is cleaved via parallel hydrogenolysis and hydrolysis. The *p*-substituted H-, CH_3-, OH- groups of diphenyl ether greatly influences the rates and reaction pathways of C-O cleavage over Ni/SiO_2. For cleaving of C-O bond in α-O-4 (benzyl phenyl ether) over dual-functional Ni/HZSM-5 catalyst, Ni, which catalyzes the hydrogenolysis of C-O bonds (major route), plays a more crucial role than HZSM-5, which catalyzes the hydrolysis (minor route) in the aqueous phase. Solvents influence the rates of catalytic phenol hydrodeoxygenation by altering the H_2 solubility and the solvent-reactant interactions, as well as by competitive solvent/reactant adsorption on the catalyst surface.

Kurzzusammenfassung

Der Mechanismus der katalytische Spaltung von C-O Bindungen und die Hydrodeoxygenierung von Lignin-Fragmentmolekülen über Metallen (Ni, Pd) und sauren Katalysatoren (HZSM-5) wurden systematisch untersucht. Über Ni/SiO_2 konnten die C-O Bindungen der α-O-4 und β-O-4 Etherbindungen selektiv durch Hydrogenolyse, bei 393 K in Gegenwart von 0.6 MPa H_2 in wässriger Phase, gespalten werden, während hingegen die C-O Bindung von 4-O-5 via paralleler Hydrogenolyse und Hydrolyse gespalten wurde. Bei der Spaltung der C-O Bindung von α-O-4 über bifunktionellen Ni/HZSM-5 Katalysatoren spielt Ni, welches die Hydrogenolyse der C-O Bindung katalysiert (Hauptroute), eine entscheidendere Rolle als HZSM-5, welcher die Hydrolyse in wässriger Phase katalysiert (Nebenroute). Die p-substituierten H-, CH_3-, OH- Gruppen des

Diphenylethers beeinflussen in großem Maße die Raten und die Reaktionswege der C-O Spaltung über Ni/SiO$_2$. Lösungsmittel beeinflussen die Rate der katalytischen Hydrodeoxygenierung von Phenol durch die Veränderung der H$_2$ Löslichkeit und der Lösungsmittel-Reaktant Wechselwirkungen als auch durch kompetitive Adsorption von Lösungsmittel/Reaktant auf der Katalysatoroberflache.

Table of Contents

Chapter 1

Introduction

1.1 General background

Nowadays, as the economy and the population grows, and as living standards improve for billions of people, the need for energy and fuels will continue to rise steadily. However, on the one hand, the supplies of traditional fossil raw materials producing fuels and energy are gradually being depleted, which makes it difficult to cope with the growing energy demand [1]. On the other hand, it is commonly believed that serious environmental pollution and problems are caused by the combustion of fossil fuels, such as acid rain (sulphur oxide and nitrogen oxide, et al.), haze (aerosol complexes arose by the reaction of sulphur oxide and sulphuric acid), and greenhouse gas (carbon dioxide) [2, 3]. Moreover, governments of many nations have created efficiency and pollution standards and other legalisation to push citizens to use the fossil fuels more responsibly and to mandate increases in the gross domestic energy and chemical production from renewable sources, especially biomass. For example, a mandatory minimum target of 10% for biofuels is requested for all European Union member states by 2020 [4]. Based on the above points, an alternative energy source has been pursued by us.

According to **Fig. 1-1** provided by Shell [5], the total world energy demand by 2050 will substantially increase to 880 EJ/year comparing to 420 EJ/year in 2000. The energy from oil will first increase to 183 EJ/year in 2020 and then decrease to 147 EJ/year in 2050. Meanwhile, the weight of oil in energy will decrease all the way from 35% in 2000 to 17% in 2050. The energy from gas would be quiet stable around 100-110 EJ/year through 2000-2050. However, the weight of gas in energy will decrease gradually from 24% in 2000 to 13% in 2050. The energy from coal will rise from 92 EJ/year in 2000 to 275 EJ/year in 2050. In percentages, the weight of coal will increase from 22% in 2000 to 31% in 2050. In other words, oil will be replaced by coal becoming as the most predominant energy source. It is very interesting to note that energy from biomass in 2050 (37 EJ/year) will be 3.5 times that in 2010 (128 EJ/year). Especially during the period of 2010-2030, the weight of biomass will be doubled from 8% to 14%. It is also forecast by ExxonMobil that the weight of biomass in global and north america liquids supply in 2040 will be more than 10 times higher than that in 2000 (**Fig. 1-2**) [6]. Therefore, biomass possessing many advantages (renewable, abundance, and sulfur free) will definitely contribute a significant part to the world energy supply.
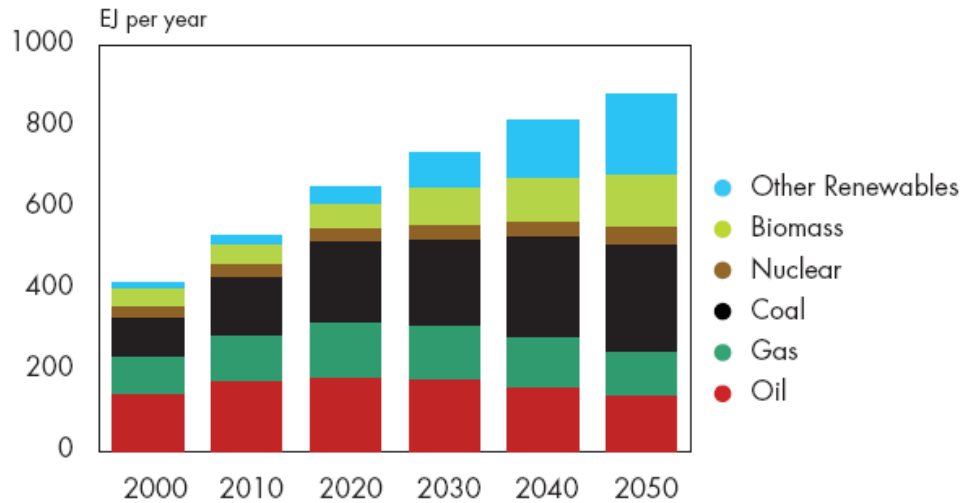
Figure 1-1 The forecast for world's primary energy to 2050 by Shell [5]. Biomass includes traditional renewables such as wood, dung, etc.
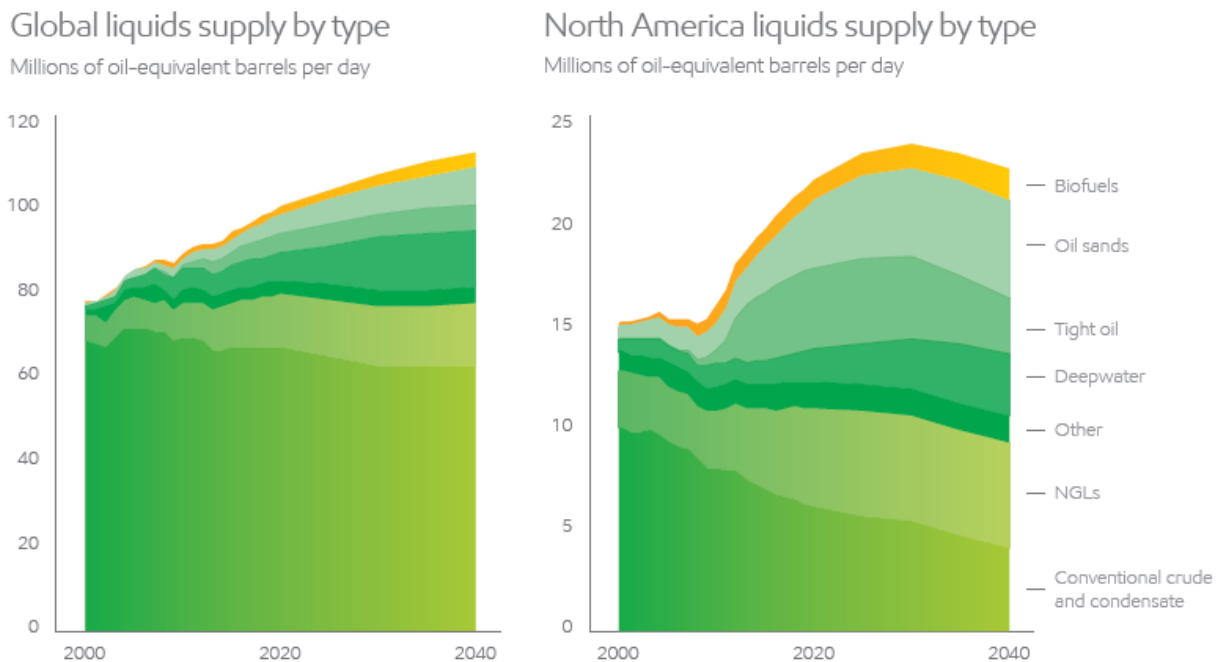
Figure 1-2. The global and north america liquids supply outlook to 2040 by ExxonMobil [6].

Biomass as a material derived from biological organisms consists of lignocellulosic biomass and triglyceride biomass. Since lignocellulosic biomass is the most abundant biomass energy

source, biomass is most often refers to lignocellulosic biomass (cellulose, hemicellulose and lignin). It can be obtained from various sources including wood (forest residues, yard clippings, wood chips, municipal and industrial solid waste) and many other types of plants (sorghum, switchgrass, hemp, willow, corn, poplar, sugarcane, bamboo, miscanthus, et al.).
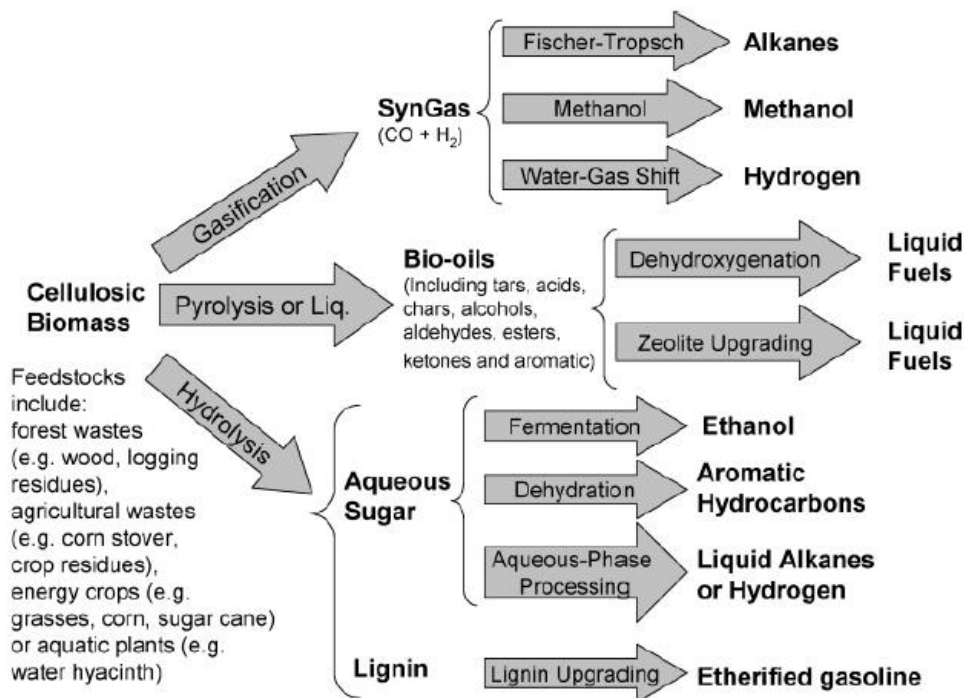
Figure 1-3. Strategies for production of fuels from lignocellulosic biomass [7].

Currently, lignocellulosic biomass can be indirectly converted to biofuels or directly burned to produce heat or electricity. For the production of biofuels, as shown in **Fig. 1-3**, gasification, pyrolysis or liquefaction and hydrolysis are three primary routes to convert lignocellulosic biomass [7]. No matter which route it takes, catalysis is regarded as a key technology for fulfilling the promise of biofuels and chemicals. In this thesis, the aryl ether compounds (lignin model

compounds) and phenolic compounds (bio-oil model compounds) are selected to study the chemical conversion of biomass via metal and/or acid catalysis.

1.2 Lignocellulosic biomass

Lignocellulosic biomass, which is mainly composed of cellulose, hemicellulose and lignin, is a very recalcitrant material and promising feedstock for providing environmentally friendly renewable chemicals and energy for the transportation sector at reasonable price.

1.2.1 Cellulose and hemicellulose

As the most abundant (40-50%) and important component in plants, cellulose, an organic polymer, has the potential to be an inexhaustible source (1.5×10^{12} ton per year as a biomass resource) for raw material to produce chemicals and energy [8]. Cellulose (chemical formula $(C_6H_{10}O_5)_n$), a long chain polymer, is formed from repeating connection of D-glucose molecules that are linked via -O- group between –OH groups of C4 and C1 carbon atoms as shown in **Fig. 1-4**. The degree of polymerization (DP), which varies depends on the source and treatment of the raw materials, determines the chain length of cellulose. The interaction between the OH-groups (hydrogen bonds) formed the hierarchical structure of the 3-D cellulose materials [9].
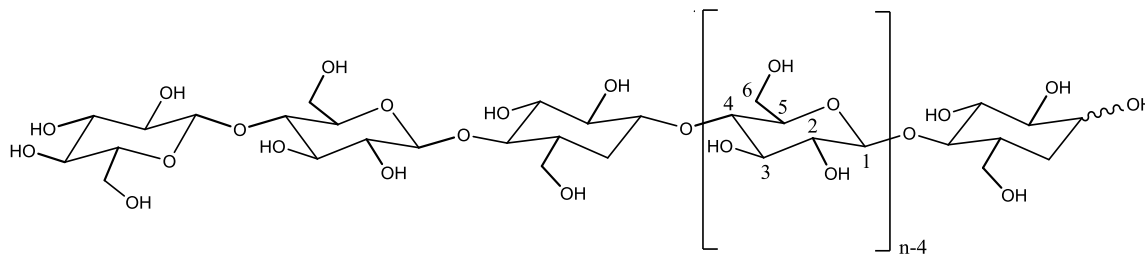
Figure 1-4 Molecular structure of cellulose (n=DP, degree of polymerization) [8].

Hemicelluloses representing 15-35% of plant biomass, are polysaccharides located in plant cell walls contributing to the strength of the cell wall by interaction with cellulose and in some conditions, with lignin [10]. Unlike cellulose, hemicellulose is not chemically homogeneous. In

other words, cellulose only contains glucose, while hemicellulose is made of various sugar monomers. It consists of a heterogeneous class of polysaccharides including arabinogalactan (in softwoods), xyloglucan (in hardwoods, grasses), galactoglucomannan (in softwoods), glucomannan (in softwoods and hardwoods), glucuronoxylan (in hardwoods), arabinoglucuronoxylan (in grasses and cereals, softwoods), arabinoxylans (in cereals), glucuronoarabinoxylans (in grasses and cereals), and homoxylans (in algae), made of pentoses, hexoses and/or uronic acids (**Fig. 1-5**). Small amount of other sugars including a-L-rhamnose a-L-fucose may present and acetyl groups may partially substitute the hydroxyl groups of sugars [10, 11].

- Xylose - ß(1,4) - Mannose - ß(1,4) - Glucose -
- alpha(1,3) - Galactose
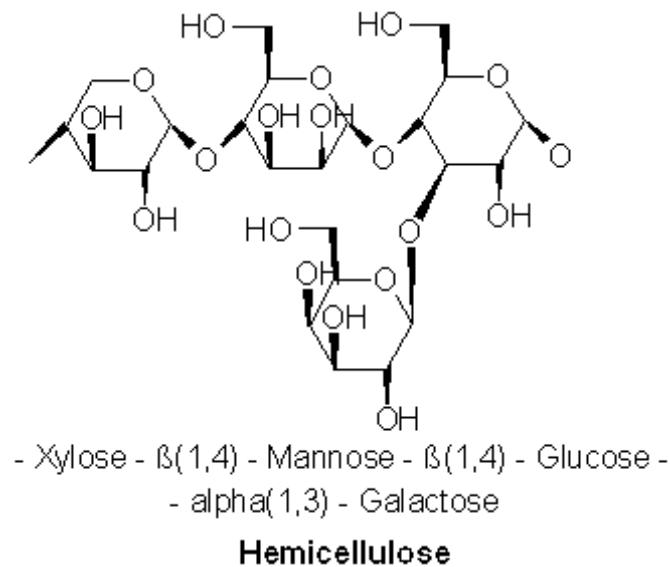
Hemicellulose

Figure 1-5 Most common motif of hemicellulose [12]

1.2.2 Lignin

Lignin, a three-dimensional amorphous polymer consisting of methoxylated phenylpropane structures [13], is one of the most abundant organic compounds on earth. From a quarter to a third of the dry mass of wood is comprised of lignin. Moreover, it contains as much as 30% of non-fossil organic carbon [14]. According to **Fig. 1-6**, lignin holds the lignocellulose material together and locates in the space between cellulose and hemicellulose in the plant cell walls.
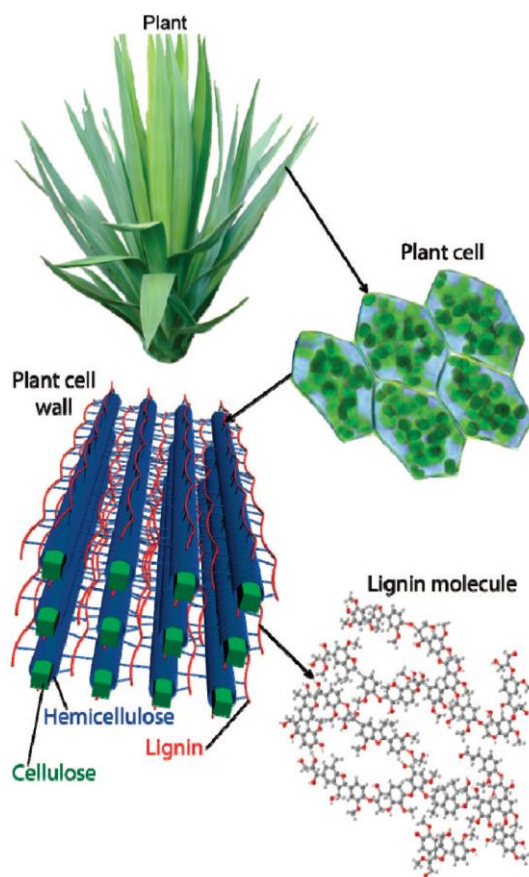
Figure 1-6 Structure of lignocellulosic biomass and the positions of cellulose, hemicellulose and lignin [15]**.**

It has been widely accepted that three types of phenyl propane units (*p*-coumary alcohol, coniferyl alcohol, sinapyl alcohol) (**Fig.1-7**) polymerize with each other to form lignin [16-18]. Due to the difference in the relative abundance of the p-coumaryl, coniferyl, and sinapyl alcohols, the composition of softwood and hardwood lignin varies accordingly. Equal amount of coniferyl
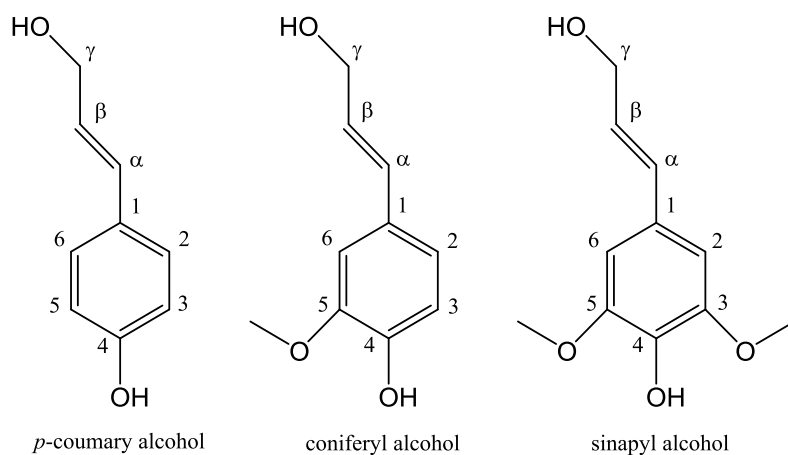
Figure 1-7 Three types of phenyl propane units (*p*-coumary alcohol, coniferyl alcohol, sinapyl alcohol) [15].
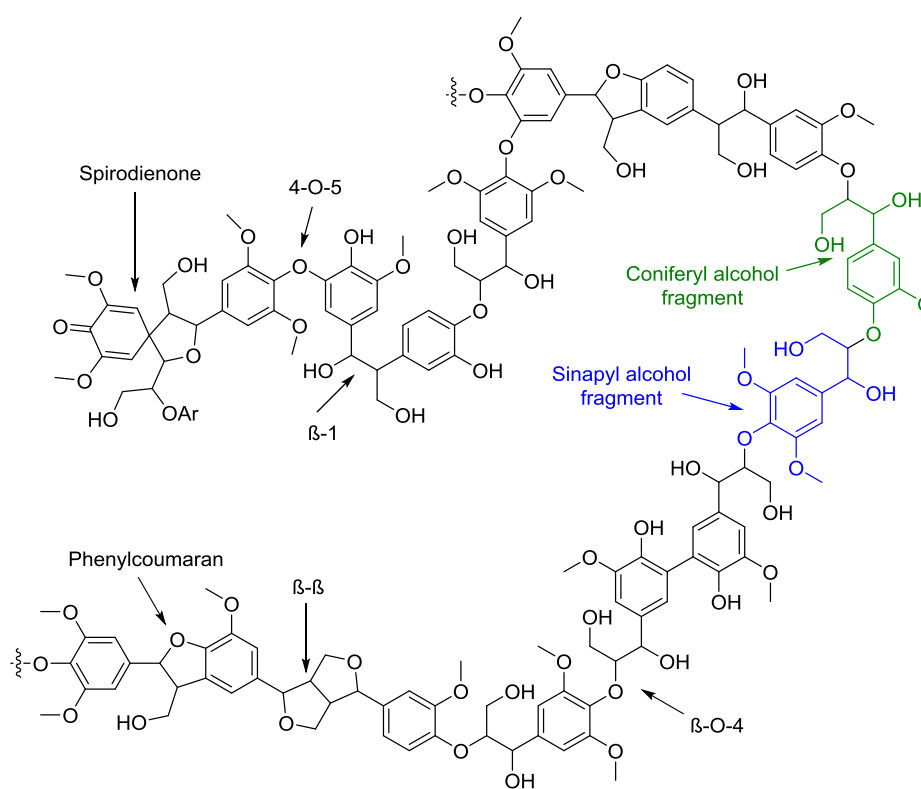
Figure 1-8 Schematic representation of hardwood lignin [15, 19].
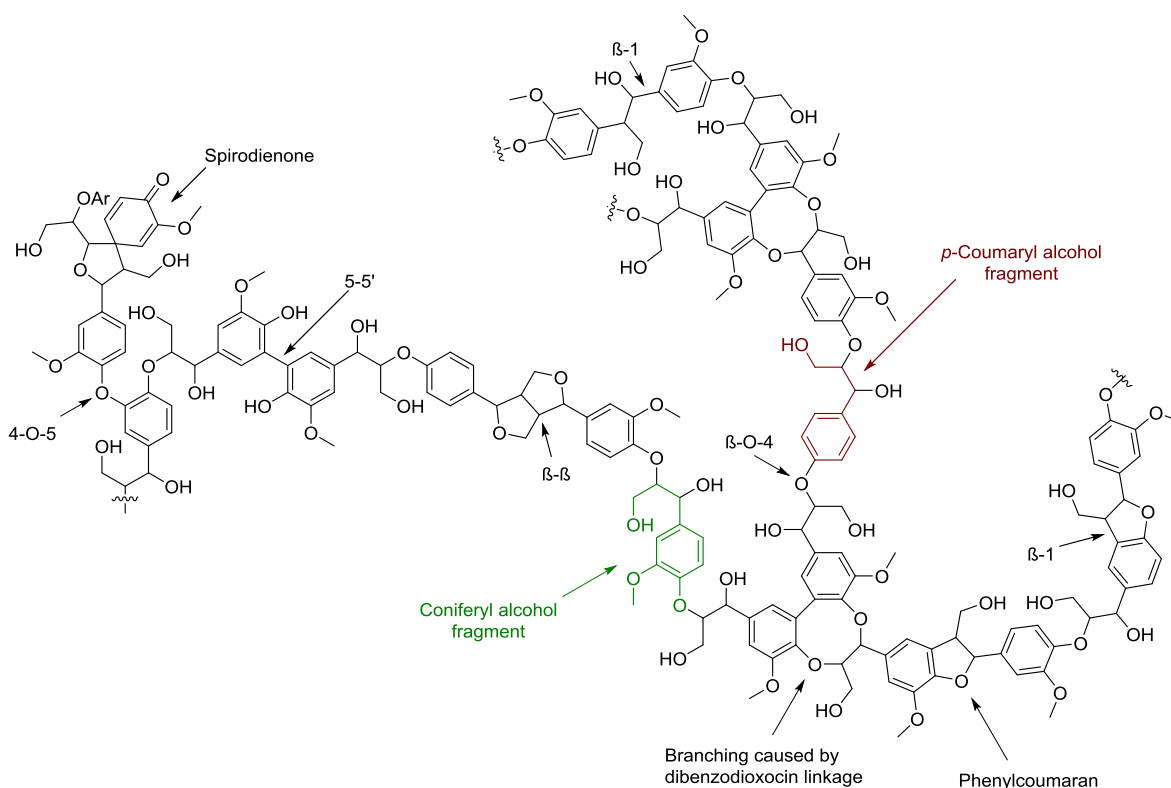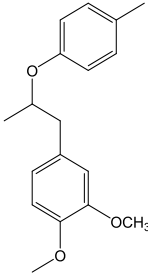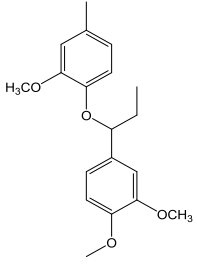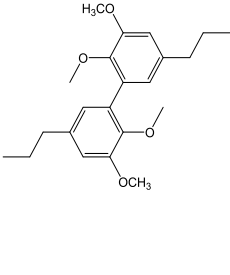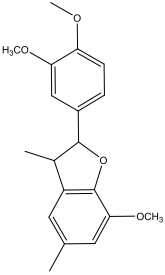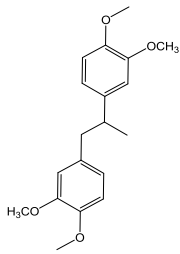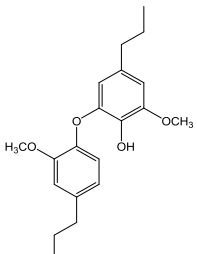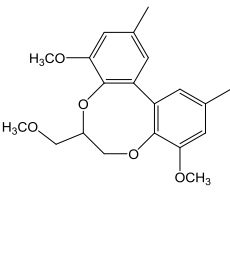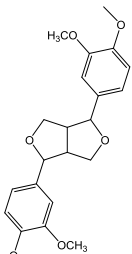
Figure 1-9 Schematic representation of softwood lignin [15].

alcohol and sinapyl alcohol constitutes hardwood lignin (**Fig. 1-8**), while almost 90% of softwood lignin (**Fig. 1-9**) is formed by coniferyl alcohol. The existence of additional methoxy groups in coniferyl alcohol and sinapyl alcohol prevents the formation of cross-linkages (5-5' and dibenzodioxocin) (**Table 1-1**) between the monomer due to steric effect in hardwood lignin. Thus, compared with softwood lignin, the structure of hardwood lignin is much more linear.

Concerning the linkages in the lignin structure, β-O-4, α-O-4, β-5, 5-5', 4-O-5, β-1, β-β, dibenzodioxocin (**Table 1-1**) are the most abundant types of connections according to the schematic representation of hardwood lignin and softwood lignin (They are also depicted in **Fig. 1-8** and **Fig.1-9**.). As shown in **Table 1-1**, in either hardwood or softwood lignin, β-O-4 is the dominant linkage; it consists of around 44-65% connection units in lignin. In addition to β-O-4, α-O-4 and 4-O-5 comprise about 6-20% and 1-9%, respectively, of the linkages containing ether bonds in lignin.

Table 1-1 Proportions of different types of linkages in softwood and hardwood lignin [13, 15, 20, 21].[a]

Linkage Source		*β-O-4*	*α-O-4*	*5-5'*	*β-5*
Pct.(%)	Softwood	45-50	6-8	18-25	9-12
	Hardwood	44-65	6-20	2-27	14
Linkage Source		*β-1*	*4-O-5*	*Dibenzodioxocin*	*β -β*
Pct.(%)	Softwood	7-10	4-8	5-7	3
	Hardwood	1-7	1-9	0-2	4-14

[a] The carbons in phenyl propane units are labelled with number or letter in **Fig. 1-7**. The dimer linkages (β-O-4, α-O-4, β-5, 5-5', 4-O-5, β-1, β-β) are named according to the carbons with which the monomers are connected.

1.3 Technology for lignocellulosic biomass conversion

Lignocellulosic biomass, as the most abundant renewable energy resource, has a bright and promising future for being an important supplement to fossil energy sources. However, nowadays it is still a challenge to convert lignocellulosic materials to liquid fuels with high efficiency. It requires more advanced technology to realize its potential. Generally, three strategies for converting the lignocellulosic biomass to transportation fuels, as shown in **Fig. 1-3** are gasification (to synthesis gas), pyrolysis or liquefaction (to bio-oil) and hydrolysis (to sugar monomers). Gasoline, diesel, methanol or other fuels could be produced from synthesis gas, which is a gas mixture containing hydrogen, carbon monoxide, and very often some carbon dioxide. Syngas could be further converted to liquid fuels or methanol via the Fisher-Tropsch process or methanol synthesis. Due to the high viscosity and oxygen content of bio-oil, it must be upgraded by hydrodeoxygenation before use as fuel. Sugar and lignin fragments could be further treated to produce gasoline, diesel, ethanol and other fuels [7].

1.3.1 Gasification

Gasification is a very old process from the 19th century. Even 80 years ago, more than 1 million cars were fuelled by biomass gasification in Europe in the 1940s [22]. It has been widely practiced to convert biomass, coal and other carbonaceous solids to syngas, producer gas, which are also referred to as town gas, blue gas or water gas [23]. Producer gas primarily consists of carbon monoxide, hydrogen, carbon dioxide, methane and nitrogen in various proportions [24-26]. The producer gas could be burned to generate electricity and heat. Due to the much higher activity of biomass than other carbonaceous solids like coal, biomass gasification required much lower temperature than coal gasification. A gasification process with greatest current interest is depicted in **Fig. 1-10**. This is so-called zero-emissions process to produce carbon monoxide and hydrogen (syngas) as the raw materials of fuels and chemicals and to act as a power station at the same time to generate electricity. The produced CO_2 is injected to a permanent geological formation.
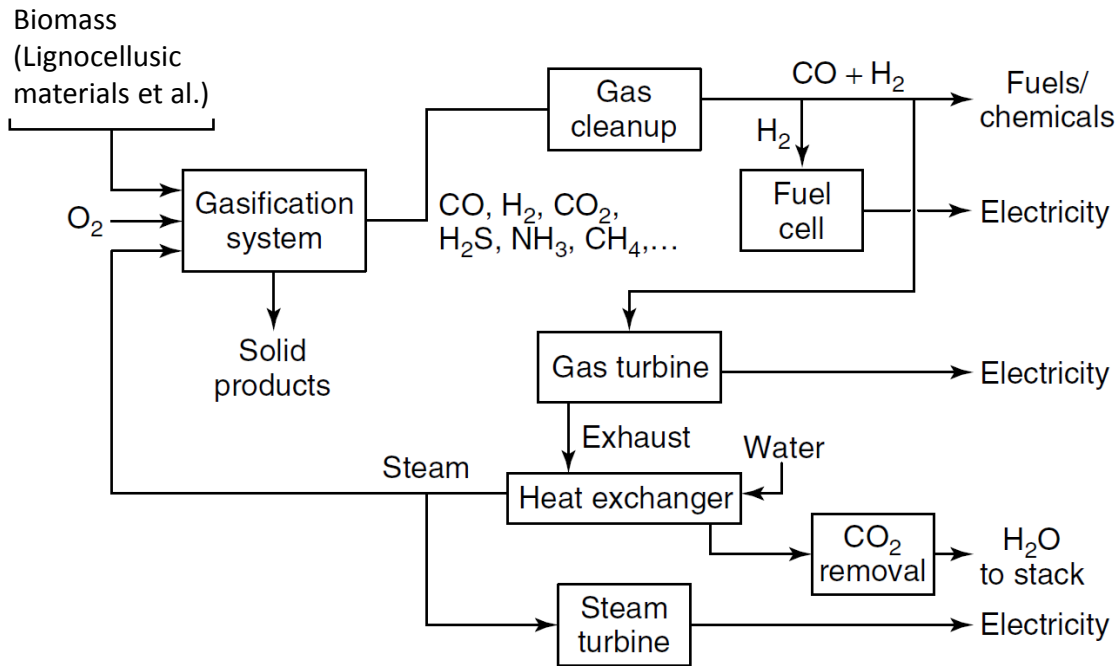
Figure 1-10 A typical gasification process [27].

The reactions occuring during gasification of biomass are very complex. They consist of pyrolysis, partial oxidation, steam gasification, water-gas shift and methanation (**Table 1-2**). Pyrolysis is a 'pure' thermal reaction to break up the bio-molecules without the participation of hydrogen and water (steam). Partial oxidation is the reaction between biomass materials and oxygen as an 'incomplete/partial combustion' requiring less oxygen than real combustion. Steam gasification uses water as the other reactant to form carbon monoxide, hydrogen and carbon dioxide. Beside these three reactions, there are still two more very important reactions including water-gas shift reaction and methanation. Water-gas shift reaction (WGSR) is a physical-chemical process to form carbon dioxide and hydrogen from a mixture of carbon monoxide and water vapor. Methanation is a reaction between carbon monoxide and hydrogen to generate methane and water. The fundamental reactions and enthalpy of selected biomass gasification reactions are summarized in **Table 1-2** [24].

Table 1-2 Fundamental Reactions and Enthalpy of Selected Cellulose Gasification Reactions [24].

classification	stoichiometry	Enthalpy (kJ/g-mol) at 300 K
pyrolysis	$C_6H_{10}O_5 \rightarrow 5CO + 5H_2 + C$	180
	$C_6H_{10}O_5 \rightarrow 5CO + CH_4 + 3H_2$	300
	$C_6H_{10}O_5 \rightarrow 5CO + CO_2 + 2CH_4 + H_2$	-142
Partial oxidation	$C_6H_{10}O_5 + \frac{1}{2} O_2 \rightarrow 6CO + 5H_2$	71
	$C_6H_{10}O_5 + O_2 \rightarrow 5CO + CO_2 + 5H_2$	-213
	$C_6H_{10}O_5 + 2O_2 \rightarrow 3CO + 3CO_2 + 5H_2$	-778
Steam gasification	$C_6H_{10}O_5 + H_2O \rightarrow 6CO + 6H_2$	310
	$C_6H_{10}O_5 + 3H_2O \rightarrow 4CO + 2CO_2 + 8H_2$	230
	$C_6H_{10}O_5 + 7H_2O \rightarrow 6CO_2 + 12H_2$	64
Water-gas shift	$CO + H_2O \rightarrow CO_2 + H_2$	-41
methanation	$CO + 3H_2 \rightarrow CH_4 + H_2O$	-206

As the reaction severity (temperature, reaction time and heating rate) increases, the gasification and pyrolysis reaction will go through three regimes including primary, secondary and tertiary stages [22]. In other words, altering the residence time and temperature could control the thermochemical process products (solid, gas or liquid). In the primary reaction stage (below 773 K), the vapor products are all very light weight molecules consisting of water, carbon monoxide, carbon dioxide and the oxygenated vapor including cellulose-derived molecules and lignin-derived phenols or analogs. Charcoal is the major solid state product. Those oxygenated molecules, which are also referred to as primary pyrolysis products or bio-oil contain the monomer fragments of lignocellulosic biomass (This will be further discussed in the following **Section 1.3.2**). In the secondary secondary stage (973-1123 K), the primary oxygenated vapor will be converted further to light hydrocarbons, aromatics, oxygenates, olefins, aromatics and gaseous carbon monoxide, carbon dioxide, water and methane in the vapor phase and primary liquids in the liquid phase. Coke is formed in the solid phase. In the tertiary reaction stage (1123-1273 K), poly-nuclear aromatics (PNA), carbon monoxide, carbon dioxide, hydrogen and water are formed. Soot is also produced in the solid phase.

.
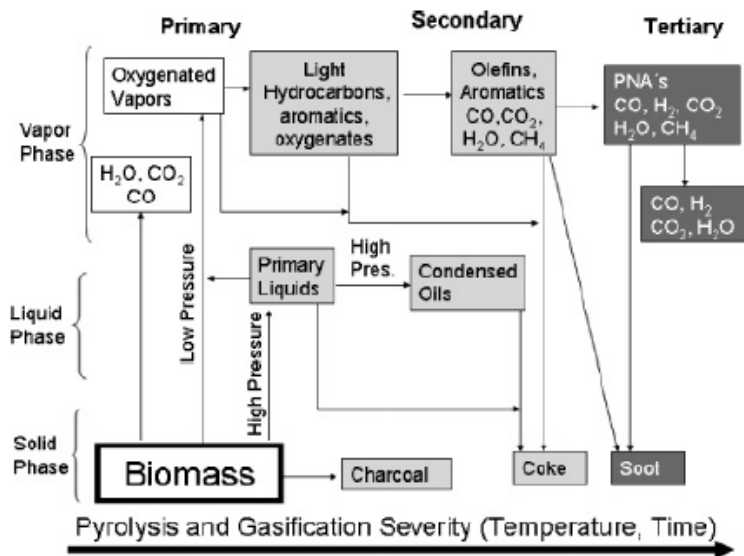
Figure 1-11 Gasification and pyrolysis reaction pathways as a function of severity of reaction conditions [22]

1.3.2 Liquefaction and Pyrolysis

Liquefaction and pyrolysis are two thermochemical treatments for biomass feedstock to produce bio-oil. As shown in **Fig.1-11**, these processes require a short residence time, fast heating rate and moderate temperature, in order to form these desired intermediate monomers of lignocellulosic materials. Normally the reaction conditions (reaction parameters) should be optimized to control the selectivity of products to desired intermediates [28-30]. Generally, pyrolysis oils are water soluble and contains more oxygen than liquefaction oils [7].

1.3.2.1 Pyrolysis

During the pyrolysis process biomass feedstock is heated in the absence of air at 648-798 K from 1×10^2 to 5×10^2 kPa. The pyrolysis includes fast pyrolysis and slow pyrolysis. The advantage of fast pyrolysis, possessing a faster heating rate than slow pyrolysis is the direct production of liquid oils which could be easily stored and transported. Slow pyrolysis is well known for producing charcoal. Fast pyrolysis is widely applied for pyrolysis oil/bio-oil (a dark

brown non-viscous liquid) production with yields up to 80 wt.% on a dry feed [7, 29]. The essential features of a fast pyrolysis are as follows: (a) a finely ground feedstock is desired for good heating and heat transfer, (b) the temperature should be strictly controlled around 773 K, and (c) the produced pyrolysis vapor has to be rapidly cooled to form the bio-oil [29]. A schematic representation of a fast pyrolysis process is shown in **Fig. 1-12**.
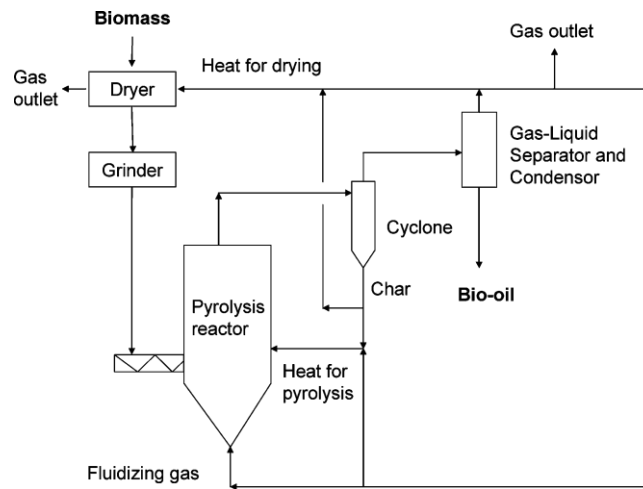
Figure 1-12 Fast pyrolysis reactor system [29].

1.3.2.2. Liquefaction

Liquefaction is a process carried out at 523-723 K under 5×10^3 - 2×10^4 kPa of H_2 (or CO) during which biomass materials together with or without solvent are converted to liquid hydrocarbons (liquefaction oil having a much lower oxygen content than pyrolysis oil) in the presence or absence of a catalyst [31]. At the same time, liquefaction has a higher capital cost than pyrolysis due to the much higher reaction pressure. Depending on the types of solvents, there are three types of liquefactions including hydropyrolysis (no solvent, only hydrogen atmosphere), hydrothermal pyrolysis (in the aqueous phase in the presence of hydrogen) and solvolysis (oil/organic liquid solvents, like creosote oil, methanol, liquefaction oil, et al.).

Regarding the solvents in liquefaction, water is considered as the most attractive one due to the low cost of water and no need to dry the biomass feedstock which has a very high water content (>20 wt.%). The produced liquefaction oil has been recycled as a solvent and shown to promote bio-oil yield. A number of organic solvents including creosote oil, alcohols, ethylene glycol and phenol are used in solvolysis.

Catalysis is also a very crucial factor to improve the efficiency of liquefaction. Three categories of catalysts are widely used in liquefaction including (I) alkali (alkaline ash components in wood, alkaline oxide, carbonates, and bicarbonates); (II) metal salts or oxides (such as formate, iodine, cobalt sulfide, zinc chloride, ferric hydroxide); (III) metal heterogeneous catalysts (such as Ni, Ru, Co, which would facilitate the hydrogenation or hydrogenolysis).

1.3.3 Hydrolysis

Hydrolysis is a reaction in which the carbohydrate sugar polymer are broken into its components by the addition of water. Hydrolysis could be catalyzed by acid or enzyme. The hydrolysis reaction of cellulose may be expressed as eq. (1).

$$(C_6H_{10}O_5)_n + n\ H_2O \xrightarrow{\text{acid or enzyme}} n\ C_6H_{12}O_6 \qquad (1)$$
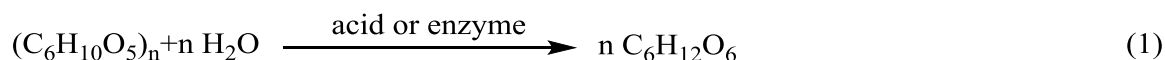
Acid catalysts are one of the most common catalysts used in lignocellulose hydrolysis. The acid catalyzed hydrolysis pathway is described in **Fig. 1-13**. In the presence of acid catalysts, cellulose may be first cleaved to glucose via oligomers. The formed glucose will be further degraded to smaller products. A part of the cellulose which could not be hydrolyzed would form the modified unreactive cellulose. The protonation of glucoside bonds is the first step in C-O-C bond cleavage in cellulose. There are two reaction pathways called A-1 and A-2 [32]. In the A-1 pathway, the proton is added to the C-O-C bond between two glucoses. In contrast, the proton reacts to the cyclic oxygen in A-2 pathway. The intermediate complex formed by proton and oxygen will be further cleaved by the addition of one water molecule (**Fig. 1-14**).
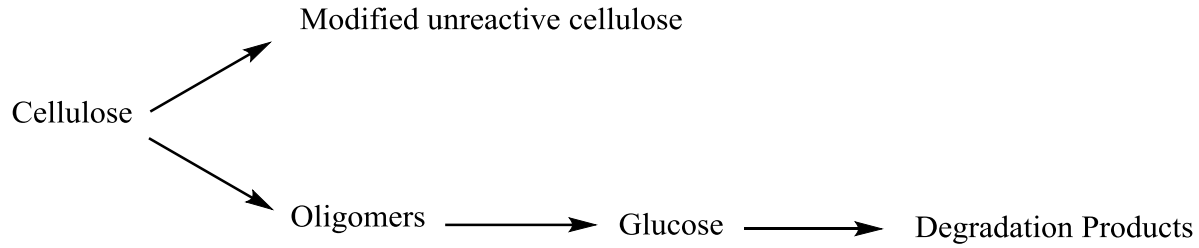
Figure 1-13 Cellulose acid-catalyzed hydrolysis pathways [33].
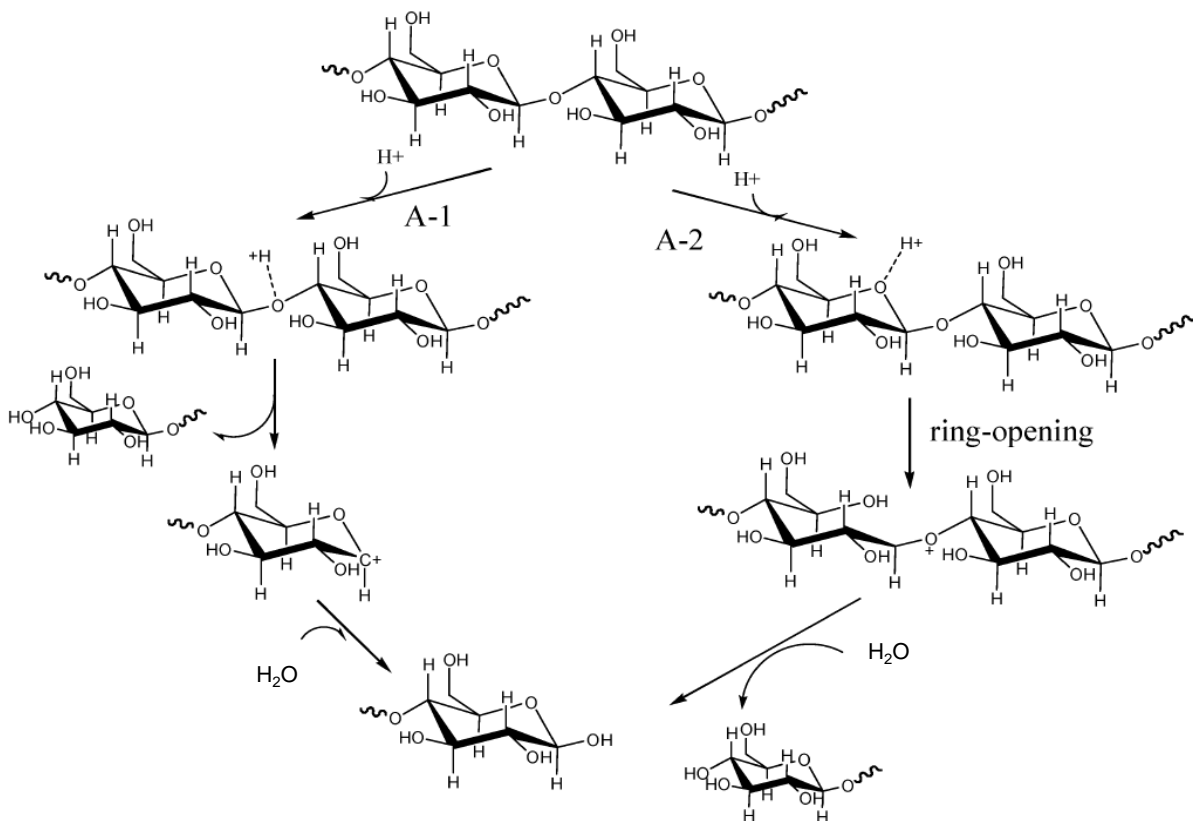
Figure 1-14 Reaction pathways of A-1 and A-2 for acid-catalyzed hydrolysis of cellulose [32].

Hydrolysis of cellulose could be also catalyzed by enzymes (cellulases). There are three major types of enzymatic reactions are catalysis by cellulases. They are (a) endoglucanases or 1,4-β-D-glucan-4-glucanohydrolases, (b) exoglucanases or 1,4-β-D-glucanglucanohydrolases and (c) β-glucosidases or β-glucoside glucohydrolases [34]. Regarding ethanol production from

lignocellulosic material, after the hydrolysis of cellulose in the lignocellulosic materials to fermentable reducing sugars, a fermentation of the sugars to ethanol may be carried out by yeasts or bacteria [35]. The factors that may affect the hydrolysis of cellulose include porosity and fiber crystallinity of cellulose and content of lignin and hemicellulose. The presence of lignin and hemicellulose prevent access of cellulase enzymes to cellulose, thus reducing the efficiency of the hydrolysis. Therefore, removal of lignin and hemicellulose, reduction of cellulose crystallinity, and increase of porosity can significantly improve the hydrolysis [36].

Hemicellulose as an amorphous polymer could be hydrolyzed by acid catalysts at much milder conditions compared with cellulose. It could even be cleaved in hot water (around 483 K) to form acetic acid, which could, in turn, act as an acid catalyst for hydrolysis. The reaction pathway for hydrolysis of hemicellulose is shown in **Fig. 1-15**.

Hemicellulose $\longrightarrow$ Oligomers $\longrightarrow$ Xylose $\longrightarrow$ Degradation Products
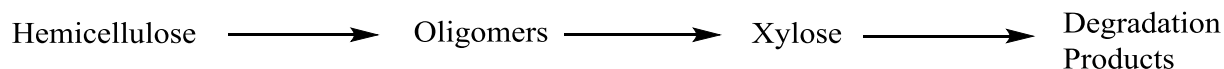
Figure 1-15 Degradation pathway for hemicellulose [33].

1.4 Hydrodeoxygenation

Since the oxygen content of biomass-derived feeds from pyrolysis or liquefaction may approach 50 wt. %, hydrodeoxygenation is considered to be the most effective method for bio-oil upgrading [7]. The low stability of the O-compounds will lead to ready polymerization during fuel combustion [37]. Normally, hydrodeoxygenation of bio-oils will be carried out at 573 to 873 K with high-pressure hydrogen in the presence of heterogeneous catalysts [7]. The hydrogen consumption and severity of the operation required for the highly effective HDO depend on the concentration and type of the O-compounds in the feed [37]. During the hydrodeoxygenation, the phenolic compounds in bio-oils dehydrate to form water and hydrogenate to form saturated C-C bonds in the presence of the catalyst in order to achieve a higher energy content and stability of the fuel.

A two-stage operation is an essential requirement for hydrotreating of bio-oils or black liquor oils [38, 39]. In the first stage, a low temperature hydrogenation/hydrogenolysis (543 K) is carried out to remove O-compounds, which would otherwise readily undergo polymerization or coking. During the first stage, the O-compounds, such as methoxyphenols, biphenols, and ethers are converted to phenols. In the second stage, a catalytic reaction at higher temperature (673 K) may be used for the hydrodeoxygnaton of phenols.

During the hydrodeoxygenation investigations, sulfided Co-Mo/Al$_2$O$_3$ and sulfided Ni-Mo/Al$_2$O$_3$ are frequently used as the catalysts for both stages [7, 37-39]. However, the conventional sulfide-based catalysts incorporate sulfur in the products as a contaminant, deactivate very fast by coke and high water content in the biomass feedstock [40-43]. Lercher group recently reported studies of reductive upgrade of bio-oils in the aqueous phase with a combination of metal and acid catalysts [44-53]. The environmentally benign aqueous phase could facilitate the separation of products, because the hydrocarbons products stay in the organic phase. The hydrodeoxygenation of the model compound, phenol, over a combination of Pd/C and H$_3$PO$_4$/HZSM-5 hydrodeoxygenation has been investigated extensively. A typical reaction pathway is shown in **Fig. 1-16**. Phenol is first hydrogenated to cyclohexanone over Pd/C, which is further hydrogenated to cyclohexanol over Pd/C, which is dehydrated to cyclohexene over acid sites, which is finally hydrogenated to cyclohexane over Pd/C.
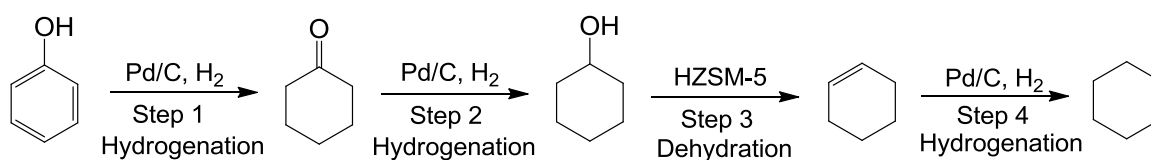
Figure 1-16. Reaction sequence of hydrodeoxygenation of phenol to cyclohexane on metal and acid catalysts using water as solvents [50].

1.5 Scope of this thesis

In this doctoral thesis, the major purpose is to explore the selective cleavage of C-O ether bonds in the lignin fragment molecules over heterogeneous transition metal catalysts under mild conditions in the aqueous phase. Our strategy for converting lignin to fuels is displayed in **Fig.1-17**. The lignin model compounds including benzyl phenyl ether (α-O-4 linkage), 2-phenylethyl phenyl ether (β-O-4 linkage), diphenyl ether (4-O-5 linkage) are selectively cleaved over Ni-based catalysts in the aqueous phase to form cyclohexanol, phenolic compounds and aromatics. The obtained fragment molecule from lignin depolymerization could be further upgraded via hydrodeoxygenation to biofuels.

In the second chapter of this thesis, a novel Ni/SiO_2 catalyzed route to selectively cleave ether bonds of (lignin derived) aromatic ethers (α-O-4 linkage, β-O-4 linkage and 4-O-5 linkage) and to hydrogenate the oxygen containing intermediates at 393K in the presence of 0.6 MPa H_2 in the aqueous phase is systematically studied in order to elucidate the reaction pathways and the fundamental chemistry that leads to the cleavage of C-O bonds in the aryl ethers. Furthermore, the kinetic parameters have been correlated to the bond dissociation energies of the model compounds and reaction pathways to elucidate the reaction mechanism.

In the third chapter, the cleavage the C−O aryl ether bonds of p-substituted H−, CH_3−, and OH− diphenyl ethers (4-O-5 linkage) has been explored over Ni-based catalyst at very mild conditions (393 K, 0.6 MPa). The influence of supports of Ni catalysts (ZrO_2, Al_2O_3 and SiO_2) and the impact of H_2 pressure on the conversion of diphenyl ether have also been explored. The kinetics of all three p-substituted diphenyl ethers were also investigated over Ni/SiO_2 in order to elucidate the influence of substituent groups on reaction pathways. In addition, the kinetic parameters are determined to elucidate the reaction mechanisms.

In the fourth chapter, catalytic pathways for the cleavage of ether bonds in benzyl phenyl ether (BPE, α-O-4 linkage) in the liquid phase (both aqueous and apolar phases) using Ni and zeolite based catalysts are systematically investigated. The role of gas atmosphere (N_2, H_2), gas pressure (0-4 MPa), metallic site (Ni/SiO_2), acidic site (HZSM-5) and the cooperation of metallic site and

acidic site (Ni/HZSM-5) have been explored via kinetics. The influence of solvents (water and undecane) on the reaction mechanism and reaction pathway is also discussed and explored by DFT calculations.

In the fifth chapter, impacts of water, methanol, and hexadecane solvents on the individual steps of phenol hydrodeoxygenation are investigated over Pd/C and HZSM-5 catalyst components at 473 K in the presence of H_2. Hydrodeoxygenation of phenol to cyclohexane includes four individual steps including phenol hydrogenation to cyclohexanone on Pd/C, cyclohexanone hydrogenation to cyclohexanol on Pd/C, cyclohexanol dehydration to cyclohexene on HZSM-5, and cyclohexene hydrogenation to cyclohexane on Pd/C. The TOFs and apparent activation energies of all individual steps in various solvents are measured. The kinetic parameters and physiochemical properties of solvents are combined to elucidate how interactions between solvent-catalyst, solvent-reactant and catalyst-reactant would affect phenol hydrodeoxygenation. In situ liquid-phase IR spectroscopy (reactor IR) is used to determine the reaction order of reactants in the aqueous phase and verify the proposed reaction pathway of phenol hydrodeoxygenation.

The final chapter concludes the whole body of research on the selective C-O ether bond cleavage of lignin model compounds and the solvent impact on phenol hydrodeoxygenation.
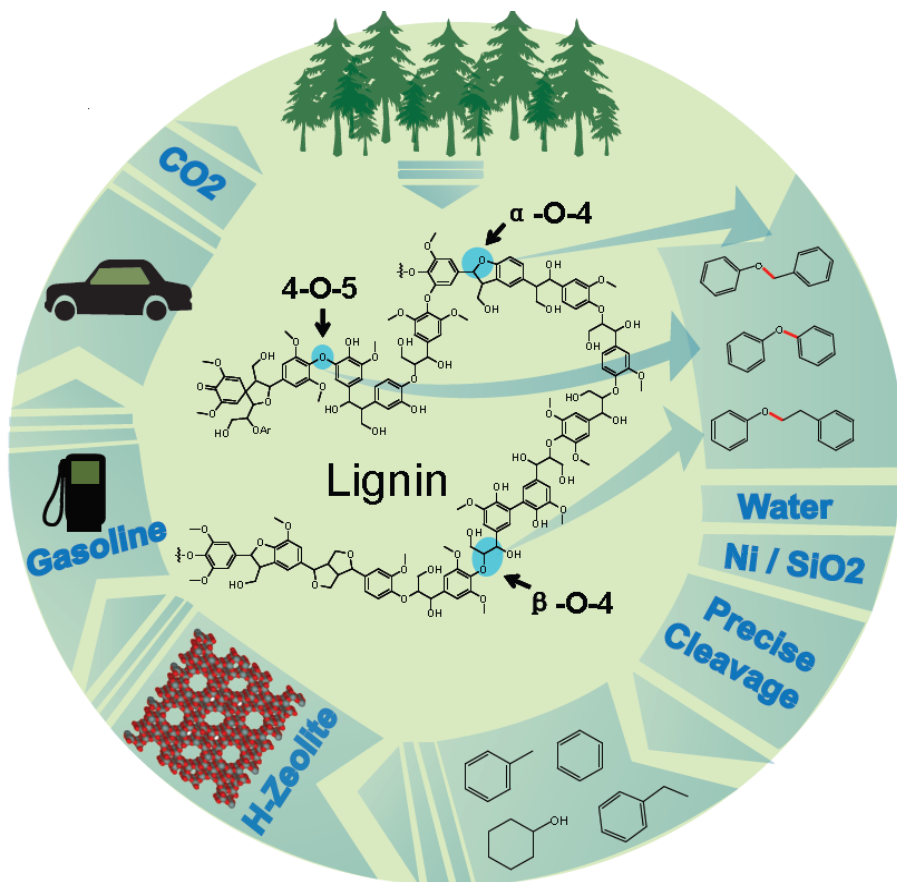
Figure 1-17 Our strategy to convert lignin to biofuel.

1.6 References

[1]   U.S.Energy Information Administration, Annual Energy Outlook 2013 With Projections to 2040, 2013.

[2]   J.S. Pandey, R. Kumar, S. Devotta, Atmos. Environ., 39 (2005) 6868.

[3]   H. Kan, C.-M. Wong, N. Vichit-Vadakan, Z. Qian, P.P. Teams, Environ. Res., 110 (2010) 258.

[4]   European Parliamennt and the Council, Directive 2009/28/EC, 2009.

[5]   Shell energy scenarios to 2050, 2008. http://www.shell.com/global/future-energy/scenarios/2050.html

[6]   The Outlook for Energy: A View to 2040, Exxonmobil, 2013.
        http://corporate.exxonmobil.com/en/energy/energy-outlook

[7]   G.W. Huber, S. Iborra, A. Corma, Chem. Rev., 106 (2006) 4044.

[8]   D. Klemm, B. Heublein, H.P. Fink, A. Bohn, Angew. Chem. Int. Ed. Engl., 44 (2005) 3358.

[9]   P. Zugenmaier, Prog. Polym. Sci., 26 (2001) 1341.

[10]   H.V. Scheller, P. Ulvskov, Annu. Rev. Plant. Biol., 61 (2010) 263.

[11]   F.M. Girio, C. Fonseca, F. Carvalheiro, L.C. Duarte, S. Marques, R. Bogel-Lukasik, Bioresour. Technol., 101 (2010) 4775.

[12]   http://en.wikipedia.org/wiki/Hemicellulose.

[13]   F.S. Chakar, A.J. Ragauskas, Ind. Corp. Prod., 20 (2004) 131.

[14]   W. Boerjan, J. Ralph, M. Baucher, Annu. Rev. Plant. Biol., 54 (2003) 519.

[15]   J. Zakzeski, P.C.A. Bruijnincx, A.L. Jongerius, B.M. Weckhuysen, Chem. Rev., 110 (2010) 3552.

[16]   N.G. Lewis, Curr. Opin. Plant Biol., 2 (1999) 153.

[17]   K.V. Sarkanen, C.H. Ludwig, Lignin, Occurrence, Formation, Structure and Reactions, Wiley/Interscience, New York, 1971.

[18]   K. Freudenberg, A.C. Neish, Constitution and biosynthesis of lignin, Springer-Verlag, New York, 1968.

[19]   D.V. Evtuguin, C.P. Neto, J. Rocha, J.D.P. de Jesus, Appl. Catal. A-Gen., 167 (1998) 123.

[20]   E.A. Capanema, M.Y. Balakshin, J.F. Kadla, J. Agric. Food. Chem., 52 (2004) 1850.

[21]   E.A. Capanema, M.Y. Balakshin, J.F. Kadla, J. Agric. Food. Chem., 53 (2005) 9639.

[22]   T.A. Milne, N. Abatzoglou, R.J. Evans, Biomass Gasifier "tars": Their Nature, Formation, and Conversion, National Renewable Energy Laboratory, 1999.

[23]   H.H. Lowry, Chemistry of coal utilization, Wiley, 1963.

[24]   D.L. Klass, Biomass for Renewable Energy, Fuels, and Chemicals, Elsevier Science, 1998.

[25]   R.C. Brown, C. Stevens, Thermochemical Processing of Biomass: Conversion into Fuels, Chemicals and Power, Wiley, 2011.

[26]   C.J. Cleveland, R.U. Ayres, Encyclopedia of Energy: Ec-Ge, Elsevier Academic Press, 2004.

[27]   G. Ertl, H. Knözinger, F. Schüth, J. Weitkamp, Handbook of Heterogeneous Catalysis, 8 Volumes, Wiley, 2008.

[28]   D. Mohan, C.U. Pittman, Jr., P.H. Steele, Energ. Fuel., 20 (2006) 848.

[29]   A.V. Bridgwater, G.V.C. Peacocke, Renew. Sust. Energ. Rev., 4 (2000) 1.

[30]   D.C. Elliott, D. Beckman, A.V. Bridgwater, J.P. Diebold, S.B. Gevert, Y. Solantausta, Energ. Fuel., 5 (1991) 399.

[31]   J.M. Moffatt, R.P. Overend, Biomass, 7 (1985) 99.

[32]   L.T. Fan, M.M. Gharpuray, Y.H. Lee, Cellulose Hydrolysis, Springer London, Limited, 2011.

[33]   W.S.L. Mok, M.J. Antal, G. Varhegyi, Ind. Eng. Chem. Res., 31 (1992) 94.

[34]   L.R. Lynd, P.J. Weimer, W.H. van Zyl, I.S. Pretorius, Microbiol. Mol. Biol. Rev., 66 (2002) 506.

[35]   Y. Sun, J.Y. Cheng, Bioresour. Technol., 83 (2002) 1.

[36]   J.D. McMillan, Pretreatment of Lignocellulosic Biomass, in: M.E. Himmel, J.O. Baker, R.P. Overend (Eds.) Enzymatic Conversion of Biomass for Fuels Production, 1994, pp. 292-324.

[37]   E. Furimsky, Appl. Catal. A-Gen., 199 (2000) 147.

[38]   D.C. Elliott, E.G. Baker, J. Piskorz, D.S. Scott, Y. Solantausta, Energ. Fuel., 2 (1988) 234.

[39]   D.C. Elliott, A. Oasmaa, Energ. Fuel., 5 (1991) 102.

[40]   E. Laurent, B. Delmon, J. Catal., 146 (1994) 281.

[41]   E. Laurent, B. Delmon, Appl. Catal. A-Gen., 109 (1994) 77.

[42]   E. Furimsky, F.E. Massoth, Catal. Today, 52 (1999) 381.

[43]   T.R. Viljava, R.S. Komulainen, A.O.I. Krause, Catal. Today, 60 (2000) 83.

[44]   C. Zhao, J.Y. He, A.A. Lemonidou, X.B. Li, J.A. Lercher, J. Catal., 280 (2011) 8.

[45]   C. Zhao, S. Kasakov, J.Y. He, J.A. Lercher, J. Catal., 296 (2012) 12.

[46]   C. Zhao, J.A. Lercher, Angew. Chem. Int. Ed. Engl., 51 (2012) 5935.

[47]   C. Zhao, Y. Yu, A. Jentys, J.A. Lercher, Appl. Catal.,B, 132 (2013) 282.

[48]   C. Zhao, Y. Kou, A.A. Lemonidou, X. Li, J.A. Lercher, Angew. Chem. Int. Ed. Engl., 48 (2009) 3987.

[49]   C. Zhao, Y. Kou, A.A. Lemonidou, X. Li, J.A. Lercher, Chem. Commun., 46 (2010) 412.

[50]   J. He, C. Zhao, J.A. Lercher, J. Catal., 309 (2014) 362.

[51]   J. He, L. Lu, C. Zhao, D. Mei, J.A. Lercher, J. Catal., 311 (2014) 41.

[52]   J. He, C. Zhao, D. Mei, J.A. Lercher, J. Catal., 309 (2014) 280.

[53]   J. He, C. Zhao, J.A. Lercher, J. Am. Chem. Soc., 134 (2012) 20768.

Chapter 2

Ni-Catalyzed Cleavage of Aryl Ethers in the Aqueous Phase

A novel Ni/SiO$_2$ catalyzed route to selectively cleave ether bonds of (lignin derived) aromatic ethers and to hydrogenate the oxygen containing intermediates at 393K in the presence of 0.6 MPa H$_2$ in the aqueous phase is reported. The C-O bonds of α-O-4 and β-O-4 linkages are cleaved by hydrogenolysis on Ni, while the C-O bond of 4-O-5 is cleaved via parallel hydrogenolysis and hydrolysis. The difference is attributed to the fact that the C$_{aliphatic}$-OH fragments generated from hydrolysis of α-O-4 and β-O-4 linkages can be further hydrogenolysed, while phenol (hydrolysis from 4-O-5 linkage) is hydrogenated to produce cyclohexanone and cyclohexanol under conditions investigated. The apparent energies of activations E$_a$ (α-O-4) < E$_a$ (β-O-4) < E$_a$ (4-O-5) vary proportionally with the bond dissociation energies. In the conversion of β-O-4 and 4-O-5 ether bonds, the C-O bond cleavage is the rate-determining step with the reactants competing with hydrogen for active sites, leading to a maximum reaction rate as a function of the H$_2$ pressure. For the very fast rate of C-O bond cleavage of the α-O-4 linkage, increasing H$_2$ pressures increase the rate-determining product desorption under conditions tested.

2.1 Introduction

Lignin is a three-dimensional, highly branched, polyphenolic substance containing an array of hydroxy- and methoxy- substituted phenylpropane units [1]. As lignin makes up 20-30 wt.% of lignocellulose, and especially contains a very high fraction of its energy content, i.e., ca. 40% in the total lignocellulosic biomass [2], its conversion to energy carriers has recently received much attention. However, due to the high strength and stability of the aryl ether bonds (**Fig. 2-1**), it is challenging to selectively depolymerize lignin into small molecules [3].

Recently, a series of interesting molecular catalysts including Ru [4], V [5], and Ni [6] complexes have shown high selectivity in cleaving C-O bonds of dimeric lignin model compounds for producing aromatic molecules in organic solvents (CD_3CN, toluene, and *m*-xylene) under rather mild conditions (353-408 K, 0.1 MPa H_2). In principle, molecular catalysts are logical choices for depolymerizing lignin, as their mobility and flexibility appears to allow reaching individual ether bonds without high steric limitation. These reported molecular catalysts, however, are sensitive to large concentrations of water, which is costly to separate from raw biomass.

More robust solid catalysts would be, therefore, better choices for the aqueous phase conversion of lignin. The strategies explored so far using heterogeneous catalysts such as $Ni/K_2CO_3/ZrO_2$, however, require high temperatures and pressures (513-673 K and 25-31 MPa) to cleave the aromatic ethers or lignin dissolved in the aqueous phase [7]. The achievable yields of the cleaved products were limited due to the recombination of products via free radical reactions even when a large excess of H_2 was present. Thus, the higher reactivity of the potential products necessitates the reactions to be carried out under very mild conditions. Ni supported on zeolite HZSM-5 showed appreciable rates of conversion and high stability for hydrodeoxygenation of ethers under moderate conditions (523 K and 5 MPa H_2) [8]. Similarly, it was shown for Pd based catalysts that combining the proximity of acid and metal sites led to high selectivity for hydrodeoxygenation of substituted phenols [9]. Combining this insight with the finding that Ni molecular catalysts can hydrogenolyse aromatic ether bonds [6], we chose to explore systematically the properties of supported Ni in the absence of adjacent acid sites on the solid support under much milder conditions.
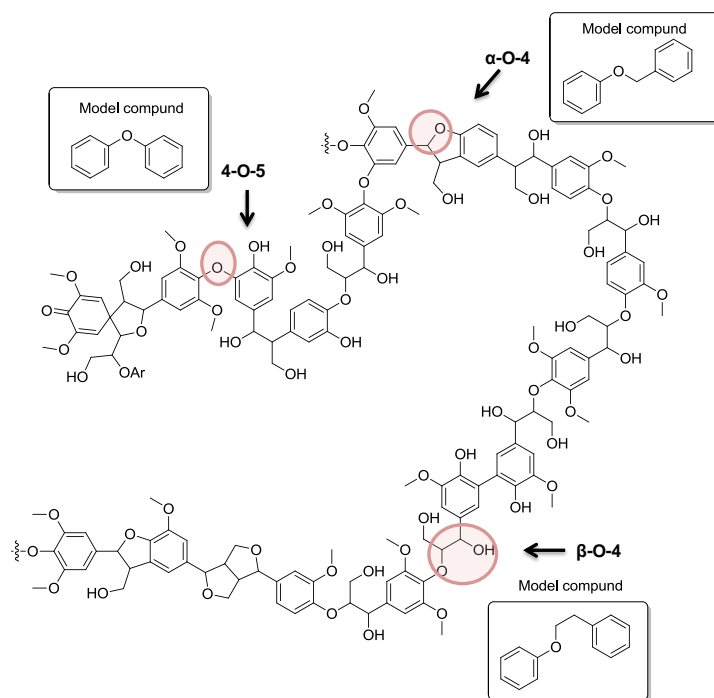
Figure 2-1. The fragment structure of hardwood lignin.

A representative fragment structure of hardwood lignin is depicted at **Fig. 2-1**. It illustrates that the β-O-4, α-O-4 and 4-O-5 linkages are three of the most frequent C-O bonds, contributing to 45-62% (the most abundant), 3-12%, and 4-9% of the ether bonds in hardwood lignin, respectively, and would, thus, be expected to determine primary products if large clusters of lignin are depolymerized [10]. 2-Phenyletheyl ether, benzyl phenyl ether, and diphenyl ether have been selected as the β-O-4, α-O-4, and 4-O-5 model compounds for exploring the reaction mechanism of C-O bond cleavage in the aqueous phase, as our previous experiments have shown that more complex substitutions hardly influence the principal chemistry [11]. Here, we show that supported Ni catalysts are able to selectively and quantitatively cleave C-O bonds in aromatic ethers such as benzyl phenyl ether (α-O-4 linkage), 2-phenylethyl ether (β-O-4 linkage), and diphenyl ether (4-O-5 linkage) to form smaller aromatic molecules, cycloalkanes and cyclohexanol under very mild conditions (393 K and 0.6 MPa H_2) in water.

2.2 Experimental section

2.2.1 Chemical

The chemicals were purchased from commercial suppliers and used as provided: benzyl phenyl ether (TCI, > 98% GC assay), 2-phenylethyl phenyl ether (Frinton Laboratories, > 99 % GC assay), diphenyl ether (Sigma-Aldrich, > 99 % GC assay), cyclohexyl phenyl ether (Sigma-Aldrich, > 95 % GC assay), benzene (Fluka, > 99.5 % GC assay), toluene (Sigma-Aldrich, > 99.5 % GC assay), ethyl benzene (Fluka, > 99 % GC assay), phenol (Sigma-Aldrich, > 99 % GC assay), ethyl acetate (Sigma-Aldrich, > 99.5 % GC assay), Ni(II) nitrate hexahydrate (Sigma-Aldrich, ≥98.5%), urea (Sigma-Aldrich, BioReagent), HNO_3 (Sigma-Aldrich, > 65 %), 5 wt.% Pd/C (Sigma-Aldrich), SiO_2 (Aerosil 200, Evonik-Degussa), H_2 (Air Liquide, >99.999%), N_2 (Air Liquide, > 99,999 %).

2.2.2 Ni/SiO₂ catalyst preparation using deposition precipitation (DP) method

First an aqueous solution (250 ml) containing $Ni(NO_3)_2{\cdot}6H_2O$ (0.14 M, 10.2 g) was divided in two parts. One (50 ml) was added with urea (0.42 M, 6.3 g), the other (200 ml) together with SiO_2 (1.9 g) and HNO_3 (65%, 0.02 M, 0.32 ml) were put into a flask thermostated at 353 K. The first part with urea was slowly added into the flask, and the suspension was rapidly heated to 363 K. After reaching 90 ℃ the suspension was magnetically stirring for 10 h. After that, the suspension was cooled to 25 ℃ and the solids were filtered and washed three times with distilled water (5/1= water/slurry). Finally, the sample was dried at 363 K for 24 h, calcined in flow air (100 ml min^{-1}) at 673, 773, 873, 973 or 1073 K, and reduced in flow H_2 (100 ml min^{-1}) at 733 K.

2.2.3 Catalytic test

The detailed reaction conditions are described in the figures as footnotes. In a typical experiment, the catalytic reactions were carried out in a slurry autoclave reactor loaded with Ni/SiO₂ using water as solvent at 393 K in the presence of 0.6 MPa H_2 (STP). The lignin model compound (0.010 mol), 57 wt.% Ni/SiO₂ (0.30 g, 2.91×10^{-3} mol Ni for β-O-4 and 4-O-5 linkages, 0.030 g, 2.91×10^{-4} mol Ni for α-O-4), H_2O (80 ml) were charged into a Parr reactor (Series 4848,

300 ml). After the reactor was flushed with H_2 three times, the autoclave was charged with 6 bar H_2 and the reaction were conducted at 393 K with a stirring speed of 700 rpm. Because it is a two-phase reaction, the kinetics data are collected at time durations. After reaction, the reactor was quenched by ice to ambient temperature, and the organic products were extracted by ethyl acetate and analyzed by gas chromatography (GC) and GC-mass spectroscopy (GC-MS) analysis on Shimadzu 2010 gas chromatograph with flame ionization detector and a Shimadzu QP 2010S GC-MS, both of them equipped with a HP-5 capillary column (30 m $\times$ 250 μm). Internal standard 2-isopropylphenol was used to calibrate the liquid product concentrations and carbon balances. The carbon balances for all reported experiments were better than 95±3%. The calculations of conversion and selectivity were on carbon mole basis. Conversion = (the amount of raw-material change during reaction/total amount of starting materials) $\times$ 100%. Selectivity = (C atoms in each product/total C atoms in the products) $\times$ 100%.

2.2.4 Catalyst characterization.

Atomic absorption spectroscopy (AAS)

A UNICAM 939 AA-Spectrometer was used to determine the concentration of nickel in Ni/SiO_2. Before measurement, a mixture of 0.5 ml of 48 wt.% hydrofluoric acid and 0.1 ml of nitro-hydrochloric acid was used to dissolve 20-40 mg of the sample at 383 K (the boiling point of the mixture).

Nuclear magnetic resonance (NMR)

The measurements of ^{1}H NMR, ^{13}C NMR and COSY NMR were performed on a JEOL 400 MHz spectrometer. $CDCl_3$ was used as the solvent for measuring.

BET surface area

The surface areas and pore diameters were determined from N_2 adsorption measurements carried out at 77 K on a PMI automated BET sorptometer. The samples were first outgassed at 523 K for 20 h before measurement.

H_2 chemisorption

The catalysts were activated at 733 K for 3 h in H_2 and then 1 h in vacuum and then cooled to 313 K. An H_2 adsorption (chemisorption and physisorption) was then taken in a pressure range from 1 kPa to 40 kPa. Then the physisorbed H_2 was removed by outgassing the sample at the same temperature for 1 h and another isotherm (physisorption) was measured. The concentration of chemisorbed hydrogen on the metal was determined by extrapolating the differential isotherm to zero H_2 pressure, and this value was used to calculate the Ni dispersions.

Transmission electron microscopy (TEM)

The images were measured on a JEM-2010 Jeol transmission electron microscope operating at 120 KV. Before measurement, the catalyst were firstly ground, and then suspended in ethanol and dispersed by ultrasonic treatment. The obtained dispersion was transferred to a copper grid-supported carbon film. Transmission electron micrographs were recorded with a magnification of 200000. The average cluster size was calculated by counting 300 metal particles.

Scanning electron microscopy (SEM)

The images were recorded on a REM JEOL 5900 LV microscopy operating at 25 kV. The power samples were used without any pretreatment.

2.3 Results and discussion

2.3.1 Catalyst synthesis strategy and catalytic measurements

We synthesized the supported Ni/SiO_2 catalysts using the deposition precipitation (DP) method with urea as hydrolysis agent. The synthesized Ni/SiO_2 catalysts had Ni loadings of ca. 40 wt. %. To alter the Ni particle size, the calcination temperatures were varied from 673 to 1073 K, which led to gradual growth of Ni particles from 4.5 to 7.9 nm (determined by transmission electron microscopy shown in **Fig. 2-2A**) due to Ni sintering at higher treatment temperatures. The hydrogenolysis of 2-phenylethyl phenyl ether (β-O-4) was conducted over these five Ni/SiO_2 catalysts at 393 K with 0.6 MPa H_2 for 90 min. in the aqueous phase. The results consistently showed that almost equal concentrations of C_6 (phenol, cyclohexanone, and cyclohexanol) and C_8 compounds (ethyl benzene) were formed under selected conditions (**Table 2-1**). The C-O bond cleavage rates normalized to accessible Ni atoms (TOF) first increased with the Ni particle size from 4.5, 4.7, 5.4, to 5.9 nm, in the sequence 7, 12, 17, to 26 h^{-1}, respectively, then dropped to 20 h^{-1} with a further increase in particle size to 8 nm (**Fig. 2-2B**). Because of the best compromise between the optimum catalytic stability and activity, we have selected a catalyst with larger particles for the in-depth study. The Ni/SiO_2 catalyst (Ni loading: 57 wt. %) had a BET surface area of 140 $m^2 \cdot g^{-1}$ with a pore volume of 0.1826 $cm^3 \cdot g^{-1}$ and a particle size of ca. 3 μm determined from SEM. The supported Ni particles had an average particle diameter of 8.0 ± 1.8 nm determined from TEM, and the atomic fraction of Ni available for catalysis was 5% measured by H_2 chemisorption (see appendix 2.6).

Table 2-1. Conversion of 2-phenylethyl phenyl ether (β-O-4) using Ni/SiO$_2$ catalysts in water. [a]

Calc. temp. (K)	Ni loading (wt.%)	d_{Ni} (nm) [b]	TOF (h^{-1}) [c]	Conv. (%)	Selectivity (%)			
					Ethyl-benzene	Cyclo-hexanol	Cyclo-hexanone	Phenol
673	42	4.5	7	5.6	51	18	4.1	27
773	41	4.7	12	12	55	25	2.3	18
873	42	5.4	17	18	50	29	2.1	19
973	46	5.9	26	21	56	31	2.0	11
1073	42	7.9	20	8.1	52	19	3.1	26

[a] Conditions: β-O-4 (1.98 g), Ni/SiO$_2$ (0.30 g), H$_2$O (80 ml), 393 K, 0.6 MPa H$_2$, 90 min, stirring at 700 rpm. [b] The Ni particle sizes are determined by TEM. [c] The TOF is normalized on the accessible Ni atoms on the surface, and the fractions of accessible Ni atoms are measured by H$_2$-chemisorption, to be 0.050, 0.057 0.051, 0.040, and 0.021 for the Ni/SiO$_2$ samples calcined at increasing temperatures, respectively. Reaction conditions are chosen to allow determining the rate below conversion of 20 %.
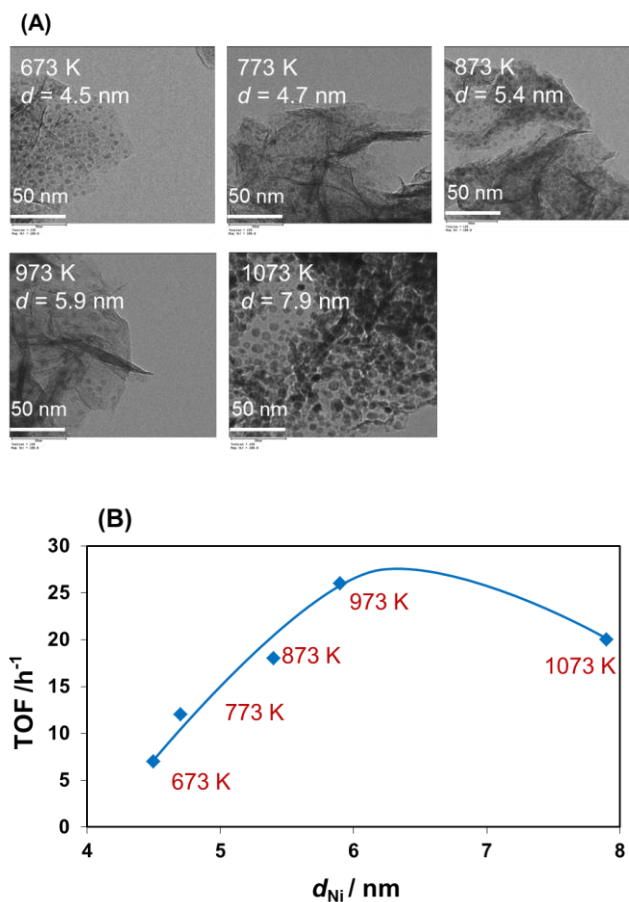
Figure 2-2. (A) TEM images of Ni/SiO$_2$ catalysts prepared by DP method at different calcination temperatures. (B) The Ni particle size versus TOF for C-O bond cleavage of 2-phenylethyl phenyl ether (β-O-4) over Ni/SiO$_2$ in water at 393 K under 0.6 MPa H$_2$.

2.3.2 Kinetics of 2-phenylethyl phenyl ether (β-O-4) conversion

Fig. 2-3a shows the product distribution for 2-phenylethyl ether (β-O-4) conversion as a function of time at 393 K in the presence of 0.6 MPa H$_2$ (STP). Cyclohexanol and ethyl benzene were the major products at reaction time t = 0, both attaining 50% selectivity during the conversion. Phenol was hardly detected, because it was completely hydrogenated to cyclohexanol,

Figure 2-3. (a) Product distributions for conversion of 2-phenylethyl phenyl ether (β-O-4) over Ni/SiO$_2$ as a function of time. Reaction conditions: 2-phenylethyl phenyl ether (β-O-4) (1.98 g, 0.010 mol), 57 wt.% Ni/SiO$_2$ (0.30 g, 2.91×10^{-3} mol Ni), H$_2$O (80 ml), 393 K, 0.6 MPa H$_2$, stirring at 700 rpm. **(b)** Reaction pathway for the cleavage of 2-phenylethyl phenyl ether (the β-O-4 bond in ether) over Ni/SiO$_2$ in the aqueous phase.

While ethyl benzene remained nearly unconverted over Ni/SiO$_2$ with the selectivity to ethyl cyclohexane being lower than 2%. The selectivity to hydrogenated single aromatic-ring products ((2-(cyclohexyloxy)ethyl)benzene and (2-cyclohexylethoxy)benzene) was below 2% independent of the conversion. The C-O-C bond was selectively cleaved at the position of the aliphatic carbon, producing phenol and ethyl benzene (**Fig. 2-3b**). The selectivities to benzene and 2-phenylethanol were lower than 1% even after 600 min. This indicates a preferred interaction of the aliphatic carbon C-O bond in 2-phenylethyl ether (β-O-4) on the Ni surface. In summary, hydrogenolysis is the dominant reaction pathway for cleaving benzyl phenyl ether (β-O-4) with Ni/SiO$_2$ in the aqueous phase, producing ethyl benzene and phenol as primary products (**Fig. 2-3b**).

This result also highlights the importance of the phenol hydroxyl group for the adsorption on Ni/SiO$_2$ as well as the different solubility of phenol (8.3g/100ml H$_2$O at 293 K) and ethyl benzene (0.018g/100 ml H$_2$O at 293 K) in hot water. Separate experiments showed that the rate of phenol hydrogenation over Ni/SiO$_2$ (130 mol·mol$_{Ni (surf)}^{-1}$·h^{-1}) was two orders of magnitude higher than that of ethyl benzene (0.8 mol·mol$_{Ni (surf)}^{-1}$·h^{-1}) in water (**Table 2-2**). In non-polar hexadecane, the rate of phenol hydrogenation (87 mol·mol$_{Ni (surf)}^{-1}$·h^{-1}) was lower than that in water (130 mol·mol$_{Ni (surf)}^{-1}$·h^{-1}) at 393 K due to differences in the solubility of reactant. The ethyl

benzene hydrogenation rate in hexadecane was still lower (13 mol·mol$_{Ni (surf)}^{-1}$·h^{-1}) than that of phenol (87 mol·mol$_{Ni (surf)}^{-1}$·h^{-1}), indicating that the capability of phenol hydroxyl group adsorption on Ni/SiO$_2$ plays a more significant role than the solvent. When phenol and ethyl benzene were added as co-reactants in water, ethyl benzene was unconverted, but phenol achieved a high hydrogenation rate with a TOF of 173 mol·mol$_{Ni (surf)}^{-1}$·h^{-1}. These results show that phenol is highly reactive, whereas ethyl benzene does hardly react on Ni/SiO$_2$ at the selected conditions.

Table 2-2. Hydrogenation of aromatic compounds on Ni/SiO$_2$ in aqueous-phase at 393 K.[a]

Entry	Reactant	Solvent	Catalyst amount (g)	Conv. (%)	TOF (h^{-1})
1	Phenol	Water	0.03	15	130
2	Phenol + Ethylbenzene	Water	0.03	20 0	173 0
3	Phenol	Hexadecane	0.03	10	87
4	Ethylbenzene	Hexadecane	0.3	16	13
5	Benzene	Water	0.3	3.4	2.9
6	Toluene	Water	0.3	2.1	1.8
7	Ethylbenzene	Water	0.3	1.0	0.8

[a] Reaction conditions: reactant (0.010 mol), H$_2$O (80 ml), 0.6 MPa H$_2$, 50 min, stirring at 700 rpm.

2.3.3 Kinetics of benzyl phenyl ether (α-O-4) conversion

The reaction of benzyl phenyl ether (α-O-4) on Ni/SiO$_2$ at 393 K with 0.6 MPa H$_2$ (**Fig. 2-4a**) showed a very high reaction rate, even in the presence of only a tenth of the catalyst used for 2-phenylethyl ether (β-O-4) conversion. The initial TOF for the C-O cleavage (1017 mol·mol$_{Ni (surf)}^{-1}$·h^{-1}) was much higher than that for the β-O-4 bond (13 mol·mol$_{Ni (surf)}^{-1}$·h^{-1}) (**Table 2-4**). The results agree well with the reports that the α-O-4 bond is thermally very unstable [12]. The primary products were toluene and phenol attaining nearly 50% selectivities each at t = 0, produced again via the direct hydrogenolysis of the aliphatic C-O bond of benzyl phenyl ether.

The phenol hydrogenation rate (130 mol·mol$_{Ni (surf)}^{-1}$·h^{-1}) was much higher than that of toluene (1.8 mol·mol$_{Ni (surf)}^{-1}$·h^{-1}) (**Table 2-2**). The very low concentration of catalysts, however, was sufficient to effectively catalyze the ether hydrogenolysis, but not the hydrogenation of the phenol aromatic ring. If the catalyst concentration was increased to that used for the β-O-4 conversion (0.30 g), 46% selectivity to toluene and 54% selectivity to cyclohexanol at 93% conversion was observed within 50 min. In summary, the reaction pathway for benzyl phenyl ether (α-O-4) conversion using Ni/SiO$_2$ in the aqueous phase is dominated by the hydrogenolysis of benzyl phenyl ether to toluene and phenol, followed by a small extent of hydrogenation of phenol to cyclohexanone and cyclohexanol (**Fig. 2-4b**).
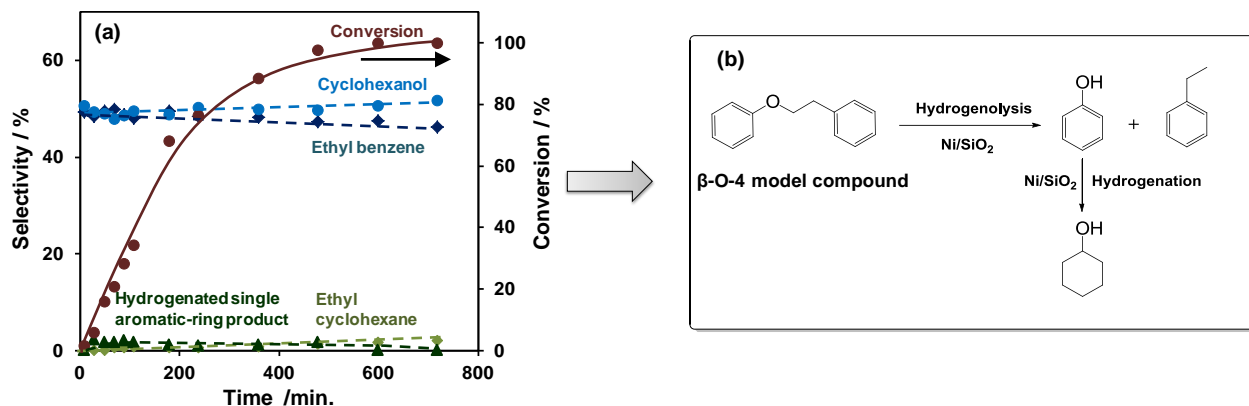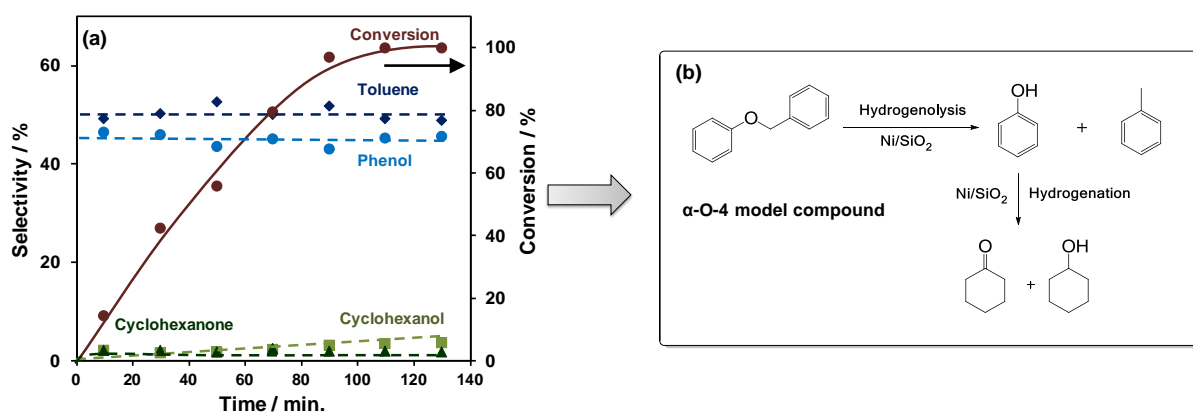

Figure 2-4. (**a**) Product distributions for conversion of benzyl phenyl ether (α-O-4) over Ni/SiO$_2$ as a function of time. Reaction conditions: Benzyl phenyl ether (α-O-4) (1.84 g, 0.010 mol), 57 wt.% Ni/SiO$_2$ (0.030 g, 2.91×10^{-4} mol Ni), H$_2$O (80 ml), 393 K , 0.6 MPa H$_2$, stirring at 700 rpm. (**b**) Reaction pathway for the cleavage of benzyl phenyl ether (the model for α-O-4 bond linkage in lignin) over Ni/SiO$_2$ in the aqueous phase.

2.3.4 Kinetics of diphenyl ether (4-O-5) conversion

The conversion of di-aryl ether was reported to be challenging, requiring severe conditions such as hydrolysis in supercritical water to cleave the C-O bond [8]. It could be also cleaved with Raney Ni in boiling methanol, but the achieved rate was extremely low (0.01 mol·mol$_{Ni}^{-1}$·h^{-1}) [13]. 4-O-5 was reacted under the same conditions reported earlier for β-O-4 (**Fig. 2-5a**). The major

products were cyclohexanol (selectivity: 25%), benzene (selectivity: 10%), and cyclohexyl phenyl ether (selectivity: 65%) at t = 0, suggesting a different reaction mechanism from that of α-O-4 and β-O-4 in which hydrogenolysis and hydrogenation were sequential. As the reaction proceeded, the yields to cyclohexanol and benzene increased steadily, and the yield to cyclohexyl phenyl ether first increased to a maximum of 13% and then decreased to 0. Cyclohexanol was formed with a high rate from phenol (130 mol·mol$_{Ni (surf)}^{-1}$·h^{-1}), much faster than the rate of benzene hydrogenation (2.9 mol·mol$_{Ni (surf)}^{-1}$·h^{-1}) (**Table 2-2**). The increasing concentration of phenol and benzene did not result from the hydrogenolysis of cyclohexyl phenyl ether. Separate reaction with cyclohexyl phenyl ether over Ni/SiO$_2$ showed that the C-O bond cleavage rate was relatively low (0.8 mol·mol$_{Ni(surf)}^{-1}$·h^{-1}), while dicyclohexyl ether did not react under the conditions used (**Table 2-3**). The rate of diphenyl ether cleavage (26 mol·mol$_{Ni(surf)}^{-1}$·h^{-1}) was much higher and we conclude that the hydrogenation-hydrogenolysis route is only the minor pathway (**Fig. 2-5b**).
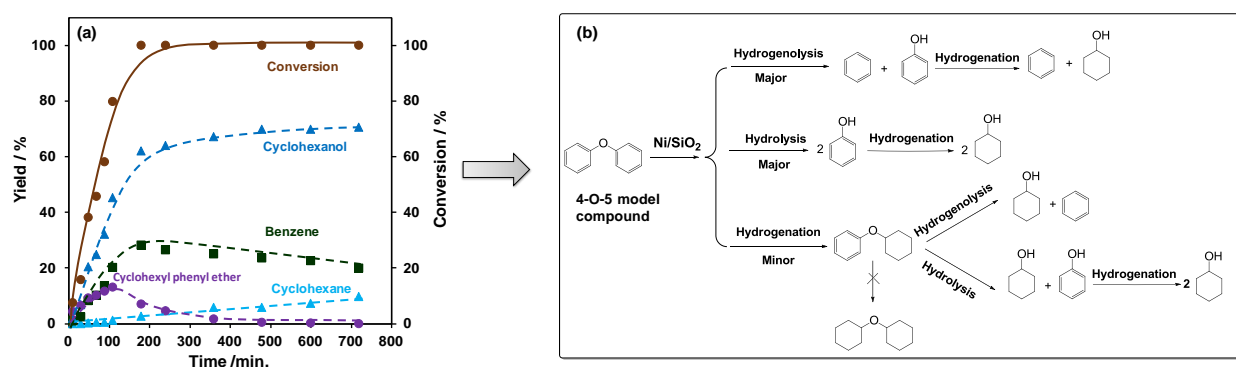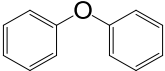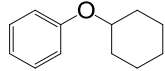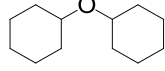
Figure 2-5. (a) Product distributions for conversion of diphenyl ether (4-O-5) over Ni/SiO$_2$ as a function of time. Reaction condition: Diphenyl ether (4-O-5) (1.70 g, 0.010 mol), 57 wt.% Ni/SiO$_2$ (0.30 g, 2.91×10^{-3} mol Ni), 393 K , 0.6 MPa H$_2$, stirring at 700 rpm. (b) Reaction pathway for the cleavage of diphenyl ether (the 4-O-5 bond in ether) over Ni/SiO$_2$ in the aqueous phase.

Table 2-3. The rates for C-O bond cleavage of diphenyl ether (4-O-5), cyclohexyl phenyl ether, and dicyclohexyl ether at 393 K.[a]

Reactant	Selectivity (%)			Conv. (%)	Initial TOF (h^{-1})
	Benzene	Cyclohexanol	CPE [b]		
	27	57	16	80	26
	32	68	-	2.1	0.8
	0	0	0	0	0

[a] Reaction conditions: reactant (0.010 mol), Ni/SiO$_2$ (57 wt. %, 0.30 g, 2.91×10^{-3} mol Ni), H$_2$O (80 ml), 0.6 MPa H$_2$, 110 min, stirring at 700 rpm. [b] CPE: Cyclohexyl phenyl ether.

The selectivity to cyclohexanol (70%) was 2.3 times higher than the selectivity to benzene (30%) at complete conversion. Considering that the selectivity to cyclohexanol (formed from phenol hydrogenation) is much higher than that to benzene, we conclude, therefore, that hydrolysis of diphenyl ether (4-O-5) occurred in parallel to hydrogenolysis producing two molecules of phenol. Thus, cyclohexanol was obtained from diphenyl ether via two routes, one relying on the sequential hydrolysis-hydrogenation, and the other relating to the sequence hydrogenolysis-hydrogenation (**Fig. 2-5b**). It is estimated that the ratio of rates of hydrogenolysis to hydrolysis is approximately 3:2.

In summary, the overall reaction pathway for diphenyl ether conversion (**Fig. 2-5b**) follows two major routes, (i) hydrogenolysis of diphenyl ether to benzene and phenol, in which phenol is rapidly hydrogenated to cyclohexanol, and (ii) hydrolysis of diphenyl ether to two molecules of phenol, which are in turn hydrogenated to cyclohexanol. Another route of minor importance is the hydrogenation of diphenyl ether to cyclohexyl phenyl ether, which is in turn hydrolyzed or hydrogenolysed to cyclohexanol, benzene, and phenol. Phenol is in turn hydrogenated to cyclohexanol and a small fraction of benzene is hydrogenated to cyclohexane.

2.3.5 Relation of the thermodynamic properties of the reactant with the kinetic parameters

After exploring the differences in kinetic behavior of three model compounds on Ni/SiO$_2$, let us explore how the bond strength of the ether bond characterized by the bond dissociation energy (BDE) correlates with the kinetic parameters (**Table 2-4**). The aryl ether bond (314 kJ·mol^{-1}) of 4-O-5 is much stronger than the aliphatic ether bonds (218 kJ·mol^{-1} for α-O-4 and 289 kJ·mol^{-1} for β-O-4). Thus, hydrogenolysis favors selectively cleaving the weaker aliphatic ether bonds. The aliphatic ether C-O bond of α-O-4 is weaker by 96 kJ·mol^{-1} than that of 4-O-5, and more easily cleaved under hydrothermal condition above 523 K even in the blank test **(**see appendix 2.6 **Fig. S2-6)**. The low bond energy (218 kJ·mol^{-1}) of α-O-4 leads to a very high initial TOF (1017 mol·mol$_{Ni\ (surf)}^{-1}$·h^{-1}) and a lower apparent activation energy (72 kJ·mol^{-1}) (**Fig. 2-6a**). By comparison, the higher bond energy of β-O-4 (289 kJ·mol^{-1}) led to a low TOF (13 mol·mol$_{Ni\ (surf)}^{-1}$·h^{-1}) and a much higher E$_a$ (86 kJ·mol^{-1}) determined from the Arrhenius plot in the temperature range of 333-393 K (**Fig. 2-6a**).
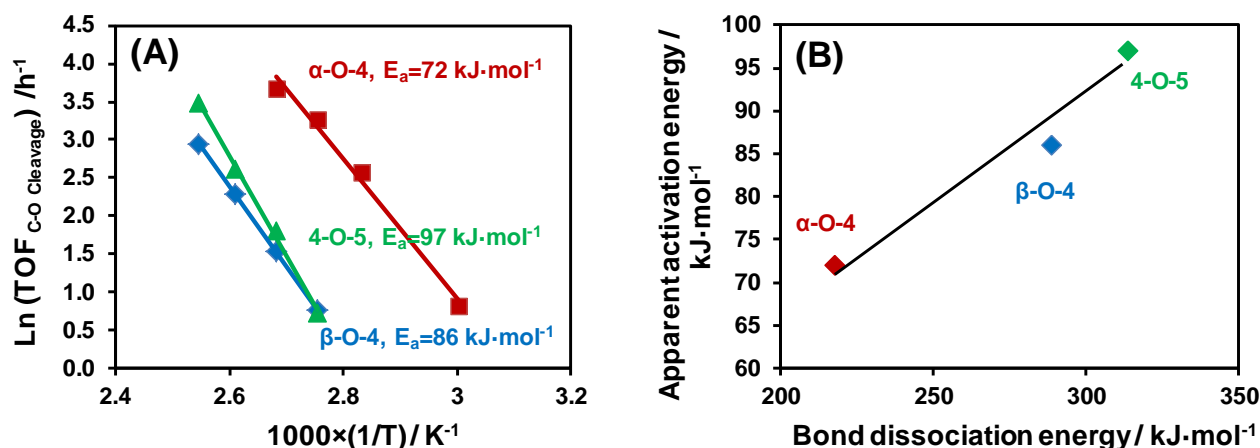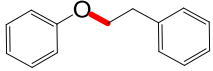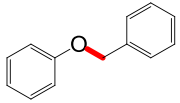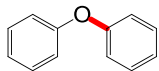
Figure 2-6. (**a**) Arrhenius plots of temperature versus Ln (TOF) on three model compounds. Reaction conditions: H$_2$O (80 ml), 6 bar H$_2$, 50 min. (i) α-O-4 (1.84 g), 57 wt % Ni/SiO$_2$ (0.03 g, 2.91 × 10^{-4} mol of Ni); (ii) β-O-4 (1.98 g), 57 wt % Ni/SiO$_2$ (0.30 g, 2.91 × 10^{-4} mol of Ni); or (iii) 4-O-5 (1.70 g), 57 wt % Ni/SiO$_2$ (0.30 g, 2.91 × 10^{-4} mol of Ni). (**b**) Relationship of apparent activation energies to bond dissociation energies on three model compounds.

Table 2-4. The bond dissociation energies (BDE), initial TOF of C-O cleavage, and apparent activation energies for C-O bond cleavage in lignin model compounds.

Linkage	Model Compound	BDE (kJ·mol⁻¹)[a]	E_a (kJ·mol⁻¹)	TOF$_{Ni/SiO_2}$ (h⁻¹)	TOF$_{H_2O}$ (h⁻¹)	TOF$_{SiO2}$ (h⁻¹)
β-O-4		289	86	13	0	0
α-O-4		218	72	1017	0	0
4-O-5		314	97	26	0	0

[a]Data from ref 14.

Compared to α-O-4 and β-O-4, the 4-O-5 bond showed very different reactivity on Ni/SiO₂. In principle, the C-O bond of 4-O-5 linkage should be the most difficult ether bond to cleave, as it has the highest bond energy (314 kJ·mol⁻¹). Previous work would also support this conclusion [8,11].The highest activation energy of 4-O-5 (97 kJ·mol⁻¹) agrees with the strongest bond dissociation energy (314 kJ·mol⁻¹). However, the reaction rate of 4-O-5 (26 mol·mol$_{Ni (surf)}^{-1}$·h⁻¹) was significantly higher than that of β-O-4 (13 mol·mol$_{Ni (surf)}^{-1}$·h⁻¹) with Ni/SiO₂ catalysts. This may be attributed to a different mechanism for the C-O bond cleavage of 4-O-5 in comparison with β-O-4. The C-O bonds in benzyl phenyl ether (α-O-4) and 2-phenylethyl ether (β-O-4) were directly cleaved by Ni catalyzed hydrogenolysis. However, the C-O bond of 4-O-5 was cleaved by parallel hydrogenolysis and hydrolysis, in which hydrolysis appears to increase the overall conversion rate. It should be noted that the apparent activation energies for cleavage of α-O-4, β-O-4, and 4-O-5 almost linearly increased with their C-O bond dissociation energies (**Fig. 2-6b**), indicating that the aryl C-O bond cleavage barriers are heavily influenced by the C-O bond dissociation energies.

To explore the specific contributions of the Ni/SiO₂ components in water, the rates of the C-O cleavage for three model compounds were compared with those in pure water, with SiO₂, and with

Ni/SiO$_2$ in the presence of 0.6 MPa H$_2$ at 393 K (**Table 2-4**). None of the ethers reacted in pure water or in the presence of SiO$_2$. With Ni/SiO$_2$ catalysts the C-O bond cleavage rates on α-O-4 (1017 mol·mol$_{Ni\ (surf)}^{-1}$·h^{-1}), β-O-4 (13 mol·mol$_{Ni\ (surf)}^{-1}$·h^{-1}), and 4-O-5 (26 mol·mol$_{Ni\ (surf)}^{-1}$·h^{-1}) dramatically increased, verifying that the Ni center is the active site for breaking the C-O bonds.

2.3.6 The impact of H$_2$ pressure

The product distributions of β-O-4, α-O-4, and 4-O-5 model compounds were recorded at conversions lower than 15% over Ni/SiO$_2$ at 393 K with varying hydrogen pressure (See appendix 2.6 **Figs. S2-7-S2-9**). In the absence of H$_2$ all three did not react. Thus, the presence of H$_2$ is also required for the hydrolysis route of diphenyl ether (4-O-5). With increasing P_{H2}, the rates of C-O bond cleavage in β-O-4 and 4-O-5 first increased to maxima at 0.6 and 1 MPa H$_2$, respectively, and then gradually decreased (**Fig. 2-7**). The C-O bond cleavage on Ni is the rate-determining step [15], suggesting that H$_2$ is competing with the organic reactant for adsorption sites. Up to medium P_{H2} the increasing surface coverage leads to an increased hydrogenolysis rate, while at high P_{H2} the rate is retarded because of the lowered ether coverage [16]. Thus, **Fig. 2-7** represents a typical change of the hydrogenolysis rate for β-O-4 and 4-O-5.
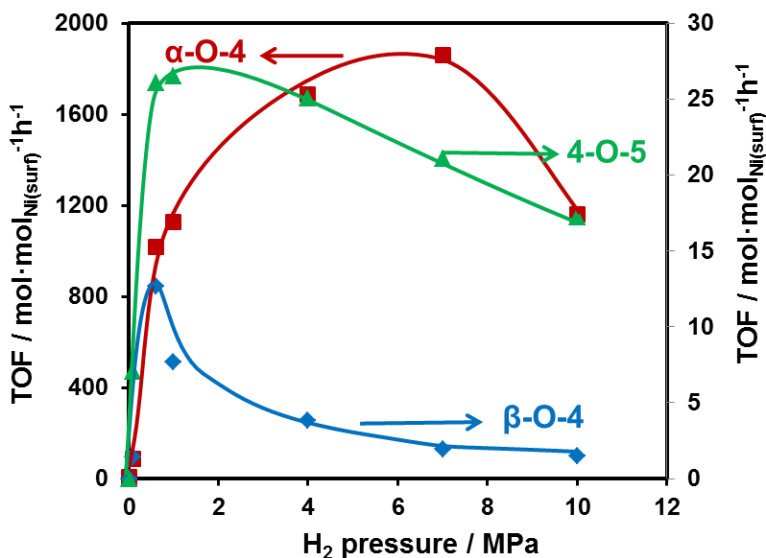
Figure 2-7. The TOFs on three model compounds over Ni/SiO$_2$ as a function of H$_2$ pressure. Detailed conditions please refer to appendix 2.6 **Figs. S2-7, S2-8, S2-9**.

In contrast, for α-O-4 the rate to C-O bond cleavage increased with P_{H2} up to 8 MPa. This is attributed to the fact that Ni/SiO$_2$ leads to a much faster rate for C-O bond cleavage in α-O-4, that is, the maximum cleavage rate being 150 and 70 times faster than those of α-O-4 and 4-O-5 (**Fig. 2-7**). This causes the product desorption to be rate-determining at lower P_{H2} and higher H$_2$ pressure facilitates product removal via H-addition and H-aided desorption. When the P_{H2} increased to 10 MPa, the TOF of C-O bond cleavage of α-O-4 decreased as the reactant coverage lowered resulting from the competition of reactant and H$_2$ adsorption on the Ni sites. Variation of the H$_2$ pressure also led to differences in the hydrogenation pathways of the model compounds. With increasing P_{H2}, the selectivity to hydrogenated single aromatic-ring products increased from 0 to 45% and to 20% for β-O-4 and 4-O-5, respectively (see appendix 2.6 **Figs. S2-7, S2-9**). However, a hydrogenated single aromatic-ring product was not observed for α-O-4 even at 10 MPa H$_2$ (see appendix 2.6 **Fig. S2-8**). This implies (i) hydrogenolysis and hydrogenation are competing reactions, and the higher H$_2$ pressure favored the hydrogenation of a single aromatic-ring of 4-O-5 and β-O-4. (ii) α-O-4 showed a different behavior, because its hydrogenolysis barrier (72 kJ·mol^{-1}) is much lower than the E$_a$ for hydrogenation of the phenolic ring (ca. 100 kJ·mol^{-1}) over Ni/SiO$_2$ [17], which results in hydrogenolysis dominating over hydrogenation at low temperatures.

2.3.7 Comparison of mechanisms of C-O bond cleavage on three model compounds

Based on the above results and discussion, the $C_{aliphatic}$-O-$C_{aromatic}$ bonds of α-O-4 and β-O-4 linkages are cleaved on the $C_{aliphatic}$-O side by the Ni catalyzed hydrogenolysis. However, for 4-O-5 the $C_{aromatic}$-O-$C_{aromatic}$ bond is cleaved by the parallel hydrogenolysis and hydrolysis routes. It is shown that the hydrolysis route on the 4-O-5 bond did not occur in the absence of H_2 (**Fig. 2-7**) or Ni/SiO$_2$ (**Table 2-4**). Hydrolysis is hypothesized to occur along the same reaction path as hydrogenolysis, cleaved by Ni and subsequently with H · and OH · (dissociated from water) addition instead of two H ·addition (**Fig. 2-8B**). For the α-O-4 and β-O-4 compounds the weaker $C_{aliphatic}$-O bonds rather than the more stable $C_{aromatic}$-O bonds are cleaved (**Fig. 2-8A**). As the C-O bond dissociation energy of α-O-4 linkage (218 kJ·mol^{-1}) is much lower than that of β-O-4 linkage (289 kJ·mol^{-1}), the hydrogenolysis rate of α-O-4 linkage over Ni/SiO$_2$ is two orders of magnitude higher than that of β-O-4 linkage (**Table 2-4**).
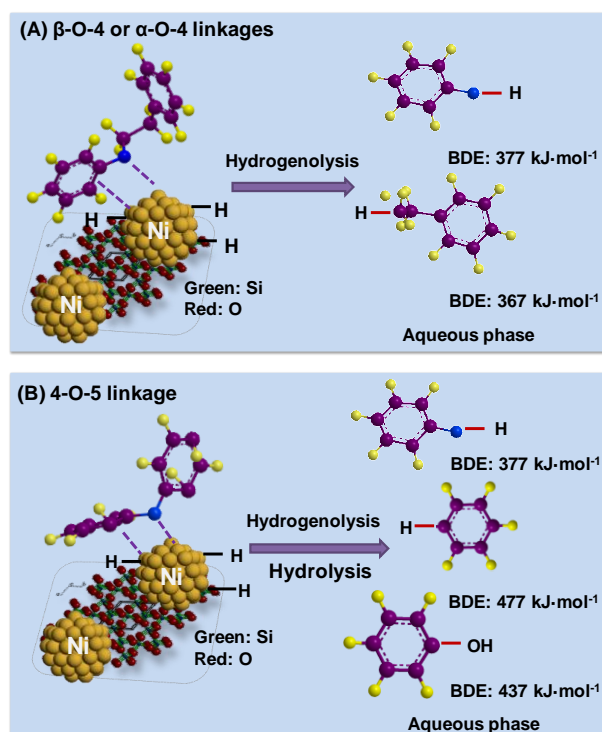
Figure 2-8. Proposed mechanisms for cleaving of C-O bonds in α-O-4, β-O-4, and 4-O-5 model compounds.

Once the $C_{aliphatic}$-O bonds of α-O-4 and β-O-4 linkages are cleaved into $C_{aliphatic}$ ·and O-$C_{aromatic}$ fragments, the dissociated abundant H ·on the Ni surface are in turn added to form methyl- or ethyl- benzene and phenol (**Fig. 2-8A**), respectively. As the bond dissociation energies of $PhCH_2CH_2$-H and $PhCH_2CH_2$-OH are 367 and 333 kJ mol^{-1} [14a], respectively, it appears that $PhCH_2CH_2$ · prefers to combine with H · but not OH · (dissociated from water) due to the much higher bond formation energy (34 kJ mol^{-1}), which makes hydrogenolysis (H ·addition) dominant. In addition, the bond dissociation energy of Ph-H (477 kJ mol^{-1}) is also much higher than that of Ph-OH (437 kJ mol^{-1}) [14a], and so hydrogenolysis rather than hydrolysis contributes a substantial fraction to the overall 4-O-5 conversion (**Fig. 2-5**). In essence, hydrolysis combined with OH ·and H · addition could occur on three model compounds in water, but the low concentrations of $PhCH_2OH$ and $PhCH_2CH_2OH$ produced can be further hydrogenolysed to $PhCH_3$ and $PhCH_2CH_3$, respectively (see appendix 2.6 **Table S2-1**), while hydrogenation is the major reaction of phenol derived from the 4-O-5 linkage to produce cyclohexanol under present conditions (**Table 2-2**). Therefore, hydrogenolysis was the major reaction pathway on overall conversion of α-O-4 and β-O-4 linkages, and the parallel hydrogenolysis and hydrolysis are the major routes on conversion of 4-O-5 linkages with Ni/SiO$_2$ catalysts in water.

2.4 Conclusions

The C-O bond linkages of model compounds α-O-4, β-O-4, and 4-O-5 representing typical bonds in lignin were selectively cleaved by a silica-supported Ni catalyst to produce aromatic and aliphatic molecules as well as cyclohexanol in aqueous media under mild conditions (393 K, 0.6 MPa H$_2$). The C-O bonds of α-O-4 and β-O-4 are cleaved by direct hydrogenolysis, which is shown to be structure-sensitive on Ni based catalysts, to be specific, the TOF of C-O bond cleavage is sensitive to the Ni particle size, while the C-O bond of 4-O-5 appeared to be cleaved by parallel hydrogenolysis and hydrolysis. The difference is attributed to the hydrogenolysis of the low concentrations of $PhCH_2OH$ and $PhCH_2CH_2OH$ intermediates from α-O-4 and β-O-4 linkages to $PhCH_3$ and $PhCH_2CH_3$, while hydrogenation converted phenol derived from 4-O-5 linkage to cyclohexanol under present conditions.

The rates for C-O bond cleavage followed the sequence r (α-O-4) > r (4-O-5) > r (β-O-4), and the increasing apparent energies of activation E_a (α-O-4) < E_a (β-O-4) < E_a (4-O-5) tracked the variations in bond dissociation energies E (α-O-4) < E (β-O-4) < E (4-O-5). The C-O bond of 4-O-5 was cleaved by parallel hydrogenolysis and hydrolysis, and the additional hydrolysis route accelerated the conversion. In the hydrogenolysis of β-O-4 and 4-O-5, an optimal H_2 pressure maximized the reaction rates for C-O bond cleavage, because the organic reactant was competing with H_2 for the active sites. In contrast, the rate to C-O bond cleavage increased continuously up to 8 MPa for α-O-4 conversion, probably because increasing higher P_{H2} facilitated product desorption from the Ni surface (rate-determining step for α-O-4 at lower P_{H2}). As the P_{H2} further increased, the TOF of C-O bond cleavage of α-O-4 decreased due to the lowered reactant coverage resulting from the competition of reactant and H_2 adsorption on the Ni sites.

The results indicate that Ni based solid catalysts are interesting and stable for the ether cleavage, and are significantly faster than related molecular catalysts. Tailoring the Ni catalysts via variation in particle size and eventually support is expected to lead to a new group of catalysts for cleaving carbon-heteroatom bonds.

2.5 Acknowledgements

2.6 Appendix

Characterization of Ni/SiO₂ catalysts (SEM and TEM)
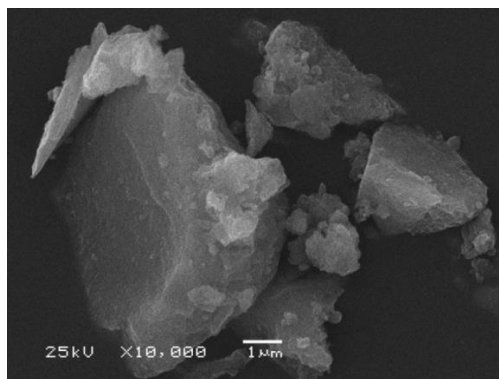
Figure S2-1. SEM image of commercial Ni/SiO₂ (metal loading: 57 wt %).
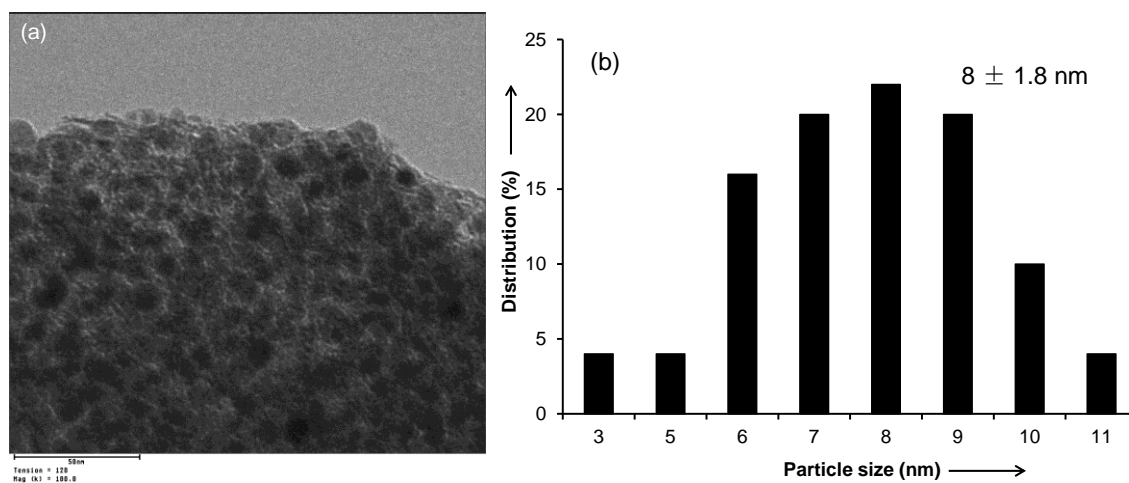
Figure S2-2. (a) TEM image of commercial Ni/SiO₂ (metal loading: 57 wt %). (b) Paticle size distribution of Ni nanoparticles on Ni/SiO₂ after couting 300 particles.

Synthesis of dicyclohexyl ether

Diphenyl ether (20.0 g) and 5 wt % Pd/C (1.0 g) were loaded in a Parr reactor (series 4848, 300 mL). After the reactor was flushed with H_2 three times, the hydrogenation reaction was conducted at 423 K in the presence of 5 MPa H_2 (ambient temperature) for 18 h with a stirring speed of 700 rpm. The catalysts were separated from liquid phase by centrifugation, and the product was separated though distillation under vacuum. Purity: > 99% (detected by GC), M_w: 182 g·mol^{-1}, Formula: $C_{12}H_{22}O$. The ^1H, ^{13}C and COSY NMR spectra are displayed in Figure S2-3, S2-2-4, S2-5.
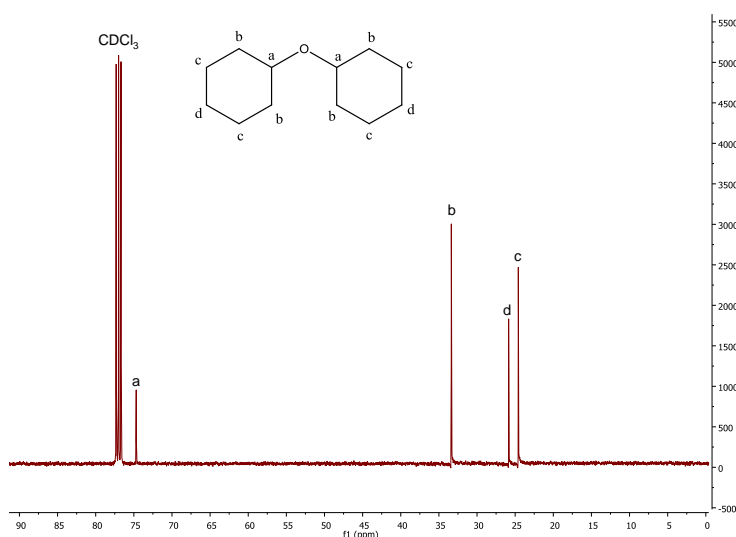
Figure S2-3. ^{13}C NMR spectrum of dicyclohexyl ether.
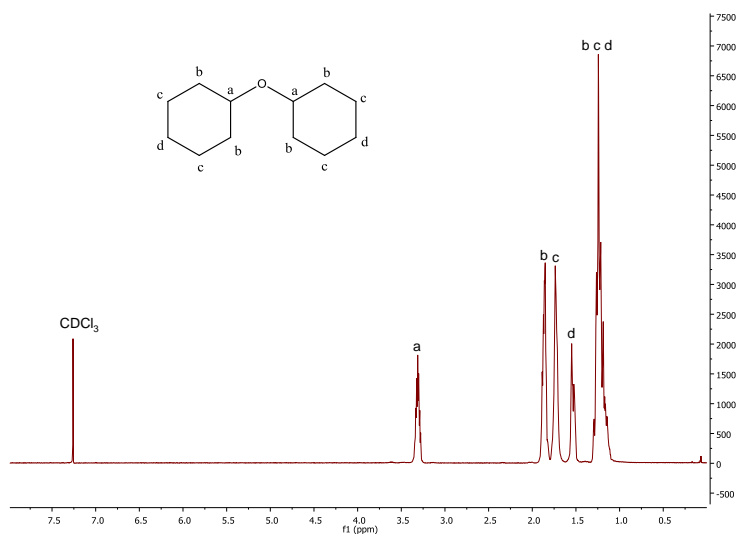
Figure S2-4. ¹H NMR spectrum of dicyclohexyl ether.
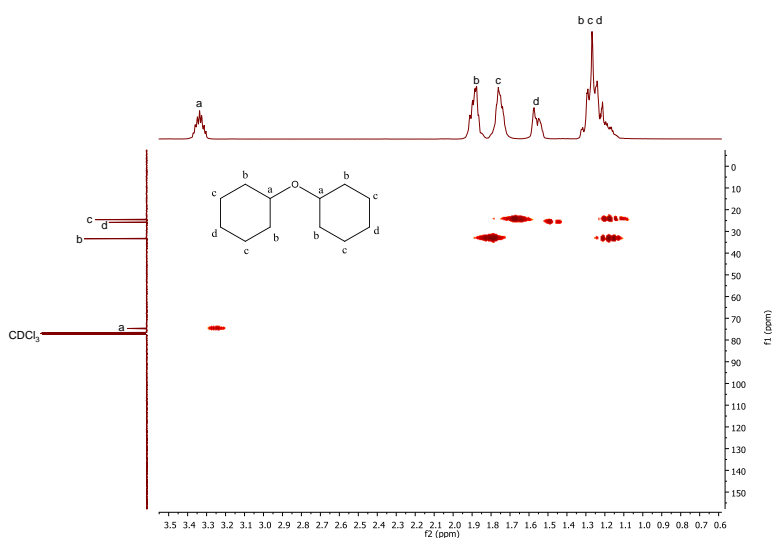
Figure S2-5. Correlation NMR spectroscopy (COSY) spectrum of dicyclohexyl ether.
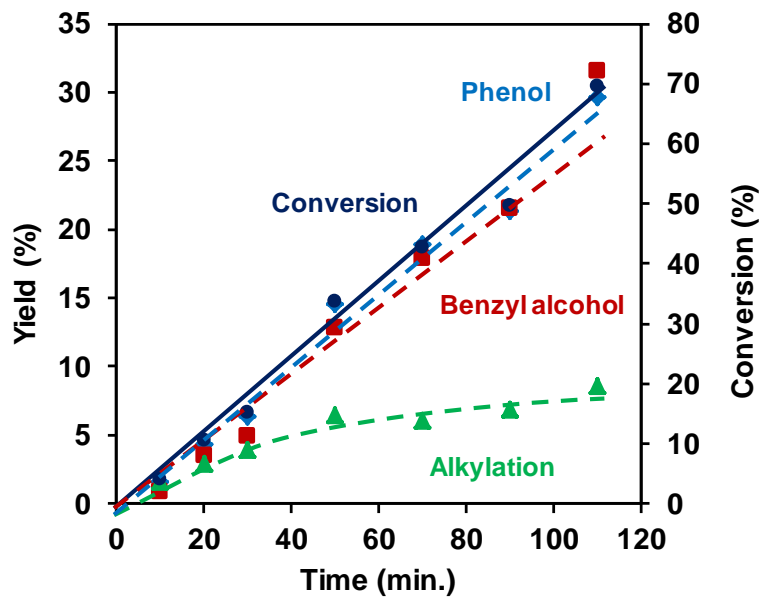
Figure S2-6. Product yields for conversion of benzyl phenyl ether in the aqueous phase in absence of H_2 as a function of time. Reaction conditions: Benzyl phenyl ether (1.84 g), H_2O (80 mL), 523 K, 4 MPa H_2, stirring at 700 rpm.

Product distribution with varying H₂ pressure
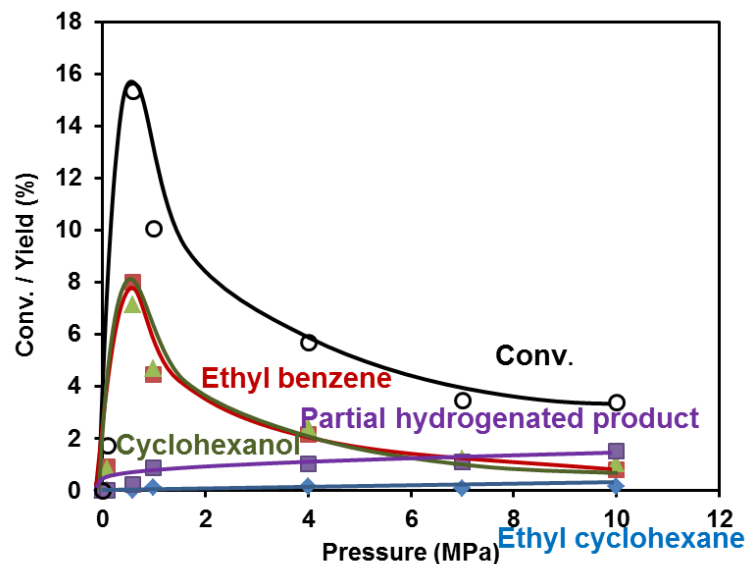
Figure S2-7. Product distribution on conversion of 2-phenylethyl phenyl ether (β-O-4) as a function of H_2 pressure. Reaction conditions: reactant (1.98 g, 0.010 mol), Ni/SiO₂ (57 wt %, 0.30 g, 2.91×10^{-3} mol Ni), H_2O (80 mL), 393 K, 50 min., stirring at 700 rpm.
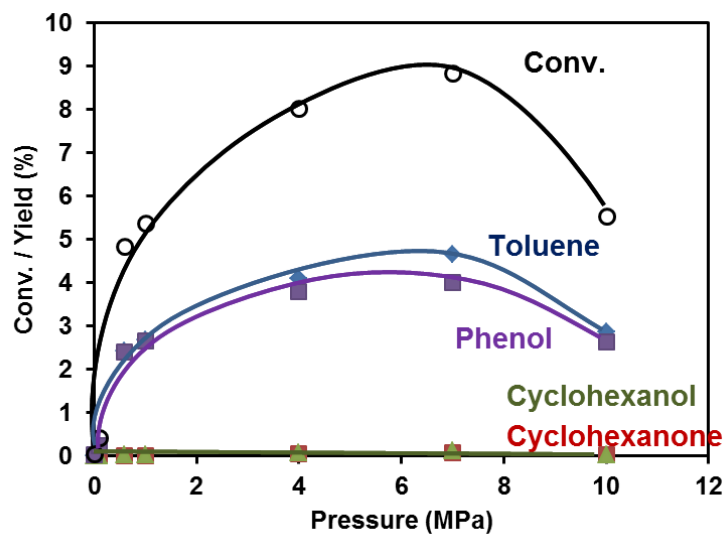
Figure S2-8. Product distribution on conversion of benzyl phenyl ether (α-O-4) as a function of H_2 pressure. Reaction conditions: reactant (9.20 g, 0.050 mol), Ni/SiO₂ (57 wt %, 0.030 g, 2.91×10^{-4} mol Ni), H_2O (80 mL), 393 K, 10 min., stirring at 700 rpm.
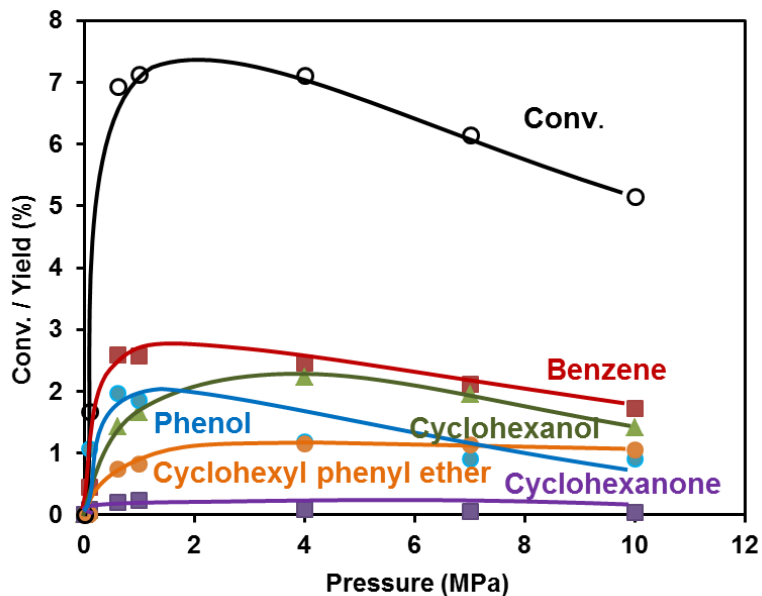
Figure S2-9. Product distribution on conversion of diphenyl ether (4-O-5) as a function of H_2 pressure. Reaction conditions: reactant (1.70 g, 0.010 mol), Ni/SiO$_2$ (57 wt %, 0.10 g, 9.7×10^{-4} mol Ni), H_2O (80 mL), 393 K, 30 min., stirring at 700 rpm.

Table S2-1. Hydrogenolysis of 2-phenylethanol and phenol-methanol over Ni/SiO$_2$ at 393 K.[a]

Entry	Reactant	Time (min)	Conv (%)	Yield (%)	TOF (h^{-1})
1	2-Phenyl-ethanol	90	1.27	1.04 (Ethyl benzene) 0.23 (Toluene)	2.0
2	Benzyl alcohol	20	4.84	4.84 (Toluene)	290

[a] reaction conditions: 2-phenylethanol (0.03 mol, Sigma-Aldrich, >99.8% GC assay), benzyl alcohol (0.03 mol, Sigma-Aldrich, ≥ 99.0% GC assay), 57 wt % Ni/SiO$_2$ (0.3 g for 2-phenylethanol, 0.03 g for benzyl alcohol), H$_2$O (80 mL), 0.6 MPa H$_2$.

2.7 Reference

[1]   M. Stöcker, Angew. Chem. Int. Ed. 47 (2008) 9200

[2]   (a) J. R. Regalbuto, Science 325 (2009) 822. (b) R. D. Perlack, L. L.Wright, A. F. Turhollow, R. L. Graham, B. J. Stokes, D. C. Erbach, U. S. Department of Energy, Biomass as Feedstock for a bioenergy and bioproducts industry: the technical feasibility of a billion-ton annual supply, 2005. (c) G. W. Huber, A. Corma, Angew. Chem. Int. Ed. 46 (2007) 7184. (d) G. W. Huber, S. Iborra, A. Corma, Chem. Rev. 106 (2006) 4044.

[3]   (a) A. Ragauskas, C. Williams, B. Davision, G. Britovsek, J. Cairney, C. Eckert, W. Frederick, J. Hallett, D. Leak, C. Liotta, J. Mielenz, R. Murphy, R. Templer, T. Tschaplinski, Science 311 (2006) 484. (b) M. C. Y. Chang, Curr. Opin. Chem. Biol. 11 (2007) 677. (c) K. Sanderson, Nature 474 (2011) S12. (d) T. D. Matson, K. Barta; A. V. Iretskii; P. C. Ford, J. Am. Chem. Soc. 133 (2011) 14090.

[4]   J. M. Nichols, L. M. Bisshop, R. G. Bergman, J. A. Ellman, J. Am. Chem. Soc. 132 (2010) 12554.

[5]   S. Son, F. D. Toste, Angew. Chem. Int. Ed. 49 (2010) 3791.

[6]   A. G. Sergeev, J. F. Hartwig, Science 332 (2011) 439.

[7]   (a) V. M. Roberts, R. T. Knapp, X. Li, J. A. Lercher, ChemCatChem 2 (2010) 1407. (b) V. M. Roberts,; V. Stein, T. Reiner, X. Li, A. A. Lemonidou, X. Li, J. A. Lercher, Eur. J. Chem. 17 (2011) 5939. (c) V. M. Roberts, S. Fendt, T. Reiner, X. Li, A. A. Lemonidou, X. Li, J. A. Lercher, Appl. Catal. B 95 (2010) 71.

[8]   C. Zhao, J. A. Lercher, Angew. Chem. Int. Ed. 51 (2012) 5935.

[9]   C. Zhao, J. A. Lercher, ChemCatChem 4 (2012) 64.

[10]   (a) J. Zakzeski, P. C. A. Bruijinincx, A. L. Jongerius, B. M. Weckhuysen, Chem. Rev. 110 (2010) 3552. (b) E. Furimsky, Appl. Catal. A. 199 (2000) 147.

[11]   (a) C. Zhao, Y. Kou, A. A. Lemonidou, X. Li, J. A. Lercher, Chem. Comm. 46 (2010) 412. (b) C. Zhao, Y. Kou, A. A. Lemonidou, X. Li, J. A. Lercher, Angew. Chem. Int. Ed. 48 (2009) 3987. (c) C. Zhao, D. M. Camaioni, J. A. Lercher, J. Catal. 288 (2012) 92. d) C. Zhao, J. He, A. A. Lemonidou, X. Li, J. A. Lercher J. Catal. 280 (2011) 8. e) C. Zhao, S. Kazacov, J. He, J. A. Lercher, J. Catal. 296 (2012) 12. f) C. Zhao, W. Song, J. A. Lercher, ACS Catalysis 2 (2012) 2714.

[12]   (a) E. Dorrestijn, L. Laarhoven, I. Arends, P. Mulder, J. Anal. Appl. Pyrolysis 54 (2000) 153. (b) P. N. Rylander, Hydrogenation Methods, Academic Press, London, 1985, pp. 157-163.

[13]   G. Chandler, W. Sasse Aust. J. Chem. 16 (1963) 20.

[14]   (a) Y. R. Luo, in Comprehensive handbook of Chemical bond energies, CRC Press, 2007. (b) M. W. Jarvis, J. W. Daily, H. Carstensen, A. M. Dean, S. Sharma, D. C. Dayton, D. J. Robichaud, M. R. Nimlos, J. Phys. Chem. A 115 (2011) 428.

[15]   S. B. Shang, C. N. Kenney, J. Catal. 134 (1992) 134.

[16]   G. C. Bond, R. H. Cunningham, J. Catal. 166 (1997) 172.

[17]   H. Hichri, A. Accary, J. Andrieu, Chem. Eng. Process. 30 (1991) 133.

Chapter 3

Mechanisms of Selective Cleavage of C−O Bonds in Di-aryl Ethers in the Aqueous Phase

A route for cleaving the C−O aryl ether bonds of p-substituted H−, CH$_3$−, and OH− diphenyl ethers has been explored over Ni/SiO$_2$ catalyst at very mild conditions (393 K, 0.6 MPa). The C−O bond of diphenyl ether is cleaved by parallel hydrogenolysis and hydrolysis (hydrogenolysis combined with HO* addition) on Ni. The rates as a function of H$_2$ pressure from 0 to 10 MPa indicate that the rate-determining step is the C−O bond cleavage on Ni surface. H* atoms compete with the organic reactant for adsorption leading to a maximum in the rate with increasing H$_2$ pressure. In contrast to diphenyl ether, hydrogenolysis is the exclusive route for cleaving a C−O bond of di-p-tolyl ether to form p-cresol and toluene. 4,4'-Dihydroxydiphenyl ether undergoes sequential surface hydrogenolysis, first to phenol and OC$_6$H$_4$OH* (adsorbed), which is then cleaved to phenol (C$_6$H$_4$OH* with added H*) and H$_2$O (O* with two added H*) in a second step. Density function theory supports the operation of this pathway. Notably, addition of H* to OC$_6$H$_4$OH* is less favorable than a further hydrogenolytic C−O bond cleavage. The TOFs of three diaryl ethers with Ni/SiO$_2$ in water follow the order 4,4'-dihydroxydiphenyl ether (69 mol mol$_{Ni\ Surf}^{-1}$ h^{-1}) > diphenyl ether (26 mol mol$_{Ni\ Surf}^{-1}$ h^{-1}) > di-p-tolyl ether (1.3 mol mol$_{Ni\ Surf}^{-1}$ h^{-1}), in line with the increasing apparent activation energies, ranging from 4,4'-dihydroxydiphenyl ether (93 kJ·mol^{-1}) < diphenyl ether (98 kJ·mol^{-1}) < di-p-tolyl ether (105 kJ·mol^{-1}).

3.1 Introduction

Lignin is an abundant natural bio-polymer with methoxylated C_9 phenyl-propane units that are connected by C−O and C−C bonds [1]. Since the C−C_{aryl} bond dissociation energy (BDE) in the linkage of lignin is as high as 384 kJ·mol^{-1}, it is reasonable to devise a strategy to selectively cleave the much weaker C_{aryl}−O or $C_{aliphatic}$−O linkages (BDE: 218-314 kJ·mol^{-1}) in lignin to form phenolic fragments [2-4]. The most abundant C−O bonds in lignin are α−O−4, β−O−4, 4−O−5, β−1, and 5−5 linkages [3]; however the 4−O−5 bond (BDE: 314 kJ mol^{-1}) [4] is the strongest. Usually diphenyl ether is selected as the simplest model compound of 4−O−5 linkage for investigating the C−O bond cleavage chemistry.

Diphenyl ether cleavage requires harsh reaction conditions, such as near- or supercritical water at high temperature 673−773 K [5, 6]. Siskin et al. reported that diphenyl ether was unreactive in the aqueous phase at temperatures lower than 733 K without catalyst but with addition of 15% phosphoric acid catalyst, diphenyl ether was hydrolyzed to 92% phenol at 588 K after three days [7]. In a comparison, the basic environment with 15% aqueous sodium formate, a 6.6% conversion, also to phenol was achieved at 588 K for three days. With 15% Na_2CO_3 solution, the reaction rate was accelerated and resulted in 33% conversion to phenol at 733 K after 1 hour. [8]. We have also reported that 100% phenol selectivity was achieved by diphenyl ether conversion over solid base catalyst K_2CO_3/ZrO_2 at 673 K [9]. Penninger et al. investigated the diphenyl ether (DPE) conversion in supercritical water at temperatures of 688–753 K with different supercritical water densities [10]. At water density below 0.3 g·mL^{-1} the radical poly-condensation dominated, forming e.g., diphenyl, phenyl–DPE, and phenoxy–diphenyl. Increasing the water density above 0.4 g·mL^{-1} forced the reaction to follow SN_1 H$^+$- catalyzed ionic hydrolysis route, yielding phenol as sole product. A NaCl concentration above 3.1 wt.% in supercritical water (SCW) greatly enhanced the hydrolysis rate of DPE [11]. This suggests that charge transfer in the water cluster surrounding the ions generated H$^+$ and OH$^-$ ions in the outer hydration shells formed the active species for diphenyl ether hydrolysis. Rinaldi et al. investigated the solvent effect on the hydrogenolysis of diphenyl ether over Raney nickel under 5 MPa H_2 at 363 K and concluded that a higher Lewis basicity of solvent such as methanol, 1,4-dioxane, and THF suppressed hydrogenation of aromatic products and showed no effect to C−O bond hydrogenolysis [12].

Apart from the traditional homogeneous or heterogeneous acid and base catalyzed hydrolysis of diphenyl ether in high temperature water, the metal catalyzed selective hydrogenolysis of diphenyl ether is also feasible. Hartwig et al. reported that a Ni(COD)$_2$ complex combined with ligand SIPr HCl and NaO^{t}Bu can selectively cleave diphenyl ether in *m*-xylene at 393 K and 0.1 MPa H$_2$, attaining 99% yields of benzene and phenol after 16 h [13,14]. While the homogeneous catalyst has minimal steric constraints on interactions with lignin model compounds and allows extremely mild conditions, the TOF with the complex Ni catalyst is as low as 0.34 h^{-1} [13]. The catalysts are also sensitive to high concentrations of water, which is ubiquitous in raw biomass. To establish a more sustainable, stable, water-tolerant, and applicable process, we have developed a supported Ni/SiO$_2$ catalyst to quantitatively convert diphenyl ether to benzene and cyclohexanol at 393 K and 0.6 MPa H$_2$ in the aqueous phase, achieving a TOF of 26 h^{-1} [15]. By changing the catalyst to Ni/HZSM-5, we have achieved an one-pot conversion of diverse lignin-derived phenolic monomers and aryl ethers to cycloalkanes at 523 K in the aqueous phase via cascade reactions of hydrolysis, hydrogenolysis, dehydration, and hydrogenation [16]. However, the detailed mechanisms of the C−O bond cleavage of di-phenolic ethers over the heterogeneous Ni catalysts have not been established. Therefore, in this contribution we investigate the mechanisms of C−O bond cleavage in *p*- (H−, CH$_3$−, OH−) substituted diphenyl ethers over SiO$_2$, ZrO$_2$, and Al$_2$O$_3$ supported Ni catalysts in the aqueous phase by investigating individual steps. Modeling using density function theory helps to elucidate the mechanism for 4,4'-dihydroxydiphenyl ether conversion.

3.2 Experimental section

3.2.1 Chemicals

All chemicals were obtained from commercial suppliers: diphenyl ether (Sigma-Aldrich, > 99% GC assay), di-*p*-tolyl ether (TCI Europe, > 98% GC assay), 4,4'-dihydroxydiphenyl ether (TCI Europe, > 98% GC assay), cyclohexyl phenyl ether (Sigma-Aldrich, > 95 % GC assay), p-cresol (TCI Europe, > 99% GC assay), hydroquinone (TCI Europe, > 99% GC assay), 1,4-

cyclohexanediol (TCI Europe, *cis-* and *trans-* mixture, > 99% GC assay), ethyl acetate (Roth, > 99.9% GC assay), phenol (Sigma-Aldrich, > 99 % GC assay), benzene (Fluka, > 99.5 % GC assay), Ni(II) nitrate hexahydrate (Sigma-Aldrich, ≥98.5%), urea (Sigma-Aldrich, BioReagent), HNO_3 (Sigma-Aldrich, > 65 %), 5 wt.% Pd/C (Sigma-Aldrich), SiO_2 (Aerosil 200, Evonik-Degussa), H_2 (Westfalen AG, 99.999 vol %), N_2 (Westfalen AG, 99.999 vol %), synthetic air (Westfalen AG, 99.999 vol %), ultra pure water system (EASYpure II, resistivity:18.2 MΩ.cm.).

3.2.2 Synthesis of dicyclohexyl ether

Diphenyl ether (20.0 g) and 5 wt % Pd/C (1.0 g) were loaded in a Parr reactor (series 4848, 300 mL). After the reactor was flushed with H_2 three times, the hydrogenation reaction was conducted at 423 K in the presence of 5.0 MPa H_2 (ambient temperature) for 18 h with a stirring speed of 700 rpm. The catalysts were separated from liquid phase by centrifugation, and the product was purified though distillation under vacuum. Purity: > 99% (detected by GC), M_w: 182 g$^.$mol^{-1}, Formula: $C_{12}H_{22}O$. The ^1H, ^{13}C, and COSY NMR spectra are displayed in **Figures S4-1-S4-3 (appendix 3.6)**.

3.2.3 Catalyst characterization

Atomic absorption spectroscopy (AAS)

With a UNICAM 939 AA-Spectrometer we determined the content of Ni in the supported catalysts.

Transmission electron micrographs (TEM)

TEM were recorded on a JEM-2010 Jeol transmission microscope operated at 120 kV. Before TEM measurement, the samples were prepared by depositing a drop of an ultrasonicated methanol suspension of the solid material onto a carbon-coated Cu grid for TEM measurement.

Scanning electron microscopy (SEM)

SEM was recorded on a JEOL 500 SEM-microscope with accelerating voltage 25 kV. The power samples were used without any pretreatment.

BET measurement

N_2 adsorption-desorption was carried out at 77.3 K using a PMI automatic BET (Brunauer-Emmett-Teller)-Sorptometer.

H_2 chemisorption

For the H_2 chemisorption measurement, the Ni catalysts were reduced under 0.1 MPa H_2 at 733 K for 4 h prior to measurement. They were activated in vacuum at 588 K for 1 h before the H_2 chemisorption and then cooled to ambient temperature. The H_2 adsorption isotherms (chemisorption and physisorption) were measured at 1 to 40 kPa. Following the first isotherms the samples were outgassed at ambient temperature for 1 h to remove the physisorbed H_2, followed by measuring another adsorption isotherm (physisorption). The Ni dispersions were calculated from the difference between extrapolated intercepts of the first and second isotherms with the assumption of H : Ni atomic ratio = 1.

3.2.4 Preparation of Ni/SiO$_2$ catalyst using deposition precipitation (DP) method

An aqueous solution (250 mL) containing $Ni(NO_3)_2 \cdot 6H_2O$ (0.14 M, 10.2 g) was first divided in two fractions. To one 50 mL portion was added urea (0.42 M, 6.3 g). The other 200 mL portion together with SiO_2 (1.1 g) and HNO_3 (65%, 0.02 M, 0.32 mL) was put into a flask thermostated at 353 K. The first part with urea was slowly added into the flask, and the suspension was rapidly heated to 363 K. After reaching 363 K the suspension was magnetically stirred for 10 h. Then the

suspension was cooled to 298 K and the solids were filtered and washed three times with distilled water (5/1 = water/slurry). Finally, the sample was dried at 363 K for 24 h, and calcinated in flowing air (100 mL·min^{-1}) at 973 K and reduced in flowing H_2 (100 mL·min^{-1}) at 733 K. The Ni/SiO$_2$ catalyst had a Ni content of 57 wt.% as analyzed by AAS.

3.2.5 Catalytic tests

In a typical experiment, the catalytic reactions were carried out in a slurry autoclave reactor with Ni/SiO$_2$ catalyst using H_2O as solvent at 393 K in the presence of 0.6 MPa H_2. The diphenyl ether (0.010 mol), 57 wt.% Ni/SiO$_2$ (0.30 g, 2.91×10^{-3} mol Ni), and H_2O (80 mL) were added into a Parr reactor (Series 4848, 300 mL). After the reactor was flushed with H_2 three times, the autoclave was charged with 0.6 MPa H_2 and the reactions were conducted at 393 K with a stirring speed of 700 rpm. It was heated from ambient temperature to 393 K in 9 min. As H_2O remained liquid under these conditions, two phases were formed as the reaction proceeded, requiring the composition determination of both phases by stopping the reaction at different times and analyzing the mixture. At the selected times, the reactor was quenched by ice to ambient temperature, and the organic products were extracted by ethyl acetate and analyzed by gas chromatography (GC) and GC-mass spectroscopy (GC-MS) analysis on a Shimadzu 2010 gas chromatograph with a flame ionization detector and a Shimadzu QP 2010S GC-MS, both were equipped with a HP-5 capillary column (30 m ×250 μm). The calculations of conversion and selectivity were on a carbon mole basis. Conversion = (the amount of raw-material decrease during reaction / original amount) ×100%. Selectivity = (C atoms in each product / total C atoms in the products) ×100%. Internal standards (i.e., 2-isopropylphenol for the organic phase and acetone for the aqueous phase) were used to determine the product concentration and carbon balance. The carbon balance was better than 95 ±3%. TOFs for C−O cleavage were calculated from the formed cleaved products per mole of active site per hour. TOF = (moles of reactants cleaved) / (moles of surface Ni sites ×reaction time in hour).

3.2.6 Computational method

To gain insight in 4,4'-dihydroxydiphenyl ether conversion over the Ni/SiO$_2$ catalyst, periodic density functional theory (DFT) calculations were carried out using the cp2k package [17]. The SiO$_2$ supported Ni catalyst was modeled by a periodic Ni (111) surface slab with four atomic Ni layers. The Ni (111) surface contained 32 atoms giving 17.2640 Å and 9.9674 Å in the x and y Cartesian directions, respectively. To avoid unphysical interactions between the periodic reactive systems, a 12 Å thickness of vacuum was inserted above the surface slabs in the z direction. All DFT calculations employed mixed Gaussian and plane-wave basis sets. Core electrons were represented with norm-conserving Goedecker-Teter-Hutter pseudopotentials [18-20], and the valence electron wave-function was expanded in a double-zeta basis set with polarization functions [21] along with an auxiliary plane wave basis set with an energy cutoff of 360 eV. The generalized gradient approximation exchange-correlation function of Perdew, Burke, and Enzerhof (PBE) [22] was used for all calculations. Each configuration was optimized with the Broyden-Fletcher-Goldfarb-Shanno (BGFS) algorithm with SCF convergence criteria of 1.0×10^{-8} au. To compensate the long-range van der Waals (vdW) interaction between the adsorbate and the zeolite, the DFT-D3 scheme [23] with an empirical damped potential term was added into the energies obtained from exchange-correlation functional in our calculations.

3.3 Results and discussion

3.3.1 The physicochemical properties of Ni/SiO$_2$

The Ni/SiO$_2$ catalyst prepared by the deposition-precipitation method had a Ni content of 57 wt.% analyzed by AAS, the surface area of 140 m^2 g^{-1} and the pore volume of 0.18 cm^3 g^{-1} determined by N$_2$ adsorption-desorption measurement (**Table 3-1**). Shown from SEM image (**Figure 3-1a**), Ni/SiO$_2$ displayed a blocky texture, with an average particle size of ca. 3 μm. The supported Ni nanoparticles had an average particle diameter of 8.0 nm with a standard deviation of 1.8 nm as determined by TEM image (**Figure 3-1b**), suggesting that the Ni nanoparticles are very uniformly dispersed. The atomic fraction of available Ni atoms on Ni/SiO$_2$ was 5.0 %, as measured by H$_2$ chemisorption.

Table 3-1. Physicochemical properties of Ni/SiO$_2$ catalyst.

Catalyst	Ni/SiO$_2$
Metal loading (wt.%)	57
BET surface area (m^{2}g^{-1})	140
Pore volume (cm^{3}g^{-1})	0.18
Pore diameter (nm)	53
Dispersion (%) (H$_2$ chemisorption)	5.0
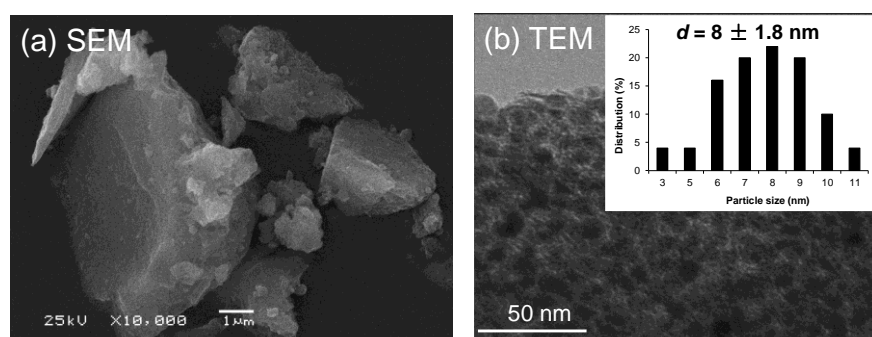
Figure 3-1. Chacterization of Ni/SiO$_2$ catalyst (a) SEM, and (b) TEM image and paticle size distribution of 300 Ni particles.

3.3.2 The kinetics and mechanisms for conversion of diphenyl ether in the aqueous phase

3.3.2.1 The kinetics and reaction pathways of diphenyl ether conversion over Ni/SiO$_2$

When converting diphenyl ether over metal sites at 393 K, three initial primary routes may exist in the aqueous phase, i.e., hydrogenolysis of a C−O bond produces equal phenol and benzene, hydrolysis of the C−O bond forms two moles of phenol, and hydrogenation of the aromatic rings

to partially hydrogenated products. Shown from the kinetics in **Fig. 3-2a** for conversion of diphenyl ether at 393 K in the presence of 0.6 MPa H_2, the initial major products were cyclohexanol, benzene, and cyclohexyl phenyl ether. It is, however, found that phenol was absent from the products although it would be an expected initial product from either the hydrogenolysis or hydrolysis route. It was found in separate experiments that the hydrogenation rate of phenol over Ni/SiO$_2$ (130 mol $mol_{Ni\,Surf}^{-1}\,h^{-1}$) was much higher than of benzene (2.9 mol $mol_{Ni\,Surf}^{-1}\,h^{-1}$; Table S1), suggesting that the primary phenol was rapidly converted to cyclohexanol [15]. This is consequent to the highly favored adsorption of phenol on the Ni/SiO$_2$ catalyst, enabling fast hydrogenation to cyclohexanol. Then, the concentration of cyclohexanol should be equal to that of benzene (**Scheme 3-1**). But the yield of cyclohexanol kept a constantly stable ratio of 7:3 to benzene, which suggests that besides the hydrogenolysis pathway there is an additional route for cleaving a C−O bond of diphenyl ether.

To understand the intrinsic mechanism and pathways for diphenyl ether C−O bond cleavage, three hypotheses are tested. One was partial hydrogenation forming cyclohexyl phenyl ether, which followed by either hydrogenolysis to produce benzene and cyclohexanol, or hydrolysis to form phenol and cyclohexanol. During diphenyl ether conversion, the yield of partially hydrogenated product increased to a maximum value of 10% at 110 min. and then decreased toward zero as reaction time extended. However, in a separate experiment, the rate of cyclohexyl phenyl ether conversion (0.8 mol $mol_{Ni\,Surf}^{-1}\,h^{-1}$) was much lower than that of diphenyl ether (26 mol $mol_{Ni\,Surf}^{-1}\,h^{-1}$) at 393 K in the presence of 0.6 MPa H_2 (see appendix 3.6 **Table S3-2**). Thus, it is concluded that the partial hydrogenation-hydrogenolysis route is of minor importance. The second route was that diphenyl ether was fully hydrogenated to dicyclohexyl ether, which was fast hydrolyzed to two moles of cyclohexanol. However, in a separate experiment dicyclohexyl ether was completely unreactive over Ni/SiO$_2$ at 393 K under 0.6 MPa H_2 (see appendix 3.6 **Table S3-2**), thus this route can also be ruled out. The third pathway was directly hydrolysis of diphenyl ether to two moles of phenol, and subsequently phenol was rapidly hydrogenated to cyclohexanol. This would reasonably explain the excess of cyclohexanol. Therefore, we conclude that diphenyl ether is also hydrolyzed to two moles phenol, which is in turn rapidly hydrogenated to cyclohexanol (**Scheme 3-1**). Therefore, cyclohexanol is formed by parallel hydrogenolysis-hydrogenation and hydrolysis-hydrogenation pathways. Since the initial yield ratio of

cyclohexanol to benzene was 7 : 3, the rate ratio of hydrogenolysis to hydrolysis routes was determined to be 3 : 2.

When H_2 pressure was increased from 0.6 MPa (**Fig. 3-2a**) to 4.0 MPa (**Fig. 3-2b**), the major products remained benzene, cyclohexanol, and cyclohexyl phenyl ether during the diphenyl ether conversion. Phenol was not found due to its rapid hydrogenation rate [24]. The yield of cyclohexyl phenyl ether was increased from 7% to 24% in the presence of the higher H_2 pressure of 4.0 MPa H_2 at 180 min., indicating that the hydrogenation of single aromatic ring of diphenyl ether is favored by the higher H_2 pressure. Cyclohexyl phenyl ether formed could be further cleaved by hydrogenolysis or hydrolysis. At the high hydrogen pressure, fully hydrogenated dicyclohexyl ether was observed with 1% yield at 110 min. (not shown in the kinetic curve of Fig. 2b). It was also found that the yield ratio of cyclohexanol to benzene remained 7:3, indicating that the hydrolysis route on DPE persisted under high H_2 pressure. The initial C−O cleavage turnover frequency (TOF) of DPE was calculated from the slope of curves in **Fig. 3-2.** In the presence of 0.6 MPa H_2, TOF for diphenyl ether cleavage was 26 mol·$mol_{Ni\ surf}^{-1}$ h^{-1}, while at higher pressure of 4 MPa it was lowered to 23 mol·$mol_{Ni\ Surf}^{-1}$ h^{-1}. The P_{H_2} impact to the C−O bond cleavage rate will be discussed in the following section.

In summary, the conversion of diphenyl ether follows two major reaction pathways (**Scheme 3-1**). The first one is that the initial hydrolysis followed by hydrogenation produces two moles of cyclohexanol. The second one is that hydrogenolysis combined with hydrogenation leads to equivalent moles of benzene and cyclohexanol. There is also a minor reaction pathway, partial hydrogenation (promoted by higher H_2 pressure) followed by hydrogenolysis or hydrolysis produces cyclohexanol and benzene, or cyclohexanol and phenol.
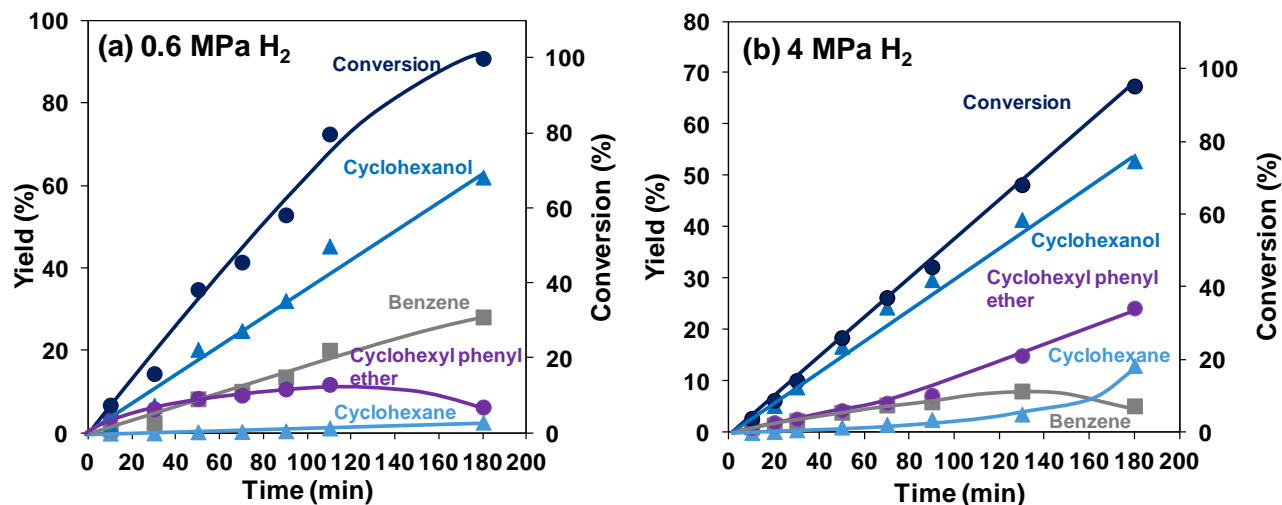
Figure 3-2. Diphenyl ether conversion over Ni/SiO$_2$ in the aqueous phase in the presence of (a) 0.6 MPa H$_2$ and (b) 4.0 MPa H$_2$. Reaction conditions: Diphenyl ether (1.70 g), H$_2$O (80 mL), 57 wt.% Ni/SiO$_2$ (0.30 g), 393 K, stirring at 700 rpm.
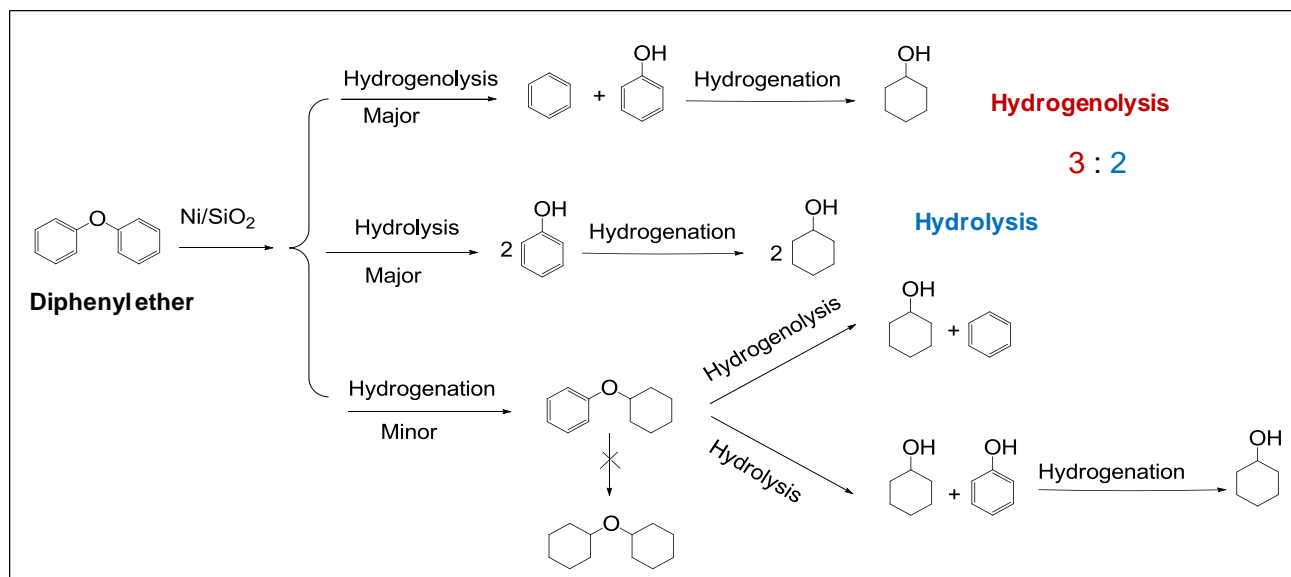
Scheme 3-1. Proposed reaction pathways of diphenyl ether conversion on Ni/SiO$_2$ in the aqueous phase.

3.3.2.1 Impact of H_2 pressure

In order to investigate the impact of H_2 pressure (from 0 to 10 MPa) to the C−O bond cleavage TOF, the product distributions from diphenyl ether were recorded at conversions lower than 15% over Ni/SiO$_2$ at 393 K (**Fig. 3-3a**). In the absence of H_2, diphenyl ether did not react indicating that H_2 is required for both hydrolysis and hydrogenolysis routes. Thus, we conclude that for both reaction pathways the cleavage of the C−O bond is identical in nature and that the difference is primarily related to the availability of H* and OH* and the probability to add to the phenyl radical. With increasing P_{H_2}, the TOFs of diphenyl ether C−O bond cleavage increased to the maxima at 0.6 and 1.0 MPa H_2 attaining 26 and 27 mol $mol_{Ni\ Surf}^{-1}$ h^{-1}, respectively, and then decreased to 17 mol $mol_{Ni\ Surf}^{-1}$ h^{-1} at 10 MPa H_2 (**Fig. 3-3a**). It also showed that the ether cleavage rate under 0.6 MPa H_2 was higher than that at 4.0 MPa, which is also fitted with the kinetic data in **Figs. 3-2a and 3-2b**.
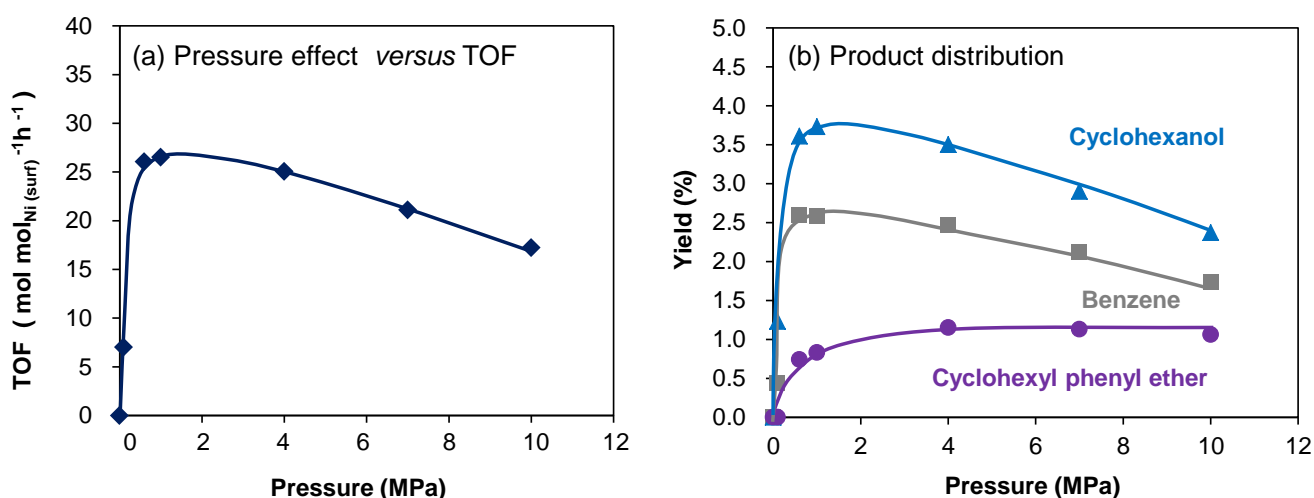
Figure 3-3. (a) TOFs for C−O bond cleavage of diphenyl ether over Ni/SiO$_2$ as a functions of H_2 pressure. Note: TOFs were calculated from the yields of cleaved products at different H_2 pressures. (b) Product distributions from conversion of diphenyl ether (4-O-5) as a function of H_2 pressure. Reaction conditions: reactant (1.70 g, 0.010 mol), 57 wt.% Ni/SiO$_2$ (0.10 g), H_2O (80 mL), 393 K, 30 min., stirring at 700 rpm.

Thus the H_2 competes with the organic reactant for adsorption sites and the rate-determining step was the C−O bond cleavage on Ni and not adsorption or desorption. Up to medium P_{H_2}, the increasing surface coverage by H* leads to an increased hydrogenolysis rate, while at high P_{H_2}, the rate is reduced due to the deficiency of DPE. **Fig. 3-3a** represents a typical change in the hydrogenolysis rate of diphenyl ether as a function of hydrogen pressure. With the increase of P_{H_2}, the selectivity for hydrogenated single aromatic-ring products increased from 0 to 20% (**Fig. 3-3b**), demonstrating that hydrogenation competes with hydrogenolysis on the Ni sites and higher H_2 pressure favored the hydrogenation of a single aromatic ring of diphenyl ether. The cyclohexanol yield increased to a maximum value at 0.6 MPa H_2 and then decreased as P_{H_2} further increased to 10 MPa. In accordance with the earlier observation in the kinetics of diphenyl ether conversion (**Fig. 3-2**), the ratio of cyclohexanol to benzene exceeded unity, confirming again the existence of a hydrolysis route for diphenyl ether cleavage.

3.3.2.2 Impact of catalyst support

To explore the effect of support, 20 wt.% of Ni was supported onto SiO_2, Al_2O_3 or ZrO_2 by the same incipient impregnation method. Reactions were carried out at identical conditions (393 K, 0.6 MPa H_2) for 1.5 h. In the blank tests with no catalyst or SiO_2 in the aqueous phase diphenyl ether was unreactive at 393 K. Even at 523 K diphenyl ether was unconverted. In contrast, benzyl phenyl ether was hydrolyzed by the hydronium ions in the water at 523 K [25]. Diphenyl ether was not hydrolyzed because of the C−O bond dissociation energy of diphenyl ether is almost 100 $kJ \cdot mol^{-1}$ higher compared to that of benzyl phenyl ether (314 $kJ \cdot mol^{-1}$ and 218 $kJ \cdot mol^{-1}$, respectively). The yields for diphenyl ether C−O bond cleaved products were 4.6%, 1.8%, and 2.8%, and TOFs were 6.4, 5.7, and 10.5 $mol \cdot mol_{Ni\ Surf}^{-1} \cdot h^{-1}$ over Ni/SiO_2, Ni/Al_2O_3, and Ni/ZrO_2 catalysts, respectively. The comparable TOFs on three oxides supported Ni catalysts show that these three supports have only a modest effect on the rates, and the heterogeneous Ni particles on the support were the active sites for cleaving the C−O bond of diphenyl ether. In the following work, Ni/SiO_2 was selected as the representative catalyst for further investigation.

Table 3-2. Data on C−O bond cleavage of diphenyl ether with Ni based catalysts.

Catalyst	Conv. (%)	Yield $_{C-O\ cleavage}$ (%)	Rate $_{C-O\ cleavage}$ (mol $\cdot$ mol$_{Ni}^{-1}$ h^{-1})	TOF $_{C-O\ cleavage}$ (mol $\cdot$ mol$_{Ni\ surf}^{-1}$ h^{-1})
None	0	0	0	0
SiO$_2$	0	0	0	0
Ni/SiO$_2$	4.9	4.6	0.30	6.4
Ni/Al$_2$O$_3$	2.1	1.8	0.12	5.7
Ni/ZrO$_2$	3.1	2.8	0.18	10.5

Conditions: diphenyl ether (1.70 g), H$_2$O (80 mL), catalyst (20 wt.% Ni, 0.30 g), 393 K, 0.6 MPa H$_2$, 90 min., stirring at 700 rpm. The Ni dispersions for Ni/SiO$_2$, Ni/Al$_2$O$_3$, and Ni/ZrO$_2$ were 4.7%, 2.1%, 1.7%, respectively, by H$_2$ chemisorption.

3.3.3 The kinetics and mechanism of conversion of di-*p*-tolyl ether over Ni/SiO$_2$ in the aqueous phase
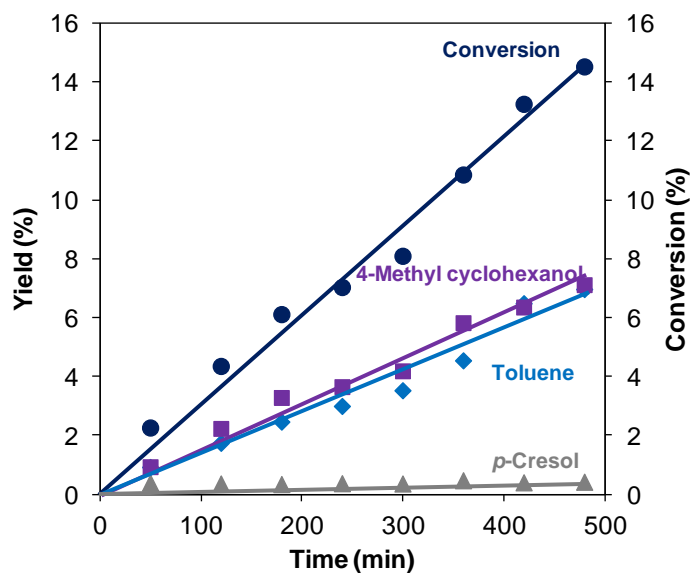
Figure 3-4. Di-*p*-Tolyl ether conversion over Ni/SiO$_2$ in the aqueous phase. Reaction conditions: Di-*p*-tolyl ether (1.98 g), H$_2$O (80 mL), 57 wt.% Ni/SiO$_2$ (0.30 g), 393 K, 0.6 MPa H$_2$, stirring at 700 rpm.

p-Dimethyl and *p*-dihydroxyl- substituted diphenyl ethers were also studied in order to elucidate the influences of the para-substituent on the C−O bond cleavage of diaryl ethers at the selected conditions (393 K, 0.6 MPa H_2). As shown in **Fig. 3-4**, 4-methylcyclohexanol and toluene were two major products from di-*p*-tolyl ether conversion. Trace amount of *p*-cresol (yield < 1%) was formed during the conversion. Because no partially hydrogenated product was detected, significant aromatic ring hydrogenation prior to di-*p*-tolyl ether scission was excluded. The hydrogenolysis route dominated, producing toluene and *p*-cresol as major products (**Scheme 3-2**). Evidently 4-methylcyclohexanol was rapidly produced from *p*-cresol hydrogenation over Ni/SiO$_2$ at same conditions.
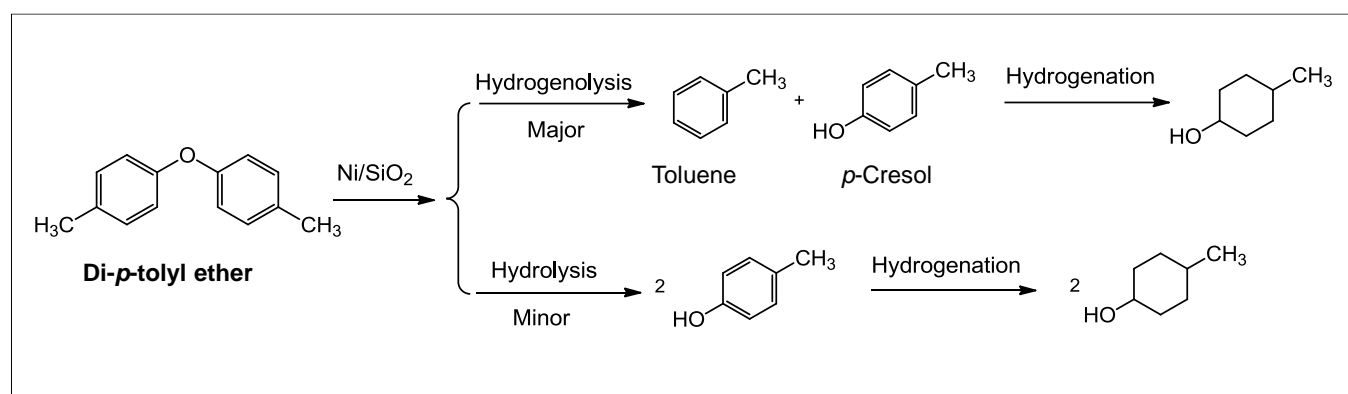
Scheme 3-2. Proposed reaction pathways on di-*p*-tolyl ether conversion on Ni/SiO$_2$ in the aqueous phase.

To test this hypothesis, a separate experiment with *p*-cresol was carried out over Ni/SiO$_2$ at 393 K and 0.6 MPa H_2 (**Fig. 3-5**). Shown from the plotted conversion data, *p*-cresol was hydrogenated to 4-methyl cyclohexanol with a selectivity exceeding 95%. The hydrogenolysed product toluene was less than 5%. *p*-Cresol was selectively hydrogenated, but not hydrogenolysed, with a rate (TOF = 100 mol $mol_{Ni\ Surf}^{-1}$ h^{-1}) being two orders of magnitude faster than the rate for cleaving the C−O bond of di-*p*-tolyl ether (1.3 h^{-1}). Thus 4-methyl cyclohexanol was the major product on di-*p*-tolyl ether conversion. The second point is that Ni/SiO$_2$ catalyzed not only hydrogenolysis of the C−O bond of di-*p*-tolyl ether, and it catalyzed also the hydrogenation of the aromatic ring of *p*-cresol at identical conditions, demonstrating that hydrogenation and

hydrogenolysis were competing on the metal sites. Such competition can be influenced by subtle modifications of the catalytic environment including temperature, pressure, and solvent. Under our conditions, the low temperature and pressure (393 K, 0.6 MPa H_2) favored the selective hydrogenolysis of the C−O bond of diaryl ether, because the hydrogenation rate of the aromatic rings of the phenolic dimer was relatively slow. On the other hand, the energy barrier for the phenolic monomer hydrogenation over Ni sites is much lower [26] than for direct cleaving of the phenolic C_{aryl}–OH group [15].

In summary, the C−O bond cleavage of di-*p*-tolyl ether over Ni/SiO$_2$ at 393 K in the aqueous phase favors a selective hydrogenolysis route, differing from diphenyl ether which is converted by parallel hydrogenolysis and hydrolysis pathways with a rate ratio of 3:2. Di-*p*-tolyl ether is hydrogenolysed over Ni/SiO$_2$ to produce toluene and *p*-cresol as initial products, and *p*-cresol rapidly hydrogenated to 4-methyl cyclohexanol. TOF of C−O bond cleavage of di-*p*-tolyl ether (1.3 mol $\cdot$mol$_{Ni\ Surf}^{-1}$ h^{-1}) was only one twentieth of diphenyl ether (26 mol $\cdot$mol$_{Ni\ Surf}^{-1}$ h^{-1}).
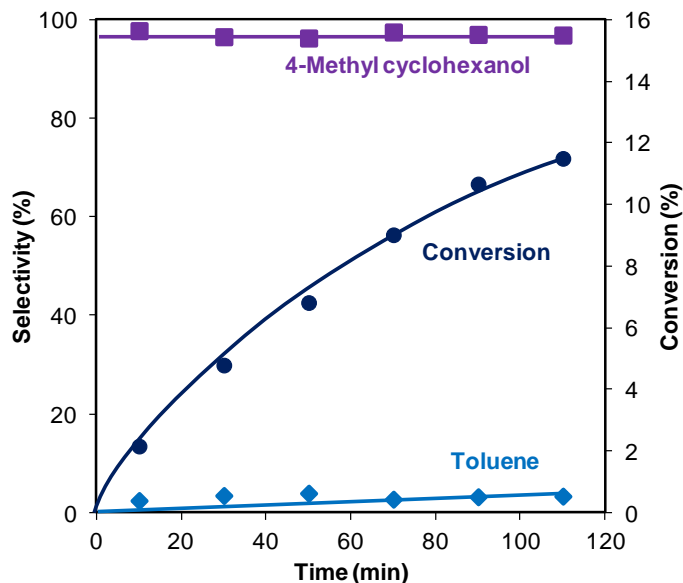
Figure 3-5. Kinetics of *p*-cresol conversion over Ni/SiO$_2$ in the aqueous phase. Reaction conditions: *p*-Cresol (2.16 g), H_2O (80 mL), 57 wt.% Ni/SiO$_2$ (0.05 g), 393 K, 0.6 MPa H_2, stirring at 700 rpm.

3.3.4 The kinetics and mechanisms of conversion of 4,4'-dihydroxydiphenyl ether over Ni/SiO$_2$ in the aqueous phase

With conversion of *p*-substituted 4,4'-dihydroxydiphenyl ether at 393 K and 0.6 MPa H$_2$ the chemistry for breaking the ether C−O bond becomes more complex. Phenol, hydroquinone, and single ring hydrogenated products were initial major products. The yield of hydroquinone increased to the maximum of 10% at 40 min., and then decreased to 1% at 80 min. (**Fig. 3-6**). The yield sum of phenol, cyclohexanone, and cyclohexanol increased dramatically with time and exceeded 85% at 1.33 h. This is difficult to rationalize, because the yield of hydroquinone should be equal to or higher than that of phenol/cyclohexanol (**Scheme 3-3**), no matter which route of hydrogenolysis, hydrolysis or partial hydrogenation-hydrogenolysis it follows. The first and third routes afford equal concentrations of hydroquinone and phenol/cyclohexanol, while the second route provides two moles of hydroquinone. It is presumed that the produced hydroquinone was rapidly hydrogenolysed to phenol, which would lower the hydroquinone concentrations relative to phenol/cyclohexanol. A study on hydroquinone conversion using Ni/SiO$_2$ was conducted in the aqueous phase at 393 K (**Fig. 3-7**).
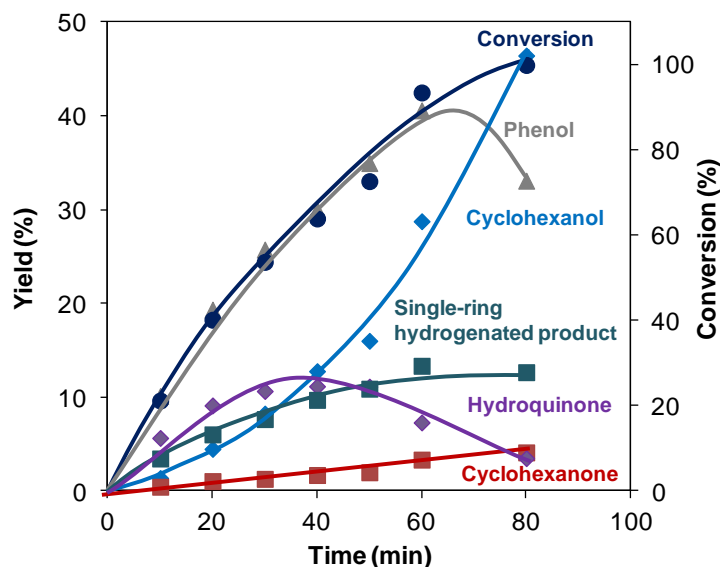
Figure 3-6. 4,4'-Dihydroxydiphenyl ether conversion over Ni/SiO$_2$ in the aqueous phase. Reaction conditions: 4,4'-Dihydroxydiphenyl ether (2.02 g), H$_2$O (80 mL), 57 wt.% Ni/SiO$_2$ (0.30 g), 393 K, 0.6 MPa H$_2$, stirring at 700 rpm.
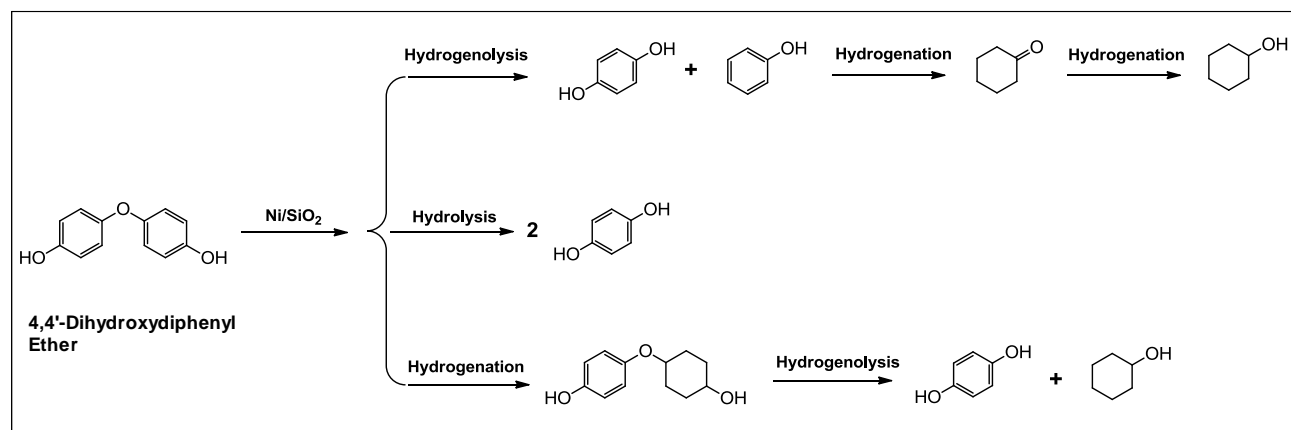
Scheme 3-3. Proposed reaction pathways of 4,4'-dihydroxydiphenyl ether conversion over Ni/SiO$_2$ in the aqueous phase.

In the conversion of hydroquinone versus reaction time shown in **Fig. 3-7**, the hydrogenated cyclohexane-1,4-dione and cyclohexane-1,4-diol and hydrogenolysis product phenol (**Scheme 3-4**) dominated. But three parallel routes might contribute to cyclohexane-1,4-diol formation from

hydrogenation of hydroquinone (**Scheme 3-4**). The first route is via isomerization to cyclohexene-1,4-dione, followed by sequential hydrogenation to cyclohexane-1,4-dione, 4-hydroxyl cyclohexanone, and cyclohexane-1,4-diol. The second one involves partial hydrogenation to cyclohexa-1,5-diene-1,4-diol, which is isomerized to 4-hydroxyclyohex-2-enone, and successive hydrogenation to 4-hydroxyl cyclohexanone and cyclohexane-1,4-diol. The third one includes partial hydrogenation to cyclohexa-1,4-diene-1,4-diol, subsequent isomerization to cyclohexane-1,4-dione, and in turn hydrogenation to 4-hydroxyl cyclohexanone, and cyclohexane-1,4-diol. Since cyclohexane-1,4-dione was the major reaction intermediate during the reaction, the first and third routes were predominant.
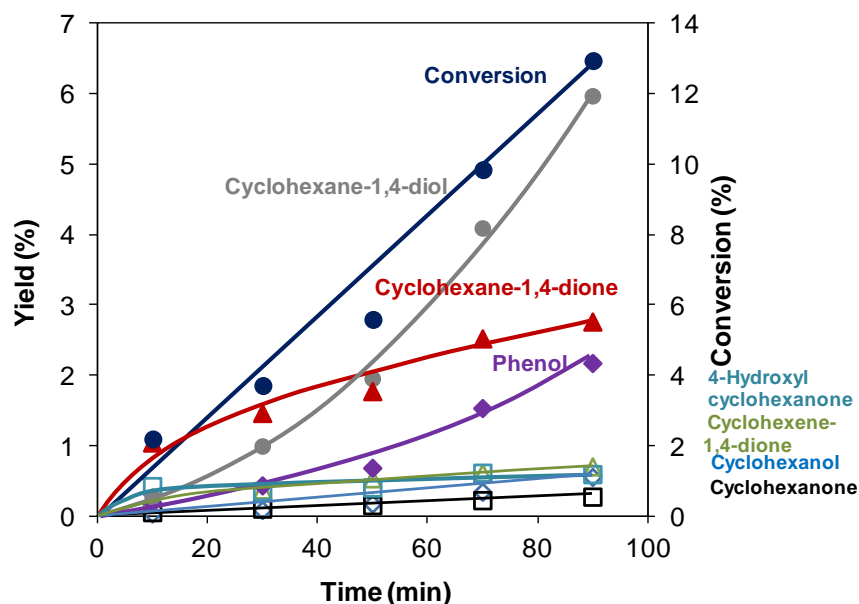
Figure 3-7. Hydroquinone conversion over Ni/SiO$_2$ in the aqueous phase. Reaction conditions: Hydroquinone (2.16 g), H$_2$O (80 mL), 57 wt.% Ni/SiO$_2$ (0.05 g), 393 K, 0.6 MPa H$_2$, stirring at 700 rpm.
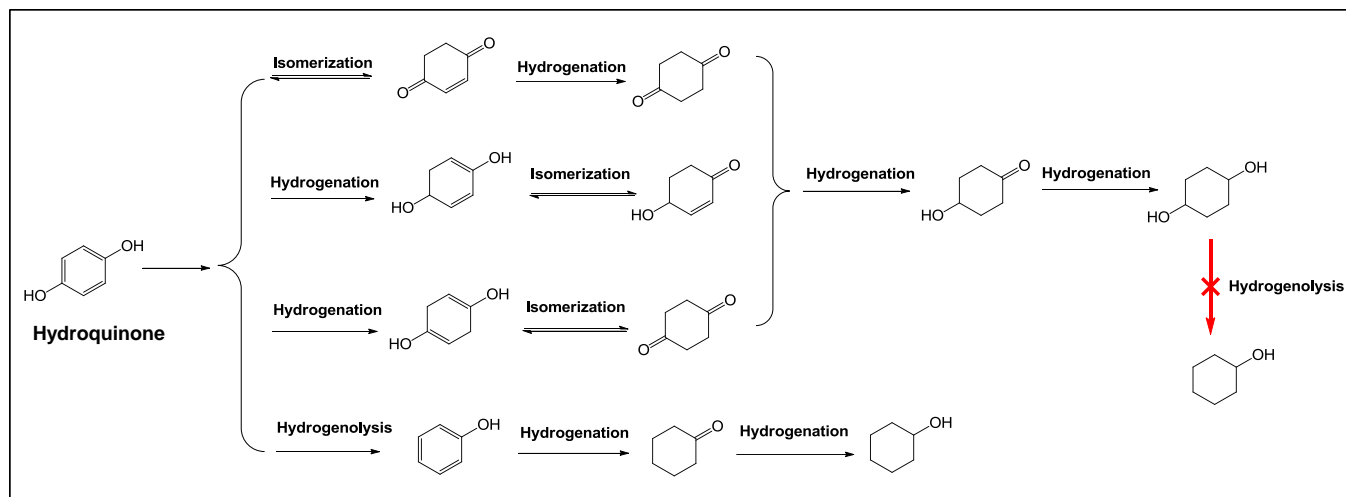
Scheme 3-4. Proposed reaction pathways of hydroquinone conversion on Ni/SiO$_2$ in the aqueous phase.

It is shown in **Fig. 3-7** that cyclohexane-1,4-dione was converted to cyclohexane-1,4-diol. But the sum of hydrogenolysis yields (3%, including phenol, cyclohexanol, and cyclohexanone) was lower than one third of hydrogenation yield (10%, cyclohexane-1,4-dione, cyclohexane-1,4-diol, and 4-hydroxyl cyclohexanone). Hydrogenation of the aromatic ring was the major reaction pathway for hydroquinone, while C−O hydrogenolysis of hydroquinone was minor and hydrogenolysis of cyclohexane-1,4-diol did not occur over Ni/SiO$_2$ at these conditions. This kinetics study also implies that intermediate phenol via hydrogenolysis of hydroquinone is in a very minor part of conversion over Ni/SiO$_2$ during 4,4'-dihydroxydiphenyl ether conversion.

We infer a mechanism for 4,4'-dihydroxydiphenyl ether conversion on Ni/SiO$_2$, as shown in **Scheme 3-5**. This two-step mechanism involves sequential cleavage of the ether C−O bonds on a metal site. The three O atoms in the adsorbate can be accommodated on the large Ni particle using two Ni sites, and H$_2$ is also dissociated on the Ni sites. In the second step the C−O ether bond was cleaved to HOC$_6$H$_4$* and OC$_6$H$_4$OH* adsorbed on the Ni surface. OC$_6$H$_4$OH* adsorbs more strongly than HOC$_6$H$_4$* onto the Ni sites due to the two oxygen atoms [27], so that OC$_6$H$_4$OH* is retained at the surface and HOC$_6$H$_4$* combines with H* to desorb as phenol.
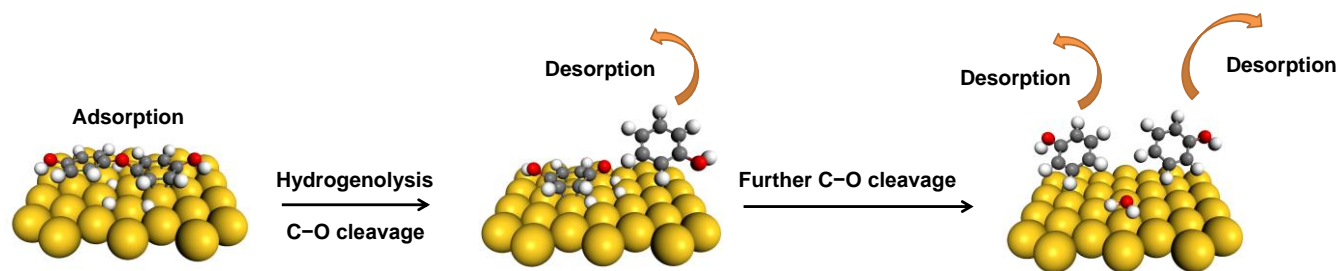
Scheme 3-5. Proposed surface reactions on 4,4'-dihydroxydiphenyl ether conversion to two moles phenol and one mole water molecules over Ni/SiO$_2$.

In the surface reaction, OC$_6$H$_4$OH* can be further cleaved to phenol and H$_2$O. Two moles of phenol are thus formed. But during quenching of the batch reactor surface OC$_6$H$_4$OH* may combine with H* to form hydroquinone. The produced hydroquinone intermediate is in a small part converted to cyclohexane-1,4-diol. The adsorbed OC$_6$H$_4$OH* is reactive, but the transformation of OC$_6$H$_4$OH* to hydroquinone is irreversible. In summary, 4,4'-dihydroxydiphenyl ether is hydrogenolyzed to phenol and OC$_6$H$_4$OH* in the first step, and OC$_6$H$_4$OH* is further cleaved to phenol and H$_2$O in the second step.

3.3.5 DFT modeling results on 4,4'-dihydroxydiphenyl ether conversion over Ni/SiO$_2$ [*]

(a) HOC$_6$H$_4$OC$_6$H$_4$OH* + 2H*

(b) HOC$_6$H$_4$* + OC$_6$H$_4$OH* + 2H*

(c) HOC$_6$H$_5$* + OC$_6$H$_4$OH* + H*

(d) HOC$_6$H$_4$* + O* + C$_6$H$_4$OH* + 2H*

(e) HOC$_6$H$_4$* + HOC$_6$H$_4$OH* + H*

(f) HOC$_6$H$_5$* + C$_6$H$_4$OH* + O* + H*

(g) HOC$_6$H$_5$* + C$_6$H$_5$OH* + O*
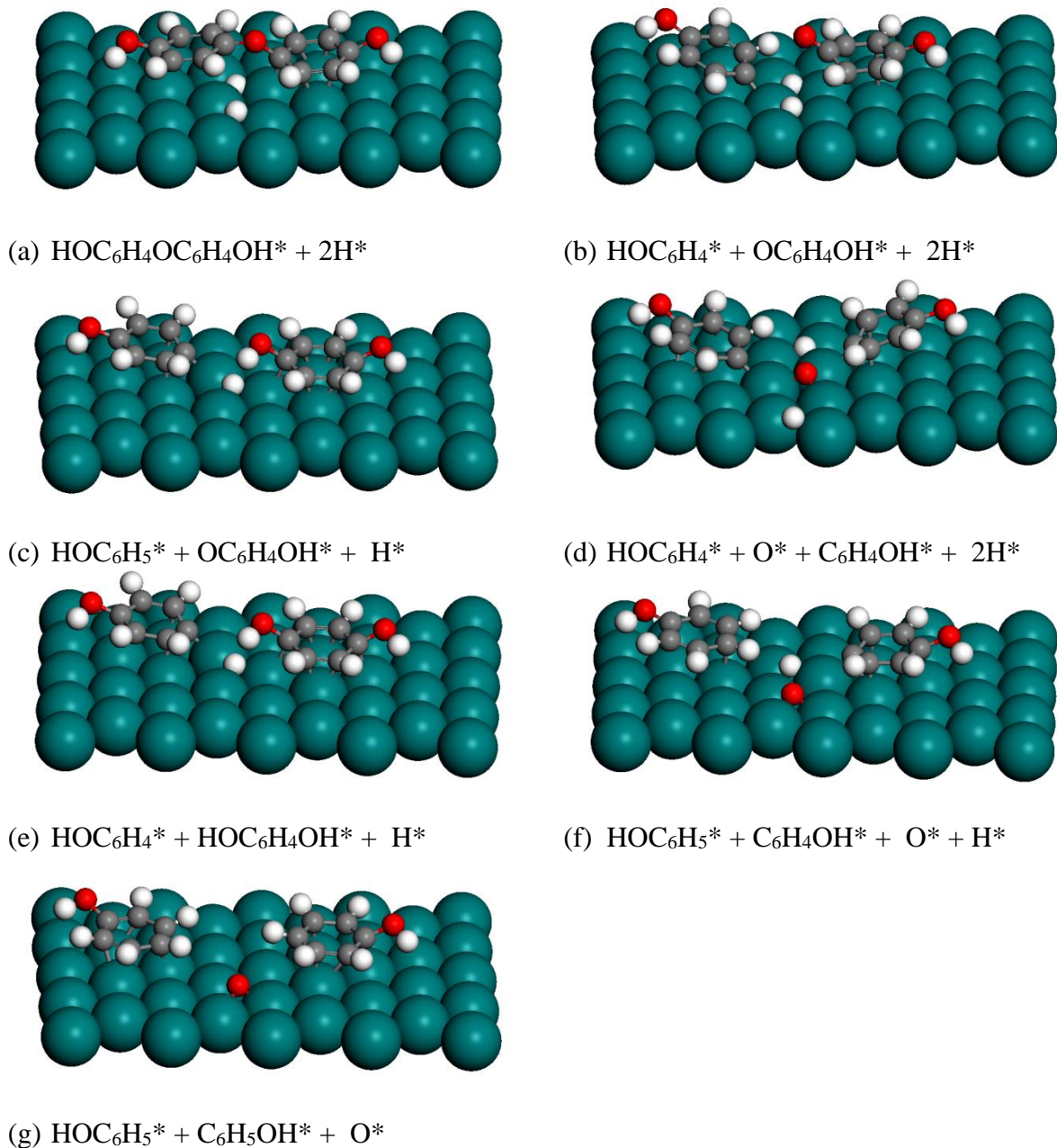
Figure 3-8. DFT calculated reaction intermediate configurations in the 4,4'-dihydroxydiphenyl ether conversion on the Ni (111) surface.

[*] *DFT calculations had been done by Dr. Donghai Mei in PNNL.*
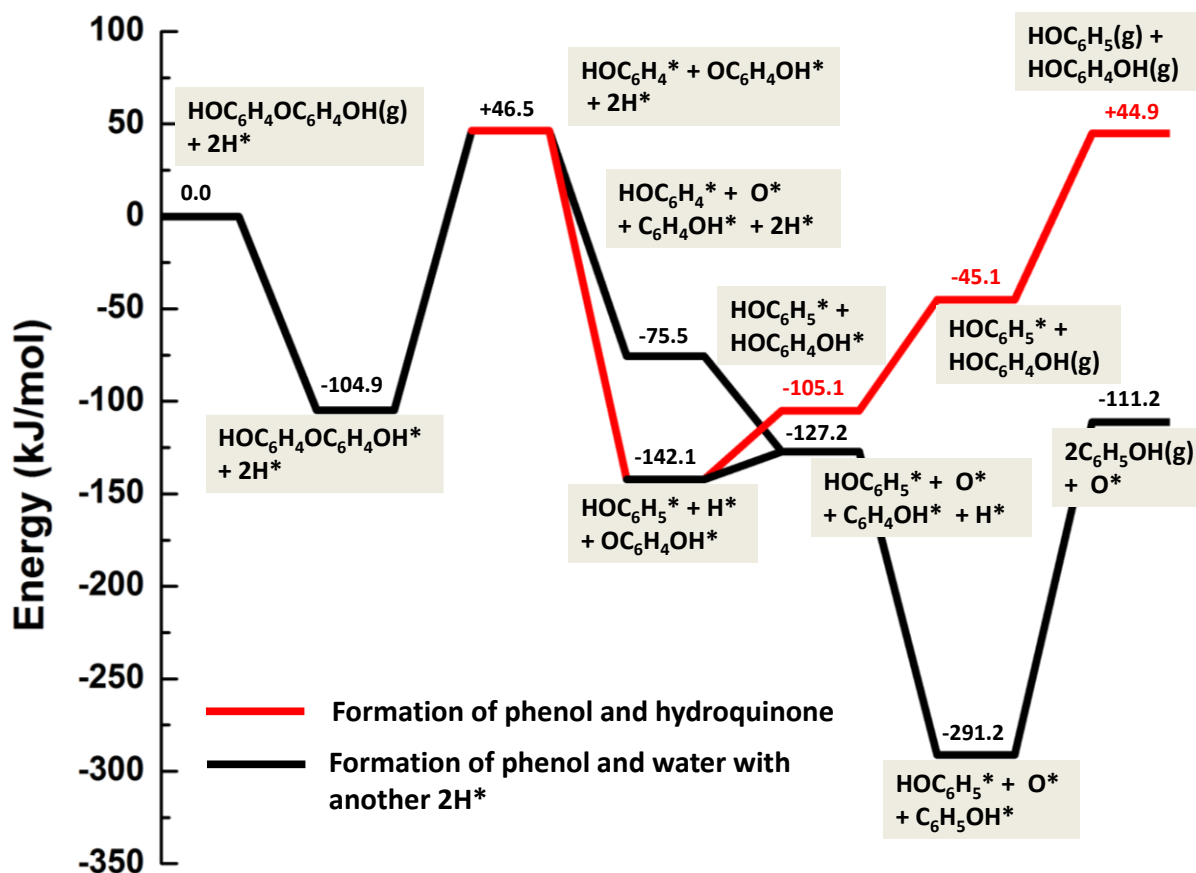
Figure 3-9. DFT calculated energy profile of the 4,4'-dihydroxydiphenyl ether conversion on the Ni (111) surface in the presence of atomic hydrogen from H_2 dissociation. The numbers listed in the figure are the energy values relative to the Ni (111) surface with two pre-adsorbed hydrogen atoms and 4,4'-dihydroxydiphenyl ether in the vacuum.

To test whether the C−O bond cleavage occurred on the surface, DFT calculation was performed on 4,4'-dihydroxydiphenyl ether conversion on the Ni (111) surface. Starting with two H* on the Ni (111) surface, our calculations showed that the most stable adsorption mode for 4,4'-dihydroxydiphenyl ether was co-planar adsorption with both phenolic rings bonding to the surface with an adsorption energy of -104.9 kJ·mol⁻¹ (**Fig. 3-9**). As shown in **Fig. 3-9**, the first C−O bond

scission of 4,4'-dihydroxydiphenyl ether led to the endothermic formation of HOC_6H_4* and OC_6H_4OH* intermediates, with a reaction energy change ΔG^0 of +151.4 kJ·mol^{-1}. Then the OC_6H_4OH* intermediate was converted to C_6H_4OH* via the second C−O bond breaking (configurations **b** to **d** in **Fig. 3-8**). In addition, the HOC_6H_4* with H* formed phenol (configurations **b** to **c** in **Fig. 3-8**). The calculation indicated that the phenol formation step from HOC_6H_4* (-188.6 kJ·mol^{-1}) is thermodynamically more favorable than the second C−O bond cleavage step on HOC_6H_4O* (-122.0 kJ·mol^{-1}). This is consistent with our experimental observation in **Fig. 3-6** that phenol is the major initial product in 4,4'-dihydroxydiphenyl ether conversion. In a similar way, hydroquinone (HOC_6H_4OH) could also be produced via H* addition to OC_6H_4OH* intermediate. The formation of hydroquinone on the surface was endothermic with ΔG^0 of +37.0 kJ·mol^{-1} (from -142.1 to -105.1 kJ·mol^{-1}), while the second C−O bond cleavage of OC_6H_4OH* was less endothermic with ΔG^0 of +14.9 kJ·mol^{-1} (from -142.1 to -127.2 kJ·mol^{-1}) on the Ni (111) surface. This implies that the formation of hydroquinone is only a minor reaction path in the 4,4'-dihydroxydiphenyl ether conversion (red line in **Fig. 3-9**), but the subsequent C−O bond cleavage of OC_6H_4OH* forming O* and C_6H_4OH* plays a major role (black line in **Fig. 3-9**). Apparently 4,4'-dihydroxydiphenyl ether undergoes first cleavage of ether C−O bond to form HOC_6H_4* (phenol precursor), and then the OC_6H_4OH* residue suffers C−O bond cleavage to produce C_6H_4OH* and O* on the Ni/SiO$_2$ catalyst. This mechanism therefore explains the abundance of phenol (or cyclohexanol) formation from 4,4'-dihydroxydiphenyl ether shown at **Fig. 3-6**.

The question now may arise, as to why it was found impossible to cleave the C−O bonds in phenol and *p*-cresol (intermediates from diphenyl ether and di-*p*-tolyl ether conversion) to form benzene and toluene under the reaction conditions chosen. The absence of these products has been rationalized by several reasons. On the one hand, the DFT calculated reaction energy of C_6H_5OH* → C_6H_5* + OH* is +124.2 kJ·mol^{-1} (endothermic), which is higher than the phenol adsorption heat of 93.4 kJ·mol^{-1} on the Ni (111) surface. This suggests that the produced phenol will desorb from the surface instead of undergoing C−O bond scission. On the other hand, the generated C_6H_5O*, which is formed from the first C−O bond scission of diphenyl ether, will quickly combine with the H* forming C_6H_5OH*. This step is exothermic (-13 kJ·mol^{-1}). In a comparison, the step
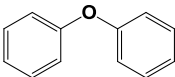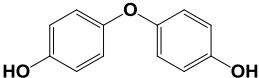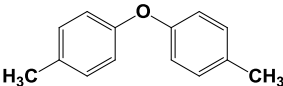
of $C_6H_5O^* \rightarrow C_6H_5^* + O^*$ is highly endothermic (70.2 kJ·mol^{-1}). Therefore, we conclude that benzene formation via the further C−O bond cleavage of phenol or $C_6H_5O^*$ species is not feasible. Similarly, although the DFT calculated reaction energy of $CH_3C_6H_4OH^* \rightarrow CH_3C_6H_4^* + OH^*$ is less endothermic (+33.3 kJ·mol^{-1}) than the *p*-cresol desorption energy of 86.5 kJ·mol^{-1}, and the kinetic activation barrier for the C−O bond-breaking is calculated to be 125.4 kJ·mol^{-1}, implying that the *p*-cresol will desorb from the catalyst surface rather than have the C−O bond cleaved. Therefore, based on DFT calculation benzene and toluene are not expected to be produced by a further cleavage of C−O bond of phenol and *p*-cresol in reactions of di-*p*-tolyl ether and diphenyl ether conversion, which is in good agreement with our experimental results.

3.3.6 The comparison of initial TOF and E_a of three diaryl ethers over Ni/SiO₂ in the aqueous phase

The initial TOFs and apparent activation energies E_a for C−O bond cleavage are compiled in **Table 3-3**. The TOF of 4,4'-dihydroxydiphenyl ether (69 mol·mol$_{Ni\ Surf}^{-1}$ h^{-1}) was two times higher than that of diphenyl ether (26 mol·mol$_{Ni\ Surf}^{-1}$ h^{-1}). This result agrees well with the observation of Siskin et al. [9] who reported that hydroxyl substituted diphenyl ether was much more reactive than diphenyl ether. This may be because the two hydrophilic hydroxyl groups in 4,4'-dihydroxydiphenyl ether can greatly enhance its solubility in water and the adsorption capability on the metal site [8]. TOF of diphenyl ether (26 mol·mol$_{Ni\ surf}^{-1}$·h^{-1}) was twenty times higher than that of di-*p*-tolyl ether (1.3 mol·mol$_{Ni\ surf}^{-1}$·h^{-1}). This associates with the fact that hydrophobic methyl group may reduce the solubility of di-*p*-tolyl ether in water and hinder the adsorption on the catalyst surface due to steric effects. Different substituents on diaryl ethers lead to different pathways for cleaving ether C−O bonds over Ni/SiO₂, that is, hydrogenolysis for di-*p*-tolyl ether, hydrogenolysis combined with hydrolysis for diphenyl ether, and sequential surface hydrogenolysis conversion for 4,4'-dihydroxydiphenyl ether. In addition, phenol as the primary product was not observed in diphenyl ether conversion, because the forward phenol hydrogenation rate constant (13000 mol$_{Ni\ surf}^{-1}$·h^{-1}) was much faster than the ether cleavage rate constant (2600 mol$_{Ni\ surf}^{-1}$·h^{-1}) over Ni/SiO₂ in the aqueous phase at 393 K. Phenol, however, appeared in 4,4'-

dihydroxydiphenyl ether conversion, as phenol formation rate constant (13800 $mol_{Ni\,surf}^{-1} \cdot h^{-1}$) was comparable to the phenol consumption rate constant (13000 $mol_{Ni\,surf}^{-1} \cdot h^{-1}$) at identical conditions.

Table 3-3. Kinetics data on conversion of three diaryl ethers over 57 wt.% Ni/SiO_2 in the aqueous phase.

Reactant	Initial TOF [a] $(mol \cdot mol_{Ni\,surf}^{-1} \cdot h^{-1})$	E_a $(kJ \cdot mol^{-1})$ [b]
	26	98
	69	93
	1.3	105

[a] Initial C-O cleavage rates are obtained from the kinetics data. [b] E_a data are determined from Figure 3-10.

81
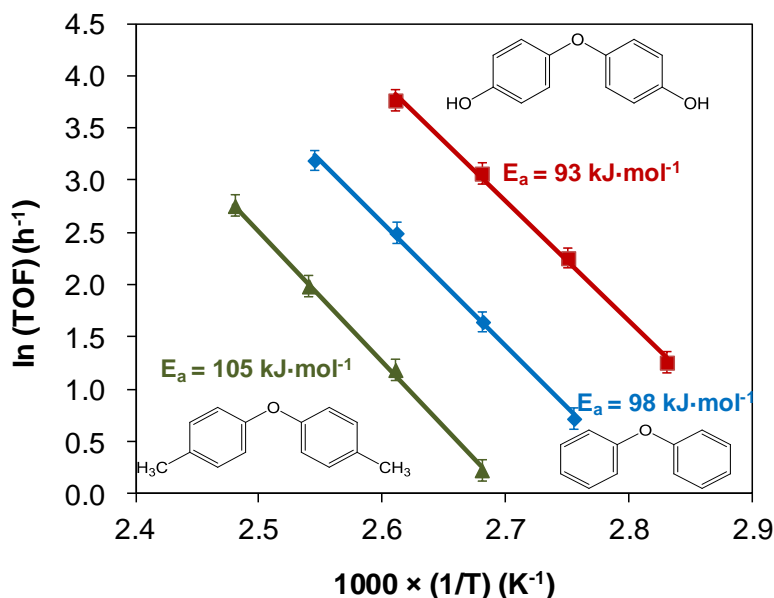
Figure 3-10. Arrhenius plots on three diaryl ether compounds at temperature range of 363 to 403 K. Reaction conditions: H_2O (80 mL), 0.6 MPa H_2, 57 wt.% Ni/SiO_2 (0.30 g), stirring at 700 rpm, with 4,4'-dihydroxydiphenyl ether (2.02 g) at 10 min; di-*p*-tolyl ether (1.98 g) at 50 min; diphenyl ether (1.70 g) at 50 min.

Apparent activation energies are obtained from the Arrhenius plots on three diaryl ether compounds in **Fig. 3-10**. TOFs of three diaryl ethers with Ni/SiO_2 in water follow the order of 4,4'-dihydroxydiphenyl ether > diphenyl ether > di-*p*-tolyl ether throughout the range of temperatures examined (363 – 403 K). The sequence of apparent activation energies (E_a) was 4,4'-dihydroxydiphenyl ether (93 kJ·mol⁻¹) < diphenyl ether (98 kJ·mol⁻¹) < di-*p*-tolyl ether (105 kJ·mol⁻¹).

The apparent activation energy can be expressed by equation [28] (1):

$$E_a^{obs} = E_a^{true} + (1- \theta_A) \Delta H_A + (1- \theta_B) \Delta H_B \qquad (1)$$

Where E_a^{obs}, E_a^{true}, θ_A, θ_B, ΔH_A, and ΔH_B represent the observed activation energy, the true activation energy, the coverage by diaryl ethers, the coverage by H^*, as well as the adsorption heat of diaryl ethers, and adsorption heat of H^*, respectively.

Concerning the range of apparent activation energies, the introduction of an electron donating −CH$_3$ group in para- position slightly strengthens the ether C−O bond, while the addition of the more electronegative −OH weakens the ether C−O bond compared to diphenyl ether. For example, the required energy for breaking C−O bonds of substituted PhO−CH$_3$ follows (p-CH$_3$)-PhO−CH$_3$ (273 kJ·mol^{-1}) > PhO−CH$_3$ (268 kJ·mol^{-1}) > (p-OH)-PhO−CH$_3$ (243 kJ·mol^{-1}) [4]. Thus, the C−O bond cleavage barrier (true activation energy) is expected to be of the order E$_a$^{true} (4,4'-dihydroxydiphenyl ether) < E$_a$^{true} (diphenyl ether) < E$_a$^{true} (di-p-tolyl ether), on consideration that C−O bond cleavage is the rate-determining step for conversion of three diaryl ethers. On the second point, the −CH$_3$ substitution on diphenyl ether may reduce the heat of adsorption ΔH$_A$, because steric hindrance and hydrophobic properties of methyl group will decrease the interactions with the aromatic rings for di-p-tolyl ether in the water, while the presence of two −OH groups in 4,4'-dihydroxydiphenyl ether strengthens the interactions with the Ni (111) surface. Thus, the absolute values of adsorption heats for three ethers on Ni/SiO$_2$ in the aqueous phase are inferred to decrease in the order ΔH$_A$ (4,4'-dihydroxydiphenyl ether) > ΔH$_A$ (diphenyl ether) > ΔH$_A$ (di-p-tolyl ether). Our DFT modeling result strongly supports this hypothesis. It shows that with one water molecule adsorbed, the absolute values of adsorption energies for three ethers on the Ni (111) surface follow the order ΔH$_{A. Cal.}$ (4,4'-dihydroxydiphenyl ether, - 271 kJ·mol^{-1}) > ΔH$_{A. Cal.}$ (diphenyl ether, - 244 kJ·mol^{-1}) > ΔH$_{A. Cal.}$ (di-p-tolyl ether, - 169 kJ·mol^{-1}) (see **Fig. 3-11**). With the overall reaction being first order as well as θ$_A$, θ$_B$ and ΔH$_B$ being comparable for three ethers, equation (1) implies that E$_a$ (di-p-tolyl ether) > E$_a$ (diphenyl ether) > E$_a$ (4,4'-dihydroxydiphenyl ether), which is perfectly in agree with the experimental data shown in **Fig. 3-10**.

| Diphenyl ether | 4,4'-Dihydrophenyl ether | Di-p-tolyl ether |

Adsorption heat: -244 kJ·mol^{-1} Adsorption heat: -271 kJ·mol^{-1} Adsorption heat: -169 kJ·mol^{-1}
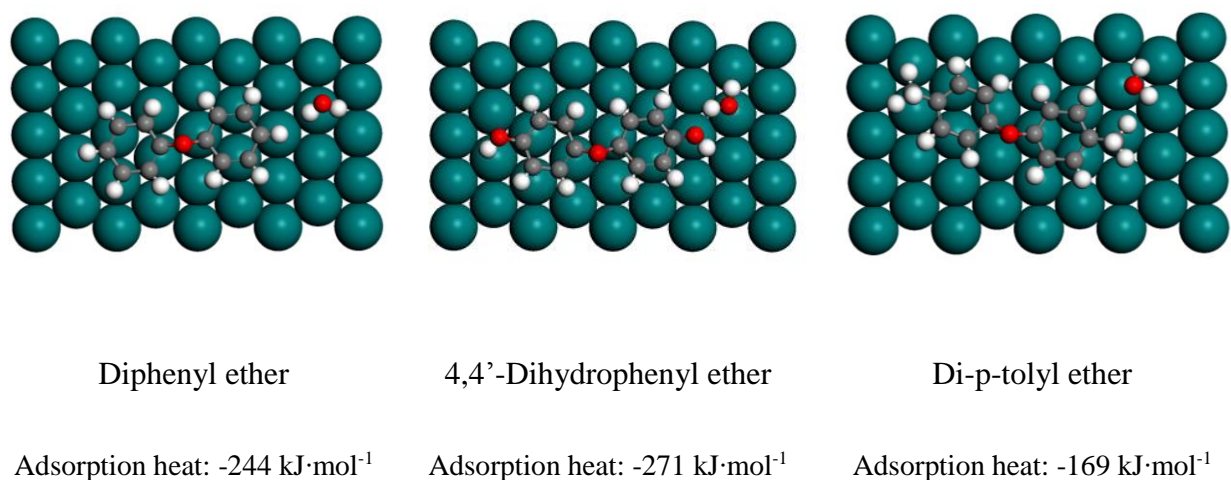
Figure 3-11. The energies of adsorption calculated by DFT modeling for adsorbing three ethers and one water molecule onto Ni (111) surface.

3.4 Conclusions

A mild route (393 K, 0.6 MPa H_2) for cleaving over Ni/SiO$_2$ the ether C−O bonds of three *p*-di-substituted H−, CH$_3$−, and OH− diphenyl ethers has been developed. The choice of SiO$_2$, Al$_2$O$_3$, or ZrO$_2$ to support the Ni had a small influence on the cleavage rate of the C−O bond of diphenyl ether. The C−O bond of diphenyl ether was cleaved by the parallel hydrogenolysis and hydrolysis routes on Ni sites. The influence of H_2 pressure indicates that the rate-determining step is the C−O bond cleavage but not adsorption or desorption on Ni, thus the H_2 competed with the organic reactant for adsorption sites which leads to a maximum rate at H_2 pressure of 0.6 MPa at 393 K. In contrast to diphenyl ether, hydrogenolysis was the exclusive route for cleaving the ether C−O bond of di-*p*-tolyl ether producing *p*-cresol and toluene. The sequential surface C−O bond hydrogenolysis contributed to 4,4'-dihydroxydiphenyl ether conversion, that is, it was first cleaved to phenol and OC$_6$H$_4$OH*, then further cleaved to phenol (H* added to C$_6$H$_4$OH*) and H_2O (2 H* added to O*) in the second step. DFT calculations confirmed this sequential C−O bond cleavage mechanism of 4,4'-dihydroxydiphenyl ether occurring on the surface of Ni. TOFs of three diaryl ethers with Ni/SiO$_2$ in water followed the order 4,4'-dihydroxydiphenyl ether (69 mol·mol$_{Ni surf}$$^-$

$^{1}\cdot h^{-1}$) > diphenyl ether (26 mol·mol$_{Ni\ surf}^{-1}\cdot h^{-1}$) > di-$p$-tolyl ether (1.3 mol·mol$_{Ni\ surf}^{-1}\cdot h^{-1}$), and in an accordance the sequence of apparent activation energies (E_a) follow 4,4'-dihydroxydiphenyl ether (93 kJ·mol^{-1}) < diphenyl ether (98 kJ·mol^{-1}) < di-p-tolyl ether (105 kJ·mol^{-1}). The lowered activation energy for 4,4'-dihydroxydiphenyl ether is attributed to the presence of two –OH groups strengthening the interaction with Ni (111) surface, leading to a much lower absolute value of the adsorption heat, which is verified by the DFT modeling investigation.

3.5 Acknowledgements

3.6 Appendix

Table S3-1. Hydrogenation of aromatic compounds on Ni/SiO$_2$ in aqueous-phase at 393 K.[a]

Entry	Reactant	Catalyst amount (g)	Conv. (%)	TOF (mol $\cdot$ mol$_{Ni\ surf}^{-1}$ h^{-1})
1	Phenol	0.03	15	130
2	Benzene	0.30	3.4	2.9

[a] Reaction conditions: reactant (0.010 mol), H$_2$O (80 ml), 0.6 MPa H$_2$, 50 min, stirring at 700 rpm.

Table S3-2. The rates for C-O bond cleavage of diphenyl ether (4-O-5), cyclohexyl phenyl ether, and dicyclohexyl ether at 393 K.[a]

Reactant	Selectivity (%)			Conv. (%)	Initial TOF (mol $\cdot$ mol$_{Ni\ surf}^{-1}$ h^{-1})
	Benzene	Cyclohexanol	CPE [b]		
	27	57	16	80	26
	32	68	-	2.1	0.8
	0	0	0	0	0

[a] Reaction conditions: reactant (0.010 mol), Ni/SiO$_2$ (57 wt. %, 0.30 g, 2.91 ×10^{-3} mol Ni), H$_2$O (80 ml), 0.6 MPa H$_2$, 110 min, stirring at 700 rpm. [b] CPE: Cyclohexyl phenyl ether.

Figure S3-1. ^{13}C NMR spectrum of dicyclohexyl ether.
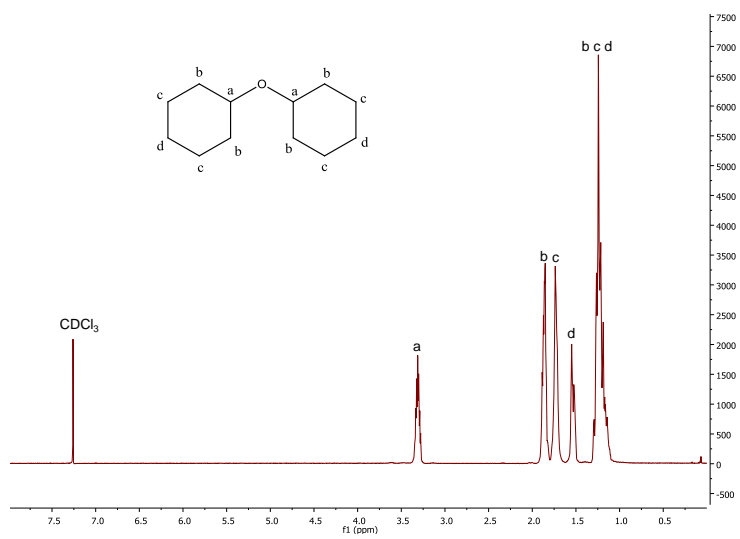
Figure S3-2. ^{1}H NMR spectrum of dicyclohexyl ether.

3.7 Reference

[1]   M. Stöcker, Angew. Chem. Int. Ed. 47 (2008) 9200.

[2]   W. Boerjan, J. Ralph, M. Baucher, Ann. Rev. Plant Biol. 54 (2003) 519.

[3]   J. Zakzeski, P. C. A. Bruijnincx, A. L. Jongerius, B. M. Weckhuysen, Chem. Rev. 110 (2010) 3552.

[4]   Y.R.Luo, Comprehensive Handbook of Chemical Bond Energies; CRC Press; Boca Raton, FL, 2007

[5]   E. Furimsky, Appl. Catal. A. 199 (2000) 147.

[6]   S. H. Townsend, M. A. Abraham, G. L. Huppert, M. T. Klein, S. C. Paspek, Ind. Eng. Chem. Res. 27 (1988) 143.

[7]   M. Siskin, A. R. Katritzky, M. Balasubramanian, Energy Fuels 5 (1991) 770.

[8]   A. R. Katritzky, R. A. Barcock, M. Balasubramanian, J.V. Greenhill, M. Siskin, W. N. Olmstead, Energy Fuels 8 (1994) 487.

[9]   V. M. Roberts, R. T. Knapp, X. Li, J. A. Lercher, ChemCatChem 2 (2010) 1407.

[10]   J. M. L. Penninger, R. J. A. Kersten, H. C. L. Baur, J. Supercritical Fluids 16 (1999) 119.

[11]   J. M. L. Penninger, R. J. A. Kersten, H. C. L. Baur, J. Supercritical Fluids 17 (2000) 215.

[12]   X.Wang, R. Rinaldi, ChemSusChem 5 (2012) 1455.

[13]   A. G. Sergeev, J. F. Hartwig, Science 332 (2011) 439.

[14]   A. G. Sergeev, J. D. Webb, J. F. Hartwig, J. Am. Chem. Soc. 134 (2012) 20226.

[15]   J. He, C. Zhao, J. A. Lercher, J. Am. Chem. Soc. 134 (2012) 20768.

[16]   C. Zhao, J. A. Lercher, Angew. Chem. Int. Ed. 51 (2012) 5935.

[17]   J. VandeVondele, M. Krack, F. Mohamed, M. Parrinello, T. Chassaing, J. Hutter, Comput. Phys. Commun. 167 (2005) 103.

[18]   S. Goedecker, M. Teter, J. Hutter, Phys. Rev. B 54 (1996) 1703.

[19]   C. Hartwigsen, S. Goedecker, J. Hutter, Phys. Rev. B 58 (1998) 3641.

[20]   M. Krack, Theor. Chem. Acc. 114 (2005) 145.

[21]   J. VandeVondele, J. Hutter, J. Chem. Phys. 127 (2007) 114105.

[22]   J.P. Perdew, K. Burke, M. Ernzerhof, Phys. Rev. Lett. 77 (1996) 3865.

[23]   S. Grimme, J. Antony, S. Ehrlich, H. Krieg, J. Chem. Phys. 132 (2010) 154104.

[24]   N. Mahata, K. V. Raghavan, V. Vishwanathan, Catal. Today 49 (1999) 65.

[25]   J. He, L. Lu, C. Zhao, D. Mei, J. A. Lercher, 2013, submitted to J. Catal.

[26]   C. Zhao, S. Kazacov, J. He, J. A. Lercher, J. Catal. 296 (2012) 12.

[27]   C. Zhao, Y. Yu, A. Jentys, J. A. Lercher, Appl. Catal. B 132 − 133 (2013) 282.

[28]   F. Kapteijn, J. A. Moulijn, R. A. van Santen, R. Wever, Stud. Surf. Sci. Catal. 123 (1999) 81.

Chapter 4

Mechanisms of Catalytic Cleavage of Benzyl Phenyl Ether in Aqueous and Apolar Phases

Catalytic pathways for the cleavage of ether bonds in benzyl phenyl ether (BPE) in liquid phase using Ni and zeolite based catalysts are explored. In the absence of catalysts, the C−O bond is selectively cleaved in water by hydrolysis, forming phenol and benzyl alcohol as intermediates, followed by alkylation. The hydronium ions catalyzing the reactions are provided by the dissociation of water at 523 K. Upon addition of HZSM-5, rates of hydrolysis and alkylation are markedly increased in relation to proton concentrations. In the presence of Ni/SiO₂, the selective hydrogenolysis dominates for cleaving the aliphatic C−O bond. Catalyzed by the dual-functional Ni/HZSM-5, hydrogenolysis occurs as the major route rather than hydrolysis (minor route). In apolar undecane the non-catalytic thermal pyrolysis route dominates. Hydrogenolysis of BPE appears to be the major reaction pathway in undecane in the presence of Ni/SiO₂ or Ni/HZSM-5, almost completely suppressing radical reactions. Density functional theory (DFT) calculations strongly support the proposed C−O bond cleavage mechanisms on BPE in aqueous and apolar phases. These calculations show that BPE is initially protonated and subsequently hydrolyzed in the aqueous phase. DFT calculations suggest that the radical reactions in non-polar solvents lead to primary benzyl and phenoxy radicals in undecane, which leads to heavier condensation products as long as metals are absent for providing dissociated hydrogen.

4.1 Introduction

Lignin is a three-dimensional amorphous polymer with methoxylated phenyl-propane units, which are randomly connected by C−O or C−C linkages [1]. It would be ideal to catalytically and efficiently convert lignin to liquid transportation fuels or fine chemicals without destroying its inherent benzene structure. However, currently lignin is primarily used as a low-grade fuel to provide heat [2,3]. Three major approaches, i.e., gasification of lignin to synthesis gas [4,5], liquefaction (pyrolysis) of lignin to bio-oil [6,7], and hydrolysis of lignin to monomeric or oligomeric units [8-10], are used to depolymerize lignin. As the hydrolysis route leads to relatively selective products under much milder reaction conditions, it is rational to select lignin model compounds such as aryl ether dimers to investigate the principal fundamental chemistry of the hydrothermal depolymerization of lignin.

The most abundant C−O bonds in lignin are α−O−4, β−O−4, 4−O−5, β−1, and 5−5 linkages [11], in which the α-O-4 bond is the most active and thermally unstable one due to the lowest bond dissociation energy of the aliphatic C−O bond (218 kJ·mol^{-1}) among these bonds [12-15]. To explore the mechanism of cleaving the α−O−4 bond, benzyl phenyl ether (BPE) has been selected as the model compound in this work.

The non-catalyzed pyrolysis of BPE has been extensively investigated in the past [16]. It is initiated by homolytic scission of the weak $C_{aliphatic}$−O bond above 548 K. Generally, pyrolysis was, however, carried out under more severe conditions above 593 K in the vapor phase or in supercritical solvents such as methanol [17], toluene [18], and tetralin [18]. The pyrolysis process produces high concentrations of benzyl and phenoxy radicals, which led to toluene and phenol formation as primary products, together with dimer and high molecular-weight products derived from the recombination of the initial radicals. The recombination yield was usually higher than 15% with a carbon balance lower than 80%. Water, in contrast, leads to higher hydrothermal conversion rates of BPE than neat pyrolysis. Klein et al. [19] reported that the pyrolysis rate of BPE in the presence of water was approximately four times higher than that in neat pyrolysis at 605 K. We have explored BPE conversion in supercritical water (between 543 − 623 K) as well

via analyzing the influence of salts (alkali carbonates) towards BPE conversion in the aqueous phase [20].

Recently we have reported that diverse lignin-derived aryl ethers can be cleaved with Ni/HZSM-5 or Ni/SiO$_2$ at 393 − 523 K via combined hydrogenolysis, hydrolysis, and hydrodeoxygenation integrated steps in the aqueous phase [21-24], however, the mechanisms for cleaving of C−O bonds in these ethers have not been unequivocally established in the presence of mono- and dual- functional metal and acid catalysts. In this work, we will, therefore, investigate the roles of gas atmosphere, acid and metal sites, as well as their cooperative action in the conversion of BPE in the aqueous phase at 523 K via exploring the detailed kinetics together with the analysis of reaction pathways and mechanisms for BPE conversion at specifically varied conditions. In addition, density functional theory (DFT) modeling is comparatively employed to explore the ether cleavage mechanisms in the aqueous and apolar phases as well.

4.2 Experimental section

4.2.1 Chemicals

The chemicals were purchased from commercial suppliers and used as received: benzyl phenyl ether (TCI, > 98 % GC assay), nickel(II) nitrate hexahydrate (Sigma-Aldrich, ≥98.5 % GC assay), SiO$_2$ (Aerosil 200, Evonik-Degussa), HZSM-5 (Clariant AG, Si/Al = 45), Ni/SiO$_2$ (Acros, Ni loading 70 %), H$_2$SO$_4$ (ROTH, ≥ 95.5 %), undecane (Sigma-Aldrich, >99 % GC assay), H$_2$ (Westfalen AG, >99.999 vol %), N$_2$ (Westfalen AG, >99.999 vol %), synthetic air (Westfalen AG, >99.999 vol %), water (EASYpure II, resistivity:18.2 MΩ.cm.).

4.2.2 Preparation of Ni/HZSM-5

Ni/HZSM-5 catalyst was synthesized by the wetness impregnation method as follows, Ni(NO$_3$)$_2$ 6H$_2$O (5.6 g) was first dissolved in H$_2$O (5.0 g) as a transparent green solution and subsequently such aqueous solution was slowly dropped into zeolite HZSM-5 powder (10 g) with stirring. After metal incorporation for 2 h, the catalyst was sequentially dried at 373 K for 12 h,

air-calcined (flow rate: 100 mL·min^{-1}) at 673 K for 4 h, and hydrogen-reduced (flow rate: 100 mL·min^{-1}) at 733 K for 4 h.

4.2.3 Catalyst characterization

Atomic absorption spectroscopy (AAS)

A UNICAM 939 AA-Spectrometer was used to measure the Ni concentrations of Ni/SiO$_2$ and Ni/HZSM-5.

BET surface area

The surface areas and pore diameters were determined by the nitrogen sorption measurement. A PMI automated BET sorptometer was used to measure the nitrogen adsorption at 77 K and before measurement the samples were first outgassed at 523 K for 20 h.

H$_2$ chemisorption

The catalysts were first activated at 733 K for 3 h in H$_2$ and 1 h in vacuum, and then cooled to 313 K. An isotherm of H$_2$ adsorption (chemisorption and physisorption) was measured within a pressure range from 1 kPa to 40 kPa. Then the physisorbed H$_2$ was removed by outgassing the sample at the same temperature for 1 h, and another adsorption isotherm (physisorption) was taken. The concentration of chemisorbed H$_2$ on the metal was determined by extrapolating the differential isotherm to zero P$_{H2}$, and this value was used to calculate the dispersion of Ni with the assumption of H:Ni atomic ratio=1.

Transmission electron microscopy (TEM)

A JEM-2010 Jeol transmission electron microscope operating at 120 KV was used to record the TEM images. Before measurement the catalyst were ground and then suspended in ethanol,

and subsequently dispersed by ultrasonic treatment. After that, the dispersion was dropped on a copper grid-supported carbon film.

IR spectra of adsorbed pyridine

IR spectroscopy with pyridine as probe molecule was used to determine the acid site concentrations and distributions. The IR spectra were measured with a PerkinElmer 2000 spectrometer operated at a resolution of 4 cm^{-1}. The sample was activated at 723 K for 2 h in vacuum and a background spectrum was recorded after the temperature decreased to 423 K. The activated sample was exposed to pyridine vapor (1.0 $\times$ 10^{-5} MPa) at 423 K for 0.5 h. After removing physisorbed pyridine by outgassing at 423 K for 0.5 h, the spectra were recorded. For quantification, molar integral extinction coefficients of 0.73 cm·μmol^{-1} and 0.96 cm·μmol^{-1} were used for Brønsted (BAS) and Lewis acid sites (LAS), respectively.

4.2.4 Catalytic test

The detailed reaction conditions are described in the corresponding figures as footnotes. In a typical experiment, the catalytic reactions were carried out in a slurry autoclave reactor loaded with Ni/HZSM-5 in the water solvent at 523 K in the presence of 4 MPa H$_2$ (STP). A mixture of benzyl phenyl ether (0.010 mol), 10 wt.% Ni/HZSM-5 (0.050 g, 8.62$\times$10^{-5} mol Ni), and H$_2$O (80 mL) were firstly added into a Parr reactor (Series 4848, 300 mL). After the reactor was flushed with H$_2$ three times, the autoclave was charged with 4 MPa H$_2$ (ambient temperature) and the reaction were conducted at 523 K with a stirring speed of 700 rpm for different reaction times. The temperature of the autoclave was increased in approximately 20 min. from ambient to reaction temperature (523 K). Because it is a two-phase reaction, the kinetics data are collected at different duration times. After reaction, the reactor was cooled by ice to ambient temperature, and the organic products were extracted by ethyl acetate and analyzed by GC and MS. The products were analyzed by a gas chromatography (GC) and GC-mass spectroscopy (GC-MS) on Shimadzu 2010 gas chromatograph with flame ionization detector and a Shimadzu QP 2010S GC-MS, both of them equipped with a HP-5 capillary column (30 m $\times$ 250 μm). Internal standard, i.e., 2-

isopropylphenol, was used to determine the liquid product concentration and carbon balance. The carbon balance for all reported experiments in the liquid phase was better than $95\pm3\%$ in this work. The calculations of conversion and selectivity were based on carbon mole basis. Conversion = (the amount of raw-material change during reaction / total amount of raw materials) $\times$ 100%. Selectivity = (C atoms in each product / total C atoms in the products) $\times$100%. Rate= (moles of reactants cleaved) / (reaction time in hour). TOF = (moles of reactants cleaved) / (moles of surface active sites $\times$ reaction time in hour).

4.2.5 Density functional theory (DFT) calculation

All the quantum chemical calculations of benzyl phenyl ether (BPE) in hot water and undecane were performed using Gaussian09 program [25]. The DFT/B3LYP functional with 6-311++G(d,p) basis set were applied. The accuracy of the B3LYP functional was checked by comparing with the second-order Möller-Plesset perturbation theory (MP2) [26]. The transition state of each reaction pathway is located using the linear (LST) and quadratic synchronous transit (QST) methods [1, 2]. A series of single point energy calculations of interpolated structures between the initial and the final states along the reaction pathway are performed. The maximum energy structure along this reaction path is used as an estimate transition state in the QST calculation. Each identified transition state was confirmed by the sole imaginary vibrational frequency. The solvation effects on the hydrolysis in water and the pyrolysis in undecane were described by the polarizable continuum model (PCM) model with dielectric constants of 78.3553 for water and 1.9910 for undecane [29].

4.3 Results and discussion

4.3.1 Catalyst characterization

The physicochemical properties of the supported metal catalyst (Ni/SiO$_2$), the acid catalyst (HZSM-5), and the dual-functional catalyst (Ni/HZSM-5) are compiled in **Table 4-1**. The Ni/SiO$_2$ catalyst had a Ni content of 70 wt.%, a BET specific surface area of 82 m^2 g^{-1}, pore volume of 0.12 cm^3 g^{-1}, and a pore diameter of 9.2 nm. The average size of supported Ni particles in Ni/SiO$_2$ was around 8.0 nm determined from the TEM image (appendix 4.6, **Fig. S4-1b**). The parent HZSM-5 had a BET surface area of 395 m^2 g^{-1}, and a total acid site concentration of 0.360 mmol·g^{-1} determined by TPD of ammonia (TPD−NH$_3$). Probed by IR of adsorbed pyridine (Py−IR), the Brønsted acid site (BAS) and Lewis acid site (LAS) concentration of HZSM-5 was 0.266 and 0.048 mmol·g^{-1}, respectively. Impregnated with Ni, the BET surface of Ni/HZSM-5 (Ni content: 10 wt.%) decreased to 374 m^2 g^{-1}. The concentration of the Brønsted acid sites decreased by approximately 20% after Ni incorporation due to the ion exchange of Brønsted acid sites for Ni^{2+}, while the Lewis acid site concentration was almost unchanged compared to parent zeolite. The average Ni particle size was 20 nm on Ni/HZSM-5 prepared by impregnation as determined by the TEM image (appendix 4.6, **Fig. S4-1a**).

Table 4-1. Physicochemical properties of catalysts

Catalyst	Ni/SiO$_2$	HZSM-5 (Si/Al=45)	Ni/HZSM-5 (Si/Al=45)
Metal loading (wt.%)	70	-	10
BET surface area (m^2 g^{-1})	82	395	374
Pore volume (cm^3 g^{-1})	0.12	0.26	0.24
Pore diameter (nm)	9.2	3.6	3.6
Metal particle diameter (nm)	8.0	-	20
Acidity (mmol·g^{-1}) (TPD-NH$_3$)	-	0.360	0.296
Conc. BAS (mmol·g^{-1})	-	0.266	0.228
Conc. LAS (mmol·g^{-1})	-	0.048	0.048
Dispersion of metal (H$_2$ chem.%)	6.9	-	0.84

4.3.2 Benzyl phenyl ether conversion in the aqueous phase

High-temperature water has a density and polarity at 573 K similar to acetone at ambient temperature [30], and acts consequently as a suitable reaction medium for dissolving organic compounds. The dielectric constant of water drops rapidly from 70 at 293 K to 27 at 523 K, and the ionic product of water is 10^{-11} at 523 K compared to 10^{-14} at 293 K [31,32]. This indicates that the high-temperature water could act as a moderately strong acid as well as a base. We structure the investigations of the influence of gas atmosphere, of a solid acid introduced in the form of HZSM-5, of metal sites introduced by Ni/SiO_2, and the presence of both sites by introducing Ni/HZSM-5, on BPE conversion at 523 K in four sections, i.e., (i) BPE conversion in the aqueous phase in the absence and presence of H_2, (ii) the influence of acid on BPE conversion in the aqueous phase in the presence of H_2, (iii) the influence of metal on BPE conversion in the presence of H_2, (iv) the influence of bifunctionality with acid and metal sites on BPE conversion in the presence of H_2.

4.3.2.1 BPE conversion in the aqueous phase in the absence and the presence of H_2

Fig. 4a shows that BPE was equally cleaved into phenol (Ph) and benzyl alcohol (BA) in water at 523 K in the absence of H_2 (0.1 MPa N_2). Without catalyst, hydronium ions from dissociated water at 523 K (pH = 5.5) catalyze the hydrolysis [31,32]. At the selected conditions, the conversion increased linearly to 31% as a function of time up to 110 min, and the yields of phenol and benzyl alcohol synchronously increased to around 13%. Besides Ph and BA, some products with 13 C atoms such as 4-benzyl phenol and 2-benzyl phenol were also observed. It was reported that these heavier products were dimers or trimers formed from BPE pyrolysis or hydrolysis via recombination of radical intermediates [20,33]. However, Siskin et al. proposed a different mechanism on BPE conversion in different temperature ranges, that is, above 623 K the radical pathway dominated, but at the lower temperature 523 K in the aqueous phase the contribution of the ionic chemistry was concluded to play a significant role [34]. Siskin et al., however, also observed the formation of phenol (41.0%), benzyl alcohol (26.4%), and alkylated products (29.6%,

including 19.6% dimers and 10% trimers) at 523 K. The higher yield of alkylated products, especially of trimers in their case is attributed to the much longer reaction time (5.5 days) than the 110 min in our case. In our work, the yield of the C−C coupled products continuously increased to 5% after achieving the specific reaction equilibrium. When the gas atmosphere was altered to H_2 (**Fig. 4-1c**), 34% conversion was attained in 110 min, which was close to the conversion obtained in the presence of 0.1 MPa N_2. The major products of Ph and BA were formed via hydrolysis by hydronium in the high-temperature water, and the C−C alkylation products have a stable yield of 5%. This indicates that gas atmosphere (P = 0.1 MPa) exerts a negligible influence to the hydrolysis of BPE in the aqueous phase.

With high-pressure N_2 (4 MPa, **Fig. 4-1b**), however, the hydrolysis rates was significantly accelarated with a high conversion of 41% in 110 min. At a high H_2 pressure (4 MPa) under hydrothermal conditions, the cleavage rates on BPE were further enhanced leading to 51% conversion in 110 min. (**Fig. 4-1d**); equal concentrations (23%) of phenol and benzyl alcohol were formed. In addition, the C−C coupling products also attained a maximum yield of 5% in water, and this constancy implied that the C−C coupling is primarily dominated by the acid catalyzed alkylation, but not by the thermal free-radical reaction [35]. Summarizing these results leads to the conclusion that the aqueous environment favors the ionic pathway in the C−O bond cleavage of BPE at 523 K. BPE is then cleaved to phenol and benzyl alcohol by hydrolysis, which is catalyzed by the protons of high-temperature water in the absence or presence of H_2. The subsequent alkylation between phenol and alcohol reaches a maximum yield of 5%.
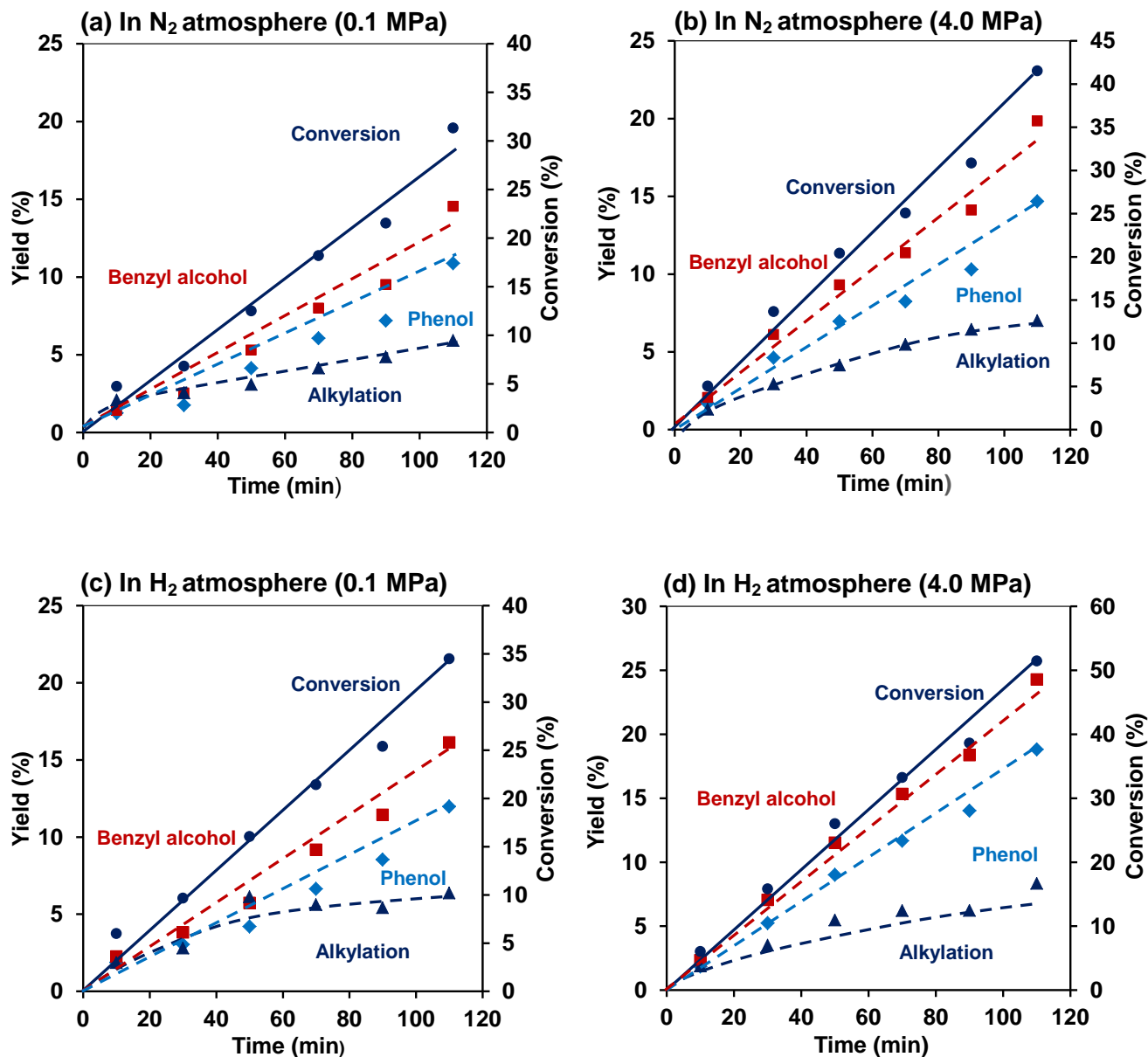
Figure 4-1. Product yields for conversion of benzyl phenyl ether in the aqueous phase in absence and presence of H_2 as a function of time. Reaction conditions: Benzyl phenyl ether (1.84 g), H_2O (80 mL), 523 K, stirring at 700 rpm, (a) 0.1 MPa N_2, (b) 4 MPa N_2, (c) 0.1 MPa H_2, (d) 4 MPa H_2.

The relationship between the hydrolysis rate and the gas pressure in the aqueous phase has been systematically investigated by Whalley et al. It has been shown that in the ether hydrolysis

based on A2 mechanism (with the rate-determining step being the bimolecular hydrolysis) the higher gas pressure enhances the ether hydrolysis rate in the aqueous phase due to a better stabilization of the transition-state via the increased gas pressure [36, 37]. The A2 mechanism of hydrolysis of benzyl phenyl ether (BPE) is described in equations 1-4. In agreement with Whalley et al. [37], our results also show that the TOF of BPE hydrolysis increased from 7.6×10^3 mol $mol_{[H+] H2O}^{-1}$ h^{-1} at 0.1 MPa H_2 to 1.1×10^4 mol $mol_{[H+] H2O}^{-1}$ h^{-1} at 4 MPa H_2.

$$H^+ \quad + \quad H_2O \quad \rightleftharpoons \quad H_3O^+ \tag{1}$$

$$\underset{C_7H_7}{\overset{C_6H_5}{>}}O \quad + \quad H_3O^+ \quad \rightleftharpoons \quad \underset{C_7H_7}{\overset{C_6H_5}{>}}OH^+ \quad + \quad H_2O \tag{2}$$

$$\underset{C_7H_7}{\overset{C_6H_5}{>}}OH^+ \quad + \quad H_2O \quad \xrightarrow{\text{slow}} \quad C_7H_7OH \quad + \quad C_6H_5O^+H_2 \tag{3}$$

$$C_6H_5O^+H_2 \quad + \quad H_2O \quad \xrightarrow{\text{fast}} \quad C_6H_5OH \quad + \quad H_3O^+ \tag{4}$$

The higher C−O cleavage rate of BPE in H_2 compared to N_2 with a pressure of 4 MPa may orignate from the different solubility of the gases in the aqueous phase. When a reaction takes place in solvents, the reactant is surrounded by solvent molecules and needs to overcome the cage of solvents to collide with reactants or catalysts. This is called the "cage effect". We speculate that the higher solubility of H_2 compared to N_2 leads to a lower equilibrium pressure and, hence, less compression and a more loose solvent cage for the reactant, facilitating reaction from the solvent cage, enhancing in turn the reaction rate with H_2 in comparison with N_2. At the present, however, we cannot fully exclude a direct positive effect of the H_2 pressure on the acid catalyzed reactions.

4.3.2.2 The influence of acid on BPE conversion in the aqueous phase in the presence of H_2

Figure 4-2. Product yields for conversion of benzyl phenyl ether with HZSM-5 in the aqueous phase in the presence of H_2 as a function of time. Reaction conditions: Benzyl phenyl ether (1.84 g), H_2O (80 mL), 523 K, 4 MPa H_2, stirring at 700 rpm, (a) HZSM-5 (0.03 g), (b) HZSM-5 (0.15 g).

The impact of the acid after loading low (0.03 g) and high (0.15 g) concentrations of HZSM-5 was subsequently investigated at 523 K in the conversion of BPE at 4 MPa H_2 (**Fig. 4-2a and 4-2b**). With a small concentration of HZSM-5 (0.03 g), the conversion was increased from 51% to 75% compared to in the neat aqueous phase with 4.0 MPa H_2 in 110 min (**Fig. 4-2a**). Meanwhile, the cleavage yields to phenol and benzyl alcohol (30%) were comparable to those (23%) in absence of acid. But it is interesting to find that the small addition of the acid remarkedly enhanced the alkylation yield from 5% to 15% at 523 K. It supports again that C_{13} products are formed by acid-catalyzed alkylation and not by free-radical reactions.

In a comparison, with a high concentration of solid acid (HZSM-5, 0.15 g). The conversion increased to 87% in the first 10 min, and further increased to 98% at 110 min, which was much higher than the conversion (only 51%) without introducing the HZSM-5 at identical conditions (**Fig. 4-2b**). This confirms that hydrolysis is indeed the major reaction pathway for BPE conversion

in the aqueous phase. It should be emphasized that the alkylation yield reached 50% under these conditions, which is much higher than that in neat water with or without hydrogen (5%), or with small concentrations of HZSM-5 (15%). This indicates that with a sufficient concentration of acid sites, the initial hydrolysis and following alkylation rates are both highly accelerated.

With the addition of HZSM-5, the major pathway was still hydrolysis for BPE in water at 523 K. The rate of hydrolysis and following alkylation between the intermediate fragments were both enhanced with a small concentration of HZSM-5. Adding a higher concentration of acid sites (higher amount of HZSM-5 added) promoted both the hydrolysis and alkylation rates to a larger extent.

4.3.2.3 The influence of metal on aqueous-phase BPE conversion in the presence of H$_2$

The metal site (Ni/SiO$_2$) expectedly catalyzed a different pathway of BPE conversion in water at 523 K (see **Fig. 4-3**). After 110 min, BPE was quantitatively cleaved to 50% phenol and 50% toluene. This suggests that the weaker C$_{aliphatic}$−O bond (bond dissociation energy: 218 kJ mol^{-1}) [14] is selectively cleaved by Ni catalyzed hydrogenolysis, but not by acid catalyzed hydrolysis. Note that the alternative products (benzene and benzyl alcohol) by cleaving of the other side of C$_{aromatic}$−O bond (bond dissociation energy: 314 kJ mol^{-1}) [14] were not observed. 5% alkylation products (catalyzed by hydronium ions formed by dissociated water at 523 K) were formed as well, indicating that the hydrolysis/alkylation route contributes to a very minor part. The alkylation yield was quite constant at 5% without the acid, as the pH value in such aqueous system is stable at 5.5 [31,32].
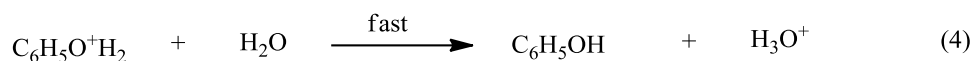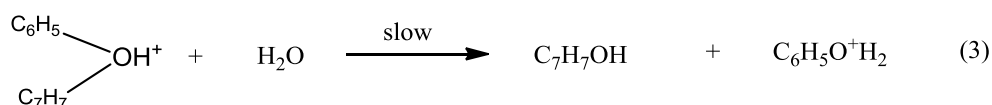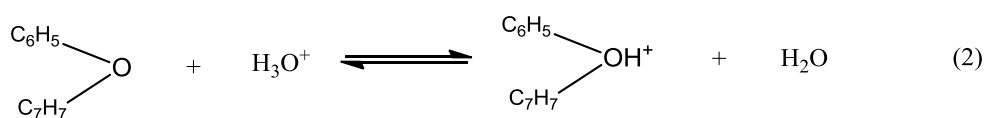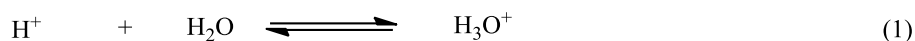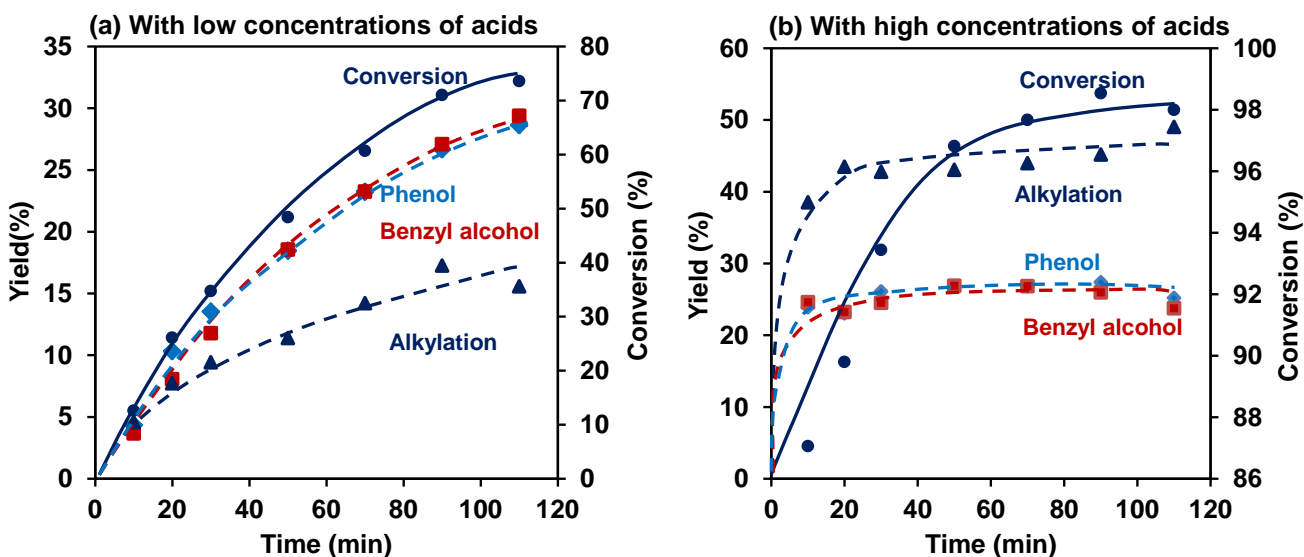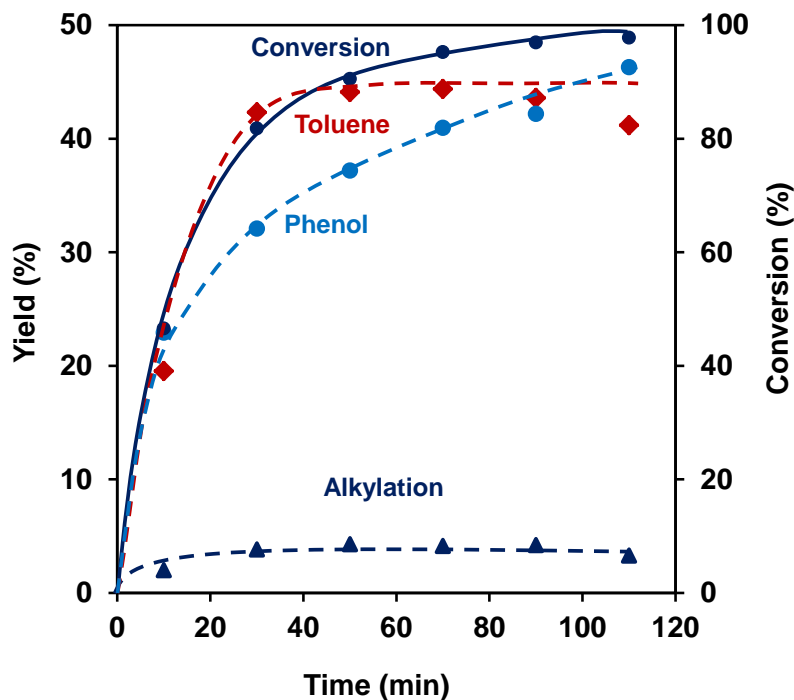
Figure 4-3. Product yields for conversion of benzyl phenyl ether with Ni/SiO$_2$ in the aqueous phase in the presence of H$_2$ as a function of time. Reaction conditions: Benzyl phenyl ether (9.20 g), Ni/SiO$_2$ (70 wt.%, 0.010 g), H$_2$O (80 mL), 523 K, 4 MPa H$_2$, stirring at 700 rpm.

The observed yield of phenol was much lower than the yield of toluene, as the hydrogenation rate of phenol (2400 h^{-1}) was much faster than the hydrogenation rate of toluene on Ni/SiO$_2$ (135 h^{-1}) at 523 K. (see appendix 4.6, **Table S4-1**). After phenol was hydrogenated to cyclohexanone and cyclohexanol on Ni, cyclohexanol was subsequently dehydrated to cyclohexene catalyzed by hydronium ions and then hydrogenated or dehydrogenated to cyclohexane or benzene, respectively. However, all these hydrodeoxygenated intermediates from phenol were detected with yields lower than 7% (not shown in **Fig. 4-3**).

In summary, the Ni-catalyzed direct hydrogenolysis on BPE is the dominating pathway for producing equal concentrations of phenol and toluene. Subsequently phenol was hydrogenated at a relatively fast rate, forming cyclohexanone and cyclohexanol as intermediates. In turn these

oxygenates were deoxygenated to cyclohexene, cyclohexane, and benzene catalyzed by the joint action of metal (Ni/SiO_2) and acid (hydronium ions in the high-temperature water).

4.3.2.4 The influence of bi-functionality with acid and metal sites on aqueous-phase BPE conversion in the presence of H_2
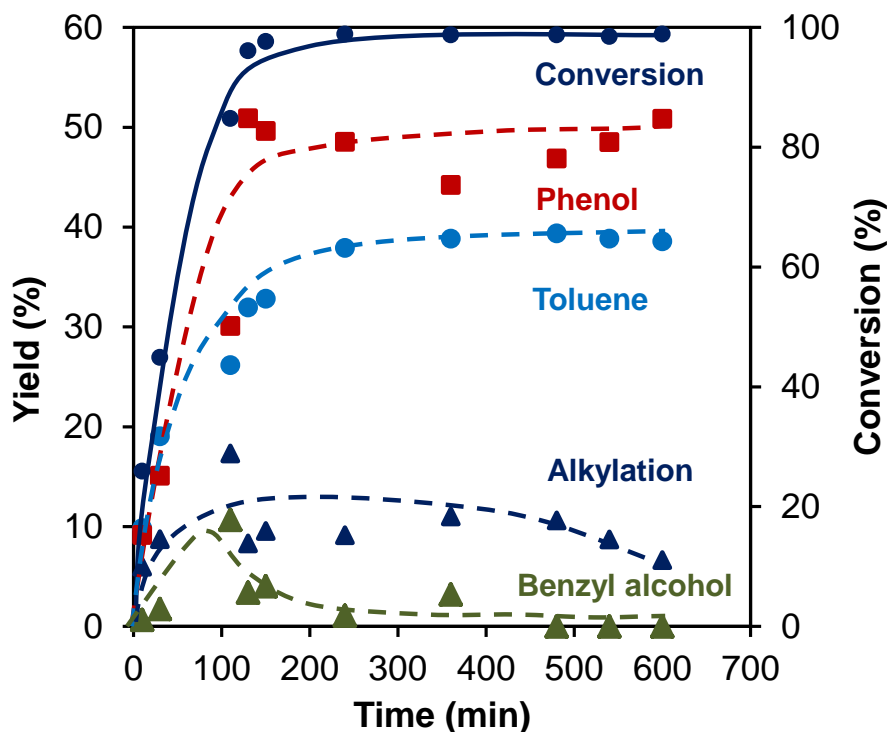
Figure 4-4. Product yields for conversion of benzyl phenyl ether with 10% Ni/HZSM-5 in the aqueous phase in the presence of H_2 as a function of time. Reaction conditions: Benzyl phenyl ether (9.20 g), 10 wt.% Ni/HZSM-5 (0.050 g), H_2O (80 mL), 523 K, 4 MPa H_2, stirring at 700 rpm.

The role of acid and metal sites in proximity on Ni/HZSM-5 were investigated in the next step. **Fig. 4-4** shows the variations of the concnetration in the reactant product mixture of BPE over Ni/HZSM-5 as a function of time. The products included 50% phenol, 40% toluene, 2% benzyl alcohol, as well as 8% C_{13} alkylated products, with quantitative conversion after 240 min. With metal and acid sites in Ni/HZSM-5, phenol and toluene (major products) were produced by metal-catalyzed hydrogenolysis, while the parallel acid-catalyzed hydrolysis (minor) pathway led to the

formation of phenol and benzyl alcohol as well as some alkylation products. The hydrolysis was catalyzed by the acid sites of Ni/HZSM-5 and protons in high-temperature water, attaining a maximum alkylation yield of 10%. It is noted that the turnover frequencies of protons/hydronium ions in the zeolite channels (**Table 4-2, Entry 4-6**) were approximately one magnitude lower than those of water dissociation. The hydrogenolysis rate was at least four times as fast as that of hydrolysis, as the yield of the hydrogenolyzed products (80%) was much higher than that of hydrolyzed (20%). Trace amounts (yields < 2%) of hydrodeoxygenation intermediates from phenol and toluene such as cyclohexanone, cyclohexanol, and methylcyclohexane were observed as well (not shown in **Fig. 4-4**).

With both catalytic sites present, the hydrogenolysis route catalyzed by metallic Ni was the major reaction pathway for cleaving the C−O bond of BPE, with producing phenol and toluene as major products. Hydrolysis was only the minor route, but hydrodeoxygenation of phenol and toluene occurred to a small extent with Ni/HZSM-5 as well. Alkylation of the cleaved products (phenol and benzyl alcohol) took place with HZSM-5 catalyst in the high-temperature water.

4.3.2.5 Different mechanisms for cleaving of the C−O bond of BPE at varying conditions in the aqueous phase

Table 4-2. The effect of gas atmosphere, HZSM-5 (acid), and Ni/SiO$_2$ (metal) on the reaction of benzyl phenyl ether (BPE) in the aqueous phase at 523 K. [a]

Entry	Gas	Active Site	Rate (mol h^{-1})	TOF (mol mol^{-1} h^{-1})
1 [b]	N$_2$ [c]	H$_2$O n ([H$^+$]$_{H_2O}$) = 2.5×10^{-7} mol	0.0017	6.8×10^3 mol mol$_{[H^+] H_2O}^{-1}$ h^{-1}
2 [b]	N$_2$	H$_2$O n ([H$^+$]$_{H_2O}$) = 2.5×10^{-7} mol	0.0022	8.8 ×10^3 mol mol$_{[H^+] H_2O}^{-1}$ h^{-1}
3 [b]	H$_2$ [c]	H$_2$O n ([H$^+$]$_{H_2O}$) = 2.5×10^{-7} mol	0.0019	7.6 ×10^3 mol mol$_{[H^+] H_2O}^{-1}$ h^{-1}
4 [b]	H$_2$	H$_2$O n ([H$^+$]$_{H_2O}$) = 2.5×10^{-7} mol	0.0028	1.1×10^4 mol mol$_{[H^+] H_2O}^{-1}$ h^{-1}
5 [b]	H$_2$	HZSM-5, H$_2$O n ([H$^+$]$_{HZSM-5}$) = 8.0 ×10^{-6} mol n ([H$^+$]$_{H_2O}$) = 2.5×10^{-7} mol	0.0090	1.1×10^3 mol mol$_{[H^+]HZSM-5}^{-1}$ h^{-1}
6 [b]	H$_2$	HZSM-5, H$_2$O n ([H$^+$]$_{HZSM-5}$) = 4.0 ×10^{-5} mol n ([H$^+$]$_{H_2O}$) = 2.5×10^{-7} mol	0.0522	1.3×10^3 mol mol$_{[H^+] HZSM-5}^{-1}$ h^{-1}
7 [d]	H$_2$	H$_2$SO$_4$, H$_2$O n ([H$^+$]$_{H_2SO_4}$) = 4.0 ×10^{-5} mol n ([H$^+$]$_{H_2O}$) = 2.5×10^{-7} mol	0.0542	1.4×10^3 mol mol$_{[H^+]}^{-1}$ h^{-1}

8 [b]	H_2	70 wt.% Ni/SiO_2, H_2O n ([Surf. Ni])= 8.5 ×10^{-6} mol, n ([H^+]$_{H_2O}$) = 2.5×10^{-7} mol	0.1410	$1.7×10^4$ mol mol$_{Surf\ Ni}^{-1}$ h^{-1}
9 [b]	H_2	10 wt.% Ni/HZSM-5, H_2O n ([Surf. Ni])=7.4 ×10^{-7} mol n ([H^+]$_{HZSM-5}$) =1.0 ×10^{-5} mol n ([H^+]$_{H_2O}$) = 2.5×10^{-7} mol	0.0777	$1.1×10^5$ mol mol$_{Surf\ Ni}^{-1}$ h^{-1}

[a] Gas pressure: 4.0 MPa. [b] The initial rate and TOF are obtained via the kinetics in the aqueous phase in Figs. 4-1 - 4-4. [c] Gas pressure: 0.1 MPa. [d] Rate and TOF are calculated based on the data listed in appendix 4.6 Table S4-2.

The variations of product distributions and reaction rates on the varying conditions in the aqueous phase are compiled in **Table 4-2**. In N_2 (P = 0.1 MPa), BPE was cleaved into phenol and benzyl alcohol by hydrolysis under the hydrothermal conditions with an initial cleavage rate of 0.0017 mol h^{-1} and a TOF of $6.8×10^3$ mol mol$_{[H^+]\,H_2O}^{-1}$ h^{-1}; 5% of alkylation products were formed at such conditions (**Table 4-2, Entry 1**). Replacing N_2 by H_2 (P = 0.1 MPa), the C−O bond cleavage rate (0.0019 mol h^{-1}) and TOF ($7.6×10^3$ mol mol$_{[H^+]\,H_2O}^{-1}$ h^{-1}) (**Table 4-2, Entry 3**) were comparable to these reactions in 0.1 MPa N_2 (0.0017 mol h^{-1} and $6.8×10^3$ mol mol$_{[H^+]\,H_2O}^{-1}$ h^{-1}). This implies that gas atmosphere make a very minor impact to the ether hydrolysis rate at a pressure of 0.1 MPa. Employing a high-pressure in the presence of N_2 (4.0 MPa), the reaction rate was accelerated leading to a conversion of 41%, with an increased initial cleavage rate of 0.0022 mol h^{-1} and TOF of $8.8×10^3$ mol mol$_{[H^+]\,H_2O}^{-1}$ h^{-1}(**Table 4-2, Entry 2**). With 4.0 MPa H_2 51% conversion was reached under identical conditions with an increased initial cleavage rate of 0.0028 mol h^{-1} and TOF of $1.1×10^4$ mol mol$_{[H^+]H_2O}^{-1}$ h^{-1} (**Table 4-2, Entry 4**). The yield of alkylation was maintained at the stable level of around 5% in the aqueous phase in the presence of H_2 or N_2, suggesting the alkylation equilibrium exists [35].

The addition of even a small amount of acid (HZSM-5, 0.030 g) increased the cleavage rate of BPE three-fold in the presence of H_2, i.e., it attains an initial cleavage rate of 0.0090 mol h^{-1}

compared to 0.0028 mol h^{-1} without the solid acid (**Table 4-2, Entry 5**). Yields of hydrolysis and alkylation were increased by 5-10% in 110 min. Employing a higher concentration of acid (HZSM-5, 0.15 g), the initial TOF (1.3×10^3 mol mol$_{[H^+]HZSM-5}^{-1}$ h^{-1}) (**Table 4-2, Entry 6**) was comparable to that with a small amount of acid (1.1×10^3 mol mol$_{[H^+]HZSM-5}^{-1}$ h^{-1}). However, the reaction rate was higher and the reaction reached full conversion with equal yields of hydrolysis (50%) and alkylation products (50%) in 110 min (**Fig. 4-2b**). We speculate that the higher concentration of HZSM-5 enhances the in situ formed concentrations of phenol and benzyl alcohol, and increases so alkylation yields. Note that the TOF of ether hydrolysis in water (1.1×10^4 mol mol$_{[H^+]\,H_2O}^{-1}$ h^{-1}) was one magnitude higher than that with HZSM-5 in the aqueous phase (1.1-1.3×10^3 mol mol$_{[H^+]HZSM-5}^{-1}$ h^{-1} (**Table 4-2, Entries 4-6**), which is attributed to the fact that liquid protons in the high-temperature water are more accessible than acid sites in the solid zeolite. To verify this hypothesis, BPE conversion with equivalent amount of liquid acid (H_2SO_4) was carried out at the same conditions, attaining an initial comparable cleavage TOF of 1.4×10^3 mol mol$_{[H^+]}^{-1}$ h^{-1} as HZSM-5 (**Table 4-2, Entry 7 and appendix 4.6 Table S4-2**). Tested in the temperature range of 483 to 543 K, the apparent activation energy of BPE hydrolysis with H_2SO_4 was 163 kJ·mol^{-1}, which was 116 kJ·mol^{-1} higher than that with HZSM-5 (E_a = 47 kJ·mol^{-1}) (**Fig. 4-5**). The much lower apparent activation energy with HZSM-5 can be ascribed to the added heat of adsorption of BPE on the HZSM-5. The preexponential factor for H_2SO_4 was 6.4×10^{19} molecules·mol$_{[H^+]}^{-1}$ h^{-1}, whereas the corresponding value for HZSM-5 was merely 4.5×10^7 molecules·mol$_{[H^+]}^{-1}$ h^{-1}, strongly indicating that the accessible acid sites with liquid H_2SO_4 is much more abundant than the confined solid acid sites in HZSM-5. Having excluded the thermal pyrolysis route on BPE in the aqueous phase, the higher hydrolysis rate in neat water can be attributed also to either OH$^-$ ions from ionization of water which can act as base to efficiently catalyze ether hydrolysis [38] or the in situ produced phenol enhances the acidity of high-temperature water during reaction at 523 K.
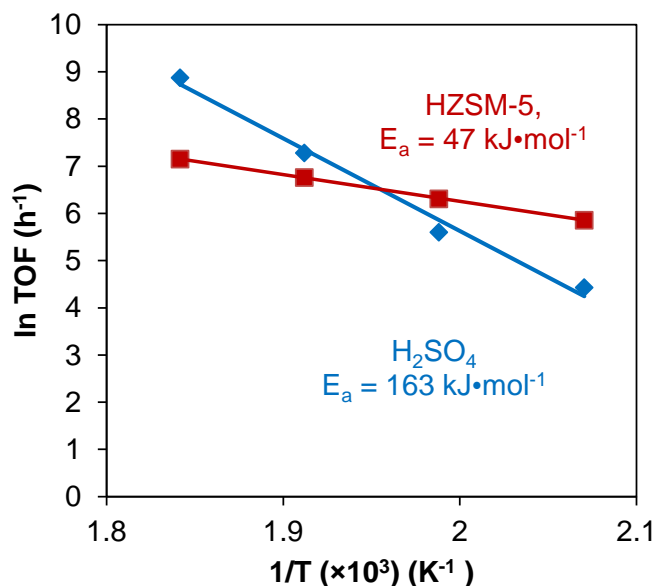
Figure 4-5. Arrhenius plots for the ln TOF (h^{-1}) with H_2SO_4 and HZSM-5 catalysts in the temperature range of 483 to 543 K in the presence of 4 MPa H_2. Reaction conditions: benzyl phenyl ether (18.4 g), H_2SO_4 solution (80 mL, $c = 2.5 \times 10^{-4}$ mol/L), 20 min.; benzyl phenyl ether (1.84 g), H_2O (80 mL), HZSM-5 (0.03 g), 30 min.

When 70 wt.% Ni/SiO_2 was introduced to the reaction mixture, Ni catalyzed the specific hydrogenolysis route on BPE to phenol and toluene formation. In addition, the C−O bond cleavage rate (0.1410 mol h^{-1}) was nearly 50 times as fast as the rate in the presence of 4.0 MPa H_2 (0.0028 mol h^{-1}) (**Table 4-2, Entry 8**). The bond cleavage TOF of Ni/SiO_2 (1.7 $\times 10^4$ mol mol$_{Surf\ Ni}^{-1}$ h^{-1}) was one magnitude higher than that with 0.03 or 0.15 g HZSM-5 (1.1$\times 10^3$ and 1.3$\times 10^3$ mol mol$_{[H^+]HZSM-5}^{-1}$ h^{-1}, respectively). These results imply that Ni atoms are the major active sites for BPE cleavage when Ni and HZSM-5 components are present together. Adding 10 wt.% Ni/HZSM-5 (**Table 4-2, Entry 9**) verifies the hypothesis that the major reaction pathway for C-O bond cleavage of BPE was Ni catalyzed hydrogenolysis and that the hydrolysis route only contributed to a minor part (**Fig. 4-4**).

Aqueous phase:
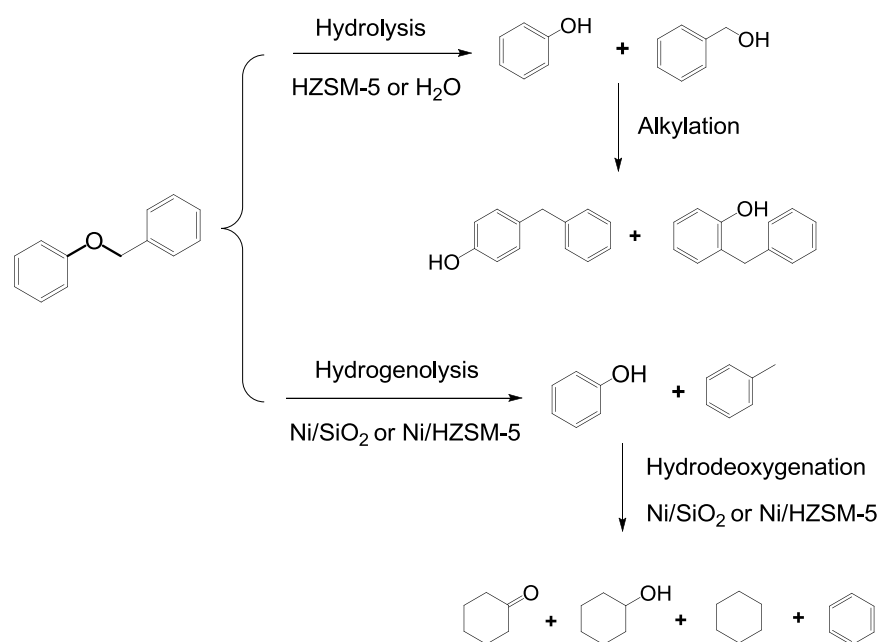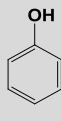
Scheme 4-1. The major reaction pathways for conversion of benzyl phenyl ether (BPE) with different catalyst components in the aqueous phase in the presence of hydrogen at 523 K.

Combing these results allows us to draw the general reaction pathways on conversion of BPE with different catalyst components in the aqueous phase at 523 K. In high-temperature water with or without HZSM-5 addition, hydrolysis is the major pathway for cleaving the C−O bond, and the following C-C coupling of alkylation takes place between the cleaved phenol and alcohol fragments. When Ni is employed with or without HZSM-5, Ni catalyzed hydrogenolysis dominates throughout the overall C-O bond cleavage reaction (**Scheme 4-1**).

4.3.3 Cleavage of C−O bond of BPE in undecane at 523 K

Table 4-3. The effect of gas atmosphere, HZSM-5 (acid), and Ni/SiO$_2$ (metal) on the reaction of benzyl phenyl ether (BPE) in undecane at 523 K. [a]

Entry	Active Center in gas atmosphere	Conv. (%)	Selectivity (C%)								Initial Rate (mol h^{-1})	TOF (mol·mol^{-1}·h^{-1})
1	N$_2$	6.8	1.8		3.8					94.4	0.0014	-
2	H$_2$	9.7	3.1		4.3					92.6	0.0019	-
3	H$_2$, HZSM-5 n ([H$^+$]$_{HZSM-5}$) = 8.0 ×10^{-6} mol	25.2	3.6		11.0					85.4	0.0050	6.3×10^2 mol·mol$_{[H^+]HZSM-5}^{-1}$·h^{-1}
4 [b,c]	H$_2$, 70 wt.% Ni/SiO$_2$ N ([Surf. Ni])= 8.5 ×10^{-6} mol	14.5	45.5	0.6	19.1	5.7	9.9	2.3	3.2	13.7	0.2172	2.6×10^4 mol·mol$_{Surf Ni}^{-1}$·h^{-1}
5 [b]	H$_2$, 10 wt.% Ni/HZSM-5 n ([Surf. Ni])=7.4 ×10^{-7} mol n ([H$^+$]$_{HZSM-5}$) =1.0 ×10^{-5} mol	25.9	32.4	0.6	19.4	2.9	2.7	2.1	3.3	36.6	0.0259	3.5×10^4 mol·mol$_{Surf Ni}^{-1}$·h^{-1}

[a] Reaction conditions: Benzyl phenyl ether (1.84 g), undecane (80 mL), HZSM-5 (Si/Al = 45, 0.030 g), Ni/SiO$_2$ (70 wt.%, 0.010 g), Ni/HZSM-5 (10 wt.%, 0.050 g), gas pressure (4 MPa), 30 min., stirring at 700 rpm. [b] Benzyl phenyl ether (9.20 g). [c] 2 min.

When changing the aqueous to apolar phase, the fundamental chemistry for cleaving of C−O bond of BPE is changed. Without catalyst either in N$_2$ or H$_2$ atmosphere (4.0 MPa), the C−O bond of BPE was cleaved by pyrolysis in undecane, but not by hydrolysis because of the absence of water. The cleavage rates in undecane were slower than those in the aqueous phase, i.e., 0.0014 vs 0.0022 mol h^{-1} in 4.0 MPa N$_2$, and 0.0019 vs. 0.0028 mol h^{-1} in 4.0 MPa H$_2$, respectively (**Table 4-3, Entries 1 and 2**). This indicates that the rate of ether hydrolysis in water is faster than pyrolysis of ether in undecane, agreeing with the observation of Klein et al [19] that in the presence of water the cleavage rate of BPE was four-fold higher than that during pyrolysis of the neat substrate at 605 K. The conversion reached 9.7% for the thermal pyrolysis of BPE at 523 K for 30 min. in the presence of H$_2$, and the main products were heavier products (selectivity: 92.6%) as well as small amounts of toluene (selectivity: 3.1%) and phenol (selectivity: 4.3%) (**Table 4-3, Entry 2**), indicating that the non-catalytic pyrolysis breaks down the weakest bond of C$_{aliphatic}$−O of BPE. The heavier products were formed from the free-radical reaction, dominating the thermal pyrolysis process (**Scheme 4-2**). When an acid component of HZSM-5 was added in the presence of H$_2$, the cleavage rate was increased to 0.0050 mol h^{-1} compared to 0.0019 mol h^{-1} without catalysts (**Table 4-3, Entry 3**). Similarly, such rate with HZSM-5 in undecane (0.0050 mol h^{-1}) was slower than that in water (0.0090 mol h^{-1}), which infers again that the hydrolysis route in the aqueous phase is much faster than the pyrolysis pathway in undecane.
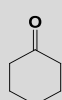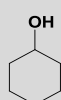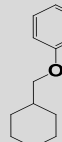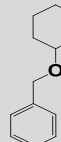
Non-polar solvent (undecane):
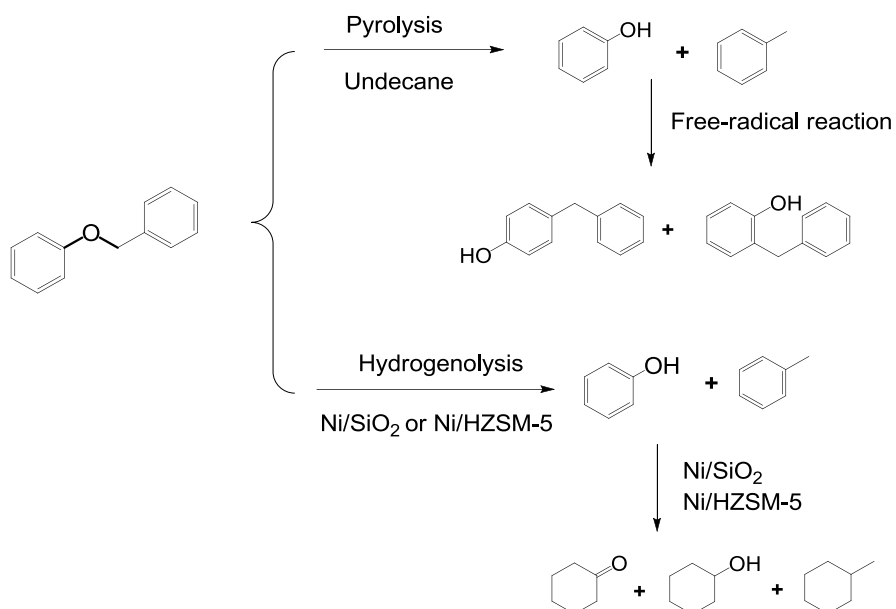
Scheme 4-2. The reaction pathways for conversion of benzyl phenyl ether (BPE) with different catalyst components in the non-polar solvent undecane in the presence of hydrogen at 523 K.

However, the metallic Ni/SiO$_2$ selectively catalyzes the hydrogenolysis of C−O bond of BPE with a cleavage rate of 0.2172 mol h^{-1}, which was 114 times as fast as the rate of pyrolysis without catalyst in the presence of 4.0 MPa H$_2$ (0.0019 mol h^{-1}) (**Table 4-3, Entry 4**). Over Ni sites, the primary products were toluene and phenol (selectivity: > 80%), while the free-radical products were highly suppressed (selectivity: 13.7%) at a conversion of 14.5%. In addition, the partial hydrogenation of aromatic ring of BPE also occurred on Ni/SiO$_2$ in undecane, producing cyclohexylmethyl phenyl ether (selectivity: 2.3%) and benzyl cyclohexyl ether (selectivity: 3.2%) (**Table 4-3, Entry 4**). The bond cleavage TOF of Ni (2.6×10^4 mol mol$_{Surf\ Ni}^{-1}$ h^{-1}) was 40 times as fast as that with HZSM-5 (6.3×10^2 mol mol$_{[H^+]HZSM-5}^{-1}$ h^{-1}). It should be addressed that in the non-polar solvent TOF for C−O bond cleavage on Ni/SiO$_2$ (2.6×10^4 mol mol$_{Surf\ Ni}^{-1}$ h^{-1}) was slightly higher than that in the aqueous phase (1.7×10^4 mol mol$_{Surf\ Ni}^{-1}$ h^{-1}). It has been consistently demonstrated that Ni surface atoms are the active sites for hydrogenolysis of C−O bond of BPE in the aqueous and apolar solvent (**Schemes 4-1 and 4-2**). The lower activity of Ni in the aqueous

phase may be attributed to the weaker adsorption of the reacting substrates in the presence of water [39]. It has been reported that in the aqueous phase, the Ni catalyst would deactivate due to water induced formation of Ni-bridged hydroxo species [40]. With Ni/HZSM-5 the major reaction pathway was hydrogenolysis of the C−O bond of BPE in undecane to produce toluene (initial selectivity: 33%) and phenol (initial selectivity: 25%) (**Scheme 4-2**). Free-radical reactions via pyrolysis were enhanced after HZSM-5 addition (together with Ni) with selectivity up to 36.6%. With Ni/HZSM-5 the C−O bond cleavage TOF in undecane (3.5×10^4 mol $\cdot$mol$_{\text{Surf Ni}}^{-1}$ h^{-1}) (**Table 4-3, Entry 5**) was much lower in water (1.1×10^5 mol $\cdot$mol$_{\text{Surf Ni}}^{-1}$ h^{-1}), which may be attributed to the fact that BPE is protonated in the high temperature water which makes the further C−O bond cleavage much easier, which is supported by the DFT calculations discussed in the following part.

4.3.4 Theoretical calculations for cleavage of C−O bond of BPE in the aqueous and apolar phases [*]

Accompanying the experimental investigation, density function theory calculations explore potential reaction routes for cleaving the C−O bonds of BPE in aqueous and apolar phases. In the aqueous phase, the direct cleavage of the C−O bond of the BPE into benzyl cation ($C_6H_5CH_2^+$) and phenoxy anion ($C_6H_5O^-$) was found to be difficult, requiring a high endothermic energy of 238 kJ $\cdot$mol^{-1}. This agrees perfectly with the reported bond strength of $C_{\text{aliphatic}}$−O bond in BPE (234 kJ $\cdot$mol^{-1}) [41]. In an alternative way, BPE was facilitated by protonation by the adjacent protons, and subsequently the protonated BPE could be readily cleaved forming phenol and benzyl cation with a low activation barrier of 9.9 kJ $\cdot$mol^{-1} (**Fig. 4-6**). Compared with the direct C-O cleavage with a high endothermic energy, the C-O cleavage of the protonated BPE is slightly exothermic.

[*] DFT calculations had been done by Dr.Donghai Mei in PNNL.
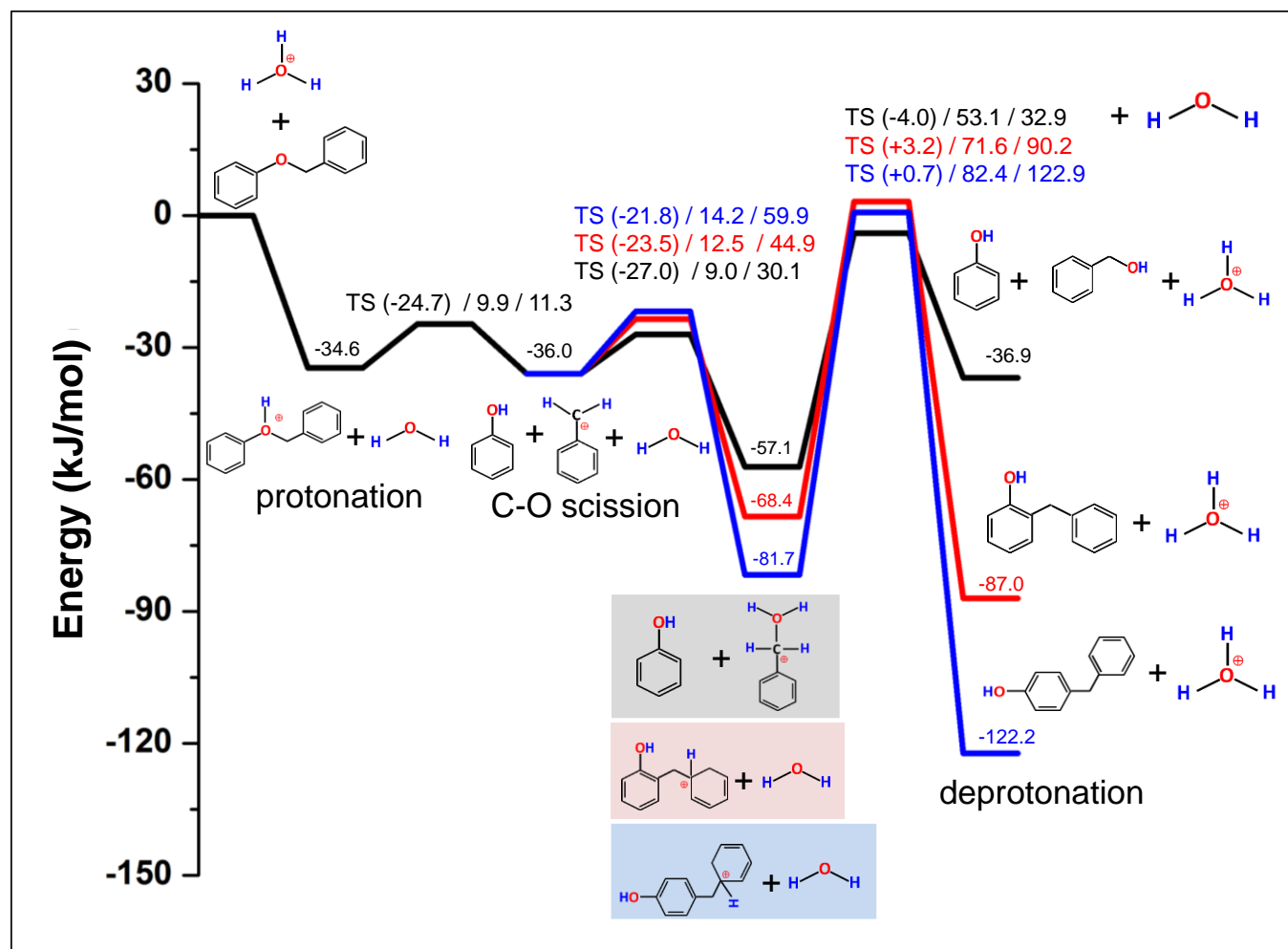
Figure 4-6. Energy profile of benzyl phenyl ether conversion in the aqueous phase calculated by DFT.

The formed benzyl cation was very active, combining with phenol or water in the aqueous phase in the next step. In essence, in the first route the benzyl cation combines with phenol to produce 2-benzylphenol or 4-benzylphenol, while in the latter pathway the benzyl alcohol ($C_6H_5CH_2OH_2^+$) formed via combination of protonated benzyl cation and water is deprotonated to benzyl alcohol. Then the produced proton is transferred to the neighboring water. Our calculations support the second route. It shows that the coupling between the benzyl cation and water ($\Delta G^{\circ}_{act} = 9.0$ kJ mol^{-1}) was almost comparable to that of coupling between the benzyl cation and phenol ($\Delta G^{\circ}_{act} = 12.5$ and 14.2 kJ mol^{-1}, respectively), whereas the deprotonation of $C_6H_5CH_2OH_2^+$ ($\Delta G^{\circ}_{act} = 53.1$ kJ mol^{-1}) was much more favored than the other two C−C coupling steps ($\Delta G^{\circ}_{act} = 71.6$ and

82.4 kJ mol^{-1}, respectively) although the deprotonation step is lightly endothermic. The calculated energy profile of BPE conversion in the aqueous phase (**Fig. 4-6**) clearly demonstrates that phenol and benzyl alcohol were the major products while 2-benzylphenol and 4-benzylphenol were formed in minor parts. This is consistent with our experimental observation that hydrolysis dominates for C−O bond cleavage in BPE, while the following C−C coupling reactions played a minor role. Our calculation also shows that the required energy was 655.5 kJ mol^{-1} for forming benzyl and phenoxy radicals from BPE in the aqueous phase, and so that the pyrolysis route was not favored in this sense.

In contrast to the major hydrolysis pathway of BPE in water, based on the experimental results the conversion of BPE followed the pyrolysis route in the apolar solvent such as undecane. Our theoretical calculations support this conclusion as well. It demonstrated that the dominant intermediates were benzyl and phenoxy radicals in undecane obtained by the C−O bond cleavage of the BPE, due to the much lower bond dissociation energy (184.3 kJ mol^{-1}) compared to that of phenyl and benzoxy radicals (332.9 kJ mol^{-1}) and that of benzyl cation and phenoxy anion (627.7 kJ mol^{-1}) (**Fig. 4-7a**). The two radicals (benzyl and phenoxy radicals) formed spontaneously recombined together with an energy drop of ~150 kJ mol^{-1} (**Fig. 4-8**), resulted in 2-$C_6H_5OCH_2C_6H_5$ and 4-$C_6H_5OCH_2C_6H_5$ radicals. In turn, the H atoms in 2-$C_6H_5OCH_2C_6H_5$ and 4-$C_6H_5OCH_2C_6H_5$ radicals stepwise shifted to the $O_{radical}$ atom via H atom transfer forming the final products of 2-benzylphenol and 4-benzylphenol (**Fig. 4-8**). The free activation barriers for the H atom transfer were 216.1 and 210.4 kJ mol^{-1} in 2-$C_6H_5OCH_2C_6H_5$ and 4-$C_6H_5OCH_2C_6H_5$, respectively. Comparing to the relative low activation barriers (9.9 kJ mol^{-1}) in the hydrolysis path of BPE in water, the activation barriers in the pyrolysis of the BPE in undecane were much higher (184.3 kJ mol^{-1}), which is in line with the experimental results that the rates of BPE conversion were slower in undecane than in water. In addition, the formation of phenol and toluene was thermodynamically favorable in undecane (**Fig. 4-7b**). However, the high H_2 dissociation energy results in the quite low concentrations of hydrogen radical without the aid of metals, which eventually leads to a low selectivity to phenol and toluene. In summary, C−O bonds of BPE in undecane are mostly cleaved by pyrolysis to produce phenyl and benzoxy radicals as intermediates, and the subsequent coupling of C−C bonds forms via radical recombination producing 2-$C_6H_5OCH_2C_6H_5$ and 4-$C_6H_5OCH_2C_6H_5$, fitting well with the previous experimental results.

(a) C−O bond cleavage mode of BPE in undecane
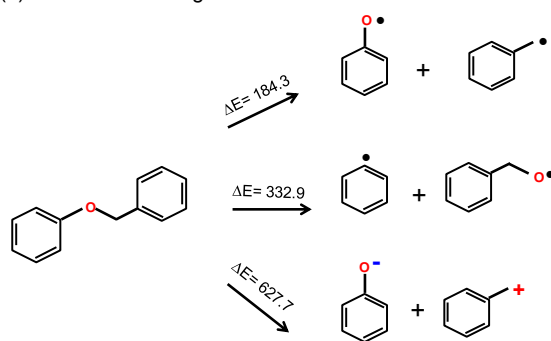
(b) Mechanism of phenol and toluene formation in undecane
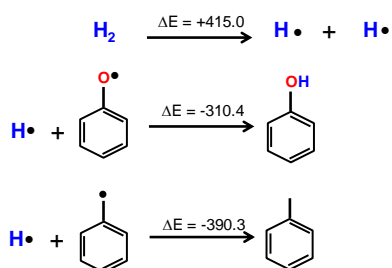
Figure 4-7. (a) Three C−O bond cleavage modes of BPE in undecane, and (b) proposed mechanism of phenol and toluene formation in undecane.
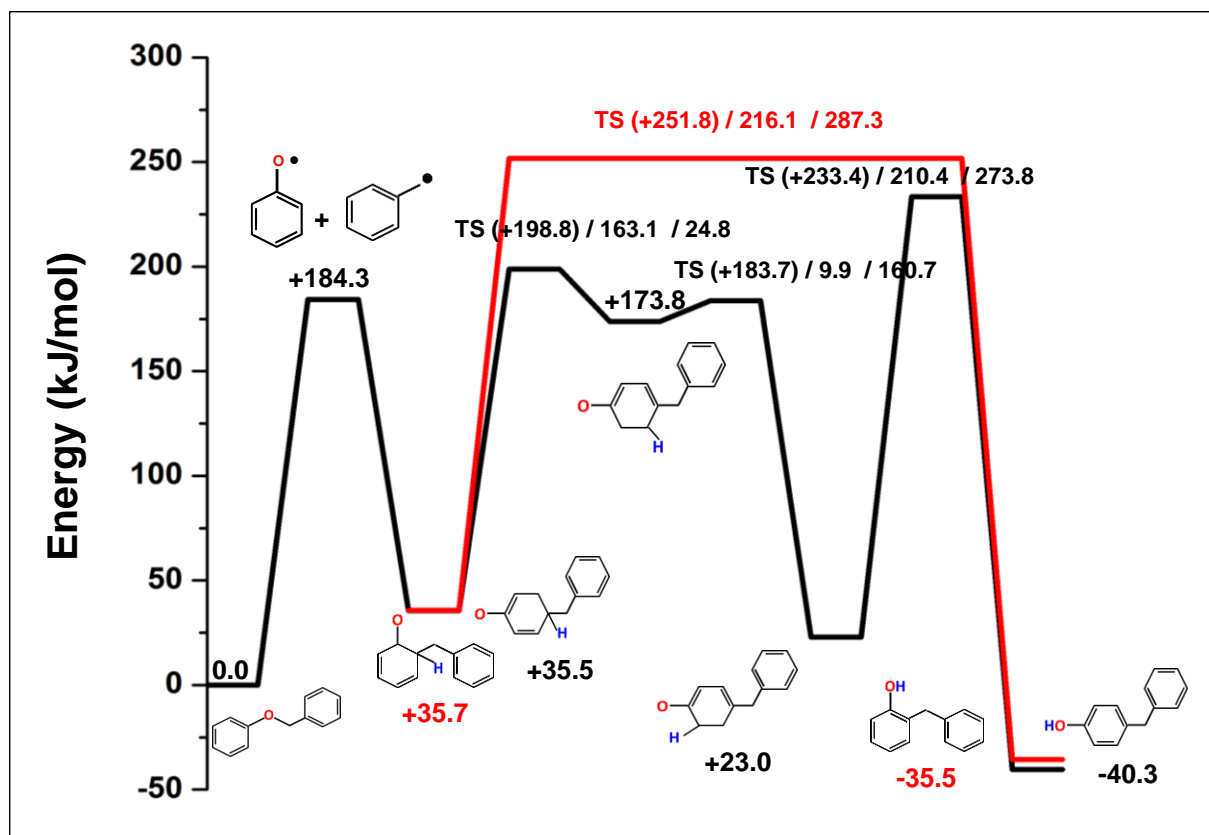
Figure 4-8. DFT calculated energy profile of benzyl phenyl ether conversion in undecane.

4.4 Conclusions

In the aqueous phase the C−O cleavage of BPE proceeds with an ionic pathway at 523 K, but not via a thermal/free radical route. In neat water in the absence or presence of H_2, the acid (hydronium ions from dissociated water) catalyzed hydrolysis route dominates, and subsequently the alkylation between the phenol and alcohol fragments follows to a small extent. In the presence of HZSM-5, both hydrolysis and alkylation rates are substantially enhanced. Ni/SiO$_2$, in contrast, leads to the quantitative and selective hydrogenolysis of C$_{aliphatic}$−O bond to form phenol and toluene in the presence of H_2. In the presence of metal and acid sites, metal (Ni) catalyzed hydrogenolysis plays a more important role for cleaving the ether bond in BPE. In apolar undecane at 523 K, non-catalytic pyrolysis cleaves the C$_{aliphatic}$−O bond of BPE, and thus, the free-radical

products dominate. When metals such as Ni/SiO₂ and Ni/HZSM-5 are involved, hydrogenolysis dominates the conversion, markedly suppressing the radical reaction. Ni/SiO₂ leads to higher hydrogenolysis rates in undecane than in water, probably because of the much weaker adsorption of reactants onto active Ni sites in the aqueous phase.

The DFT calculations support the proposed C−O bond cleavage mechanisms in the aqueous and apolar phases. Modeling results show that the protonation of BPE rather than the direct cleavage of the ether bond is the initial primary route in the aqueous phase due to the lower activation energy. In turn the protonated BPE is readily cleaved to form phenol and benzyl cation. Therefore, hydrolysis is demonstrated to be the main route for BPE conversion in the aqueous phase. In contrast, the radical reaction plays a dominant role in undecane, and the high concentrations radicals generate high concentrations of condensed heavier products. The phenol and toluene formed are present in small concentrations in the pyrolysis process due to the low concentrations hydrogen radicals produced without metals.

4.5 Acknowledgements

4.6 Appendix

Figure S4-1. TEM images of (**a**) Ni/HZSM-5 (Ni loading 10 wt.%) and (**b**) Ni/SiO$_2$ (Ni loading: 70 wt.%).

Table S4-1. Hydrogenation of aromatic compounds on Ni/SiO$_2$ in aqueous-phase at 523 K.[a]

Entry	Reactant	Selectivity (%)	Conv. (%)	TOF (h^{-1})
1[b]	Phenol	Benzene 3.0 Cyclohexane 3.0, Cyclohexanol 45, Cyclohexanone 49	20	2400
2	Toluene	Methyl cyclohexane 98, Methyl cyclohex-1-ene 2.0	19	135

[a] Reaction conditions: Reactant (0.050 mol), H$_2$O (80 mL), 70 wt.% Ni/SiO$_2$ (0.10 g), 4 MPa H$_2$, stirred at 700 rpm, 50 min.

[b] 70 wt.% Ni/SiO$_2$ (0.010 g), 30 min.

Table S4-2. Hydrolysis of benzyl phenyl ether in the mineral acidic solution. [a]

Entry	Conv. (%)	Selectivity (%)		
		phenol	Benzyl alcohol	Alkylation products
1	18	38	52	10

[a] Reaction conditions: reactant (18.4 g, 0.10 mol), H_2O (80 mL), 523 K, 4 MPa H_2, c (H_2SO_4) = 2.5×10^{-4} mol/L, 20 min., stirring at 700 rpm.

4.7 Reference

[1]   M. Stöcker, Angew. Chem. Int. Ed. 47 (2008) 9200.

[2]   W. Boerjan, J. Ralph, M. Baucher, Ann. Rev. Plant Biol. 54 (2003) 519.

[3]   E. Sjöström, Wood Chemistry: Fundamentals and Applications. Academic Press, Orlando, 1993.

[4]   T. Yoshida, Y. Oshima, Ind. Eng. Chem. Res. 43 (2004) 4097.

[5]   M. Osada, O. Sato, M. Watanabe, K. Arai, M. Shirai, Energy Fuels 20 (2006) 930.

[6]   F. P. Petrocelli, M. T. Klein, Ind. Eng. Chem. Prod. Res. Dev. 24 (1985) 635.

[7]   C. Amen-Chen, H. Pakdel, C. Roy, Bioresour. Technol.79 (2001) 277.

[8]   M. Saisu, T. Sato, M. Watanabe, T. Adschiri, K. Arai, Energy Fuels 17 (2003) 922.

[9]   Q. Song, F. Wang, J. Xu, Chem. Commun. 48 (2012) 7019.

[10]   Q. Song, F. Wang, J. Cai, Y. Wang, J. Zhang, W. Yu, J. Xu, Energy Environ. Sci. 6 (2013) 994.

[11]   Zakzeski, P. C. A. Bruijinincx, A. L. Jongerius, B. M. Weckhuysen, Chem. Rev.110 (2010) 3552.

[12]   E. Dorrestijn, L. Laarhoven, I. Arends, P. Mulder, J. Anal. Appl. Pyrolysis 54 (2000) 153.

[13]   P. N. Rylander, Hydrogenation Methods, Academic Press, London, 1985, pp. 157

[14]   Y. R. Luo, Comprehensive Handbook of Chemical Bond Energies, CRC Press, 2007.

[15]   M. W. Jarvis, J. W. Daily, H. Carstensen, A. M. Dean, S. Sharma, D. C. Dayton, D. J. Robichaud, M. R. Nimlos, J. Phys. Chem. A 115 (2011) 428.

[16]   T. Suzuki, H. Yamada, P. L. Sears, Y. Watanabe, Energy Fuels 3 (1989) 707.

[17]   B. C. Wu, M. T. Klein, S. I. Sandler, Energy Fuels 5 (1991) 453.

[18]   B. C. Wu, M. T. Klein, S. I. Sandler, AIChE J. 36 (1990) 1129.

[19]   S. H. Townsend, M. T. Klein, Am. Chem. Soc., Div. Petr. Chem. 32 (1987) 133.

[20]   V. Roberts, S. Fendt, A. A. Lemonidou, X. Li, J. A. Lercher, Appl. Catal. B 95 (2010) 71.

[21]   C. Zhao, J. A. Lercher, Angew. Chem. Int. Ed., 51 (2012) 5935.

[22]   J. He, C. Zhao, J. A. Lercher, J. Catal. 309 (2014) 362.

[23]   J. He, L. Lu, C. Zhao, D. Mei, J. A. Lercher, J. Catal. 309 (2014) 280.

[24]   J. He, C. Zhao, J. A. Lercher, J. Am. Chem. Soc. 134 (2012) 20768.

[25]   G.W.T. M. J. Frisch, H. B. Schlegel, G. E. Scuseria, M. A. Robb, J. R. Cheeseman, G. Scalmani, V. Barone, B. Mennucci, G. A. Petersson, H. Nakatsuji, M. Caricato, X. Li, H. P. Hratchian, A. F. Izmaylov, J. Bloino, G. Zheng, J. L. Sonnenberg, M. Hada, M. Ehara, K. Toyota, R. Fukuda, J. Hasegawa, M. Ishida, T. Nakajima, Y. Honda, O. Kitao, H. Nakai, T. Vreven, J. A. Montgomery, Jr., J. E. Peralta, F. Ogliaro, M. Bearpark, J. J. Heyd, E. Brothers, K. N. Kudin, V. N. Staroverov, R. Kobayashi, J. Normand, K. Raghavachari, A. Rendell, J. C. Burant, S. S. Iyengar, J. Tomasi, M. Cossi, N. Rega, J. M. Millam, M. Klene, J. E. Knox, J. B. Cross, V. Bakken, C. Adamo, J. Jaramillo, R. Gomperts, R. E. Stratmann, O. Yazyev, A. J. Austin, R. Cammi, C. Pomelli, J. W. Ochterski, R. L. Martin, K. Morokuma, V. G. Zakrzewski, G. A. Voth, P. Salvador, J. J. Dannenberg, S. Dapprich, A. D. Daniels, Ö. Farkas, J. B. Foresman, J. V. Ortiz, J. Cioslowski, and D. J. Fox, Gaussian, Inc., Wallingford CT, 2009.

[26]   C. Moller, M. S. Plesset, Phys. Rev. 46 (1934) 0618.

[27]   N. Govind, M. Petersen, G. Fitzgerald, D. King-Smith, J. Andzelm, Comp. Mater. Sci. 28 (2003) 250-258.

[28]   T.A. Halgren, W.N. Lipscomb, Chem. Phys. Lett. 49 (1977) 225-232.

[29]   M. Cossi, V. Barone, M. A. Robb, J. Chem. Phys. 111 (1999) 5295.

[30]   E. U. Franck, J. Chem. Thermodyn. 19 (1987) 225.

[31]   M. L. Marshall, E. U. Franck, J. Phys. Chem. Ref. Data 10 (1981), 295.

[32]   G. C. Akerlof, H. I. Oshry, J. Am. Chem. Soc. 72 (1950) 2844.

[33]   R. H. Schlosberg, W. H. Davis, T. R. Ashe, Fuel 60 (1981) 201.

[34]   M. Siskin, G. Brons, S. N. Vaughn, Energy Fuels 4 (1990) 488.

[35]   C. Zhao, D. M. Camaioni, J. A. Lercher, J. Catal. 288 (2012) 92.

[36]   E. Whalley, T. Faraday Soc. 55 (1959) 798.

[37]   J.Koskikallio, E. Whalley, Can. J. Chem. 37 (1959) 788.

[38]   V. M. Roberts, R. T. Knapp, X. Li, J. A. Lercher, ChemCatChem 2 (2010) 1407.

[39]   R. L. Cowan, R. W. Staehle, J. Electrochem. Soc. 118 (1971) 557.

[40]   J. Conella, E. Gomez-Bengoa, R. Martin, J. Am. Chem. Soc. 135 (2013) 1997.

[41]   E. Dorrestijn, L.J.J. Laarhoven, I. Arends, P. Mulder, J. Anal. Appl. Pyrolysis 54 (2000) 153.

Chapter 5

Impact of Solvent for Individual Steps of Phenol Hydrodeoxygenation with Pd/C and HZSM-5 as Catalysts

Impacts of water, methanol, and hexadecane solvents on the individual steps of phenol hydrodeoxygenation are investigated over Pd/C and HZSM-5 catalyst components at 473 K in the presence of H_2. Hydrodeoxygenation of phenol to cyclohexane includes four individual steps of phenol hydrogenation to cyclohexanone on Pd/C, cyclohexanone hydrogenation to cyclohexanol on Pd/C, cyclohexanol dehydration to cyclohexene on HZSM-5, and cyclohexene hydrogenation to cyclohexane on Pd/C. Individual phenol and cyclohexanone hydrogenation rates are much lower in methanol and hexadecane than in water, while rates of cyclohexanol dehydration and cyclohexene hydrogenation are similar in the three solvents. The slow rate in methanol is due to the strong solvation of reactants and the adsorption of methanol on Pd, as well as to the reaction between methanol and the cyclohexanone intermediate. The low solubility of phenol and strong interaction of hexadecane with Pd lead to the slow rate in hexadecane. The apparent activation energies for hydrogenation follow the order $E_{a\ phenol} > E_{a\ cyclohexanone} > E_{a\ cyclohexene}$, and the sequences of individual reaction rates are reversed in the three solvents. The dehydration rates ($1.1 - 1.8 \times 10^3\ mol \cdot mol_{BAS}^{-1} \cdot h^{-1}$) and apparent activation energies ($115 - 124\ kJ \cdot mol^{-1}$) are comparable in the three solvents.

5.1 Introduction

Hydrodeoxygenation is considered an effective approach to remove oxygen from the products of low rank coal and oil shale, and especially from biomass liquifaction [1]. Since the oxygen content of biomass (up to 50 wt.%) markedly exceeds that of coal (below 10 wt.%), advanced catalytic approaches are required for economically feasible deoxygenation of biomass and its derivatives. Solvents dramatically influence the rates and selectivity in these catalytic processes, by changing the reactive state of these complex bio-polymers and the products in the thermal reactions. Therefore, the selection of a proper solvent is of great importance for an efficient catalytic process. However, information about the relation between solvent nature, the activity and selectivity of the catalysts, and the state of the reactant is limited in the three-phase system (gas, liquid, and solid phases) during the hydrodeoxygenation.

Recently, we reported that the hydrodeoxygenation of bio-derived phenolic components to cycloalkanes can be quantitatively achieved using metallic (Pd, Pt, and Ni) and liquid (H_3PO_4) or solid acid catalysts (Nafion, SO_4^{2-}/ZrO_2, HZSM-5, and HBEA,) at 473 - 523 K in water [2-7]. The reaction sequence of phenol hydrodeoxygenation with bifunctional sites of metal and acid sites in the aqueous phase is concluded to follow initial phenol hydrogenation to cylcohexenol/cyclohexanone and subsequent cyclohexanone hydrogenation to cyclohexanol catalyzed by metals, and then acid catalyzed dehydration of cyclohexanol to cyclohexene, and final cyclohexene hydrogenation to cyclohexane [2-4]. It is, however, important to explore and compare the fundamental chemistry of hydrodeoxygenation of phenolic compounds in solvents of varying properties in order to understand, how the solvent environment modifies the solvent-catalyst, solvent-reactant, and reactant-catalyst interactions and how it might influence the catalyst itself.

Water comprises typically 30 wt. % of raw bio-oil and is a suitable solvent for an upgrading process. Methanol has been successfully used for lignocellulose conversion especially for lignin liquefaction [8], and non-polar solvents such as hexadecane and toluene have been employed for related hydrotreating of synthetic crude coal and oil shale [9,10]. The solvent for hydrodeoxygenation should, therefore, (i) be stable with respect to the process temperature,

pressure, and catalyst, (ii) hold reactants and intermediates in solution; (iii) dissolve and transport H_2, and (iv) dissipate the heat of the highly exothermic reactions.

In this contribution, we report the detailed kinetics of individual steps for phenol hydrodeoxygenation with Pd/C or HZSM-5 in water, methanol, and hexadecane. The turnover frequencies (TOFs) and apparent activation energies for individual steps are explored. The relationships between the chemical nature of the solvents and the interactions at the gas-liquid-solid interfaces are investigated in order to understand the fundamental differences between the reactions occurring in media with differing properties. The solvent-catalyst, solvent-reactant, and reactant-catalyst interactions and their influence on the activity are discussed in this work as well. In situ liquid phase IR spectroscopy is employed to monitor the concentrations of the reactants and products during individual reaction steps in water to obtain kinetic information.

5.2 Experimental Section

5.2.1 Chemicals

All chemicals were provided from commercial suppliers: phenol (Sigma-Aldrich, 99% GC assay), cyclohexene (Sigma-Aldrich, 99% GC assay), cyclohexanol (Sigma-Aldrich, 99% GC assay), cyclohexanone (Sigma-Aldrich, ≥99.5%, GC assay), ethyl acetate (Sigma-Aldrich, ≥99.5%, GC assay), methanol (Sigma-Aldrich, ≥99.93%, GC assay), hexadecane (Merck, >99%, GC assay), toluene (Sigma-Aldrich, ≥99.5%, GC assay), hydrogen (Westfalen AG, 99.999 vol %), nitrogen (Westfalen AG, 99.999 vol %), synthetic air (Westfalen AG, 99.999 vol %), ultra water system (EASYpure II, resistivity:18.2 MΩ·cm).

5.2.2 Catalysts

The Pd/C was obtained from Sigma-Aldrich (Sigma-Aldrich, 1 wt.% Pd), and HZSM-5 (Si/Al = 45) was supplied by Clariant AG. They were used without further treatment.

5.2.3 Catalyst characterization

BET surface area and pore diameters

The surface areas and pore diameters were determined by N_2 adsorption. The N_2 adsorption was carried out at 77 K on a PMI automated BET sorptometer. Prior to the measurements, the samples were outgassed at 523 K for 20 h. The specific surface areas, micropore and mesopore distributions were calculated based on the BET and BJH models.

H_2 chemisorption

The Pd supported on activated carbon was first reduced at 588 K in the presence of 0.1 MPa H_2 for 4 h before measurement. The reduced catalyst was activated at 588 K for 1 h in vacuum and then cooled to 313 K. The H_2 chemisorption and physisorption were subsequently measured in a pressure range from 1 kPa to 40 kPa. Then, the physisorbed H_2 was removed by outgassing the sample at the same temperature for 1 h. A second adsorption isotherm (physisorption) was measured. The concentration of chemisorbed hydrogen on the metal was determined by extrapolating the difference isotherm to zero H_2 pressure, and this value was used to calculate the dispersion of metal on supports.

Transmission electron microscopy (TEM)

TEM images were measured on a JEM-2010 Jeol transmission electron microscope operating at 120 kV. Prior to measurements catalyst was ground, suspended in ethanol and dispersed by ultrasonic treatment. The dispersion was dropped on a copper grid-supported carbon film. The average cluster size was calculated by counting 300 Pd particles.

Temperature-programmed desorption (TPD)

HZSM-5 was activated in flowing He at 623 K for 1h using a heating rate of 5 K $\cdot$min^{-1} from room temperature to 623 K. NH$_3$ was adsorbed by adding 10 vol.% to the He carrier gas (total flow 30 mL $\cdot$min^{-1}) at 423 K. The sample was purged with He for 2 h to remove physisorbed molecules. For TPD, the sample was heated in He at a rate of 10 K $\cdot$min^{-1} from 373 K to 1033 K for NH$_3$ desorption. The species desorbing were monitored by mass spectrometry (Balzers QME 200). For quantification, a reference material with known acid site concentration (HZSM-5 with Si/Al = 45) was used.

IR spectra of adsorbed pyridine

IR spectroscopy with pyridine as probe molecule was used to determine the acid site concentrations and distributions. The IR spectra were measured with a PerkinElmer 2000 spectrometer operated at a resolution of 4 cm^{-1}. The sample was activated at 723 K for 2 h in vacuum and a background spectrum was recorded after the temperature decreased to 423 K. The activated sample was exposed to pyridine vapor (1.0×10^{-5} MPa) at 423 K for 0.5 h. After removing physisorbed pyridine by outgassing at 423 K for 0.5 h, the spectra were recorded.

Atomic absorption spectroscopy (AAS)

A UNICAM 939 AA-Spectrometer was used to determine the concentration of noble metals in the carbon supported catalyst. Before measurement, 20–40 mg of the sample was dissolved in a mixture of 1.0 mL of 37 wt.% hydrochloric acid and 1.0 mL of 65 wt.% nitric acid at the boiling point of the mixture.

5.2.4 Measurement of catalytic reactions

5.2.4.1 Individual steps of phenol hydrodeoxygenation with Pd/C and HZSM-5 catalysts

The hydrodeoxygenation of phenol to cyclohexane includes four steps, **Step 1:** phenol hydrogenation to cyclohexanone on Pd/C, **Step 2:** cyclohexanone hydrogenation to cyclohexanol on Pd/C, **Step 3:** cyclohexanol dehydration to cyclohexene on HZSM-5, **Step 4:** cyclohexene hydrogenation to cyclohexane on Pd/C. Exploration of reaction rates was carried out at 473 K in three solvents (water, methanol, and hexadecane). Apparent activation energies were calculated from rates measured at 433, 453, 473 and 493 K.

The turnover frequencies (TOFs) defining initial reaction rates were expressed as per mole of converted reactant on per mole of surface Pd atom (or per mole of Brönsted acid site) per hour at conversions lower than 15% (except for the very fast cyclohexene hydrogenation) at 473 K in the presence of 4 MPa H_2. To control conversions in this range, the ratios of reactant to catalyst have been manipulated (**Fig. 5-2, 5-4, 5-5 and 5-7**). H_2 gas was introduced to the reactor at the reaction temperature of 473 K in order to make the conversion data start from zero at t = 0.

5.2.4.1.1 Kinetics of individual steps of phenol hydrodeoxygenation in water

The reaction conditions for the TOF measurements are reported as footnotes in the corresponding figures. In a typical experiment exemplified by **Step 1** of phenol hydrogenation, phenol (12.5 g), Pd/C (0.020 g, 1 wt.%), and H_2O (80 mL) were loaded in a Parr reactor (Series 4848, 300 mL), then the autoclave was charged with 0.1 MPa N_2. After the temperature was increased to 473 K, P_{H2} (partial pressure for hydrogen) was charged to 4.0 MPa (ambient temperature). Then stirring was initiated and the reaction time was recorded from that point. Reactions were conducted at 473 K with different duration times, or at 433, 453, 473 and 493 K for 0.5 h, with a stirring speed of 700 rpm. After reaction the reactor was quenched by ice to ambient temperature and the organic products were extracted with ethyl acetate and analyzed by

GC / MS. Because two phases existed in the four individual steps in water, the kinetics data was collected from separate batches with varying reaction times. The number of surface Pd atoms is determined by H_2-chemisorption measurement. The Brønsted acid measured by IR spectroscopy of adsorbed pyridine is used to calculate the dehydration TOF. The measurements for calculation of apparent activation energy were conducted at 433, 453, 473 and 493 K with the reaction times of 0.5 h.

5.2.4.1.2 Kinetics of individual steps of phenol hydrodeoxygenation in methanol

For the reactions carried out in methanol, the procedures were similar to those described in water. But because reactants, intermediates, and products were all soluble in methanol the in-situ sampling was enabled and the solvent extractions are unnecessary. The detailed reaction conditions are presented as footnotes of the corresponding figures. For **Steps 1, 2, 3, and 4**, the samples were collected with in situ sampling enabled by solubility in methanol, and then analyzed by GC/MS.

5.2.4.1.3 Kinetics of individual steps of phenol hydrodeoxygenation in hexadecane

When using hexadecane as solvent, the samples were collected from separate batch modes at varying durations for **Step 1** (phenol hydrogenation on Pd/C) because the phenol reactant is insoluble in hexadecane. After reaction the catalysts were collected by filtration, and toluene was added to the reactor to dissolve all organics. The homogeneous solution was analyzed by GC/MS. For **Steps 2, 3, and 4**, because reactants, intermediates, and products were all soluble in hexadecane, the in-situ sampling was enabled and the solvent extractions are unnecessary. The detailed reaction conditions are presented as footnotes of the corresponding figures. The samples were collected with in situ sampling enabled, when reactants and products are soluble in hexadecane, and then analyzed by GC/MS.

5.2.5 In situ liquid phase IR spectroscopy for measuring individual steps of phenol hydrodeoxygenation in water

The in situ liquid IR measurements were performed with a React IR 1000 spectrometer (Mettler Toledo) connected to an autoclave (100 mL, Parr). A diamond placed in the bottom of the autoclave was used as a probe to collect the in situ liquid IR spectra in the liquid phase. First, a background was collected with the working system containing water solvent (50 mL) and catalyst (1 wt.% Pd/C 0.10 g or HZSM-5 0.040 g) at 473 K in the presence of 4.0 MPa H_2. Second, after the reactor was cooled to ambient temperature, the individual reactions for phenol and cyclohexanone hydrogenation (**Steps 1 and 2**) were carried out at 473 K. When the temperature reached 473 K, a 4.0 MPa H_2 was introduced to the autoclave and the IR spectroscopy initiated. For dehydration of cyclohexanol (**Step 3**), the autoclave was charged with 1.5 MPa H_2 at ambient temperature and the IR spectrometer started. The IR spectra were collected every 10 min for 240 min during the overall reaction. Background spectra were subtracted before analysis.

5.3 Results and discussion

5.3.1 Catalyst characterizations

The physicochemical properties of 1 wt.% Pd/C and HZSM-5 catalysts are compiled in **Table 5-1**. Pd/C had a high BET surface area of 1103 m^2g^{-1} and pore volume of 0.58 cm^3g^{-1} with a Pd dispersion of 51% determined by H_2 chemisorption. The average Pd nanoparticle size was 2.6 nm measured by TEM (displayed in appendix 5.6, Fig. S5-1), agreeing reasonably well with the H_2 chemisorption result (2.2 nm). For HZSM-5 the apparent BET specific surface area was 395 m^2g^{-1} and the pore volume was 0.26 cm^3g^{-1} determined by N_2 sorption. The total acid concentration of HZSM-5 was 0.359 mmol·g^{-1}. The Brønsted acid sites (BAS) and Lewis acid sites (LAS) were 0.278 mmol·g^{-1} and 0.048 mmol·g^{-1}, respectively, measured by IR spectra of adsorbed pyridine (Py-IR) (**Table 5-1**). The acid concentration determined by TPD-NH_3 was 10% higher than those

analyzed by Py-IR, because the smaller size of probe molecule NH_3 allows it to reach more sterically limited acid sites comparing to pyridine.

Table 5-1. Physicochemical properties of the selected catalysts

Catalyst	Pd/C	HZSM-5 (Si/Al = 45)
Metal Loading (wt.%)	1.0	-
BET Surface Area (m^2g^{-1})	1103	395
Mesopore Surface Area (m^2g^{-1})	107	173
Micropore Surface Area (m^2g^{-1})	996	222
Pore Volume (cm^3g^{-1})	0.58	0.26
Mesopore Volume (cm^3g^{-1})	0.14	0.18
Micropore Volume (cm^3g^{-1})	0.44	0.08
Pd Dispersion (%)	51	-
Pd Particle Diameter (nm) (H_2 Chemisorption)	2.2	-
Pd Particle Diameter (nm) (TEM)	2.6	-
Acidity ($mmol·g^{-1}$) (TPD)	-	0.359
Acidity ($mmol·g^{-1}$) (Py-IR)	-	BAS: 0.278 LAS: 0.048

5.3.2 Hydrodeoxygenation of phenol in three solvents

Table 5-2. Solvent polarity index and H_2 solubility in the three solvents (298 K and 0.1 MPa H_2). [11-13].

Solvent	Polarity	H_2 solubility (mol·cm^{-3})
Water	9.0	7.8×10^{-7}
Methanol	6.6	3.5×10^{-6}
Hexadecane	ca. 0.3*	4.7×10^{-6}

*The value is estimated from the polarity index of n-decane (0.3), n-octane (0.4), and n-hexane (0).

We have previously evaluated combinations of mono-functional catalysts with metal or acid sites for hydrodeoxygenation of phenol in water [2-6]. We now investigate the kinetics of individual steps of phenol hydrodeoxygenation with a specific combination of supported Pd and HZSM-5 in water, methanol, or hexadecane. Water has a highest polarity index 9.0 (**Table 5-2**), methanol is lower at 6.6 and hexadecane is non-polar with the lowest polarity index of 0.3 [11]. H_2 solubility at 298 K and 0.1 MPa H_2, decreases from hexadecane (4.7×10^{-6} mol·cm^{-3}) via methanol (3.5×10^{-6} mol·cm^{-3}) to water (7.8×10^{-7} mol·cm^{-3}) (**Table 5-2**) [12,13].

Table 5-3. Solubility of phenol, cyclohexanone, cyclohexanol, cyclohexene, and cyclohexane at 298 K (g·(100 mL)$^{-1}$).[12]

Solvent	Phenol	Cyclohexanone	Cyclohexanol	Cyclohexene	Cyclohexane
Water	8.3	5.0	3.6	0.025	Immiscible
Methanol	> 62.5	> 62.5	> 62.5	> 62.5	30-33
Hexadecane	Insoluble	> 62.5	> 62.5	> 62.5	> 62.5

We expect the solubility of reactants, intermediates, and products to influence the reaction rates and apparent energies of activation through variations of solvent-catalyst, solvent-reactant, and reactant-catalyst interactions, as well as via potentially induced diffusion limitations. Vigorous stirring of the liquid phase ensures the absence of external gas-liquid mass transfer diffusion limitations in this four-phase reaction, verified in the previous kinetic study in water that the individual reaction steps were not influenced by stirring speeds varied from 700 to 1000 rpm, or varied reactant/water or reactant/catalyst ratios [4]. In addition, solubility of phenol, its derived intermediates, and products is different in various solvents. (**Table 5-3**). Water is partially miscible with phenol, cyclohexanone, and cyclohexanol at 298 K, but cyclohexene and cyclohexane are nearly immiscible in water. Phenol, ketone, alcohol and alkene/ane are soluble in methanol at 298 K. In hexadecane phenol is completely insoluble, but the other intermediates and ketone, alcohol, and alkene/ane product are highly soluble at 298 K (**Table 5-3**) [14].

5.3.2.1 Reaction sequence of phenol hydrodeoxygenation to cyclohexane

5.3.2.1.1 Reaction pathways of phenol hydrodeoxygenation in water and in hexadecane

It has been established that with a combination of two mono-functional catalysts phenol hydrodeoxygenation to cycloalkane proceeds in the aqueous phase through four steps (**Scheme 5-1**), i.e., phenol hydrogenation to cyclohexanol/cyclohexanone on metal sites (**Step 1**), sequential cyclohexanone hydrogenation to cyclohexanol on metal sites (**Step 2**), cyclohexanol dehydration to cyclohexene on acid sites (**Step 3**) and finally cyclohexene hydrogenation to cyclohexane on metal sites (**Step 4**). In hexadecane or water, the reaction pathways are identical for phenol hydrodeoxygenation with Pd/C and HZSM-5; hydrogenation is followed by dehydration (**Scheme. 5-1**), but in methanol the reaction pathway is more complex because of the acetal reactions between the cyclohexanone intermediate and methanol.
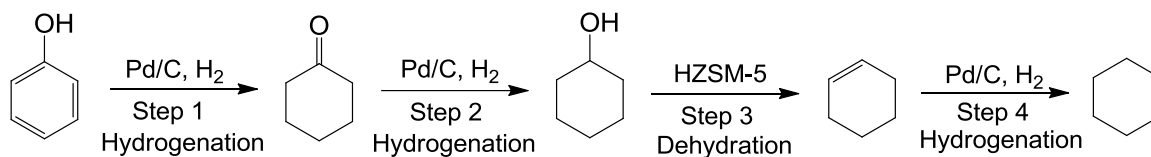
Scheme 5-1. Reaction sequence on hydrodeoxygenation of phenol to cyclohexane on metal and acid catalysts using water or hexadecane as solvents.

5.3.2.1.2 Hydrodeoxygenation pathway of phenol in methanol
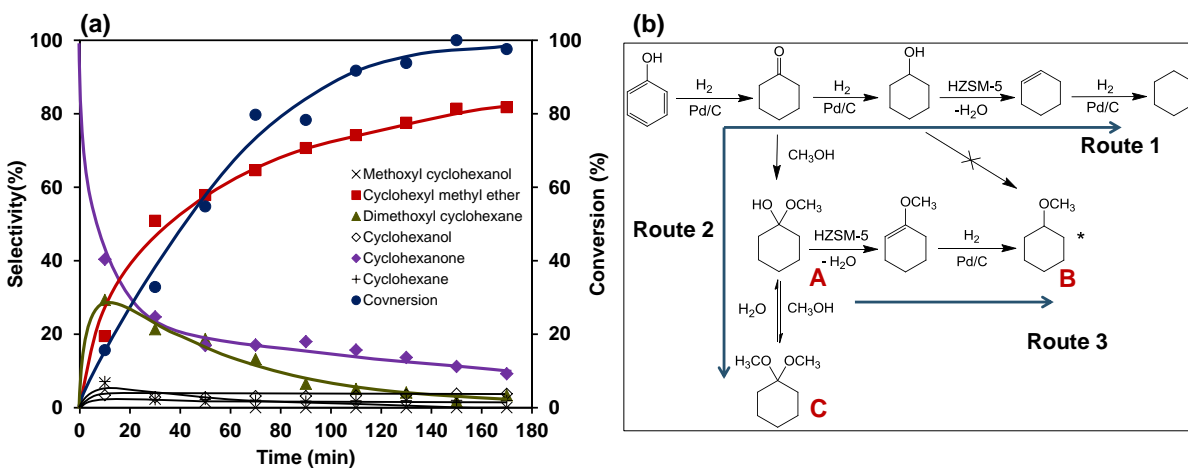
Figure 5-1. (a) The product distributions during phenol hydrodeoxygenation in methanol at 473 K and 4 MPa H_2. Reaction condition: Phenol (10.0 g), CH_3OH (80 mL), Pd/C (1 wt.%, 0.20 g), HZSM-5 (Si/Al = 45, 0.02 g), stirring at 700 rpm. (b) Reaction pathways for phenol hydrodeoxygenation over Pd/C and HZSM-5 catalysts in methanol at 473 K.

The product distribution from phenol conversion in methanol is plotted in **Fig. 5-1a** as a function of time with Pd/C and HZSM-5 at 473 K. At t = 0 the primary product was cyclohexanone [4]. The ketone was rapidly consumed via the acetal reaction (**Route 2** in **Fig. 5-1b**) but not by the parallel hydrogenation route (**Route 1** in **Fig. 5-1b**). The selectivity to the primary acetal product (Compound **A,** methoxycyclohexanol formed from cyclohexanone and methanol, **Fig. 5-1b**) remained very low (< 5 C%) during the reaction. Compound **A** was either rapidly dehydrated by HZSM-5 (**Route 3**) and hydrogenated over Pd to cyclohexyl methyl ether (Compound **B**), or this intermediate reacted further with methanol to form 1,1'-dimethoxycyclohexane (Compound **C**, **Route 2**, slower than **Route 3**) (**Fig. 5-1b**). Thus, cyclohexyl methyl ether (Compound **B**) became the major product with 81% selectivity at 170 min.

The selectivity to 1,1'-dimethoxycyclohexane (Compound **C**) first increased to a maximum of 29% at 10 min and then decreased to 3.3% at 170 min. The initial selectivity increased, because the acetal product was able to react with a large excess of methanol. The subsequent decrease in selectivity is mainly related to the fact that the increasing concentrations of water formed from the

dehydration of methoxycyclohexanol (Compound **A**) shifted the equilibrium of 1,1'-dimethoxycyclohexane (Compound **C**) to methoxycyclohexanol (Compound **A**) (**Fig. 5-1b**), and thus, decreased the selectivity of 1,1'-dimethoxycyclohexane (Compound **C**).

With methanol as solvent, cyclohexane was produced with selectivity as low as 1.9% at 100% conversion after 170 min. via **Route 1**. The fast acetal reaction between ketone and methanol (**Route 2**) dominated the phenol conversion in methanol. The acetal reaction was much faster than cyclohexanone hydrogenation on Pd/C in methanol under these reaction conditions (**Fig. 5-1b**). Thus, alcohols or polyols are not suitable solvents for hydrodeoxygenation of phenolic compounds to produce hydrocarbon biofuels, although it has been reported that lignin is efficiently converted in supercritical methanol [15].

5.3.2.2 Turnover frequencies (TOFs) of individual steps for phenol hydrodeoxygenation in three solvents

5.3.2.2.1 TOFs for phenol hydrogenation over Pd/C
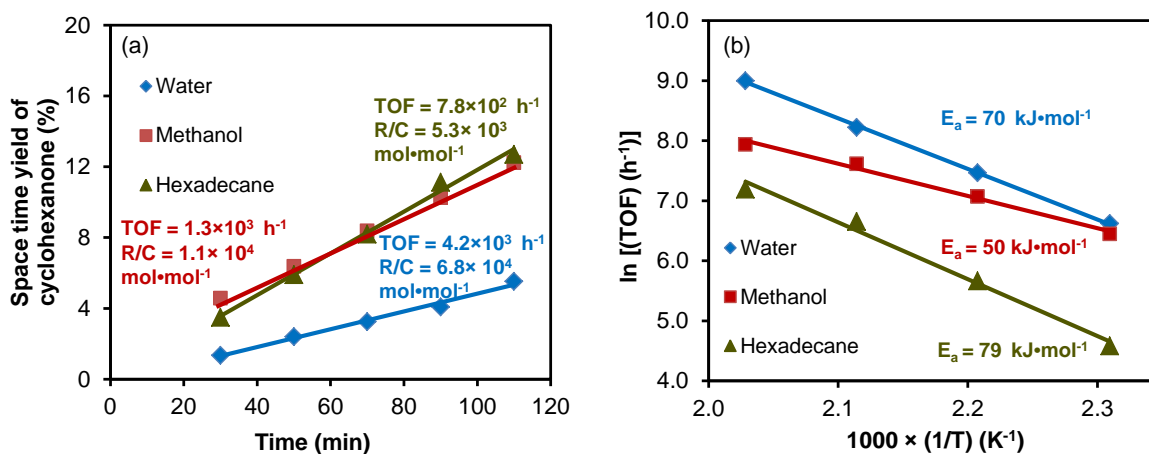

Figure 5-2. (a) TOFs on phenol hydrogenation over Pd/C in three solvents at 473 K and 4 MPa H$_2$ at a stirring speed of 700 rpm. Note: R/C is mol (reactant) to mol (catalyst) ratio. Reaction conditions: phenol (12.5 g), H$_2$O (80 mL), and Pd/C (1 wt.%, 0.020 g); phenol (15.0 g), CH$_3$OH (80 mL), and Pd/C (1 wt.%, 0.15 g); phenol (5.0 g), hexadecane (80 mL), and Pd/C (1 wt.%, 0.10

g). (b) The TOF values for Arrhenius plots were recorded after 30 min. at 433, 453, 473, and 493 K.

In the first phenol hydrogenation step on Pd/C (**Step 1,** the first individual step), the initial TOFs in methanol (1.3 $\times 10^3$ mol·mol$_{Pd\ surf.}^{-1}$h^{-1}) and hexadecane (7.8 $\times 10^2$ mol·mol$_{Pd\ surf.}^{-1}$h^{-1}) were significantly lower than in water (4.2 $\times 10^3$ mol·mol$_{Pd\ surf.}^{-1}$h^{-1}) (**Fig. 5-2, Table 5-4**). Three factors influence the initial hydrogenation rates in methanol. The first is the solvation of phenol (solvent-reactant interaction). In the case of acetophenone conversion, Bertero et al. [16] reported that its solvation increased in the sequence 2-propanol < 1-propanol < ethanol < methanol. The opposite trend was observed for acetophenone hydrogenation rates with Ni/SiO$_2$, explained by the fact that stronger solvent-reactant interaction (solvation) reduced the surface coverage of the reactant. The hydrogenation rate showed 0-1 reaction order with respect to the phenol concentrations, e.g., a reaction order of 0.65 was obtained on Pd/Ca-Al$_2$O$_3$ at 503 K [17]. Thus, we hypothesize that the stronger solvation of phenol in methanol than in water or hexadecane reduces its adsorption on Pd and lowers the phenol hydrogenation rate.

The second consideration is related to the interaction of methanol with the Pd surface (solvent-catalyst interaction). Solvent adsorption on the catalyst surface may have strongly influenced the Pd activity for phenol hydrogenation. For example, methanol may compete for the catalyst surface and decrease surface coverage of phenol. Sexton et al. [18] reported that CH$_3$OH adsorbed more strongly than water on Pd, and thus, affects the surface phenol coverage more strongly than water.

The third impact results from the reaction between cyclohexanone and methanol (**Fig. 5-1**). The hydrogenated cyclohexanone reacted quickly with methanol to form a series of products via the acetal reaction (**Fig. S5-2**). Consequently, the acetal products cyclohexyl methyl ether and dimethoxycyclohexane dominated with selectivity exceeding 85%. However, if 1,1'-dimethoxycyclohexane were preferably adsorbed on Pd sites, phenol hydrogenation would have been inhibited.

In hexadecane, the rate of phenol hydrogenation was lowered by two major factors. One is the low solubility of phenol in hexadecane (**Table 5-3**), limiting the phenol concentrations (0.26 mg·L^{-1} at 298 K, detected by GC) close to the accessible Pd/C sites and inducing a diffusion

limitation. The second is related to the solvent-Pd interaction, as the phenol hydrogenation rate decreased with increased strength of solvent adsorption on the Pd surface. It has been reported that the adsorption energies of hexadecane on Pd (111) and Pt (111) were ca. 118 kJ·mol^{-1} [19], while in a comparative study the adsorption energy of water on Pd (111) was 50 kJ·mol^{-1} [20]. This indicates again that the hexadecane-Pd interaction is much stronger than the water-Pd interaction, which would reduce the surface concentration of phenol on Pd. In line with this argument note that the hydrogenation rate in water is five times that in hexadecane.

In comparison with methanol and hexadecane, water gave the highest phenol hydrogenation rate. Phenol had low solubility in water (8.3 g·100 mL^{-1}) at ambient temperature, but the phenol solubility increased to completely miscible in water at 338 K. Thus, the solubility of phenol in water at 473 K would not limit the reaction rate. In the second consideration, the H_2 solubility in water is lower (7.8 $\times 10^{-7}$ mol·cm^{-3}) than in hexadecane (4.7 $\times 10^{-6}$ mol·cm^{-3}) or methanol (3.5 $\times 10^{-6}$ mol·cm^{-3}), and the soluble H_2 concentration in water was 0.0232 mol·cm^{-3} at 473 K in the presence of 4 MPa H_2 [21]. The result shows that the hydrogenation rates are more affected by the solvent properties, but not (as to be expected) by the H_2 solubility at conditions selected, which is in accordance with the previous report for hydrogenation of aromatics [22].

5.3.2.2.2 TOFs of cyclohexanone hydrogenation over Pd/C

Cyclohexanone reacted with methanol to form methoxycyclohexanol (Compound **A**) as initial product through the acetal reaction (**Figs. 5-3a and 5-3b**) and further to form 1,1-dimethoxycyclohexane (Compound **C**) via **Route 1** (**Fig. 5-3b**). The methoxycyclohexanol (Compound **A**) intermediate can also dehydrate to cyclohexenylmethyl ether catalyzed by protons in hot water (**Route 2** in **Fig. 5-3b**), and hydrogenate to cyclohexylmethyl ether (Compound **B**, major product at selectivity of 50% at 110 min.). In a separate experiment on cyclohexanol conversion in methanol using Pd/C, the ether yield was only 0.4%, and, thus, another possible route (**Route 3**) via intermolecular dehydration forming cyclohexyl methyl ether is excluded. The kinetics of cyclohexanone conversion in methanol with Pd/C showed that conversion already attained 15% at t = 0 after the pre-heating process (**Fig. 5-3a**), and it is concluded that this conversion is due to the non-catalytic acetal reaction between cyclohexanol and methanol at 473

K. This is supported by the separate blank test that the cyclohexanone already reached 13% conversion after 15 min.. In the first 10 minutes this acetal reaction between cyclohexanone and methanol consumed 15% of the cyclohexanone. This would slow the rate for **Step 2** over Pd/C as the cyclohexanone hydrogenation rate had nearly first order (n = 0.8) dependence on the reactant concentration [23]. It is estimated that with the lowered cyclohexanone concentration, the rate in methanol would be increased to 4.1×10^3 mol·mol$_{Pd\ surf.}^{-1}$h^{-1} over Pd/C, which is slightly higher than the experimental rate (3.5×10^3 mol·mol$_{Pd\ surf.}^{-1}$h^{-1}). Strong solvation of cyclohexanone and the Pd surface by methanol [18] further decreased the cyclohexanone hydrogenation rate (experimental result: 3.5×10^3 mol·mol$_{Pd\ surf.}^{-1}$h^{-1}; expected: 4.1×10^3 mol·mol$_{Pd\ surf.}^{-1}$h^{-1}. Since 15% of cyclohexanone had been consumed by acetal reaction during the heating process from room temperature to 473 K, the concentration of cyclohexanone at the beginning of reaction at 473 K was only 85% of the initial one.).
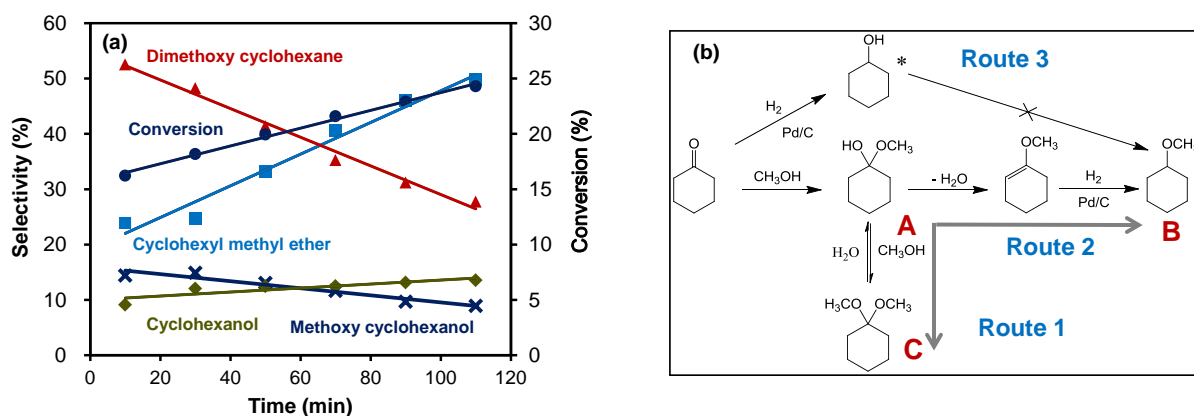
Figure 5-3. (a) The conversion/selectivity of cyclohexanone hydrogenation in methanol at 473 K and 4 MPa H$_2$ at a stirring speed of 700 rpm. Reaction condition: cyclohexanone (20.0 g), CH$_3$OH (80 mL), and Pd/C (1 wt.%, 0.010 g). (b) Reaction pathways for cyclohexanone hydrogenation over Pd/C in methanol.

In the cyclohexanone hydrogenation rate in water over Pd/C (TOF = 2.1×10^4 mol·mol$_{Pd\ surf.}^{-1}$h^{-1}) was six times that in methanol (TOF = 3.5×10^3 mol·mol$_{Pd\ surf.}^{-1}$h^{-1}) and four times that in hexadecane (TOF = 5.3×10^3 mol·mol$_{Pd\ surf.}^{-1}$h^{-1}) (**Fig. 5-4a, Table 5-4**). The rates of cyclohexanone hydrogenation were three to seven times those of phenol hydrogenation (**Table 5-**

4), because Pd metal sites have a stronger interaction with a ketone functional group than with the aromatic ring. Since cyclohexanone did not populate Pd active sites, a lower rate of cyclohexanone hydrogenation was observed in hexadecane. This is because hexadecane has much stronger adsorption strength than water to Pd as noted previously [19,20].
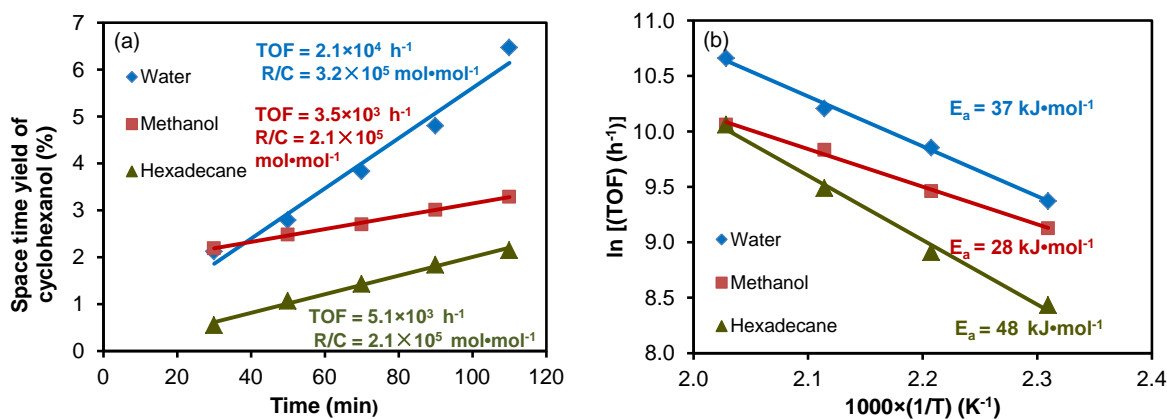
Figure 5-4. (a) TOFs of cyclohexanone hydrogenation over Pd/C in three solvents at 473 K and 4 MPa H_2 at a stirring speed of 700 rpm. Note: R/C stands for mol (reactant) to mol (catalyst sites). Reaction conditions: cyclohexanone (60.0 g), H_2O (80 mL), and Pd/C (1 wt.%, 0.020 g); cyclohexanone (20.0 g), CH_3OH (80 mL), and Pd/C (1 wt.%, 0.010 g); cyclohexanone (20.0 g), hexadecane (80 mL), and Pd/C (1 wt.%, 0.010 g). (b) The TOF values for Arrhenius plots are recorded after 30 min. at 433, 453, 473, and 493 K.

5.3.2.2.3 TOFs for cyclohexanol dehydration over HZSM-5

The TOFs of cyclohexanol dehydration (**Step 3**, the third individual step) were similar at 1.1 $\times 10^3 - 1.8 \times 10^3$ mol·mol$_{BAS}^{-1}$·h^{-1} in water, methanol, and hexadecane, respectively (**Fig. 5-5a and Table 5-4**). HZSM-5-catalyzed dehydration rates in water (1.6 $\times 10^3$ mol·mol$_{BAS}^{-1}$·h^{-1}) were two orders of magnitude higher than H_3PO_4 (15 mol·mol$_{[H^+]}^{-1}$·h^{-1}) [4]. The water solvent shifted the dehydration-hydration equilibrium and inhibited dehydration. It has been reported that Lewis acid sites are ineffective for dehydration in the aqueous phase, because water blocks Lewis active sites

[24]. Consequently, the Brønsted acid sites in the pores of zeolite are concluded to be the active catalytic sites for dehydration. We attribute the high dehydration rates on HZSM-5 to the unique properties of zeolite stabilizing a favorable transition state. High alcohol adsorption capacity even in aqueous solution [25] as well as micropore size of HZSM-5 only allows the smaller alcohol monomers to approach the zeolite BAS sites. Thus, the alcohol monomer-oligomer equilibrium is rapidly shifted towards monomers to accelerate the dehydration rate [26].
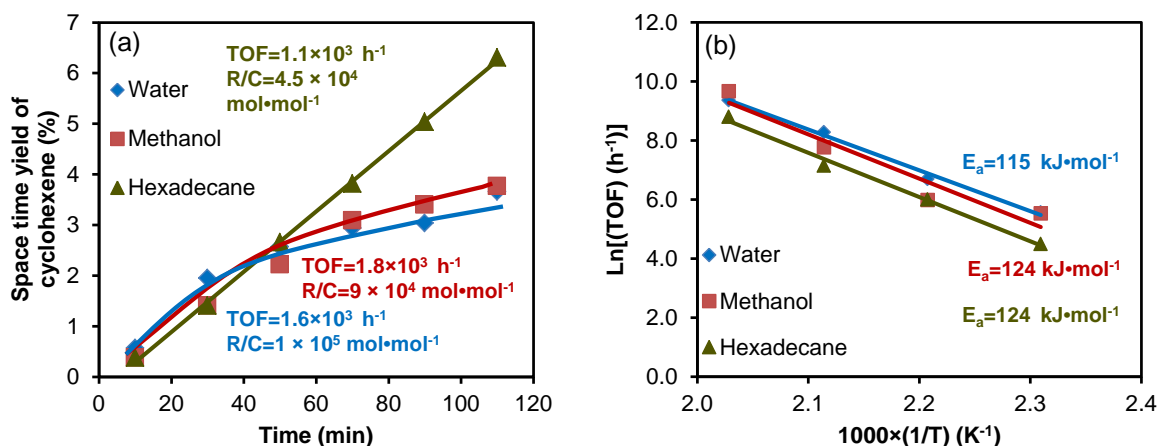
Figure 5-5. (a) TOFs of cyclohexanol dehydration in three solvents at 473 K in the presence of 4 MPa H_2 at a stirring speed of 700 rpm. R/C stands for mol (reactant) to mol (catalyst sites). Reaction conditions: cyclohexanol (140.0 g), H_2O (80 mL), HZSM-5 (0.050 g); cyclohexanol (50.0 g), CH_3OH (80 mL), HZSM-5 (0.020 g); cyclohexanol (50.0 g), hexadecane (80 mL), HZSM-5 (0.040 g). (b) The TOF values for Arrhenius plots are recorded after 30 min. at 433, 453, 473, and 493 K.

The initial activity for alcohol dehydration of HZSM-5 dropped by 60% in methanol and water after 40 min. (**Fig. 5-5a**), indicating deactivation appears in the liquid phase of high concentrations of cyclohexanol (38.5 - 63.6 wt.%, see conditions in **Fig. 5-5a**). We also found that the color of HZSM-5 changed from white to brown, which may be caused by carbon deposition in the autoclave after reaction in water or methanol, while the color of the catalyst in hexadecane was unchanged. Noller et al. [27] reported that the gas phase alcohol dehydration was accompanied by

carbon deposition from the oligomerization of the formed olefins in the zeolite. Haw et al. [28] also observed with ^{13}C MAS NMR oligomerized cyclohexene from cyclohexanol on HZSM-5. In fact, more carbon was deposited from the concentrated cyclohexanol liquid phase (38.5 - 63.6 wt.%) than from the gas phase after considering the different densities of the two phases. The decreased catalytic activities in water and methanol are mainly due to the carbon deposition formation on the catalytic material.

The catalyst, however, did not deactivate in hexadecane and this may be attributed to the different stability of carbenium ions (from cyclohexanol) in the three solvents. The counter ion and the carbenium ion may have a range of associations, from a covalent bond, tight ion pair (un-separated), to solvent-separated ion pair (partially separated) and free ions (completely dissociated) (**Scheme 5-2**) [29, 30]. The covalent bond association is strongest and the association of free ions is weakest [30]. In cationic polymerization, the ions are in equilibrium between an associated ion pair and free ions [29]. Ion pair separation is favored by more polar solvents. Since free ions are more reactive than ion pairs, the rate of propagation is faster in more polar solvents. Therefore, polar water (polarity index: 9.0) and methanol (polarity index: 6.6) yield higher polymerization selectivity than hexadecane (polarity index: 0.3).

$\sim\!\!\sim\!\! RX$ $\sim\!\!\sim\!\! R^+X^-$ $\sim\!\!\sim\!\! R^+/X^-$ $\sim\!\!\sim\!\! R^+ + X^-$

covalent   tight ion pair   solvent-separated ion pair   free ions
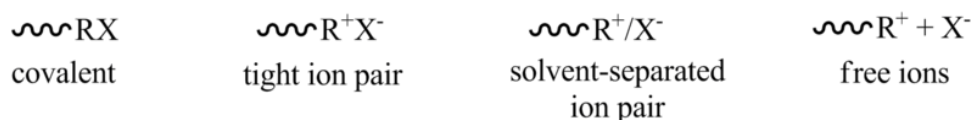
Scheme 5-2. Range of associations between the carbenium ion (R^+) and anion (X^-).

The intermolecular dehydration of cyclohexanol in water formed bicyclohexyl ether with 10% selectivity at 110 min. Cyclohexanol reacted with methanol via intermolecular reaction as well. Shown from the kinetics of cyclohexanol dehydration (**Fig. 5-6a**), the parallel routes of intra-molecular dehydration producing cyclohexene and of intermolecular dehydration forming cyclohexyl methyl ether maintained individual selectivities of 75% and 25% during the conversion (**Fig. 5-6b**), respectively.
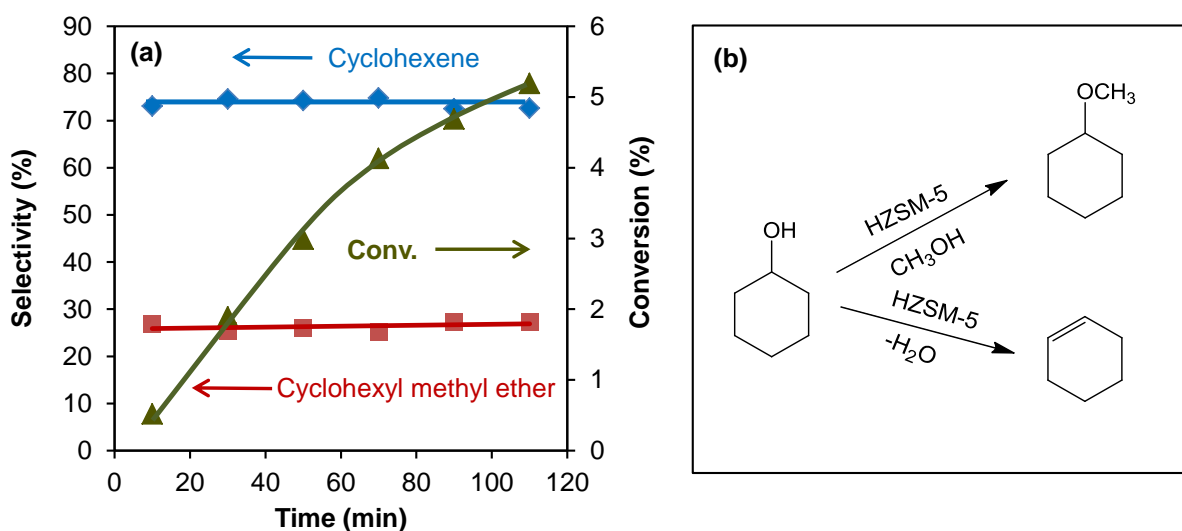
Figure 5-6. (a) The product distribution from cyclohexanol dehydration in methanol at 473 K in the presence of 4 MPa H_2. Reaction condition: cyclohexanol (50.0 g), CH_3OH (80 mL), HZSM-5 (Si/Al = 45, 0.020 g). (b) Reaction route for cyclohexanol dehydration over HZSM-5 in methanol.

5.3.2.2.4 TOFs for cyclohexene hydrogenation over Pd/C
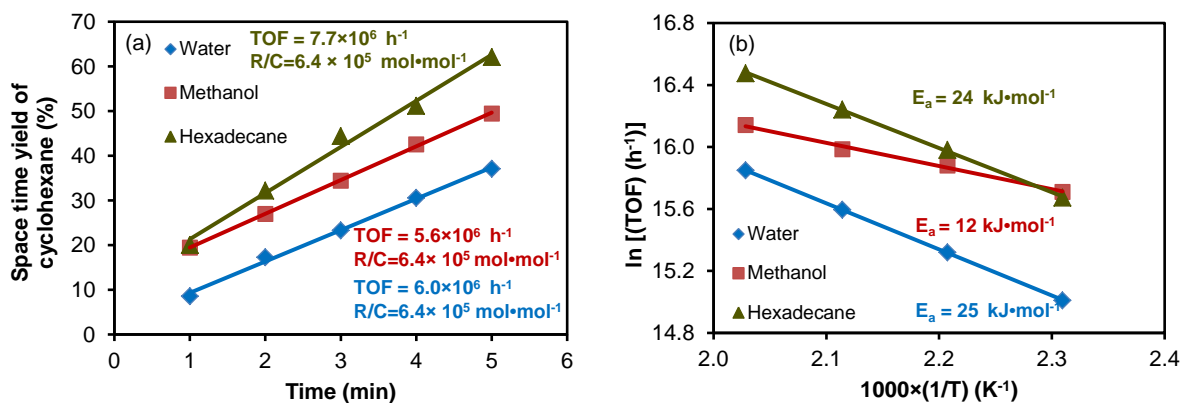
Figure 5-7. (a) TOFs of cyclohexene hydrogenation over Pd/C in water, methanol and hexadecane at 473 K in 4 MPa H_2 at a stirring speed of 700 rpm. Note: R/C stands for mol (reactant) to mol (catalyst sites). Reaction conditions: cyclohexene (50.0 g), H_2O (80 mL), Pd/C (1 wt. %, 0.010 g); cyclohexene (50.0 g), CH_3OH (80 mL), Pd/C (1 wt.%, 0.010 g); cyclohexene (50.0 g), hexadecane

(80 mL), Pd/C (1 wt.%, 0.010 g). (b) The TOF values for Arrhenius plots were recorded after 3 min. at 433, 453, 473, and 493 K.

Cyclohexene hydrogenation rates (**Step 4**, the fourth individual step) were similar in these three solvents at attaining TOFs of $5.6 \times 10^6 - 7.7 \times 10^6$ mol·mol$_{Pd\ surf.}^{-1}$h^{-1} (**Fig. 5-7, Table 5-4**). This is in line with results obtained by Gonzo and Boudart [31], who also reported the absence of a solvent effect for hydrogenation of cyclohexene on Pd/SiO$_2$ after studying the influence of diverse solvents including methanol, *n*-heptane, ethyl acetate, and cyclohexane at 308 K.

Combining all the data obtained from kinetics of the four individual reactions distinguishes the rate-determining step for the phenol hydrodeoxygenation in the three solvents (**Table 5-4**). In water, cyclohexanol dehydration (**Step 3**) was the slowest step. The rate-determining step in methanol and hexadecane was phenol hydrogenation (**Step 1**). Based on these results, it is expected that in the use of dual-functional catalysts of Pd/C and HZSM-5 for phenol hydrodeoxygenation in water, if not considering the competitive adsorption of the reactants in the overall kinetics, the most abundant product is cyclohexanol as dehydration (**Step 3**) is relatively slow compared to hydrogenation. When phenol starts to be hydrogenated on Pd/C (**Step 1**) in hexadecane, cyclohexane is expected to appear as the major product in a short time, because the rates of cyclohexanone hydrogenation (**Step 2**), via cyclohexanol dehydration (**Step 3**), to cyclohexene hydrogenation (**Step 4**) are accelerated step by step. Rates of cyclohexanol dehydration and cyclohexene hydrogenation were similar in three solvents, but the rates of hydrogenation of phenol and cyclcohexanone were much slower in methanol and hexadecane compared to the rates in water.

Table 5- 4. TOFs of hydrodeoxygenation of phenol in three solvents (473 K, 4 MPa H_2).

Solvent	Phenol hydrogenation over Pd/C	Cyclohexanone hydrogenation over Pd/C	Cyclohexanol dehydration over HZSM-5	Cyclohexene hydrogenation over Pd/C
	TOF_1 (mol·mol$_{Pd\ surf.}^{-1}$·h^{-1})	TOF_2 (mol·mol$_{Pd\ surf.}^{-1}$·h^{-1})	TOF_3 (mol·mol$_{BAS}^{-1}$·h^{-1})	TOF_4 (mol·mol$_{Pd\ surf}^{-1}$·h^{-1})
Water	4.2×10^3	2.1×10^4	1.6×10^3	6.0×10^6
Methanol	1.3×10^3	3.5×10^3	1.8×10^3	5.6×10^6
Hexadecane	7.8×10^2	5.1×10^3	1.1×10^3	7.7×10^6

5.3.2.3 E_a of the individual steps in phenol hydrodeoxygenation

The individual steps during phenol hydrodeoxygenation can be grouped into (i) hydrogenations of aromatic ring, ketone, and alkene on Pd and (ii) dehydration of cyclohexanol on HZSM-5. For the three hydrogenation steps, it was found that the apparent activation energies for hydrogenation were similar in hexadecane and water, but significantly lower in methanol (**Table 5-5**).

Table 5-5. E_a (kJ mol^{-1}) on hydrodeoxygenation of phenol in three solvents (473 K, 4 MPa H$_2$).

Solvent	Phenol hydrogenation over Pd/C	Cyclohexanone hydrogenation over Pd/C	Cyclohexanol dehydration over HZSM-5	Cyclohexene hydrogenation over Pd/C
	E_{a1}	E_{a2}	E_{a3}	E_{a4}
Water	70	37	115	25
Methanol	50	28	124	12
Hexadecane	79	48	124	24

The observed activation energy equation can be expressed as [32]:

$$E_a^{obs} = E_a^{true} + (1-\theta_A) \Delta H_A - \theta_B \Delta H_B \qquad (1)$$

Where E_a^{obs}, E_a^{true} θ_A, θ_B, ΔH_A, and ΔH_B represents the observed activation energy, the true activation energy, the coverage by reactant, the coverage by product, the reactant heat of adsorption, and the product heat of adsorption, respectively.

The phenol hydrogenation rates were recorded in three solvents at 433, 453, 473, and 493 K. Based on the Arrhenius law, the activation energies (E_a) were calculated to be 70, 50, and 79 kJ mol^{-1} in water, methanol, and hexadecane, respectively. Vishwanathan et al. [33] obtained an apparent activation energy of 65 kJ mol^{-1} for phenol hydrogenation over Pd/MgO in the gas phase in fair agreement of our result (**Table 5-5**). By comparison, E_a for the phenol hydrogenation in hexadecane was similar to that in water at 70-79 kJ mol^{-1}. E_a in methanol was significantly lower at 50 kJ mol^{-1} (**Table 5-5**). We attribute this to the strong solvation of both phenol [16] and surface Pd [18] by methanol. Solvation would lower the θ_A and θ_B in equation (1). Consequently E_a^{obs} in methanol would be lower than in water or hexadecane. Moreover, the reaction with methanol of

the cyclohexanone generated from phenol hydrogenation would also decrease θ_A and θ_B because of competing by-product adsorption, and thus lower E_a^{obs} in methanol.

The E_a of cyclohexanone hydrogenation followed the same trend as phenol hydrogenation; hexadecane (48 kJ mol^{-1}) > water (37 kJ mol^{-1}) > methanol (28 kJ mol^{-1}). E_a for the hydrogenation reaction in methanol was significantly lower than that in water or hexadecane (**Table 5-5**). Due to the similar hydrogenation mechanisms, the strong solvation of cyclohexanone by methanol [16] (**Table 5-3**) and the stronger adsorption of methanol on Pd [18] decreased the θ_A and θ_B, and therefore, lowered the apparent activation energy.

The E_a values for cyclohexanol dehydration were 115, 124, and 124 kJ mol^{-1} with HZSM-5 in water, methanol, and hexadecane, respectively. Knözinger et al. [34] measured E_a for cyclohexanol dehydration (110 kJ mol^{-1}) over γ-Al$_2$O$_3$ in a continuous flow reactor at low conversion (< 10%). In our preliminary work, E_a for H$_3$PO$_4$-catalyzed cyclohexanol dehydration was calculated to be 120 kJ mol^{-1}. In the present study (**Table 5-5**), E_a for HZSM-5 catalyzed cyclohexanol dehydration in water (115 kJ mol^{-1}) was similar to that in hexadecane (124 kJ mol^{-1}) and in methanol (124 kJ mol^{-1}), and to Ni/ZSM-5 catalyzed cyclohexanol dehydration (E_a: 112 kJ mol^{-1}) in our other work [35, 36].

In the cyclohexene hydrogenation E_a in water (25 kJ mol^{-1}) and in hexadecane (24 kJ mol^{-1}) were almost the same. E_a in methanol was only 12 kJ mol^{-1}. The E_a of cyclohexene hydrogenation was 32 kJ mol^{-1} in the liquid phase over Pd/SiO$_2$ reported by Gonzo and Boudart. [31], which was a bit higher than our result. The adduct formation from methanol and cyclohexene [37] may lead to a much lower apparent E_{a4} in methanol.

Summarizing the three hydrogenation reactions in the sequence at 473 K, the activation energies decreased in the order $E_{a\ phenol\ hydrogenation}$ > $E_{a\ cyclohexanone\ hydrogenation}$ > $E_{a\ cyclohexene\ hydrogenation}$, while the reaction rates rose in the reverse sequence $TOF_{phenol\ hydrogenation}$ < $TOF_{cyclohexanone\ hydrogenation}$ < $TOF_{cyclohexene\ hydrogenation}$. It also shows that the three hydrogenation reaction apparent activation energies were much lower in methanol than in water or hexadecane, apparently due to the solvent effect including methanol-phenol and methanol-Pd interactions. The interactions of methanol with phenol, cyclohexanone or cyclohexene altered the occupancy of Pd sites by decreasing the reactant

coverage, and thus also lower the apparent activation energies eventually. The rates and activation energies for dehydration catalyzed by HZSM-5 were similar in the three solvents, indicating that they led to similar interactions with reactant-HZSM-5 and product-HZSM-5.

5.3.3 In situ liquid phase IR spectroscopy for measuring the individual steps in aqueous-phase phenol hydrodeoxygenation

In order to detect the intermediates and products formed in situ during phenol conversion, and to estimate and compare the rates of individual steps, variations in concentrations of compounds are monitored by attenuated total reflectance (ATR) IR spectroscopy using diamond as a probe window for phenol hydrogenation, cyclohexanone hydrogenation, and cyclohexanol dehydration reactions in the aqueous phase. The standard IR reference spectra of water solvent with reactant, intermediates, and products are displayed in Figure S5-3. The IR signals of cyclohexene hydrogenation are not observable in the aqueous phase, because cyclohexene and cyclohexane are immiscible in water (**Table 5-3**). With the IR diamond probe on the reactor floor, three individual reactions (**Steps 1, 2,** and **3**) were carried out in the aqueous phase at 473 K and 4.0 MPa H_2.

During phenol hydrogenation over Pd/C, the intensity of the characteristic IR peak of phenol at 1228 cm^{-1} steadily decreased throughout the run shown in **Fig. 5-8a**. The intensity of the peak characteristic of cyclohexanone (partial hydrogenated from phenol) at 1698 cm^{-1} initially increased from 0 to 0.085 at 100 min., and then decreased from 0.085 to 0 at extended time up to 240 min. The intensity of the characteristic peak of cyclohexanol at 1058 cm^{-1} increased very slowly in the initial 100 min., because cyclohexanol was formed by direct hydrogenation from phenol in the beginning. Then, the intensity rose more steeply from 100 to 240 min., as both of phenol and cyclohexanone were converted to cyclohexanol at this time interval. This interesting kinetic performance is consistent with step-wise hydrogenation of phenol to cyclohexanone, and subsequent hydrogenation to cyclohexanol (**Fig. 5-8b**). From the plotted data of IR absorbance versus reaction time (**Fig. 5-8c**), it can be calculated that the phenol hydrogenation rate was 5.0 × 10^3 mol·mol$_{Pd\ surf.}$$^{-1}$h^{-1}, which is similar to that obtained value from the above kinetic measurement detected by GC (4.2 × 10^3 mol·mol$_{Pd\ surf.}$$^{-1}$h^{-1}). In addition, if assuming that it was first-order to

phenol concentration, the fitted curve can be perfectly matched with the experimental data with a rate constant of 9.1×10^{-3} min^{-1} (**Fig. 5-8d** and **Table 5-6**).
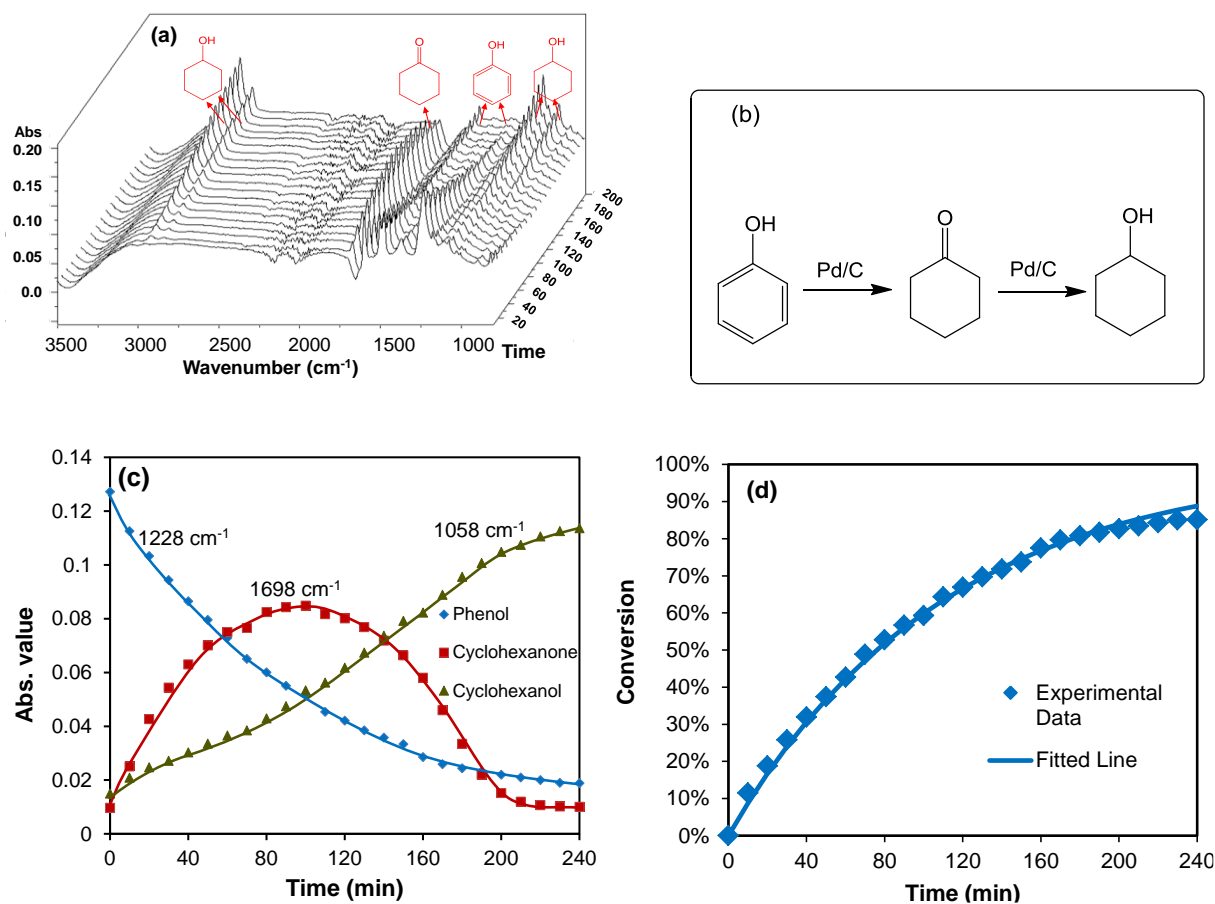
Figure 5-8. (a) In situ liquid IR spectra for aqueous phase phenol hydrogenation. Reaction conditions: phenol (10.0 g), H_2O (50.0 mL), 1wt.% Pd/C (0.10 g), 4 MPa H_2, 473 K, stirred at 700 rpm. The spectra were collected every 10 min. for 240 min. (b) Reaction pathway for phenol conversion on Pd/C in the aqueous phase. (c) IR absorbance as a function of reaction time. (d) Fitted line and experimental conversion data as a function of time based on the assumption of first order dependence to phenol concentrations.
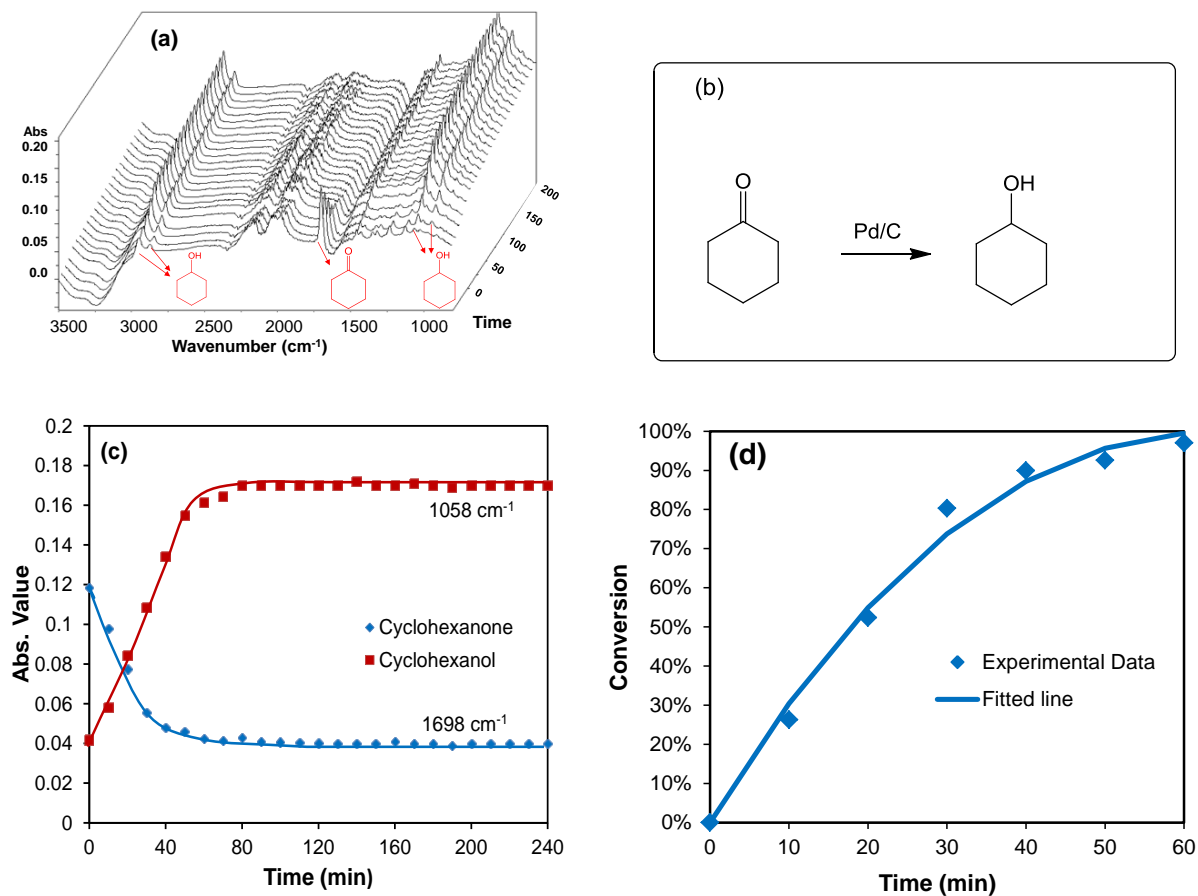
Figure 5-9. (a) In situ liquid IR spectra during aqueous phase cyclohexanone hydrogenation. Reaction conditions: cyclohexanone (10.0 g), H_2O (50.0 mL), 1wt.% Pd/C (0.10 g), 4 MPa H_2, 473 K, stirred at 700 rpm. The spectra were collected every 10 min. for 240 min. (b) Reaction pathway for cyclohexanone conversion on Pd/C in the aqueous phase. (c) IR absorbance as a function of reaction time. (d) Fitted line and experimental conversion data as a function of time based on the assumption that the order dependence to cyclohexanone concentrations is 0.55.

In the conversion of cyclohexanone hydrogenation over Pd/C (**Fig. 5-9a**), the intensity of the characteristic IR absorbance of cyclohexanone reactant at 1698 cm^{-1} decreased rapidly and vanished at 60 min., while the intensity of characteristic IR absorbance of cyclohexanol at 1058 cm^{-1} increased quickly accordingly. The fast loss of cyclohexanone is agreement with the high cyclohexanone hydrogenation TOF. The rate of cyclohexanone hydrogenation was shown to be

much faster than phenol hydrogenation through the comparison of two in situ liquid IR spectra (**Figs. 5-8a** and **5-9a**). The cyclohexanone hydrogenation rate was 1.8×10^4 mol·mol$_{Pd\ surf}^{-1}$·h^{-1} calculated from the plots of IR absorbance versus reaction time (**Fig. 5-9c**), consistent with the value 2.1×10^4 mol·mol$_{Pd\ surf}^{-1}$·h^{-1} monitored by GC. Shown in **Fig. 5-9d** the cyclohexanone hydrogenation rate showed the order dependence to cyclohexanone concentrations of 0.55, attaining the rate constant of 4.6×10^{-2} mol$^{0.45}$·L$^{-0.45}$·min^{-1}.
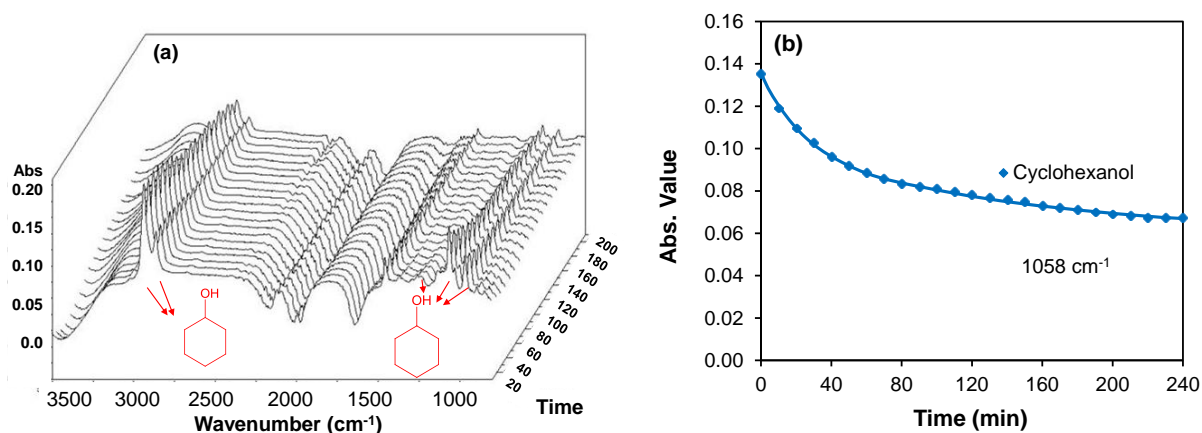
Figure 5-10. (a) In situ liquid IR spectra during aqueous phase cyclohexanol dehydration. Reaction conditions: cyclohexanol (10.0 g), H_2O (50.0 mL), HZSM-5 (0.040 g), 4 MPa H_2, 473 K, stirred at 700 rpm. The spectra were collected every 10 min. for 240 min. (b) IR absorbance versus reaction time.

In a sequence of IR spectra taken during cyclohexanol dehydration in water over HZSM-5 (**Fig. 5-10a**) only the characteristic IR band of cyclohexanol varied, because the cyclohexene floated on the aqueous phase and was not detected by the IR detector in the bottom of the autoclave. The intensity of the cyclohexanol absorbance at 1058 cm^{-1} decreased more slowly than the former two individual reactions, in accordance with the kinetic measurement that dehydration is the rate-determining step in aqueous-phase phenol hydrodeoxygenation. Determined from the IR absorbance versus reaction time (**Fig. 5-10b**), the cyclohexanol dehydration rate was 2.2×10^3

$mol \cdot mol_{BAS}^{-1} \cdot h^{-1}$, agreeing with the rate of 1.6×10^3 $mol \cdot mol_{BAS}^{-1} \cdot h^{-1}$ derived from chromatographic evidence.

The dehydration-hydration reaction of cyclohexanol is equilibrated over HZSM-5 in the aqueous phase following equation (2):
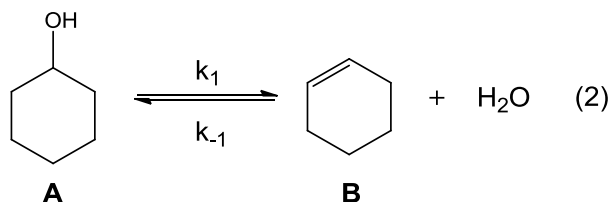
For the 1st order reversible reaction with excess water:

$$-\frac{d[A]}{dt} = k_1[A] - k_{-1}[B] \quad (3)$$

$$[B] = [B]_0 + ([A]_0 - [A]) \quad (4)$$

$$\text{So} -\frac{d[A]}{dt} = k_1[A] - k_{-1}([B]_0 + ([A]_0 - [A])) \quad (5)$$

At equilibrium, $-\frac{d[A]}{dt} = 0$ and $[A]_{eq} = \frac{k_{-1}}{k_1+k_{-1}}([B]_0 + [A]_0) \quad (6)$

$$-\frac{d([A] - [A]_{eq})}{dt} = -\frac{d[A]}{dt} = (k_1 + k_{-1})([A] - [A]_{eq}) \quad (7)$$

$$[A] - [A]_{eq} = ([A]_0 - [A]_{eq})e^{-(k_1+k_{-1})t} \quad (8)$$

$$t = \frac{\ln([A]-[A]_{eq})}{-(k_1+k_{-1})} + \frac{\ln([A]_0-[A]_{eq})}{(k_1+k_{-1})} \quad (9)$$
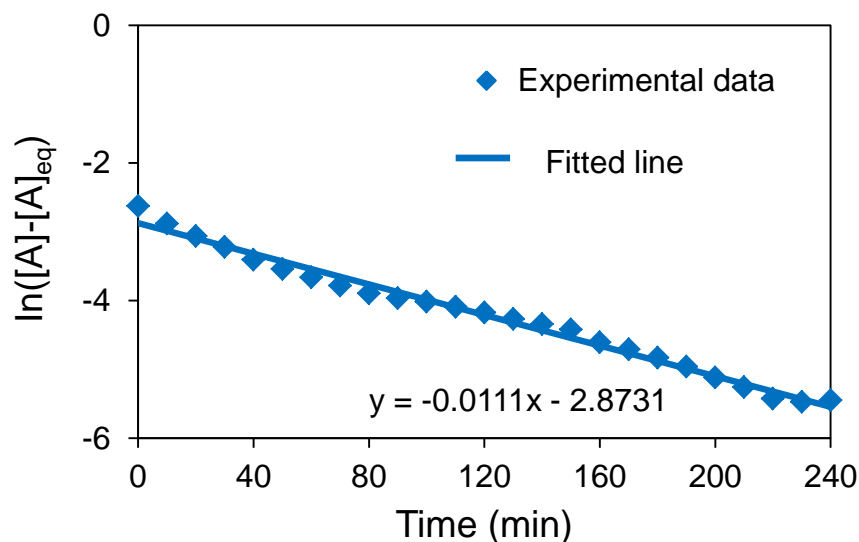
Figure 5-11. Estimation the validity of a first order reaction rate hypothesis for the cyclohexanol dehydration via ln ([Cyclohexanol]−[Cyclohexanol]$_{eq}$) versus time.

As shown from **Fig. 5-11**, cyclohexanol dehydration was determined to be a first-order reaction with HZSM-5 at 473 K in the aqueous phase, and k_1+k_{-1} equaled to 1.1×10^{-2} min^{-1}.

Table 5-6. Kinetic data for individual steps of phenol hydrodeoxygenation in the aqueous phase determined by in situ liquid IR and GC measurements (Normalized to the conditions in the in situ liquid IR experiments).

Reactions / Kinetic data	Phenol hydrogenation	Cyclohexanone hydrogenation	Cyclohexanol dehydration	Cyclohexene hydrogenation
In situ liquid IR TOF	5.0×10^3 mol·mol$_{Pd\ surf}^{-1}$.h^{-1}	1.8×10^4 mol·mol$_{Pd\ surf}^{-1}$. h^{-1}	2.2×10^3 mol·mol$_{BAS}^{-1}$·h^{-1}	-
Reaction order	$n_{(Phenol)}$: 1	$n_{(Cyclohexanone)}$: 0.55	$n_{(Cyclohexanol)}$: 1	-
Rate constant	9.1×10^{-3} min^{-1}	4.6×10^{-2} mol$^{0.45}$·L$^{-0.45}$·min^{-1}	1.1×10^{-2} min$^{-1\ a}$	-

GC	4.2×10^3	2.1×10^4	1.6×10^3	6.0×10^6
TOF	$mol \cdot mol_{Pd\ surf.}^{-1} h^{-1}$	$mol \cdot mol_{Pd\ surf.}^{-1} h^{-1}$	$mol \cdot mol_{BAS}^{-1} \cdot h^{-1}$	$mol \cdot mol_{Pd\ surf.}^{-1} h^{-1}$
Reaction order	n (Phenol): 1	n (Cyclohexanone): 0.55	n (Cyclohexanol): 1	n (Cyclohexene): 0
Rate constant	$3.3 \times 10^{-3}\ min^{-1}$	4.5×10^{-2} $mol^{0.45} \cdot L^{-0.45} \cdot min^{-1}$	$7.5 \times 10^{-3}\ min^{-1\ b}$	5.0×10^{-2} $mol \cdot L^{-1} \cdot min^{-1}$

a: The value represents the sum of $k_{dehydration}$ and $k_{hydration}$ in the aqueous phase.

b: The value represents the $k_{dehydration}$ in the aqueous and organic phases.

The rate constants, reaction orders, and TOFs of three individual steps in the aqueous phase, as determined by GC and in situ liquid IR detectors, are compiled in **Table 5-6**. The reaction orders in the aqueous solution have been identified by in situ liquid IR spectroscopy, that is, phenol and cyclohexanone hydrogenation over Pd/C followed reaction orders of 1.0 and 0.55, respectively. Conversion of cyclohexanol with HZSM-5 shows first-order dependence in the dehydration-hydration equilibrium. The TOFs of three aqueous phase individual steps determined from GC measurement were very close to the values from in situ liquid IR, with minor differences of 10%-20%. Shown in **Table 5-6**, the rate constants for phenol and cyclohexanone hydrogenation were comparable. Phenol hydrogenation attained a rate constant of 9.1×10^{-3} and $3.3 \times 10^{-3}\ min^{-1}$ as measured by in situ liquid IR spectroscopy and GC, respectively, while cyclohexanone hydrogenation showed a rate constant of 4.6×10^{-2} and $4.5 \times 10^{-2}\ mol^{0.45} \cdot L^{-0.45} \cdot min^{-1}$ from these two techniques. It is notable the dehydration rate constants were quite different from two approaches, because in situ liquid phase IR spectroscopy estimates the sum of $k_{dehydration}$ and $k_{hydration}$ ($1.1 \times 10^{-2}\ min^{-1}$) in the aqueous phase, while the GC analysis determines $k_{dehydration}$ ($7.5 \times 10^{-3}\ min^{-1}$) in the sum of aqueous and organic phases. The rate constant for cyclohexene hydrogenation was calculated to be $5.0 \times 10^{-2}\ mol \cdot L^{-1} \cdot min^{-1}$ from GC measurement, as the reaction order towards cyclohexene concentration is assumed to be 0 [31].
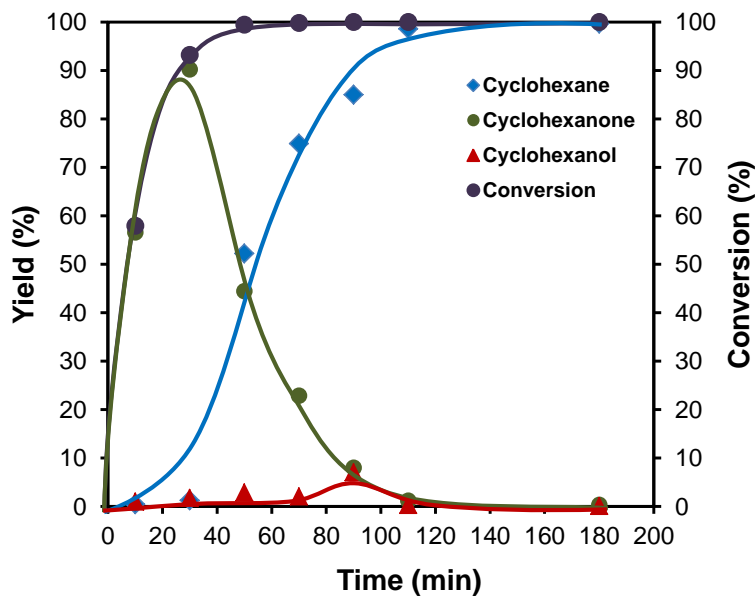
Figure 5-12. The product distributions during phenol hydrodeoxygenation in the aqueous phase in the presence of Pd/C and HZSM-5. Reaction Conditions: Phenol (1.0 g), 1 wt.% PdC (0.040 g), HZSM-5 (0.20 g), H_2O (80 mL), 473 K, 40 MPa H_2, stirring at 700 rpm.

In a comparative study, we also performed the overall phenol hydrodeoxygenation with dual Pd/C and HZSM-5 components in the aqueous phase in order to demonstrate the cooperative effect of acid and metal sites (**Figure 5-12**). Phenol was quantitatively converted to cyclohexane at 473 K and 4 MPa H_2 along the reaction routes discussed above. Due to the fast hydrogenation of cyclohexene intermediate on Pd/C it was not observed in the presence of the catalyst mixture. This result agrees well with our previous studies on hydrodeoxygenation of phenol monomers and dimers as well as bio-oil with bifunctional catalysts consisting of Pd and acids [4-6]. The elementary steps in the overall phenol hydrodeoxygenation include phenol hydrogenation to produce cyclohexanone (k_1), subsequently cyclohexanone hydrogenation to afford cyclohexanol (k_2) which is in equilibrium with cyclohexanol dehydrogenation to cyclohexanone (k_{-2}), in turn cyclohexanol is dehydrated and hydrogenated to cyclohexane (k_3) (**Scheme 5-3**).
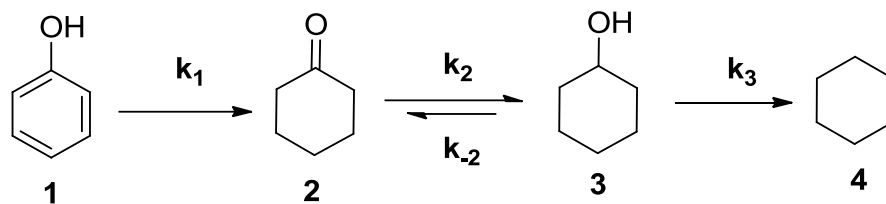
Scheme 5-3. Proposed elementary reaction steps in the overall phenol hydrodeoxygenation.
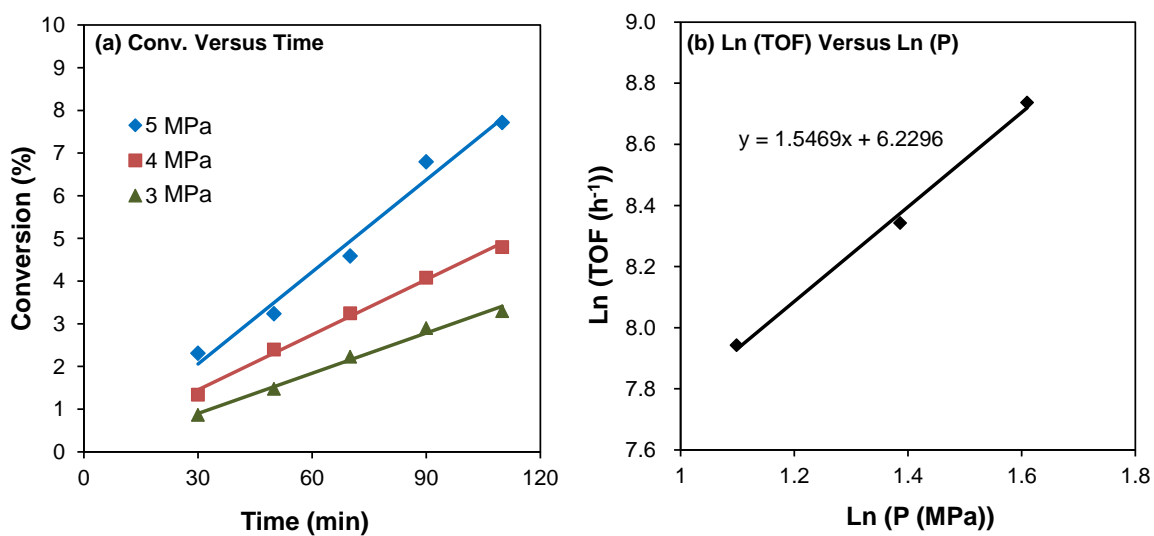
Figure 5-13. Hydrogenation of phenol over Pd/C with varying hydrogen pressures. Reaction conditions: phenol (12.5 g), H_2O (80 mL), 1 wt.% Pd/C (0.02 g), 473 K, stirring at 700 rpm.
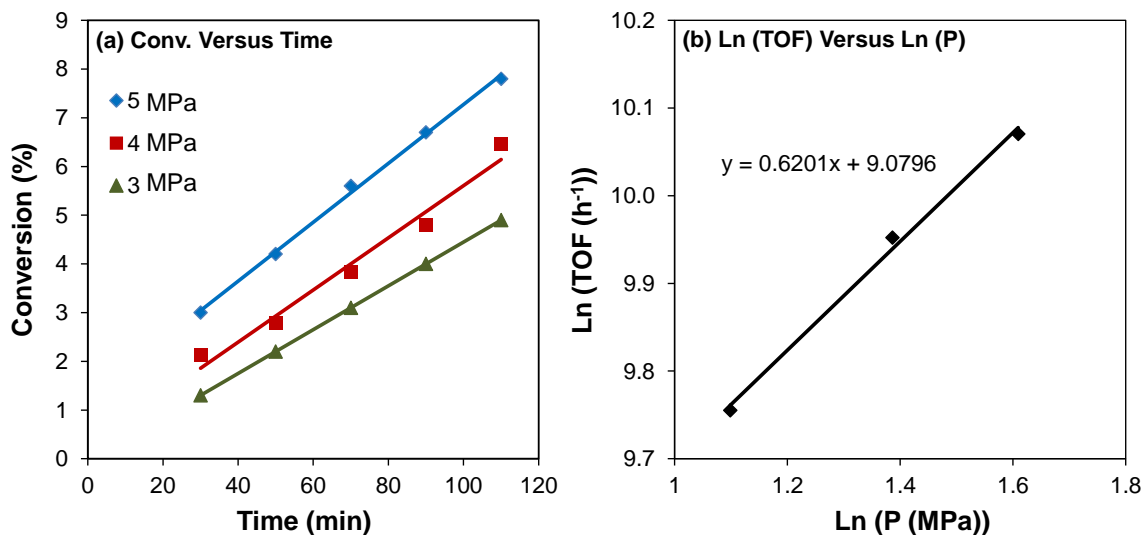
Figure 5-14. Hydrogenation of cyclohexanone over Pd/C with varying hydrogen pressures. Reaction conditions: cyclohexanone (60.0 g), H_2O (80 mL), 1 wt.% Pd/C (0.02 g), 473 K, stirring at 700 rpm.

For hydrogenation of phenol and cyclohexanone over Pd/C with varying hydrogen pressures of 3, 4, and 5 MPa, the reaction orders of hydrogen concentration for phenol and cyclohexanone hydrogenation were determined to be 1.5 and 0.6, respectively (see **Figs. 5-13 and 5-14**). It was observed that the hydrogen pressure before and after reaction remained constant, thus, the hydrogen pressures were considered as constant values in the elementary rate equations.

It is assumed first reaction-order to phenol, cyclohexanone, cyclohexanol concentrations and zero reaction-order to cyclohexene concentration. Therefore, the overall phenol hydrodeoxygenation includes the following elementary rate equations (10-13):

$$\frac{dc_1}{dt} = -k_1 \times c_1 \quad (10)$$

$$\frac{dc_2}{dt} = k_1 \times c_1 - k_2 \times c_2 + k_{-2} \times c_2 \quad (11)$$

$$\frac{dc_3}{dt} = k_2 \times c_2 - k_{-2} \times c_2 - k_3 \times c_3 \times c(H^+) \quad (12)$$

$$\frac{dc_4}{dt} = k_3 \times c_3 \times c(H^+) \quad (13)$$

Table 5-7. Comparison of fitted rate constants in the overall phenol hydrodeoxygenation and in the individual steps analyzed by GC measurements. (Conditions: phenol (1.0 g), 1 wt.% Pd/C (0.04 g), HZSM-5 (0.20 g), 473 K, 4 MPa H_2)

Reaction rate constants	k_1 (min^{-1})	k_2 (min^{-1})	k_{-2} (min^{-1})	k_3 (min^{-1})	Fitness parameter
Fitted elementary steps in the overall HDO	9.0×10^{-2}	3.0×10^{-1}	5.4	4.0×10^{-1}	0.46
Data from individual steps analyzed by GC [a]	1.4×10^{-2}	1.8×10^{-1}	n.d.	3.8×10^{-1}	-

a: Normalized to the conditions in the overall phenol hydrodeoxygenation experiment.
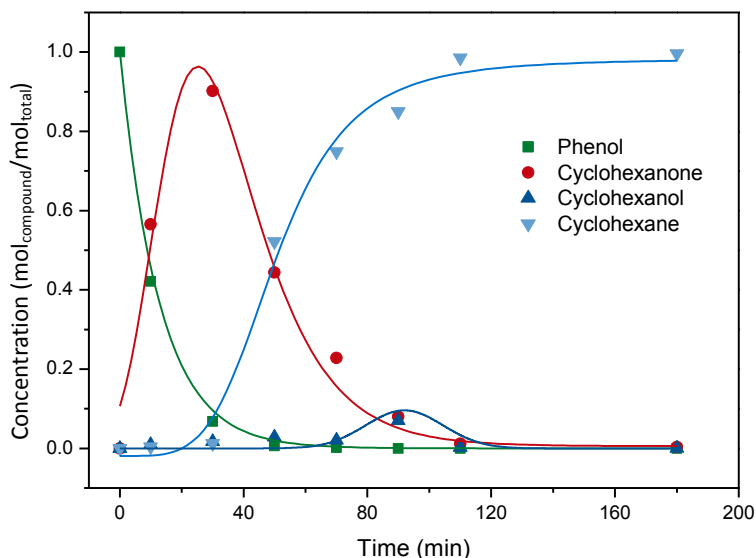
Figure 5-15. Fitting the experimental data of phenol hydrodeoxygenation with Pd/C and HZSM-5 catalysts in the presence of hydrogen, solid points: experiment data, line: fitted curve. Conditions: phenol (1.0 g), 1 wt.% Pd/C (0.04 g), HZSM-5 (0.20 g), 473 K, 4 MPa H_2.

Fitting the pseudo rate constants of the individual steps of phenol hydrodeoxygenation (**Table 5-7** and **Figure 5-15**), the fitted phenol hydrogenation rate constant (9.0×10^{-2} min^{-1}) was much higher than the value (1.4×10^{-2} min^{-1}) deduced as the first step in individual measurements, probably due to the added acid effect for accelerating hydrogenation rates in the overall phenol hydrodeoxygenation. But fitted apparent rate constants (3.0×10^{-1} min^{-1}) in the subsequent cyclohexanone hydrogenation elementary steps varied from that determined in individual steps (1.8×10^{-1} min^{-1}) (**Table 5-7**) due to strong competitive adsorption of phenol and cyclohexanone onto active sites during the overall phenol hydrodeoxygenation. The fitted cyclohexanol dehydration rate constant (4.0×10^{-1} min^{-1}) was slightly higher than the value (3.8×10^{-1} min^{-1}) analyzed by the individual measurement as well, because the dehydration-hydration equilibrium is shifted by the subsequent cyclohexene hydrogenation over combined Pd/C and HZSM-5 catalysts.

5.4 Conclusions

Solvents influence the rates of catalytic phenol hydrodeoxygenation by altering the H_2 solubility and the solvent-reactant interactions, as well as by competitive solvent/reactant adsorption on the catalyst surface. Impacts of water, methanol, and hexadecane solvents on the individual steps of phenol hydrodeoxygenation are investigated over Pd/C or HZSM-5 catalyst at 473 K in the presence of hydrogen. Hydrodeoxygenation of phenol to cyclohexane includes four individual steps of phenol hydrogenation to cyclohexanone on Pd/C, cyclohexanone hydrogenation to cyclohexanol on Pd/C, cyclohexanol dehydration to cyclohexene on HZSM-5, and cyclohexene hydrogenation to cyclohexane on Pd/C. Methanol provides an additional acetal reaction route of cyclohexanone with methanol during phenol hydrodeoxygenation, compared to water and hexadecane. The hydrogenation reactions, especially of phenol and cyclohexanone, show lower rates in methanol than in water or hexadecane. Methanol not only strongly solvates phenol and cyclohexanone but also adsorbs strongly on Pd. This strong adsorption either prevents cyclohexanone/phenol from interacting with Pd active sites or reduces the cyclohexanone/phenol coverage on the Pd/C surface, affording slower cyclohexanone/phenol hydrogenation in methanol. The low solubility of phenol and strong interaction of hexadecane-Pd surface in hexadecane lead to the slow hydrogenation rate.

The apparent activation energies for hydrogenation show the order $E_{a\ phenol\ hydrogenation} > E_{a\ cyclohexanone\ hydrogenation} > E_{a\ cyclohexene\ hydrogenation}$, and the reaction rates follow $TOF_{cyclohexene\ hydrogenation} > TOF_{cyclohexanone\ hydrogenation} > TOF_{phenol\ hydrogenation}$ at 473 K. The in situ liquid IR spectroscopy results confirm that the rates are consistent with kinetics derived from chromatographic evidence in the aqueous phase, and verify that hydrogenation of phenol and cyclohexanone follows reaction orders of 1.0 and 0.55 over Pd/C, respectively. Conversion of cyclohexanol with HZSM-5 shows first-order dependence in the dehydration-hydration equilibrium. The dehydration rates and apparent activation energies are comparable in three solvents. The control of the balance between metal and acid sites is crucial to optimize the cascade reactions consisting of the integrated hydrogenation and dehydration steps, which allows developing active and stable catalysts.

5.5 Acknowledgements

J.H. gratefully acknowledges the support of the TUM graduate school's faculty graduate center of chemistry (FGCh) at the Technische Universität München, the Elitenetzwerk Bayern (graduate school NanoCat). We acknowledge the support from the US Department of Energy, Office of Basic Energy Sciences. Pacific Northwest National Laboratory (PNNL) is a multiprogram national laboratory operated for DOE by Battelle.

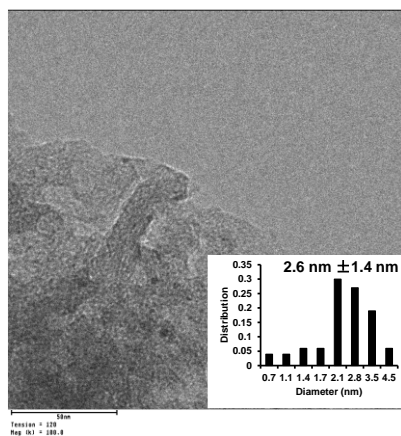# 5.6 Appendix

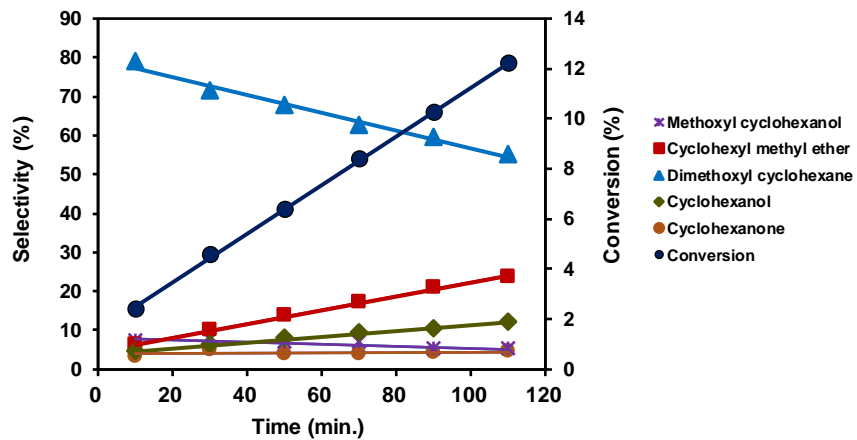**Figure S5-1.** TEM images of 1 wt.% Pd/C.

Figure S5-2. The product distributions of phenol hydrogenation in methanol over Pd/C at 473 K in the presence of 4 MPa H_2. Reaction condition: phenol (15.0 g), CH_3OH (80 ml), Pd/C (1 wt.%, 0.15 g), stirring at 700 rpm.
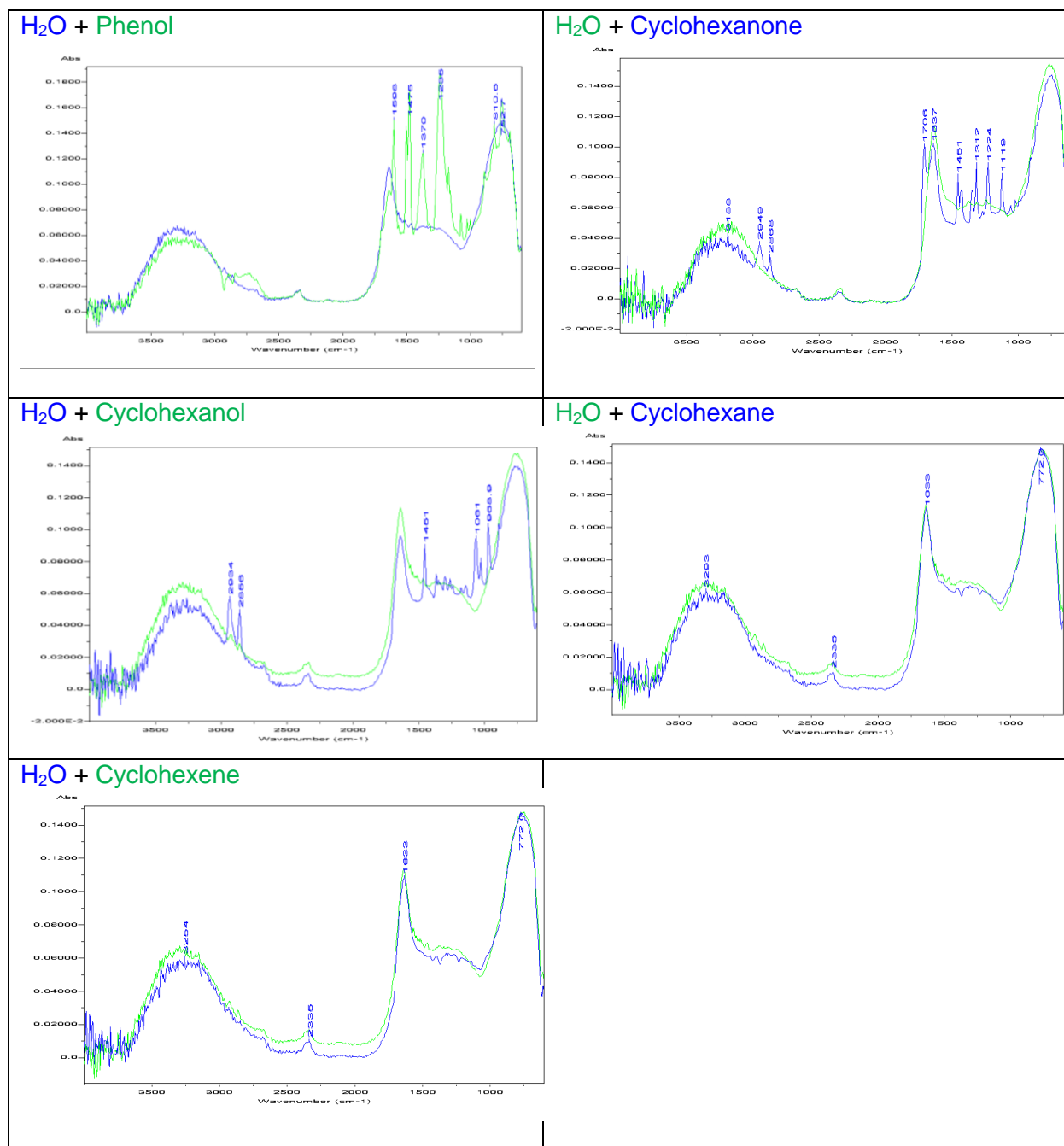
Figure S5-3. The standard IR reference spectra of solvent with reactants, intermediates, and products.

5.7 Reference

[1]   E. Furimsky, Appl. Catal. A 199 (2000) 147.

[2]   C. Zhao, Y. Kou, A. A. Lemonidou, X. Li, J. A. Lercher, Angew. Chem. Int. Ed. 48 (2009) 3987.

[3]   C. Zhao, J. A. Lercher, Angew. Chem. Int. Ed. 51 (2012) 5935.

[4]   C. Zhao, J. He, A. A. Lemonidou, X. Li, J. A. Lercher, J. Catal. 280 (2011) 8.

[5]   C. Zhao, D.M. Camaioni, J.A. Lercher, J. Catal. 288 (2012) 92.

[6]   C. Zhao, J. A. Lercher, ChemCatChem 4 (2012) 64.

[7]   J. He, C. Zhao, J. A. Lercher, J. Am. Chem. Soc. 134 (2012), 20768.

[8]   J. S. Shabtai, W. W. Zmierczak, E. Chornet, 2001, US Patent, The University of Utah Research Foundation, 6,172,272 B1.

[9]   C.-L. Li, Z.-R. Xu, Z.-A. Cao, B.C. Gates, AIChE J. 31 (1985) 170.

[10]   Y.Q. Yang, C. T. Tye, K. J. Smith, Catal. Commun. 9 (2008) 1364.

[11]   L.R. Snyder, J. Chromatogr. 92 (1974) 223.

[12]   U.K. Singh, M.A. Vannice, Appl. Catal. A 213 (2001) 1.

[13]   M. Boudart, D.J. Sajkowski, Faraday Discuss. 92 (1991) 57.

[14]   Y. Xiang, L. Ma, C. Lu, Q. Zhang, X. Li, Green Chem. 10 (2008) 939.

[15]   J. S. Shabtai, W. W. Zmierczak, E. Chornet, 1999, US Patent, The University of Utah Research Foundation, 5,959,167.

[16]   N. M. Bertero, A. F. Trasarti, C. R. Apesteguia , A.J. Marchi, Appl. Catal. A 394 (2011) 228.

[17]   N. Mahata, K.V. Raghavan, V. Vishwanathan, Catal. Today 49 (1999) 65.

[18]   B. A. Sexton, K. D. Rendulic and A. E. Hughes, Surf. Sci. 121 (1982) 181.

[19]   Y. Morikawa, H. Ishii, K. Seki, Phys. Rev. B 69 (2004) 041403.

[20]   S. Andersson, c. Nyberg, C.G. Tengstål, Chem. Phys. Lett. 104 (1984) 305.

[21]   H. A. Pray, C. E. Schweickert, B. H. Minnich, Ind. Eng. Chem. 44 (1952) 1146.

[22]   A. Drelinkiewicza, A. Waksmundzka, W. Makowski, J.W. Sobczak, A. Król, A. Zieba, Catal. Lett. 94 (2004) 143.

[23]   K. A. Manbeck, N. E. Musselwhite, L. M. Carl, C. A. Kauffman, O. D. Lyons, J. K.Navin, A. L.Marsh, Appl. Catal. A 384 (2010) 58.

[24]   B. Peng, C. Zhao, I. Mejá-Centenoa, G. A. Fuentesa, A. Jentys, J. A. Lercher, Catal. Today 183 (2012) 3.

[25]   R. Krishna, J. M. van Baten, Langmuir 26 (2010) 10854.

[26]   J. Macht, M. J. Janik, M. Neurock, E. Iglesia, Angew. Chem. Int. Ed. 46 (2007) 7864.

[27]   H. Noller, W. Kladnig, Catal. Rev. 13 (1976) 149.

[28]   T. Xu, J. F. Haw, J. Am. Chem. Soc. 116 (1994) 7753.

[29]   G. Odian, Principles of Polymerization (4th ed.). Hoboken, NJ: Wiley-Interscience, 2004.

[30]   J.M. G. Cowie, V. Arrighi, Polymers Chemistry and Physics of Modern Materials (3rd ed.). Boca Raton: Taylor & Francis, 2008.

[31]   E. E. Gonzo, M. Boudart, J. Catal. 52 (1978) 462.

[32]   F. Kapteijn, J. A. Moulijn, R. A. van Santen, R. Wever, Stud. Surf. Sci. Catal. 123 (1999) 81.

[33]   N. Mahata, V. Vishwanathan, J. Mol. Catal. A 120 (1997) 267.

[34]   H. Knözinger, K. Kochloef, H. Bühl J. Catal. 24 (1972) 57.

[35]   C. Zhao, Y. Yu, A. Jentys, J. A. Lercher, Appl. Catal. B 132-133 (2013) 282.

[36]   C. Zhao, S. Kasakov, J. He, J. A. Lercher, J. Catal. 296 (2012) 12.

[37]   R. West, J. Am. Chem. Soc. 81 (1959) 1614.

Chapter 6

Summary and Conclusions

The incentive of this dissertation includes (i) the selective cleavage of C-O bonds of lignin-derived dimers (the aryl ethers, the model compounds for C-O bond linkages in lignin) to form monomers in mild conditions (393 K, 0.6 MPa H_2) and (ii) the solvent impact on the hydrodeoxygenation of phenol (the monomer of lignin) to cyclohexane (gasoline component) . The aim of selective C-O bond cleavage of lignin model compounds is dual: practically, the depolymersization of lignin to form bulk chemicals or fuels with highly efficient catalytic system could provide an alternative solution for sustainable energy in the future. Fundamentally, far from sufficient knowledge has been available for the mechanistic details of the cleavage of dimer's C-O bonds over metal and acid sites in the aqueous phase, i.e the reaction pathway and rate for C-O bond cleavage. The focus of the phenol hydrodeoxygenation is the impact of various solvents (water, methanol and hexadecane) on all four individual steps (Step 1: hydrogenation of phenol to cyclohexanone over metal; Step 2: hydrogenation of cyclohexanone to cyclohexanol over metal; Step 3: dehydration of cyclohexanone to cyclohexene over acid; Step 4: hydrogenation of cyclohexene to cyclohexane over metal).

Compared to the mild reaction conditions (353-393 K, 0.1 MPa H_2) of homogeneous catalysts for C-O bond cleavage of aryl ethers, the heterogeneous catalysts normally require much harsher conditions (513-673 K and 25-31 MPa). In the current thesis work, the C-O bond linkages of model compounds α-O-4, β-O-4, and 4-O-5 representing typical bonds in lignin were selectively cleaved by a silica-supported Ni catalyst to produce aromatic and aliphatic molecules as well as cyclohexanol in aqueous media under mild conditions (393 K, 0.6 MPa H_2). The C-O bonds of α-O-4 and β-O-4 are cleaved by direct hydrogenolysis, which is shown to be structure-sensitive on Ni based catalysts, to be specific, the TOF of C-O bond cleavage is sensitive to the Ni particle size, while the C-O bond of 4-O-5 appeared to be cleaved by parallel hydrogenolysis and hydrolysis. The difference is attributed to the hydrogenolysis of the low concentrations of $PhCH_2OH$ and $PhCH_2CH_2OH$ intermediates from α-O-4 and β-O-4 linkages to $PhCH_3$ and $PhCH_2CH_3$, while hydrogenation converted phenol derived from 4-O-5 linkage to cyclohexanol under present conditions. The rates for C-O bond cleavage followed the sequence r (α-O-4) > r (4-O-5) > r (β-O-4), and the increasing apparent energies of activation E_a (α-O-4) < E_a (β-O-4) < E_a (4-O-5) tracked the variations in bond dissociation energies E (α-O-4) < E (β-O-4) < E (4-O-5).

Among the three most abundant C−O bonds (α−O−4, β−O−4, 4−O−5) in lignin, the 4−O−5 bond (BDE: 314 kJ mol^{-1}) is the strongest. The diphenyl ether, which is selected as the simplest model compound of 4−O−5 linkage for investigating the C−O bond cleavage chemistry, shows a very unusual reaction pathway (parallel hydrogenolysis and hydrolysis) over Ni/SiO$_2$ in comparison to α−O−4, β−O−4. In this work, the ether C−O bonds cleavage of three *p*-di-substituted H−, CH$_3$−, and OH− diphenyl ethers has been investigated in very mild conditions (393 K, 0.6 MPa H$_2$) over Ni/SiO$_2$. The C−O bond of diphenyl ether was cleaved by the parallel hydrogenolysis and hydrolysis routes on Ni sites. In contrast to diphenyl ether, hydrogenolysis was the exclusive route for cleaving the ether C−O bond of di-*p*-tolyl ether producing *p*-cresol and toluene. The sequential surface C−O bond hydrogenolysis contributed to 4,4'-dihydroxydiphenyl ether conversion, that is, it was first cleaved to phenol and OC$_6$H$_4$OH*, then further cleaved to phenol (C$_6$H$_4$OH* with H* added) and H$_2$O (O* with 2 H* added) in the second step. DFT calculations confirmed this sequential C−O bond cleavage mechanism of 4,4'-dihydroxydiphenyl ether occurring on the surface of Ni. TOFs of the three diaryl ethers with Ni/SiO$_2$ in water followed the order 4,4'-dihydroxydiphenyl ether (69 mol·mol$_{Ni\ surf}$$^{-1}$·h^{-1}) > diphenyl ether (26 mol·mol$_{Ni\ surf}$$^{-1}$·h^{-1}) > di-*p*-tolyl ether (1.3 mol·mol$_{Ni\ surf}$$^{-1}$·h^{-1}), and is in accordance with the sequence of apparent activation energies (E$_a$) follow 4,4'-dihydroxydiphenyl ether (93 kJ·mol^{-1}) < diphenyl ether (98 kJ·mol^{-1}) < di-*p*-tolyl ether (105 kJ·mol^{-1}).

The α-O-4 bond is the most active and thermally unstable one due to the lowest bond dissociation energy of the aliphatic C−O bond (218 kJ·mol^{-1}) among these bonds. To explore the mechanism of cleaving the α−O−4 bond, benzyl phenyl ether (BPE) has been selected as the model compound in this work. In the aqueous phase the C−O cleavage of BPE proceeds with an ionic pathway at 523 K, but not via a thermal/free radical route. In neat water in the absence or presence of H$_2$, the acid (hydronium ions from dissociated water) catalyzed hydrolysis route dominates, and subsequently the alkylation between the phenol and alcohol fragments follows to a small extent. In the presence of HZSM-5, both hydrolysis and alkylation rates are substantially enhanced. Ni/SiO$_2$, in contrast, leads to the quantitative and selective hydrogenolysis of C$_{aliphatic}$−O bond to form phenol and toluene in the presence of H$_2$. In the presence of metal and acid sites, metal (Ni) catalyzed hydrogenolysis plays a more important role for cleaving the ether bond in BPE. In apolar undecane at 523 K, non-catalytic pyrolysis cleaves the C$_{aliphatic}$−O bond of BPE, and thus, the free-

radical products dominate. When metals such as Ni/SiO_2 and Ni/HZSM-5 are involved, hydrogenolysis dominates the conversion, markedly suppressing the radical reaction. Ni/SiO_2 leads to higher hydrogenolysis rates in undecane than in water, probably because of the much weaker adsorption of reactants onto active Ni sites in the aqueous phase.

The phenolic compounds obtained from depolymerization of lignin contains very high oxygen content, advanced catalytic approaches are required for economically feasible deoxygenation. Water, methanol and non-polar solvents such as hexadecane and toluene have been frequently employed for related hydrotreating of biomass, synthetic crude coal and oil shale. Solvents influence the rates of catalytic phenol hydrodeoxygenation by altering the H_2 solubility and the solvent-reactant interactions, as well as by competitive solvent/reactant adsorption on the catalyst surface. Impacts of water, methanol, and hexadecane solvents on the individual steps of phenol hydrodeoxygenation were investigated over Pd/C or HZSM-5 catalyst at 473 K in the presence of hydrogen. Hydrodeoxygenation of phenol to cyclohexane includes four individual steps of phenol hydrogenation to cyclohexanone on Pd/C, cyclohexanone hydrogenation to cyclohexanol on Pd/C, cyclohexanol dehydration to cyclohexene on HZSM-5, and cyclohexene hydrogenation to cyclohexane on Pd/C. Methanol provides an additional acetal reaction route of cyclohexanone with methanol during phenol hydrodeoxygenation, compared to water and hexadecane. The hydrogenation reactions, especially of phenol and cyclohexanone, show lower rates in methanol than in water or hexadecane. Methanol not only strongly solvates phenol and cyclohexanone but also adsorbs strongly on Pd. This strong adsorption either prevents cyclohexanone/phenol from interacting with Pd active sites or reduces the cyclohexanone/phenol coverage on the Pd/C surface, affording slower cyclohexanone/phenol hydrogenation in methanol. The low solubility of phenol and strong interaction of hexadecane-Pd surface in hexadecane lead to the slow hydrogenation rate. The apparent activation energies for hydrogenation show the order $E_{a\ phenol\ hydrogenation} > E_{a\ cyclohexanone\ hydrogenation} > E_{a\ cyclohexene\ hydrogenation}$, and the reaction rates follow the order $TOF_{cyclohexene\ hydrogenation} > TOF_{cyclohexanone\ hydrogenation} > TOF_{phenol\ hydrogenation}$ at 473 K.

Chapter 7

Zusammenfassung und Schlussfolgerungen

Die Motivation dieser Dissertation beinhaltet (i) das selektive Spalten von C-O Bindungen von Lignin abgeleiteten Dimeren (Arylether als Modelverbindungen von C-O-Bindungen in Lignin) um Monomere unter milden Bedingungen zu erzeugen (393 K, 0.6 MPa H$_2$) und (ii) den Einfluss des Lösungsmittels auf die Hydrodeoxygenierung von Phenol (das Monomer des Lignins) zu Cyclohexan (Benzin Additiv). Das Ziel der selektiven Spaltung von C-O-Bindungen in Modelkomponenten des Lignins ist zweierlei: Die Depolymerisation von Lignin, um Grundchemikalien und Treibstoffe mit hocheffizienten katalytischen Systemen zu erzeugen, könnte eine alternative Lösung für nachhaltige Energie der Zukunft sein. Grundsätzlich ist kein ausreichendes Wissen über die mechanistischen Details der C-O-Bindungsspaltung der Dimere mit Metall- und Säurezentren in wässriger Phase, d.h. die Reaktionspfade und Raten der C-O-Bindungsspaltung, verfügbar. Der Fokus der Hydrodeoxygenierung von Phenol ist auf dem Einfluss verschiedener Lösungsmittel (Wasser, Methanol und Hexadekan) auf alle vier Einzelschritte (Schritt 1: Metall katalysierte Hydrierung von Phenol zu Cyclohexanon; Schritt 2: Metall katalysierte Hydrierung von Cyclohexanon zu Cyclohexanol; Schritt 3: Sauer katalysierte Dehydratisierung von Cyclohexanon zu Cyclohexen; Schritt 4: Metall katalysierte Hydrierung von Cyclohexen zu Cyclohexan).

Verglichen mit den milden Reaktionsbedingungen (353-393 K, 0.1 MPa H$_2$) von homogenen Katalysatoren zur C-O-Bindungsspaltung von Arylethern, erfordern die heterogenen Katalysatoren normalerweise viel extremere Bedingungen (513-673 K und 25-31 MPa). In der aktuellen Arbeit repräsentieren die C-O-Bindungen von Modellkomponenten α-O-4, β-O-4 und 4-O-5 typische Bindungen in Lignin, welche selektiv von Siliziumdioxid geträgerten Ni Katalysatoren gespalten werden um aromatische und aliphatische Moleküle sowie Cyclohexanol in wässrigem Medium unter milden Bedingungen (393 K, 0.6 MPa H$_2$) zu produzieren. Die C-O-Bindungen von a-O-4 und b-O-4 werden durch direkte Hydrogenolyse gespalten, welche auf Ni basierenden Katalysatoren struktursensitiv ist, genauer gesagt, die TOF der C-O-Bindungsspaltung ist abhängig von der Größe der Ni Partikel, wohingegen sich zeigte, dass die C-O-Bindungen von 4-O-5 durch parallele Hydrogenolyse und Hydrolyse gespalten wird. Der Unterschied wird der Hydrogenolyse von PhCH$_2$OH bei geringer Konzentration und PhCH$_2$CH$_2$OH Zwischenprodukten mit α-O-4 und β-O-4 Verknüpfungen zu PhCH$_3$ und PhCH$_2$CH$_3$ zugeschrieben, wohingegen Phenol, abgeleitet von 4-O-5 Verknüpfungen, unter den

vorliegenden Bedingung durch Hydrierung zu Cyclohexanol umgesetzt wird. Die Raten der C-O-Bindungsspaltung folgen der Reihe r (α-O-4) > r (4-O-5) > r (β-O-4) und die steigende scheinbare Aktivierungsenergie E_a (α-O-4) < E_a (β-O-4) < E_a (4-O-5) folgt der unterschiedlichen Bindungsdissoziationsenergie E (α-O-4) < E (β-O-4) < E (4-O-5).

Unter den drei am häufigsten vorkommenden C-O-Bindungen (α−O−4, β−O−4, 4−O−5) in Lignin ist die 4-O-5-Bindung (BDE: 314 kJ mol^{-1}) die stärkste. Diphenylether, welches als einfachste Modelverbindung für 4-O-5 zur Untersuchung der C-O-Bindungsspaltungschemie ausgesucht wird, zeigt einen sehr unüblichen Reaktionspfad (parallele Hydrogenolyse und Hydrolyse) über Ni/SiO$_2$ im Vergleich zu α−O−4, β−O−4. In dieser Arbeit ist die C-O-Bindungsspaltung von Ethern mit drei *p*-di-substituierten H-, CH$_3$- und OH- Diphenylethern unter sehr milden Bedingungen (393 K, 0.6 MPa H$_2$) über Ni/SiO$_2$ untersucht worden. Die C-O-Bindung von Diphenylether wurde durch parallele Hydrogenolyse- und Hydrolyseroute an Ni-Zentren gespalten. Im Gegensatz zu Diphenylether war Hydrogenolyse die ausschließliche Route um die C-O-Etherbindung von Di-*p*-tolylether zu spalten und *p*-Kresol und Toluol zu bilden. Die schrittweise Hydrolyse der C-O-Bindungen an der Oberfläche trägt zum Umsatz des 4,4'-Dihydroxydiphenylethers bei, und zwar wird dieser zuerst zu Phenol und OC$_6$H$_4$OH* , dann im zweiten Schritt weiter zu Phenol (C$_6$H$_4$OH* mit H*) und H$_2$O (O* mit 2 H*) gespalten. DFT-Berechnungen bestätigen, dass dieser Mechanismus der C-O-Bindungsspaltung von 4,4'-Dihydroxydiphenylether schrittweise auf der Oberfläche von Ni abläuft. Die TOFs der drei Diarylether mit Ni/SiO$_2$ in Wasser folgen der Reihenfolge 4,4'-Dihydroxydiphenylether (69 mol·mol$_{Ni\,surf}^{-1}$·h^{-1}) > Diphenylether (26 mol·mol$_{Ni\,surf}^{-1}$·h^{-1}) > Di-*p*-tolylether (1.3 mol·mol$_{Ni\,surf}^{-1}$·h^{-1}) und übereinstimmend folgen die scheinbaren Aktivierungsenergien (E_a) 4,4'-Dihydroxydiphenylether (93 kJ·mol^{-1}) < Diphenylether (98 kJ·mol^{-1}) < Di-*p*-tolylether (105 kJ·mol^{-1}).

Die α-O-4 Bindung ist die aktivste und thermisch instabilste wegen der geringsten Bindungsdissoziationsenergie der aliphatischen C-O-Bindung (218 kJ mol^{-1}) unter diesen Bindungen. Um den Mechanismus der Spaltung der α−O−4 Bindung zu untersuchen, wurde in dieser Arbeit Benzylphenylether (BPE) als Modelkomponente ausgewählt. In wässriger Phase verläuft die C-O-Spaltung in BPE auf einem ionischen Pfad bei 523 K, aber nicht über eine

thermische Route oder über freie Radikale. In ausschließlich Wasser und An- oder Abwesenheit von H_2 herrscht die Säure katalysierte Hydrolyseroute vor (Hydroniumionen von dissoziiertem Wasser) und anschließend folgt die Alkylierung zwischen Phenol und Alkohol in geringem Ausmaß. In Gegenwart von HZSM-5 werden sowohl die Raten von Hydrolyse als auch Alkylierung beachtlich erhöht. Im Unterschied dazu führt Ni/SiO_2 zu quantitativer und selektiver Hydrogenolyse der $C_{aliphatisch}{-}O$ Bindung um in der Anwesenheit von H_2 Phenol und Toluol zu bilden. In Anwesenheit von Metall- und Säurezentren spielt Metall (Ni) katalysierte Hydrogenolyse für die Spaltung der Etherbindung in BPE eine wichtige Rolle. In unpolarem Undekan bei 523 K wird die $C_{aliphatisch}{-}O$ Bindung von BPE durch nicht-katalytische Pyrolyse gespalten und somit dominieren freie radikalische Produkte. Wenn Metalle wie Ni/SiO_2 und Ni/HZSM-5 beteiligt sind, dominiert Hydrogenolyse die Umsetzung merklich und unterdrückt die radikalische Reaktion. Ni/SiO_2 führt zu höheren Hydrogenolyseraten in Undekan als in Wasser – wahrscheinlich, weil die Reaktanden in wässriger Phase viel schwächer auf den aktiven Ni-Zentren adsorbieren.

Die phenolischen Komponenten, erhalten durch Depolymerisation von Lignin, enthalten einen sehr hohen Sauerstoffgehalt. Für eine ökonomisch machbare Deoxygenierung sind fortschrittliche katalytische Herangehensweisen notwendig. Wasser, Methanol und unpolare Lösungsmittel wie Hexadekan und Toluol sind häufig für das verwandte Hydrotreating von Biomasse, synthetisches Rohöl und Ölschiefer angewendet worden. Lösungsmittel beeinflussen die Raten der katalytischen Phenol Hydrodeoxygenierung, indem sie die H_2 Löslichkeit und die Lösungsmittel-Edukt-Wechselwirkung verändern; sowie die kompetitive Lösungsmittel/Edukt Adsorption auf der Katalysatoroberfläche. Der Einfluss der Lösungsmittel Wasser, Methanol und Hexadekan auf die Einzelschritte der Phenol Hydrodeoxygenierung auf Pd/C oder HZSM-5 Katalysator wird bei 473 K in Gegenwart von Wasserstoff untersucht. Die Hydrodeoxygenierung von Phenol zu Cyclohexan schließt vier Einzelschritte mit ein - Die Hydrierung von Phenol zu Cyclohexanon auf Pd/C, Hydrierung von Cyclohexanon zu Cyclohexanol auf Pd/C, Dehydratisierung von Cyclohexanol zu Cyclohexen auf HZSM-5 und Hydrierung von Cyclohexen zu Cyclohexan auf Pd/C. Im Vergleich mit Wasser und Hexadekan eröffnet Methanol eine zusätzliche Reaktionsroute von Cyclohexanon mit Methanol bei der Hydrodeoxygenierung von Phenol. Die Hydrierungsreaktionen, vor allem von Phenol und Cyclohexanon, besitzen in

Methanol geringere Raten als in Wasser oder Hexadekan. Methanol löst Phenol und Cyclohexanon nicht nur stark, sondern adsorbiert auch stark auf Pd. Diese starke Adsorption hindert Cyclohexanon/Phenol entweder daran mit den aktiven Zentren des Pd wechselzuwirken oder verringert die Bedeckung von Cyclohexanon/Phenol auf der Pd/C Oberfläche, was zu langsamerer Hydrierung von Cyclohexanon/Phenol in Methanol führt. Die geringe Löslichkeit von Phenol und die starke Wechselwirkung von Hexadekan mit der Pd-Oberfläche in Hexadekan führen zu einer langsamen Hydrierungsrate. Die scheinbaren Aktivierungsenergien der Hydrierungen besitzen die Reihenfolge $E_{a\ Phenol\ Hydrierung} > E_{a\ Cyclohexanon\ Hydrierung} > E_{a\ Cyclohexen\ Hydrierung}$, und die Raten folglich $TOF_{Cyclohexen\ Hydrierung} > TOF_{Cyclohexanon\ Hydrierung} > TOF_{Phenol\ Hydrierung}$ bei 473 K.

Curriculum vitae

Jiayue He was born on December 29th, 1984 in Nanchang, China. With his performance at high school and "*Bronze Medal of Chemistry Olympiad (National High School Chemistry Competition)*", he was matriculated into the Department of Chemistry at Nankai University (Tianjin, China) without requiring entrance examinations, where he received his bachelor's degree in Science in June 2008. In August 2008, he started the study in the joint program (Industrial Chemistry) of National University of Singapore and Technische Universität München as a master student under the supervision of Prof. Fritz E. Kühn. In February 2010, he earned the degree of master in Science, with the thesis titled "*Immobilization of Weakly Coordinating Anions B(C$_6$F$_5$)$^{4-}$ Merrifield Resin and Their Potential Applications in Supported Molecular Catalysis*". During his master's study, he was awarded "*GIST-DAAD scholarship*" by German Academic Exchange Service and "*Book prize*" by Technische Universität München. In March of the same year, he joined the research group of Prof. Johannes A. Lercher and started his Ph.D study at the Chair of Technical Chemistry II at Technische Universität München, Germany. His recent research focuses on the selective cleavage of C-O bonds and hydrodeoxygenation of lignin fragment molecules. During his Ph.D study, he was awarded "*Chinese Government Award for Outstanding Self-financed Students Abroad*" by Chinese Government.

List of Publications

Jiayue He, Lu Lu, Chen Zhao, Donghai Mei, Johannes A. Lercher " *Mechanisms of Catalytic Cleavage of Benzyl Phenyl Ether in Aqueous and Apolar Phases*" Journal of Catalysis 311 (2014) 41-51

Jiayue He, Chen Zhao, Johannes A. Lercher "*Impact of Solvent for Individual Steps of Phenol Hydrodeoxygenation with Pd/C and HZSM-5 as Catalysts*" Journal of Catalysis 309 (2014) 362-375

Jiayue He, Chen Zhao, Donghai Mei, Johannes A. Lercher "*Mechanisms of Selective Cleavage of C–O Bonds in Di-aryl Ethers in Aqueous Phase*" Journal of Catalysis 309 (2014) 280-290

Jiayue He, Chen Zhao, Johannes A. Lercher "*Ni-Catalyzed Cleavage of Aryl Ethers in the Aqueous Phase*" Journal of the American Chemical Society 134 (2012), 20768–20775

Jiayue He, Harry Ranger, Donghai Mei, Chen Zhao, Eszter Baráth, Johannes A. Lercher "*Solvent Impact on the Conversion of Di-aryl Ethers over Ni/SiO$_2$*" in preparation

Jiayue He, Yu Lou, Albert Albert, Chen Zhao, Eszter Baráth, Johannes A. Lercher " *Catalytic Cleavage of Five C-O and C-C Linkages of Lignin in the Aqueous Phase*" in preparation

Jiayue He, Harry Ranger, Haiyan Li, Gokulnath Dilibabu, Donghai Mei, Chen Zhao, Eszter Baráth, Johannes A. Lercher "*Hydrogenolysis and Hydrogenation of Diverse Lignin-derived Alcohols and Ethers*" in preparation

Jiayue He, Miriam Pfab, Yu Lou, Donghai Mei, Chen Zhao, Eszter Baráth, Johannes A. Lercher "*Mechanisms into C-O Bond Cleavage of 2-Phenylethyl Phenyl Ether in the Aqueous Phase: Experimental and Theoretical Study*" in preparation

Chen Zhao, Stanislav Kasakov, <u>Jiayue He,</u> Johannes A. Lercher "*Comparison of kinetics, activity and stability of Ni/HZSM-5 and Ni/Al$_2$O$_3$-HZSM-5 for phenol hydrodeoxygenation*" Journal of Catalysis 296 (2012) 12-23

Chen Zhao, <u>Jiayue He,</u> Angeliki A. Lemonidou, Xuebing Li, Johannes A. Lercher "*Aqueous-phase hydrodeoxygenation of bio-derived phenols to cycloalkanes*" Journal of Catalysis 280 (2011) 8-16

Yang Li, <u>Jiayue He,</u> Vineeta Khankhoje, Eberhardt Herdtweck, Klaus Kohler, Oksana Storcheva, Mirza Cokoja, Fritz E. Kühn " *Copper(II) Complexes Incorporating Poly/Perfluorinated Alkoxyaluminate-type Weakly Coordinating Anions: Syntheses, Characterization and Catalytic Application in Stereoselective Olefin Aziridination*" Dalton Transactions 40 (2011) 5746-5754

Yu Liu, Rui Cao, Yong Chen, <u>Jia-yue He</u> "*Effect of beta-cyclodextrin charge type on the molecular recognition thermodynamics of reactions with (ferrocenylmethyl)dimethylaminium derivatives* " Journal of Physical Chemistry B 112 (2008) 1445-1450

List of Presentations

<u>Jiayue He,</u> Lu Lu, Donghai Mei, Chen Zhao, Johannes A. Lercher "*Mechanisms of Catalytic Conversion of lignin-derived Benzyl Phenyl Ether in Aqueous and Apolar Phase*" (Oral Presentation) 247th ACS National Meeting and Exposition, 2014, Dallas, TX, USA.

<u>Jiayue He,</u> Chen Zhao, Johannes A. Lercher "*Mechanisms of Selective Cleavage of Aryl Ether Bond in the Lignin-Derived Dimer in the Aqueous Phase*" (Oral Presentation) 246th ACS National Meeting and Exposition, 2013, Indianapolis, IN, USA.

<u>Jiayue He,</u> Chen Zhao, Johannes A. Lercher "*Selective Cleavage of Aryl Ether Bonds in Lignin Model Compounds Using Ni Based Catalysts in Water*".(Oral Presentation) 45. Jahrestreffen Deutscher Katalytiker, 2012, Weimar, Germany.

<u>Jiayue He,</u> Chen Zhao, Johannes A. Lercher "*Catalytic Cleavage of Ether Bonds in Lignin Model Compounds Using Ni Based Catalysts in Water*"(Oral Presentation) 15th International Catalysis Conference, 2012, Munich, Germany

<u>Jiayue He,</u> Lu Lu, Donghai Mei, Chen Zhao, Johannes A. Lercher "*Mechanisms of Catalytic Conversion of lignin-derived Benzyl Phenyl Ether in Aqueous and Apolar Phase*" (Poster Presentation) 247th ACS National Meeting and Exposition, 2014, Dallas, TX, USA.

<u>Jiayue He,</u> Chen Zhao, Johannes A. Lercher "*The Metal and/or Acid Effect on the Cleavage of the Ether Bond of Benzyl Phenyl Ether (BPE) in Aqueous Phase*"(Poster Presentation) 46. Jahrestreffen Deutscher Katalytiker, 2013, Weimar, Germany.

<u>Jiayue He,</u> Chen Zhao, Johannes A. Lercher "*Kinetics of Hydrodeoxygenation of Phenol on Dual Functional Catalysts*"(Poster Presentation) European Graduate School Summer School "Energy and Materials from The Sun", 2011, Rolduc Abbey, The Netherlands

Jiayue He, Chen Zhao, Johannes A. Lercher "*Solvent Effect on Phenol Hydrodeoxygenation over Pd/C and HZSM-5*" (Poster Presentation) IDECAT/ERIC-JCAT Conference on Catalysis, 2011, Bertinoro, Italy.

Jiayue He, Chen Zhao, Johannes A. Lercher "*Bio-derived Phenols Hydrodeoxygenation in Aqueous-Phase*"(Poster Presentation) European Graduate School Winter School, 2010, Nyborg, Denmark